SCIENTIFIC PROGRAMME

SIMULATION
OF
SIGNAL
AND
IMAGE
PROCESSING

EMERGENT COMPUTATION AND IMAGE PROCESSING - FEATURE EXTRACTION PATTERNS GENERATED BY THE INTERACTIONS BETWEEN SIMPLE AGENTS AND THEIR IMAGE ENVIRONMENT.

Jeff Jones
Mohammed Saeed
Steve Lewis
University College Chester
Parkgate Road, Chester
CH1 4BJ, United Kingdom
E-mail: jeff.jones@chester.ac.uk

KEYWORDS
Multi agent systems, image processing, stigmergy, feature extraction, emergent computation, persistence, data-driven, physical systems.

ABSTRACT

Conventional image processing techniques regard the image merely as data to be processed by the chosen algorithm. We propose that by treating the image data as a landscape upon which a large population of agents live, feature extraction can be regarded as a persistent pattern resulting from the dynamics between the agents' behaviour and their environment. We describe a system that both situates the dynamic agents in their environment and provides parallel environmental effects, such as erosion and diffusion. Agents can explore their landscape, be affected in their behaviour by the landscape, and modify the landscape, for example by laying a trail, leaving specific marks or directly changing the landscape 'data'. The agents act locally and independently in a simple behavioural manner, reacting to simple stigmergic cues from the landscape configuration. We demonstrate different 'breeds' of agent whose behaviour, combined with environmental effects, produces persistent patterns in the landscape data. These persistent patterns provide image feature extraction behaviour. Examples results are shown and the importance of giving data an active role in its own processing is stressed, as opposed to being merely treated as 'fodder' to be processed by a complex algorithm.

INTRODUCTION AND PREVIOUS WORK

Image processing is typically regarded as transforming an input image data using a specified algorithm giving output data that contains the desired features. This places a greater emphasis on the algorithm as opposed to the data. In images the desired features are usually distributed in nature across many pixels and finding these features is a non-trivial problem. Many different algorithms exist to discover certain features within digital images, such as edges and lines, regular shapes, and higher level features such as eyes or entire faces. It is difficult to specify such features in terms of their basic components, single pixels, as the features and patterns are distributed in the relationships between many different pixels. The distributed nature of the desired data within an image is responsible for the difficulty in designing image processing/analysis algorithms.

The high level nature of the data patterns stored within images parallels the behaviour of simple agent based systems. In this case the agents possess very simple behaviours and their interactions result in a global pattern of emergent behaviour that is not specified in their underlying component behaviours. Much of the research into simple agent systems comes from studies of social insects (Deneubourg et al, 1991) and this research has shown that much of the complexity in the patterns of agent behaviour come from the interactions between the individual agents and their environment. One form of the interactions seen is known as stigmergy (Grasse, 1959), an indirect communication where the agents receive behavioural cues from stimuli in their environment. Agents in turn can also influence other agent behaviour by laying down their own stimuli in the environment. Stigmergic communication can be based on the amount of stimuli sensed, or based upon different types of stimuli sensed (Holland and Melhuish, 1999).

The use of multi agent systems for tasks such as image processing/analysis would seem ideal since the image data 'landscape' presents rich environmental stimuli for agents. Although agent behaviours are influenced by the landscape at the pixel level, any emergent patterns seen from a group of interacting agents would hopefully be strongly influenced by the high level patterns stored within the data. Furthermore, stigmergy is a simple communications paradigm to implement, eliminating the need for complex agent-agent communication protocols since the communication between agents is mediated entirely by the environment.

The use of simple behavioural multi agent systems (as opposed to the traditional AI complex *knowledge based* agent) in image processing/analysis has been seen in recent years. Liu and Tang used reproducing agents to reduce the time to perform image processing and analysis operations such as edge detection (Liu and Tang, 1997). Ramos and Almeida developed ant like agents inspired by the Ant Colony Optimisation research of Dorigo and Gambardella (1997) to explore group behaviour in pattern recognition (Ramos and Almeida, 2000). Recently, specific applications of multi agent feature extraction have been developed. Guillaud used groups of simple agents to perform edge detection and ring continuity on fish otolith images (Guillaud et al, 2002).

Toffoli also examined the fact that features in images are macroscopic patterns (lines, shapes etc) in a fine-grained substrate (pixels). He proposed emergent fine-grained computation based on the cellular automata paradigm as a way of making the high level features that are 'latent' in an image apparent. He also espoused the development of approaches that modelled physical systems, such as chemical staining, Brownian motion, etching and plating, in order to achieve feature extraction (Toffoli, 1999).

IMAGES AS DYNAMIC ENVIRONMENTS.

We present a system that uses the concept of multiple agents habituated in a dynamic environment. The environment 'landscape' (Figure 1) is a digitised grey-scale image. For an 8-bit image this provides 256 different possible 'heights'.

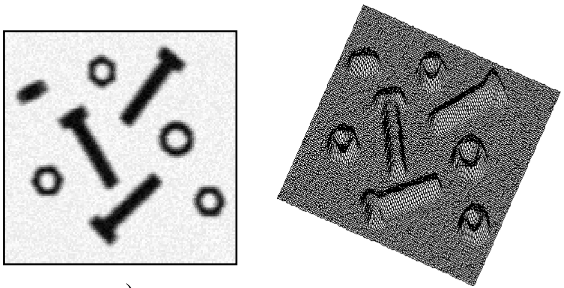

a) b)

Figure 1: Sample input image (1a) and representation of image as an environment landscape (1b).

The environment is itself a dynamic system that operates in real time and all areas in the environment update synchronously. The updating of the environment in parallel adheres to the cellular automata paradigm and provides possibilities for increased emergent interactions with the agents. The environment dynamics available include erosion (similar to water erosion or wind effects) – where areas of the environment, trails or marks can be eroded subject to certain conditions specified by the user at the start of an experimental run. These conditions can apply evenly to all cells or can be dependent on certain qualities of the cells: for example the erosion of marks may be dependent on the level of mark at a particular cell. This is analogous to staining or washing where a more 'stubborn' heavily deposited mark will be more resistant to erosion than a more lightly deposited mark. Another example of an environmental dynamic is diffusion where levels of trails or marks may diffuse across (subject to user specified parameters) into other cells.

FEATURES OF BASIC AGENTS

A decision was made not to model the behaviour of the agents specifically on any single model, such as ant models, in order keep the system as flexible as possible. The agents are habituated within the dynamic image environment. Agents all contain the same basic features: They are able to move independently in their environment from cell to cell in any of the 8 compass directions. They can sense their position and height in the landscape and deposit certain signals in their environment – trails and a more general 'mark', or even modify the landscape height directly. The agents can sense the presence of other agents and they can also have the ability to 'teleport' to any unoccupied point in the landscape. Agents do not communicate directly with one another – all communication is indirect via the environment using the stigmergy paradigm. Specific breeds of agent can be extended from this basic agent in order to provide more specialised features.

EXAMPLE RESULTS OF DIFFERENT AGENT BREEDS.

Examples of the different 'breeds' of agent are shown below. All different breeds extend the functionality of the basic agent. The interactions between the agents and their environment result in emergent patterns being created. Some of these patterns may persist over time and it is these patterns which provide the feature extraction behaviour of the system. The proscribed behaviours of the agents were made as simple as possible, since by specifying simple behaviours it would be easier to show the generation of emergent patterns. By choosing simple behaviours it is also be easier to ascertain whether or not any patterns formed were simply due to artefacts of the algorithm.

Walking Agent.

This agent has a very simple proscribed behaviour given by the following pseudocode:

```
Take a step forwards in the current direction
If the cell at the FRONT LEFT is less in intensity
than the cell at the FRONT RIGHT:
    Turn left 45 degrees
Else if the cell at the FRONT RIGHT is less in
intensity than the cell at the FRONT LEFT:
    Turn right 45 degrees
```

Figure 2 below shows the original image (2a), an image of 600 agents (the dots on the image) moving within their landscape (2b), the trail patterns left by the agents at 200 steps (2c), and at 2000 steps (2d).

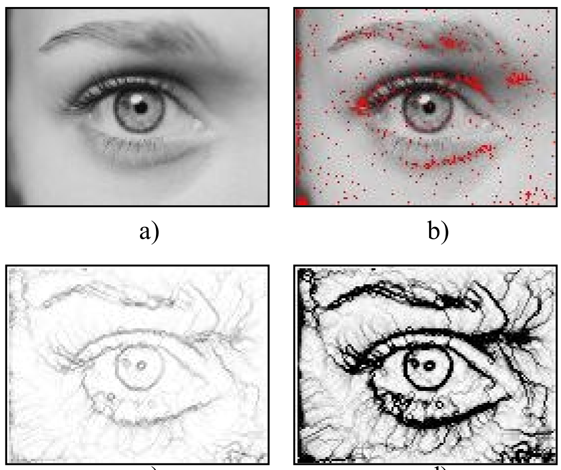

a) b) c) d)

Figure 2: Sample outputs from Walking Agent experiment

For the walking agent experiment, the 600 agents were initially placed randomly within their environment and were sensitive to changes of landscape intensity of 1. It is possible for the user to adjust this sensitivity parameter. For example a sensitivity parameter of 5 will ensure that the agents respond only to environment changes if the deviation between the current cell and the target cell is greater than 5 – thus making the agent sensitive only to large deviations of intensity.

The results show an emergent pattern 'developing', consisting of trails left behind by the agents as they move. The final output at 2000 iterations of the system clearly shows latent 'channels' that the agents move down that are not apparent in the original image.

Gravity Agent Experiment.

This example illustrates how edge detection can arise from an algorithm with no apparent connection to image feature extraction. The pseudocode for each agent is given below:

```
Take a step forwards in the current direction.
If there is a neighbouring cell that is lower in value
than the current cell:
        Turn to face that cell
Else:
        Leave a mark and Teleport to a new
        random location
```

Figure 3 below shows the mark patterns left by 3000 Gravity Agents in 3 experiments, each applying this behaviour for 1000 iterations, and with different sensitivity parameters.

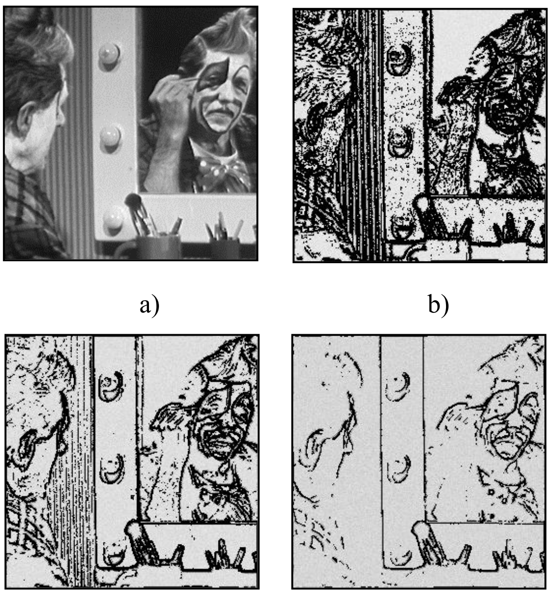

a) b) c) d)

Figure 3: Original 'Clown' image (3a), sensitivity value of 10 (3b), sensitivity of 20 (3c), sensitivity of 40 (3d)

DISCUSSION AND FURTHER WORK

We have described a system that performs image feature extraction ('higher level' features which are distributed among many pixels), seen as a persistent emergent pattern produced by the interactions between agents and their environment. This takes a broader approach to multi agent systems than the approaches influenced purely by social insects The system is also influenced by the phenomena seen in physical systems, the environment dynamics within a system and the interactions between the agents and their environment. The system is extensible with many different agent 'breeds' and further work is in progress to explore more fully the agent-environment dynamics. Experiments currently being evaluated are based on image skeletonisation and noise reduction via environmental influences. Some challenges remain, notably that of deciding when the image processing has finished – something that is usually trivial using conventional algorithms but proves more difficult with emergent computation approaches.

The component agents in the system are specifically designed to be simple in nature in order to place the emphasis on the importance of the data in its processing and analysis. Since the desired data is stored within the image in a distributed high level pattern, a suitable means of achieving the extraction of the data may be to get the data to drive the behaviour of the agents. By doing so, the emergence of a persistent pattern left behind will leave a 'footprint' that represents the desired result.

REFERENCES

Deneubourg, J.-L., Goss, S., Franks, N., Sendova-Franks A., Detrain, C., Chretien, L. "The dynamics of Collective Sorting: Robot-like ants, and Ant-like robots" In proceedings first conference on simulation of adaptive behaviour: From animals to animats, MIT press 1991., 356-365.

Dorigo, M. and Gambardella, L.M. (1997). Ant Colonies for the Traveling Salesman Problem. *BioSystems,* **43**:73-81.

Grassé, P-P. (1959) La reconstruction du nid et le coordinations inter-individuelles chez Bellicositermes natalensis et cubitermes sp. La theorie de la stigmergie: Essai d'interpretation du comportement des termites constructeurs. Insectes sociaux, **6**, 41-81.

Guillaud, A., Benzinou, A., Troadec, H., Rodin, V. and Le Bihan, J. (2002) Autonomous agents for edge detection and continuity perception on otolith images, *Image and Vision Computing*, **20**, 955-968.

Holland, O.E. and Melhuish C. (1999) Stigmergy, Self-Organization, and sorting in collective robotics. *Artificial Life* **Vol. 5,** 173-202.

Liu, J. and Tang Y. Y. (1997) An evolutionary autonomous agents approach to image feature extraction, in: *IEEE Transactions on Evolutionary Computation,* Vol. **1**, **No. 2**, pp 141-158.

Ramos, V. and Almeida, F. (2000) Artificial ant colonies in digital image habitats – A mass behaviour effect study on pattern recognition, ANTS'2000 – 2nd Int. Workshop on Ant Algorithms (From Ant Colonies to Artificial Ants), M. Dorigo, M. Middendorf & T. Stüzle (Eds.), Brussels, Belgium, 7-9 Sep. 2000., pp 113-116.

Toffoli, T. (1999) Programmable matter methods, *Future Generation Computer Systems Special issue on Cellular Automata (Eds Talia, D. and Sloot P.)*, **16:2-3**, 187-201.

ARABIC DOCUMENT UP/DOWN ORIENTATION DETERMINATION

Ahmed M. Zeki
Dept of Computer Science
International Islamic Univ. Malaysia
Jln. Gombak 53100, KL, Malaysia
amzeki@iiu.edu.my

Mohamad S. Zakaria
Dept of Computer Science
National Univ. of Malaysia
Bangi, 43600, Selangor, Malaysia
msz@pkrisk.cc.ukm.my

KEYWORDS
Arabic Documents, Up/Down Orientation, Orientation Determination

ABSTRACT

A method to determine the up/down orientation of an Arabic document is described here. The document consists of Arabic characters and numerals. The algorithm assumes that the document being substantially text and well vertically aligned with respect to the scanner axes. Three main zones were identified for the Arabic characters, namely: upper, middle and lower zones. The algorithm is based on the fact that the Arabic characters are asymmetric on these zones, hence producing asymmetric horizontal histogram. The algorithm is tested on a diverse sample of Arabic documents varying in size, number of lines, font style and font size and achieved 100% accuracy.

1. INTRODUCTION

Human brain can determine the orientation of a document easily, instinctively and intuitively. A mathematical algorithm needs to be developed and implemented in a program in order to give the computer the capability of determining the orientation.
Inverted documents (i.e. upside down) may arise from scanning paper documents into a computer, from faxes received via a fax modem or from rotated document images for a reason or another. The problem discussed here is a subset of the skew detection/correction problem.
Skew detection is an essential stage for character recognition as well as many other applications in pattern recognition and image processing. It should be considered as one of the earliest steps in the preprocessing stage. The problem can be studied from four perspectives:

1. *Determining the skew angle* if the document is not vertically or horizontally aligned. Several methods have been proposed by researchers for skew detection (Yu et al. 1995) (Chaudhuri and Pal 1997) (Smith 1995). However, this level of detection may not look into the up/down orientation of the text at the first place.

2. *Detecting the vertical/horizontal orientation*. Several researchers (Akiyama and Hagita 1990) (Farrow et al. 1994) (Le et al. 1994) successfully solved this problem by determining whether the document is fed into the system vertically (portrait) or horizontally (landscape). The method relies on text having frequent interline gaps of similar size to character heights, but smaller and 'vertically' unaligned intraline gaps (Caprari 2000). However, this step is not enough for character recognition and should be followed by the up/down orientation determination.

3. *Determination of the up/down orientation*, which is the scope of this paper and will be discussed in details in the following sections.

4. *Skew Correction*. Once the document is found to be skewed, there is a need to correct or deskew it for further processing, see for example (Ali 1997). This stage is out of the scope of this paper.

A typical character recognition system should have the above four stages as part of the preprocessing stage. Most of the work was found to be dealing with English and European documents and none has been found to deal with Arabic documents. This research paper is focused on the Arabic characters, and specially the printed ones.

2. THE ALGORITHM

This research is based on the work of Caprari (2000) in which he designed an algorithm and applied it on English characters and Arabic numerals. In this paper, the same method is modified and used to determine the up/down orientation of the Arabic documents.
The algorithm operates on a page of scanned text represented as an array. The effectiveness of the algorithm relies on the document being substantially text. Hence, it does not work for non-textual images.
The method is slightly modified to be suitable for Arabic documents. It should work properly for other alphabets as well with minor modifications.
Basically, it is based on studying the shape of the Arabic characters and determining the different zones of the character. These natural zones will have an impact on the horizontal histogram of the document. The algorithm assumes that the original document is well vertically aligned with respect to the scanner axes; otherwise, skew correction process is necessary.
The distinction between upright and inverted text is based on the asymmetry feature of the Arabic character shape which is neither horizontally nor vertically symmetric as illustrated in Figure 1.
By looking at the characters in Figure 1, three zones can be recognized easily; the upper, middle and lower zone. Different fonts have slightly different zone height. However, it can be noticed that the upper zone is slightly bigger than half of the total height, the middle zone is about

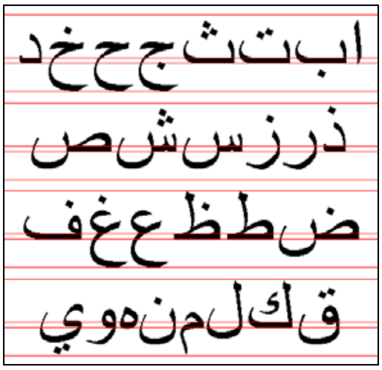

Figure 1: The Separated Arabic Characters and their Zones, using Arabic Transparent Font.

10% or less, and the lower zone is slightly bigger than one third of the total height.

The middle zone is known as the *text-baseline*, mainly contains the horizontal strokes that connect the characters together, it is so small that it can't contain any character, and even sometimes it is represented by a 1-pixel line. Extracting the middle zone is extremely useful in character recognition because some characters completely fall in the upper and middle zone, and some fall in the middle and lower. The algorithm is described in the following steps through an example:

Step 1: Compute the horizontal projection of the document using formula (1), Figure 2(a) shows a sample of an Arabic document and Figure 2(b) shows its horizontal projection graph.

$$p(i) = \sum page(i, j) \qquad (1)$$

The asymmetry attribute of the Arabic text line is clear in the graph, the longest spike represents the base-line, and the upper zone is slightly bigger and thicker than the lower zone.

Step 2: The projection *p* is differentiated *dp* by a *forward difference method formula* (Formula 2) and the graph is shown in figure (2c).

$$dp(i) = p(i+1) - p(i) \qquad (2)$$

Notice from graph (2c) that each text line is characterized by one large positive spike and one smaller negative spike. This verifies that the text up/down asymmetry has persisted through to this stage of the algorithm.

Step 3: *Squared differentiated projection sdp* is computed using formula (3), and the graph is shown in figure (2d):

$$sdp(i) = dp^2(i) \qquad (3)$$

Step 4: To restore the sign of *dp* which was destroyed by squaring *dp*, *sdp* is multiplied by the sign of *dp* using formula (4) as shown in figure (2e).

$$ssdp(i) = sdp(i) * sign(dp(i)) \qquad (4)$$

Step 5: Finally, to know whether the graph is symmetric or asymmetric, the sum of *ssdp* is divided by the sum of *sdp* over all rows using formula (5). The result is a scalar, the document will be upright if the scalar is negative and inverted if it is positive.

$$asym = -\frac{\sum ssdtp(i)}{\sum sdtp(i)} \qquad (5)$$

3. EXPERIMENTAL RESULTS

The algorithm described in this paper was implemented in MATLAB® v.6.5 and tested on a diverse sample of Arabic documents. Testing was conducted on 31 different documents varying in size, number of lines, font style and font size. All images were monochrome images. The font size ranged between 8 and 72 points. There were 18 upright documents and 13 inverted.

No deskewing of page images was undertaken because the documents were very well vertically aligned. No noise has been added to the images. The orientation of all documents was correctly determined. It has been noted that smaller font sizes and smaller text region reduce the algorithm effectiveness.

4. REFERENCES

Yu, Chiu L., Yuan Y. Tang and Ching Y. Suen. 1995. "Document Skew Detection Based on the Fractal and Least Squares Method". *Proceeding of the Third International Conference on Document Analysis and Recognition (ICDAR'95)*, pp. 1149-1152.

Chaudhuri, B. B. and Pal U. 1997. "Skew Angle Detection of Digitized Indian Script Documents". *IEEE Transactions on Pattern Analysis and Machine Intelligence*, Vol. 19, No. 2, pp. 182-186.

Smith, Ray. 1995. "A Simple and Efficient Skew Detection Algorithm via Text Row Accumulation". *Proceeding of the Third International Conference on Document Analysis and Recognition (ICDAR'95)*, pp. 1145-1148.

Akiyama, T. and Hagita, N. 1990. "Automated Entry System for Printed Documents". *Pattern Recognition* 23, 1141-1154.

Farrow, G., M. Ireton, and C. Xydeas. 1994. "Detecting the Skew Angle in Document Images". *Signal Processing: Image Communication* 6, 101-114.

Le, D., G. Thoma, and H. Wechsler. 1994. "Automated Page Orientation and Skew Angle Detection for Binary Document Images". *Pattern Recognition* 27, pp. 1325-1344.

Caprari, Robert S. 2000. "Algorithm for Text Page Up/Down Orientation Determination". *Pattern Recognition Letters*, Vol. 21, pp. 311-317.

Ali, M., 1997. "An Object/Segment Oriented Skew-Correction Technique for Document Images". *Proceedings of the Fourth International Conference on Document Analysis Recognition*, pp. 671-674.

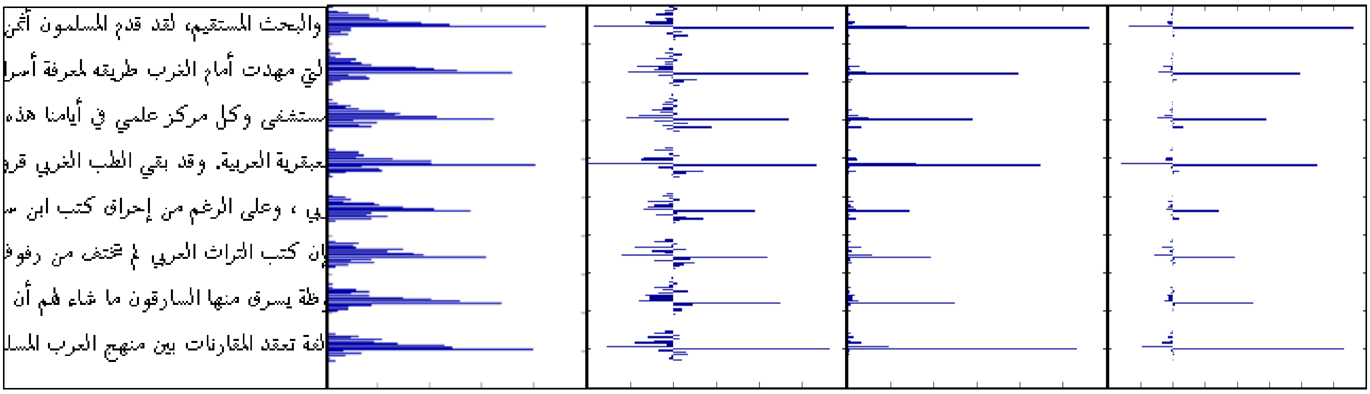

(a) (b) (c) (d) (e)

Figure 2: (a) A Sample of an Arabic Document written in Traditional Arabic Font, Size 12 (b) The Horizontal Projection *p* (c) Differentiated Projection *dp* (d) Squared Differentiated Projection *sdp* (e) Signed Squared Differentiated Projection *ssdp*

FAST AND SPACE EFFICIENT EDGE DETECTION FOR GREY-SCALE AND COLOUR IMAGES BY MEANS OF A GENETIC ALGORITHM TO EVOLVE RELATIVE VALUED CELLULAR AUTOMATA.

Jeff Jones
Mohammed Saeed
Steve Lewis
University College Chester
Parkgate Road, Chester
CH1 4BJ, United Kingdom
E-mail: jeff.jones@chester.ac.uk

KEYWORDS
Cellular Automata, Edge Detection, Genetic algorithms, Grey-scale, Colour, Evolutionary computation, Parallelism, Canny operator

ABSTRACT
The architectural similarity between two-dimensional cellular automata and digital images naturally suggests their use in image processing operations. However, increasing the number of different colour values, or intensity levels in grey-scale images, dramatically increases the look-up table size of traditional cellular automata. We introduce a method to reduce the rule table size in cellular automata using relative pixel intensity values, enabling the processing of images with large ranges of pixel intensity. A genetic algorithm is used to evolve cellular automata rule tables using this relative value method. A parameter to increase or decrease the sensitivity of the image processing automaton is described and examples of its use are illustrated. Edge detection results using this cellular automaton are shown in comparison to the popular Canny operator. Advantages of this method are that the rule table size is reduced so that it can easily be stored within the computer memory. This maintains the operational speed of the processing and avoids the need to specify rules algebraically. This method is a fast, efficient and inherently parallel means of achieving edge detection behaviour. Results and further possible work are discussed.

INTRODUCTION AND PREVIOUS WORK

Cellular automata as suggested by Ulam and implemented by von Neumann (von Neumann, 1966) are discrete dynamical systems composed of a lattice of simple computational elements. Each element has an internal state and this state is governed by a transition function. The transition function considers both the internal state and the state of the neighbouring elements (‘cells’). Typically, the cells are updated in a synchronous manner, they obey the same transition function and the cells are arranged in a regular lattice.

Although cellular automata may be seen in one, two, and three dimensional variants, the similarity between the architecture of a two dimensional cellular automaton and a stored discrete digital image makes them naturally suitable for the task of image processing (Preston and Duff, 1984), (Toffoli, 1999). Each picture element (‘pixel’) in a digital image has a value, corresponding to the light intensity value in a grey-scale image, or a colour value in a colour image (itself consisting of separate colour components such as Red, Green and Blue values). A digital image, like a two dimensional cellular automaton, is arranged in a regular lattice and each pixel is surrounded by neighbouring pixel ‘cells’. Image processing is the process of modifying the data within an image in order to highlight certain features. Edge detection is one such procedure, where the edges in an image (discontinuities in intensity or texture, steps or lines) are enhanced and a great many different algorithms exist to perform this operation (Ziou and Tabbone, 1997). Poli has suggested that all image feature extraction behaviours can be stated as being filters, for whichever feature is being enhanced, all other features are being filtered out (Poli, 1996).

The transition function of a cellular automaton can be implemented in a rule table, or look-up table. The state of the current cell and its neighbours creates a unique value corresponding to an entry in the table that determines the new state of the cell in the next step of the automaton. The rule table contains every possible configuration of the cell’s state combined with every possible configuration of neighbouring states. The size of the rule table is dependent on both the number of different possible states and the size of the neighbourhood.

The two most common neighbourhoods in two-dimensional automata are the von Neumann neighbourhood and the Moore neighbourhood. The von Neumann neighbourhood consists of the central cell undergoing the transition function and its four neighbours, visualised as the main compass points (N,S,E,W). The Moore neighbourhood extends the von Neumann neighbourhood by also including the extra diagonal corners of the neighbourhood (NE, NW, SE, SW).

Since the neighbourhood of the transition function is usually fixed, the biggest influence on look up table size will be the number of possible states per cell. For example, in a binary (two-state) automaton with the Moore neighbourhood the number of different possible cell/neighbourhood configurations will be 2^9 (512) and the number of different possible rule tables will be 2^{512}. As the number of cell states increases, the size of the rule table, and therefore the space of all possible rule tables, increases dramatically.

As the complexity and size of the rule table increases, it is often simpler to state the cell transition rule algebraically rather than in terms of an explicit look-up table. For example, Conway's popular automaton, Life (2 states, Moore neighbourhood) may have its transition function expressed in the following manner (Gardner, 1970):

> If a cell is currently alive (1) and has exactly two or three neighbouring cells that are alive, remain alive in the next generation, otherwise die (0) in the next generation.
>
> If a cell is currently dead and has exactly three neighbours that are alive, come alive in the next generation, otherwise remain dead in the next generation.

Describing the transition rule algebraically has the advantage that the transition rule is more understandable, certainly more so than reading entries in a binary look up table. In some respects it is also space efficient, since the rule table for the Life automaton (512 combinations) need not be stored in memory. An algebraic encoding of transition rules has also been used chosen for grey-scale image processing in cellular automata (Wongthanavasu and Sadananda, 2003).

Disadvantages to this approach however are that the operation of an automaton using an algebraic expression will be slower than one that simply 'jumps' blindly to an entry in a look up table. The second, and perhaps more pertinent disadvantage is that it is more difficult to optimise the transition rule for more efficient operation of the automaton. This must be done in a 'trial-and-error' manner in order to try and achieve different results. The use of evolutionary algorithms to evolve improvements in transition function rules is one possibility. Poli used genetic programming techniques to evolve algebraic image processing functions, though he was forced to limit the number of component functions in order to reduce both the size of the search space and the cost of excessive computation time (Poli, 1996).

RELATIVE PIXEL INTENSITY VALUE ENCODING

The use of evolutionary algorithms to evolve simple rule tables for cellular automata is a simpler process than trying to evolve algebraic transition functions. The fixed size of the rule table 'genome' enables the use of simpler genetic algorithms to be used. However there is the problem of the number of possible states for each cell in the automaton to contend with.

A cellular automaton look-up table increases in size dramatically in relation to the number of states possible in each cell. This imposes a severe memory constraint when considering even a small range of grey scale levels. A solution we have devised is to consider the intensity of the cell not in absolute intensity values, but relative to the intensity of its neighbours.

This method only requires three states to be stored for each cell – no matter how large the range of intensity values for each cell. The only values that need to be stored is whether the cell is of a greater intensity, a lesser intensity, or has the same intensity as its neighbouring cells. Figure 1 illustrates the concept for both the Moore neighbourhood (1a) and the von Neumann neighbourhood (1b).

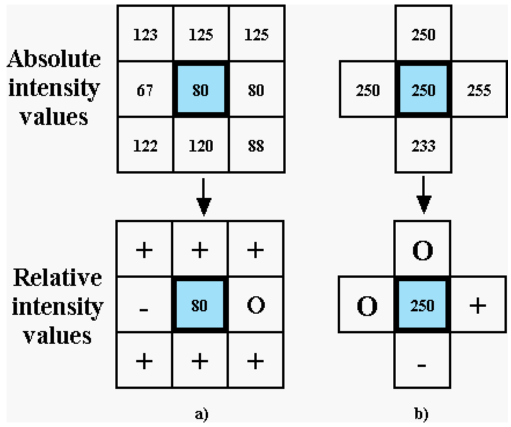

Figure 1: Absolute pixel intensity values translated to relative pixel intensity values

It can be seen that by only encoding the relative changes in intensity – greater than ('+'), less than ('-'), or the same ('0') – a great economy in the size of the look-up table can be achieved. This economy is further increased when we consider that we do not have to include the centre cell in the rule table. Thus the Moore neighbourhood entries consist of only eight cells and the von Neumann neighbourhood entries now consist of only four cells. Because we are only considering three possible states per cell, the size of the rule table is further reduced. The look-up table for a von Neumann neighbourhood will only be 3^4 entries long (81 entries), and the look-up table for the Moore neighbourhood is only 3^8 entries long – 6561 entries. This is a somewhat larger table than for the von Neumann neighbourhood but easily within the memory capacity of modern personal computers. This encoding of relative intensity values enables us to consider images with many grey scale levels and even colour images with a great many colour ranges, for example 32bit colour ranges for each pixel. The output from each look up table entry, giving the state of the cell in the next 'step', can be of three possible values: an increase in pixel intensity for that cell, a decrease in pixel intensity, or no change in pixel intensity. The amount of the increase/decrease in pixel intensity may be specified by the user at the start of the experiment.

RELATIVE PIXEL SENSITIVITY PARAMETER

The encoding of the rule table specifies whether the neighbourhood cells' intensity differ from the centre cell (greater, lesser or the same). It is useful to introduce a sensitivity parameter that specifies how large the deviation between the intensity values of the pixels must be in order for the difference to register. For example, a sensitivity parameter value of 1 means that, if a neighbouring pixel is greater in intensity by a value of one or more, then that neighbour will be given the '+' code. However if the sensitivity parameter is set to 5, a neighbour with an intensity difference of 1 will not be enough to trigger a difference, and that neighbour will be given the '0' (same) code. The sensitivity parameter thus acts to specify the sensitivity of changes in image intensity values.

It is possible to view the effect of the sensitivity parameter and its effect on the distribution of rule table entries, if we consider the von Neumann neighbourhood with 81 different possible rule table entries and give each entry a different colour value. Figure 2a illustrates an original grey scale image (256 possible grey levels). Figure 2b illustrates the rule table distribution with a sensitivity parameter value of 1 and figure 2c illustrates the rule table distribution with the sensitivity parameter of 5. It can be seen that this feature in itself acts as a rudimentary image filtering operation.

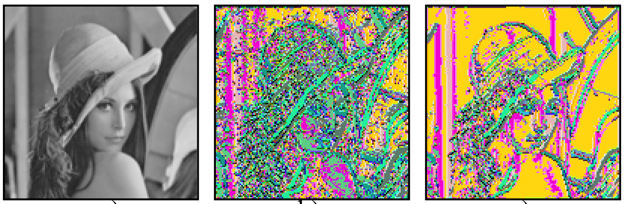

a) b) c)

Figure 2: a) Original 'Lena' image, b) rule-table entry distribution with sensitivity of 1, c) rule table distribution with sensitivity 5.

EVOLVING RELATIVE VALUED CELLULAR AUTOMATA FOR EDGE DETECTION.

A genetic algorithm was developed to assess the suitability of using relative valued cellular automata for edge detection on images. The algorithm generates a population of cellular automata whose genomes consist of rule tables. The rule tables can be either 81 entries long (von Neumann neighbourhood) or 6561 entries long (Moore neighbourhood). The initial output values in the rule tables were generated randomly. The user specifies the sensitivity parameter, the amount to increment/decrement each cell's pixel intensity value, number of CA iterations, number of generations, CA boundary conditions and neighbourhood type. A typical run consisted of a population size of 30, a recombination probability (single point, randomly selected) of 1, and a mutation probability of .001.

Each CA was given an 8-bit (256 different states) source grey scale image as an initial input and the outputs from the CA were compared to an edge detection reference generated by the popular Canny algorithm (Canny, 1986). Fitness was assessed by calculating how much the output from the CA differed from the output from the Canny operator, i.e. the most fit were those who minimised the error difference between the CA output and the Canny reference. Population fitness was ranked and the next generation was generated by keeping the fittest member unchanged (elitist strategy) and generating the next population by recombining the fittest and second fittest members' genomes at a random location. The population, excepting the fittest member, was subject to mutation at the rate specified by the user.

RESULTS AND DISCUSSION

The results in Figure 3 show one run of the GA after 350 generations. The input image was the 8bit greyscale image shown in Figure 2a. Figure 3a shows the output from the Canny operator used to test fitness and 3b shows the output from the fittest CA (Single iteration, Moore neighbourhood, sensitivity: 15, intensity increment/decrement: 255, cloned-edge boundary conditions, recombination probability: 1, mutation probability: .001).

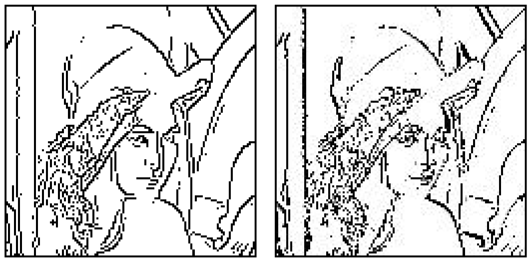

Figure 3: The output from the Canny operator to test fitness (3a) and a sample output from one run of the GA (3b).

Our results show that it is possible to evolve a cellular automaton to perform edge detection operations on images with a large (effectively unlimited) intensity range. Furthermore the automaton is fast (operates in a single computational 'step'), and space efficient – overcoming the traditional problem of rule table size in multi-state automata. The system would be possible to parallelise as each cell is computationally very simple. The system can also process colour images by processing each colour channel separately and combining the results for the output. The use of a sensitivity parameter enables the automaton to be tailored by the user for different applications.

Further work in progress includes examining the use of non-uniform transition rules and to further explore the effects of adjusting the CA parameters, such as number of CA iterations, different boundary conditions and variations in the rule table output levels to increase/decrease intensity values of the cells.

REFERENCES

Canny, J. F. (1986) A computational approach to edge-detection, *IEEE Transactions on Pattern Analysis and Machine Intelligence*, **vol 8 (6)**, pp 679-714.

Gardner, M. (1970) The fantastic combinations of John Conway's new Solitaire game 'Life', *Scientific American*, **223**, 120-123.

Poli, R., 1996, Genetic Programming for Image Analysis, in Koza, J.R., Goldberg, D.E., Fogel, D.B. and Riolo, R.L. (Eds.), *Genetic Programming 96, Proc. of the 1 st Annual Conference*, Stanford Univ., MIT Press, pp. 363-368.

Preston, K. Duff, M. (1984) Modern cellular automata, advanced applications in pattern recognition, New York, Plenum, pp317-328.

Toffoli, T. (1999) Programmable matter methods, *Future Generation Computer Systems Special issue on Cellular Automata (Eds Talia, D. and Sloot P.)*, **16:2-3**, 187-201.

von Neumann, J. (1966) *Theory of self-reproducing automata (Edited and completed by Burks, A.),* University of Illinois Press.

Wongthanavasu, S. and Sadananda, R. (2003) A CA-based edge operator and its performance evaluation, J. Vis. Commun. Image R., **14**, 83-96.

Ziou, D. and Tabbone, S. (1997) Edge detection techniques- an overview. Technical Report AI Memo 833, Massachusetts Institute of Technology, Artificial Intelligence Laboratory, 1997. 135.

MELANOMA-PATTERN EXTRACTION USING HISTOGRAM-THRESHOLDING APPROACH

Imène Khanfir
Amin Kallel
Mohamed Salim Bouhlel
Khaled Taouil
Ecole Nationale d'Ingénieurs de Sfax
B.P.W, 3038 Sfax, Tunisie
Tél: (216)74.27.40.88 Fax: (216)74.27.55.95
E-mail : imene.kk@37.com ; amin.kallel@37.com

KEYWORDS
Image, Segmentation, Thresholding, Histogram, melanoma.

ABSTRACT

The melanoma is a form of skin cancer that can causes a great number of deaths. The physician community has long relied on visual observation of the skin's surface to determine if the lesion is malign or benign. A convenient and painless process to detect melanoma of the skin can allow a quick diagnosis, and give doctors a close-up view about the nature of the lesion. The first step to get such tool is to extract the lesion from the healthy skin. Five automatic methods for segmentation of pigmented lesion images are presented in this paper. The methods allow converting a gray-level image into a binary one by using the histogram based thresholding approach. Thus we will be able to determine efficiently three of the four clinical features known as the ABCDs of melanoma.

INTRODUCTION

The interest accorded to the image processing is growing while the image became an essential support and a privileged source of information. The interpretation-quality of an image strongly depends on his analysis. The first problem we face is that of segmentation. That is, in order to extract valuable information from the image at hand, we first need to divide the image into distinctive components, which can then be further analysed. This is needed, in order to separate the "interesting" components from the subordinate ones, since computers have much difficulty in performing classification compared to human brain.
A general, and an automatic, segmentation method is difficult to conceive because of the several varieties of area-shapes that can be presented in one image. Hence we will proove that the segmentation by the histogram-based thresholding approach is one of the most adapted for the pigmented-skin-lesion images in dermatology.
In section 2, a medical-description of the melanomas and theirs characteristics is given. This is followed by a brief review about the image segmentation. We present in detail the segmentation by the histogram-based thresholding approach in section 4. The algorithm procedures that we propose will be summarized in section 5. The application to pigmented skin lesions is illustrated and discussed in section 6.

MEDICAL DESCRIPTION

Skin cancers are the most common form of human cancers. The malignant melanoma is considered as the most deadly of them. Its originer cames from the fact that the skin cells, melanocytes, produce more than necessary the dark, protective pigment called melanin. However, melanoma is almost always curable when detected in its early stages.
Warning signs of melanoma include: changes in the surface of a mole, scaliness, oozing, bleeding or the appearance of a new bump; spread of pigment from the border into surrounding skin.
These clinical features are known as the ABCDs of melanoma [1]:
- **A**symmetry: One half doesn't match the other half (figure 1.a).
- **B**order irregularity: The edges ragged notched or blurred (figure 1.b).
- **C**olor: The pigmentation is not uniform. Shades of tan, brown and black are present. Dashes of red, white and blue add to the mottled appearance (figure 1.c).
- **D**iameter: The width is greater than six millimetres (about the size of a pencil eraser). Any growth of a mole should be of cancern (figure 1.d).

(a) Asymetry (b) Border irregularity

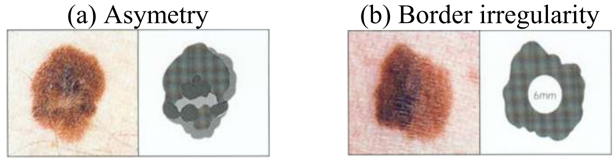

(c) Color (d) Diameter

Figures 1: ABCDs criteria

Consequently image analysis techniques for measuring these features have been developed. Melanoma diagnosis requires that the lesions will be detected and localized in image. It is essential that lesion boundaries are determined precisely so that measurements can be accurately computed. For this, various image segmentation methods have been developed. Many of them use gray level image to extract the lesion from the healthy skin.

IMAGE SEGMENTATION

Image segmentation is perhaps the most studied area in computer vision, with numerous methods. It consists in extracting the region of interest in an image. In our case the principal region of interest is the lesion and our objective consists to delimit it and to determine as precisely as possible its contour. A segmentation method is usually designed taking into consideration the properties of a particular class of images, thus it can be performed in many different ways [3-20]:

- One common approach is to perform Edge-Detection, in order to find all edges in the image, thus implying the borders of shapes in the given image [3-8].
- A second approach is to try and detect whole shapes, given the fact that these shapes usually tend to have distinctive properties as opposed to the background they are aligned against: it is the region-growing approach [9-11].
- A third approach consists in converting the gray-level image into a binary one according to a critical value called threshold. This threshold is chosen after an histogram processing which can be total or adaptive: The thresholding is total if the same critical value is used over the whole image. Otherwise, it is adaptive if each area of the image has its own threshold [12-20].

To get optimal results, these three approaches are sometimes combined.

For the following of this paper, we shall concentrate on the third approche.

HISTOGRAM THRESHOLDING

The gray-level histogram of an image is a function which gives the appearance-frequency of each gray-level in the image. Thresholding aims to segment an image in many classes by only using the histogram. Thus, we suppose that each class can be characterized by only its own gray level distribution. So, to each peak of the histogram is associated a class. There are many histogram thresholding methods [12-20]. These methods were very often developed to treat the particular case of the segmentation in two classes. In this case, the image thresholding converts a gray-level image into a binary one. The two binary levels may represent objects and background or, more generally, two classes in an image (in our case it consists in extracting the lesion from the healthy skin). Pixels whose value exceeds a critical value are assigned to one category, and the rest to the other (figure 2). The threshold is global if the same critical value is used across the whole image. Many algorithms have been proposed for automatically selecting the threshold appropriate for a given image [12-20]. Some algorithms simply use the histogram of values in the image, whereas others use contextual information such as gray level occurrences in adjacent pixels. Global histogram based algorithms are most commonly used, despite the benefits that can accrue from using contextual information and allowing the threshold to vary over an image. They are simple to understand and implement, and computationally fast once the histogram has been obtained.

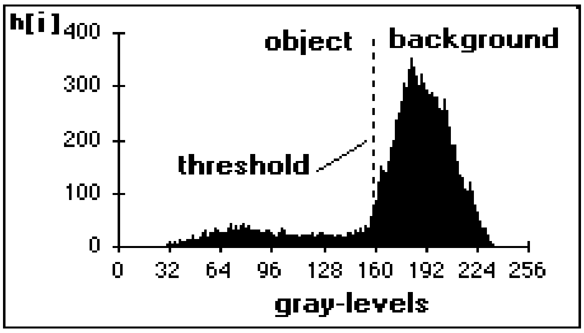

Figures 2: A bimodal- image Histogram.

The histogram will be denoted h(1), h(2), h(3)... h(n-1), h(n), where h(i) is the number of pixels in the image having the gray level i, and n is the maximum gray-level reached (typically n=255). The threshold value is an integer, denoted t [13]. The original image is defined by the function I(x, y) where x and y are the coordinates of a pixel. The binary image Ib is defined by the function:

$$Ib(x,y)=\begin{cases}0 & \mathit{If}\quad I(x,y)\le t\\ 255 & \mathit{If}\quad I(x,y)>t\end{cases}\qquad (1)$$

ALGORITHMS

Subsequent algorithms can be computed efficiently if the following partial sums are obtained.

For J = 0...,n :

$$\begin{cases} A_j=\sum_{i=0}^{j} h(i) & B_j=\sum_{i=0}^{j} i\,h(i)\\ C_j=\sum_{i=0}^{j} i^2\,h(i) & D_j=\sum_{i=0}^{j} i^3\,h(i)\end{cases}\qquad (2)$$

Moments

This algorithm due to Tsai [15], chooses t such that the binary image has the same first three moments as the original one. Thus, the value of t is such that A_t/A_n is the value of the fraction closest to the value of x_0 where:

$$\begin{cases} x_0=\frac{1}{2}-\frac{B_n/A_n+x_2/2}{\sqrt{(x_2^2-4x_1)}}\\ x_1=\frac{B_nD_n-C_n^2}{A_nC_n-B_n^2}\quad x_2=\frac{B_nC_n-A_nD_n}{A_nC_n-B_n^2}\end{cases}\qquad (3)$$

Entropy

The entropy E of a discreet source of observations, which values are in {0...j} is defined by:

$$E_j=\sum_{i=0}^{j} h(i)\log(h(i))\quad \text{for } j=0,\ldots\ldots,n\qquad (4)$$

One of several maximum entropy algorithms, due to Kapur and Al [16], consists in evaluating, for any j= 0...n, the following expression:

$$E_j/A_j-\log(A_j)+(E_n-E_j)/(A_n-A_j)-\log(A_n-A_j)\qquad (5)$$

The value of the threshold t is the j's one which minimized this expression.

Iterative Intermeans

Ridler and Calvard [17], and Trussel [18] proposed an iterative method: From an initial guess for t, the mean gray-levels in the two classes defined by the threshold, that is, below and above it, are computed as:

$$\begin{cases} \mu_t = B_t / A_t \\ \nu_t = (B_n - B_t)/(B_n - A_t) \end{cases} \tag{6}$$

The threshold **t** is recalculated to be half-way between these means that is the integer part of (μt + νt)/2. Then μ and ν are recomputed, and a new value of t is obtained. This is repeated until convergence, which is a repeat of the same value of t on two consecutive iterations.

Intermeans

A closely related algorithm to the precedent one, INTERMEANS, due to Otsu [19], requires the between-class sum of squares

$X_j=A_j\ (A_n - A_j)\ (\mu_j - \nu_j)^2$ (7)

The above equation will be evaluated for j=0...n-1. The threshold t is set to the value of j at which Xj is maximized. Although it is not immediately apparent from the algebraic formulation, this has the effect of positioning the threshold midway between the means of the two classes.

Triangle

This technique due to Zack [20] is illustrated in Figure 3. A line is constructed between the maximum of the histogram at brightness i_{max} and the lowest value i_{min} = (p=0)% in the image. The distance d between the line and the histogram h[i] is computed for all values of b from i = i_{min} to i = i_{max}. The brightness value i_o where the distance between h[i_o] and the line is maximal is the threshold value, that is, t = i_o. This technique is particularly effective when the object pixels produce a weak peak in the histogram.

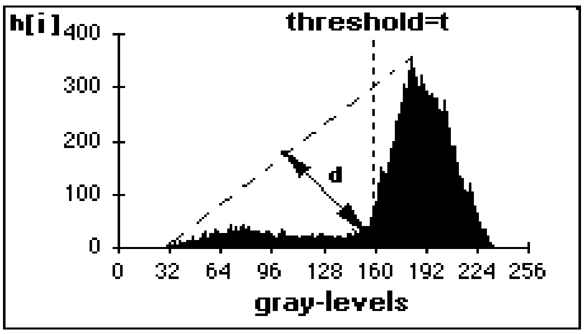

Figure 3: Triangle algorithm.

D: y=a*x+c → D: a*x-y+c=0

D passes by the two points whish coordinates are (i_{min}, MIN) and (i_{max}, MAX) thus:

$$\begin{cases} a = (MAX - MIN)/(i_{max} - i_{min}) \\ c = (MIN.i_{max} - MAX.i_{min})/(i_{max} - i_{min}) \end{cases} \tag{8}$$

So the distance d between the point (i , h(i)) and the line D is:

$$d = \frac{|a.i - h(i) + c|}{\sqrt{a^2 + c^2}} \tag{9}$$

The threshold t takes the value of i which maximized d.

RESULTS AND DISCUSSION

To validate the methods previously presented we applied them on 62 images lesions. The visual evaluation of these methods is presented in figure 4 for four different images. For each method we superpose the contour of the segmented image (white edge) on the original image. The Table 1 gathers the threshold values t for the five methods tested on the four images of lesions.

According to these results, we can classify the five methods previously presented in two categories. To carry out a such classification, we chose the two following criteria: the produced threshold value, and the obtained quality of the segmentation (psycho-visual criterion).

A first class gathers the two following methods: Intermeans [19], and Intermeans Iterative [17,18]. Indeed they give a very close threshold values which are lower than those produced by the three other methods. The obtained thresholds allow a good extraction of the lesion from its background.

For the second category in which we classify the three methods Triangle [20], Entropy [16], and Moments [15], we note similar results, and threshold values higher than those of the preceding class. For this category, the shape extraction of the melanoma in the produced binary images is less precise.

Thus, it is abvious that the methods of the first class are better for the lesion-image-segmentation.

CONCLUSION

In this paper we were interested in the histogram-based-thresholding techniques. Five methods were presented and applied on sixty-two images of melanoma. Although these methods are relatively simple and that we have not recourse to complex techniques, we obtained very satisfying results especially those which we gathered in the first class. We estimate that we have contributed to the first links of a medical help for diagnostic-data-processing tool dedicated to the classification of the melanoma. It is thought that the use of the color melanoma can give another dimension to this work. Thus we will be able to define a color space which will be better adapted to the segmentation.

REFERENCES

[1] NIH Consensus Conference, Diagnosis and treatment of early melanoma, JAMA 268 (10) (1992) 1314-1319.

[2] K. Taouil., "Faisabilité en détection des mélanomes", Thèse INSA de ROUEN, 1995.

[3] M. S. Bouhlel, H. Trichili, N. Derbel., "Synthesis and comparison of different segmentation methods using edge detector's approach". The Third Middle East Symposium on

Simulation and Modeling, Amman Jordan, September, 3-5, 2001.
[4] M. S. Bouhlel, H. Trichili, N. Derbel and L. Kamoun., “fusion des approaches contours et région en vue d’une segmentation meilleure des images scintigraphiques”. TAIMA01 Tunis, 8-12, Octobre 2001.
[5] M. S. Bouhlel, H. Trichili, N. Derbel., “Robustness of methods using edge detection approach towards different noise types”. 20th International Conference on Computational Aspects and Their Application in Electrical Engineering, CATAEE’02, Amman, Jordan, Mach 2002.
[6] M. S. Bouhlel, H. Trichili, N. Derbel, L. Kamoun., “Evaluation de la méthode de Canny pour la segmentation des images en couleur en termes de robustesse aux bruits, durées de traitement et qualités de contours”. Deuxième Conférence Internationale des Journées Tunisiennes d'Electrotechniques et d'Automatique., JTEA'02, 21-23 Mars 2002, Sousse Nord, Tunisie.
[7] J. Canny., “A Computational Approch to edge detection”, IEEETrans. Pattern Anal. Mach. Intell. PAMI-8.N0.6, 1986, pp.679-698.
[8] R. Dériche., “Using Canny's criteria to derive a recursively implemented optimal edge detector”, Inter.jour.of Vision, p.167, Boston 1987.
[9] D. Micollet., “Edge détection from inhomoge-neous background QCAV95”, conférence internationale sur le contrôle qualité par vision artificielle, IUT LE CREUSOT (1995), pp.183-188.
[10] M. Fontaine., “Segmentation non supervisée d'images par analyse de la connexité”. ISIVC 2000.
[11] H. Trichili, M. S. Bouhlel, N. Derbel, L. Kamoun., “Fusion des approche contour et région en vue d’une segmentation meilleur des images scintigraphiques”, Conférence : Traitement et Analyse d'Images (TAIMA'2001), Hammamet, Tunisia, 8-12 Octobre 2001.
[12] N. Milstein., “Image segmentation by adaptive thresholding”, FCS, 1998.
[13] C. A. Glasbey., “An analysis of histogram-based thresholding algorithms”, CVGIP: Graphical Models And Image Processing, Vol. 55, No. 6, pp. 532-537, 1993.
[14] J. M. S. Prewitt and M. L. Mendelsohn., “The analysis of cell images”, in Ann. New York Acad. Sci., Vol. 128, pp. 1035-1053, New York Acad. Sci., New York, 1966.
[15] W. Tsai., “Moment-preserving thresholding: A new approach”, Comput. Vision Graphics Image Process. 29, 1985, 377-393.
[16] J. N. Kapur, P. K. Sahoo, and A. K. C. Wong., “A new method for gray-level picture thresholding using the entropy of the histogram”, comput. Vision Graphics Image Process. 29, 1985, 273-285.
[17] T. Ridler and S. Calvard., “Picture thresholding using an iterative selection method”, IEEE Trans. Systems Man Cybernet. SMC-8, 1978, 630-632.
[18] H. J. Trussel., “Comments on Picture thresholding using an iterative selection method”, IEEE Trans. Systems Man Cybernet. SMC-9, 1979, 311.
[19] N. Otsu., “A treshold selection method from gray-level histogram”, IEEE Trans. Systems Man Cybernet. SMC-8, 1978, 62-66.
[20] Zack, G.W., W.E. Rogers, and S.A. Latt., “Automatic Measurement of Sister Chromatid Exchange Frequency”. 1977. 25(7): p. 741-753.

Table 1: Threshold values t for the five methods tested on the four images of lesions.

	Image 1	Image 2	Image 3	Image 4
$t_{moments}$	175	167	147	198
$t_{entropy}$	192	182	148	217
$t_{iterative\ intermeans}$	154	151	117	196
$t_{intermeans}$	152	149	115	194
$t_{triangle}$	187	185	141	221

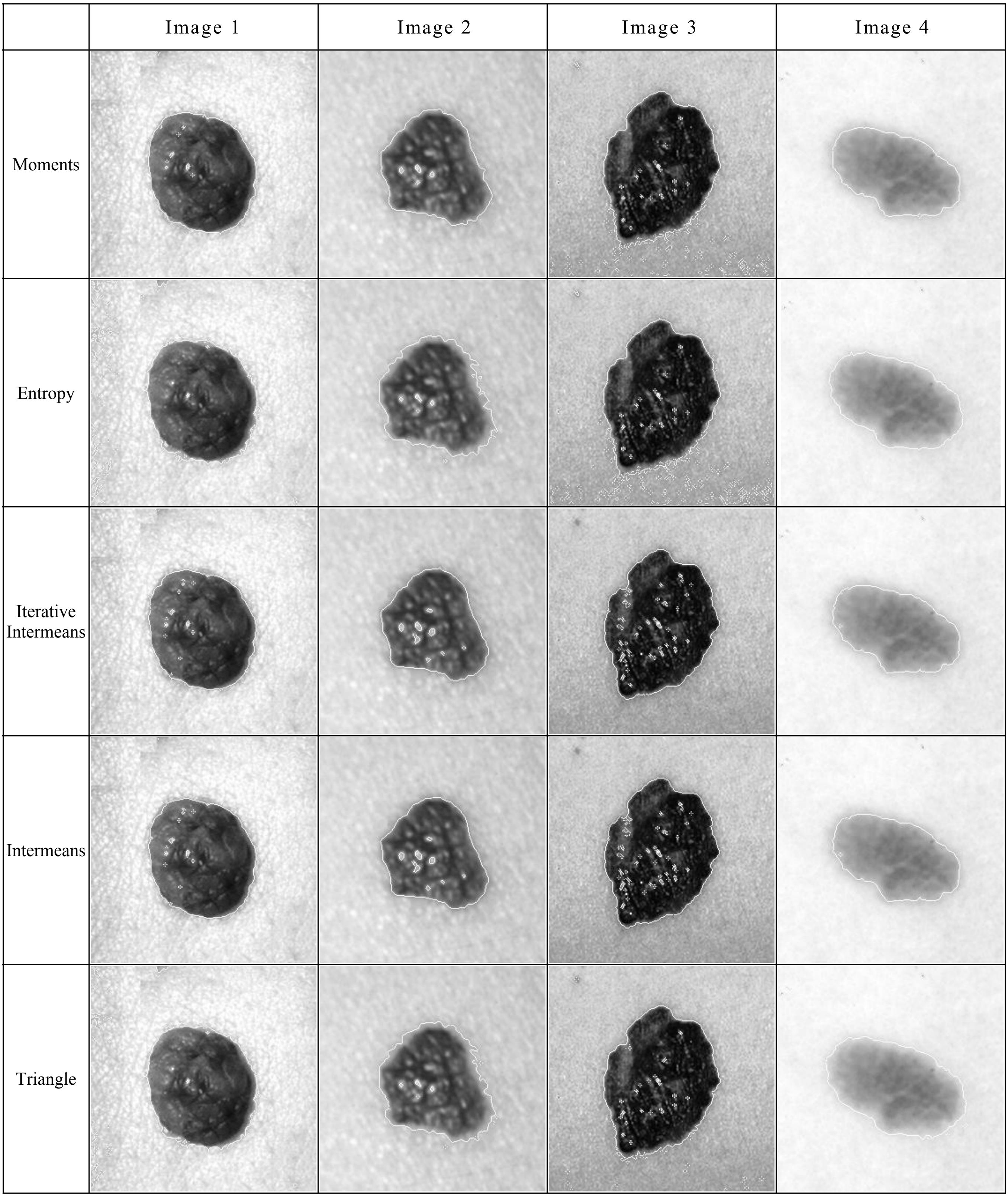

Figures 4: Results of segmentation

SIMULATION OF DIGITAL WATERMARKING

A Blind Digital Watermarking scheme based on the Lower and Upper bit sequences

Abdulrrazaq Ali Aburas
Ittihad University,
Department of Computer Sciences
P.O. Box: 2286, Ras Al Khaimah, United Arab Emirates
Tel: +971 7 236 2323 Fax: +971 7 236 2121
Phone Home: 00971 7 2331096

Email: abdulrrazaq01@hotmail.com

Key Word: hidden data, Lower bit, Upper bit, sequences, digital watermarking.

Abstract

Digital watermarking is the unique solution that can be used for protecting all the digital multimedia data from any illegal use. In this work, we present a new method as blind watermarking to embed data into digital images, digital audio and scanned text. The method is based on the lower and the upper bit sequences. Each pixel in the digital media keeping the quality as it is. The new technique is very simple for embedding and extractions of the hidden data.

1. Introduction

Over the last view years, many different watermarking algorithms schemes have been developed for a large variety of digital data types [1] [2]. New digital media has improved, with existing new hardware and software dealing with the multimedia application have increased the demand not just for producing new digital media (such as images, audio, movies, et..) but also increased the demand for protections of all these new products from unknown customers or illegal users[3][4]. Digital watermarking comes to the front as new application to give the protection needed in the world of digital multimedia. Digital watermarking is the process of embedding particular information (watermark message) into or onto the digital media and retrieving it from other digital data. The theory of the digital watermarking have been investigated [5][6][7]. The reliability of the digital watermarking information is dependent on the texture of the original digital image or audio [8]. In this paper, we present a new method of embedding the watermarking into the digital image based on the lower and upper bit sequences of each pixel. The proposed method is presented in section 2. in section 3, we explain the basic idea behind the structure of the lower and upper bit sequences and the reference database table for the embedding method. In section 4, we introduce the embedding and extraction (detection) system and how it works. In section 5, we give some examples experimental results as test for the new blind watermarking technique and show how to deal with it. In section 6, we show some results of using the new method of the blind embedding and extraction of the watermarks under some common attacks. In the last section, we concluded our presentation work.

2. Proposed Method

Digital watermarking uses one of the following two methods to embed a payload. One way involves special algorithms that can change the intensity or luminance of individual pixels of a digital picture to encode a predetermined number of bits of embedded, but imperceptible data. The other method involves changing the image in the frequency domain, by slightly altering the discrete cosine transform (DCT) coefficients (at the heart of the compression algorithms used in MPEG and JPEG). Our work based on the special domain, the pixel of which is the 8-bits length. Some work has been done using the least significant bits [11], and others used some other method such as flappable and shuffling [9] [10]. In this research work, we looked closely to the sequences of all the bits that represented each pixel in the digital image or the digital media. By dividing (portions) the bits sequence into two parts, the lower bit sequence (part 0) which starts from bit number 0 to bit number 3 and the upper bit sequences (part 1) which starts from bit number 4 to bit number 7 right to left direction which is from the lower to the higher bit order.

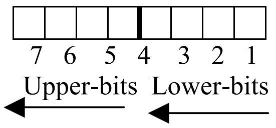

Figure 1: The bit sequences of the pixel.

Figure 1; illustrate the lower and the upper bits sequences. By splitting the data pixels into two parts, the lower and the upper parts, in fact we divide the digital image into two levels. The low level is the data pixel of the digital image or media valued from 0 to 8 in real data. The upper level is the digital image or media valued from 16 to 255 in real data. By introducing these two level, we construct a database (see Figure 2) based on these levels or sequences to build up the embedded for the digital watermark.

3. Data base structure

To evaluate each data pixel of the digital media, we have constructed a database table as shown in Figure 2.

Range	Upper-bits data	Lower-bits Data	Value	Level –No.
15	15	0	0	0
15	31	16	1	1
15	47	32	2	2
15	63	48	3	3
15	79	64	4	4
15	95	80	5	5
15	111	96	6	6
15	127	112	7	7
15	143	128	8	8
15	159	144	9	9
15	175	160	10	10
15	191	176	11	11
15	207	192	12	12
15	223	208	13	13
15	239	224	14	14
15	255	240	15	15

Figure 2: The Database (Table) structures

The database (table) divided into five parts directed from left to right. Part one is the level-no. That indicates the lower value and the upper value in each level. Part two is the replacing value for each data pixel to calculate the watermarking message. Part three is the lower bit sequences. Part four is the upper bit sequences and part five is the range between each level.

4. Embedding and Extraction Systems

This is a new method is known blind digital watermarking method. This method is different from others [2] [9] [10] [11] such that it does not require the original digital image or media to extract or detect the hidden data (watermark message).

4.1 The Embedding Algorithm

Based on the database from Figure 2, the embedding algorithm is described as following:

1) For each data pixel from the original image, extract and replace with equivalent number from the table that exists between its lower or upper data value.
2) Add the all the equivalent numbers and then take the average.
3) Extract the watermark number (value) from the table that exists between the lower and upper data value of any level.
4) Add the watermark to the original data pixel of the image.

Figure 3, shows the embedding system. The embedding system uses a straightforward process and uses a segmented 8x8 data pixel of a digital image (original image) as sample to explain the procedure of the new embedding system. Each data pixel in the digital image, there is a cross-pounding value number that can be computed from the database-table (see Figure 2). After completing the replacements of all the data pixels, the embedded computes the digital watermark by summing up all these value numbers then taking the average value and extracting again the cross-pounding value from the table to get the watermark number (value) that is to be added to the original segmented digital image(marked image).

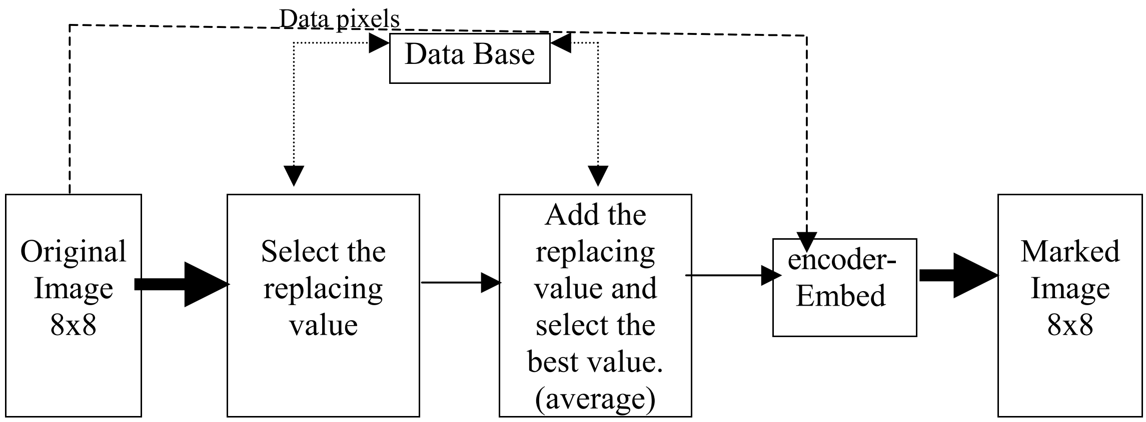

Figure 3: The Embedding System.

4.2 The Extraction-Detection Algorithm

After embedding the digital watermark, which is a very small data value, it is range from 0 to 15, such that it does not affect the quality of the marked image or media.

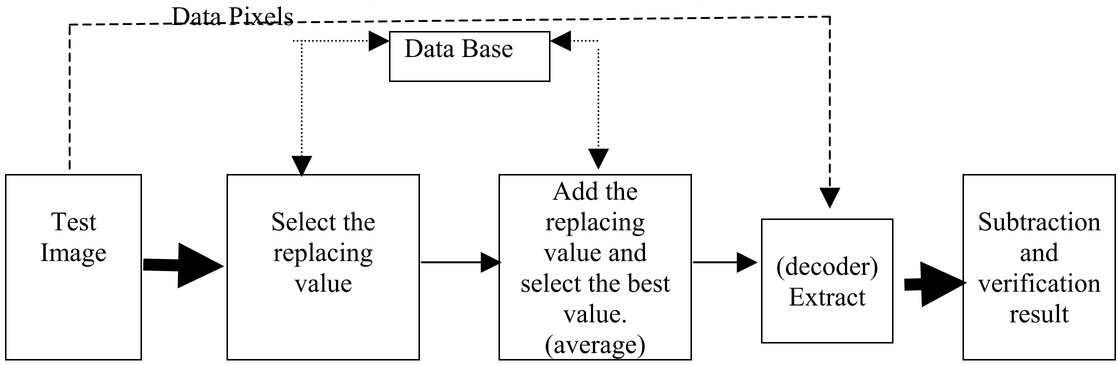

Figure 4: The Extraction (Detection) System.

Figure 4; illustrated the extraction algorithm for the hidden watermark which is very simple and the description of the algorithm is as following:

1- For each data pixel of the marked image, replace it with its cross-pounding valued number from the database or the table.
2- Sum up all the valued numbers and then take the average.
3- Extract the equivalent valued number from the database or the table and i.e., the marked message (hiding data) if exist.
4- Subtract the watermark from the marked image to obtain the original digital image (data value).

In Figure 4, the extraction system also employs a straightforward process for the extraction of the watermark from the marked image or media. Except that after computing and getting the valued number from the database or the table, the system subtracts the valued number from the marked image to get back the original digital data.

5. Applying the New Method

As result of blind digital watermarking technique, the embedded can embed the watermark message to a particular location or the entire image itself. After applying the new method over different types of digital images, we have got a good quality marked images. Figure 5; Shows some results after applying the new method using only one random 8x8 segmented block to be as watermark (hidden) in the target image.

(a) Original Image

(b) marked Image

(c) Original Image

(d) Marked Image

6. Experiments

The blind watermarking based bit sequences system was tested on 2000 images using reference mark image of size 8x8 pixels taking from the original image. The message embedded was in range [0 – 15] that is obtained from the table illustrated in Figure 2. The message obtained was small compared to other existing techniques. Since the message is bounded the system had a measured of over 99%.

7. The new method with common attackers

The new method has given good results of recognizing the watermarks after applying some attackers such as JPEG compression where the compression ratio was 20:1 and another attacker such as adding noise (Gaussian). This is because of the range capacity available from the data base or the table (see Figure 2). For each level has a range from 0 to 15 of valued number; and that will help either for the embedded or for the extractor to recover from most (any) attacker. The capacity level is one of the best advantage exist in this blind digital watermarking method.

8. Conclusion

In this paper, we presented a new blind digital watermarking scheme using the lower and the upper bit sequences to embed and extract the watermark message. The new method has given good quality of marked images or media after embedding the watermark message. The new method can allow embedding the watermark into a segmented part (i.e. only 8x8 block size) or into all images and it can extract the marked message anywhere in the image target. The new method has survived from most common attackers such as standard JPEF compression [20:1] and additive noise.

9. References:

[**1**] M.D. Swanson, B. Zhu, A.H. Tewfik: ”Robust Data Hiding for Images”, IEEE DSP Workshop, 1996.

[**2**] C. Podilchuk, W. Zeng: “Image Adaptive Using Visual Models”, IEEE JSAC, vol.16, no.4, 1998.

[**3**] K. Matsui, K. Tanaka:”Video-steganography: How to secretly Embed a Signature in a Picture”, Proc of IMA intellectual Property Project, Vol.1, no. 1, 1994.

[**4**] N. F. Maxemchuk, S. Low: “Marking Text Documents”, ICIP,1997.
[**5**] B. Chen and G. W. Wornell: “Provably robust digital watermarking”, Proc. SPIE:Multimedia Sysyetms and Appilcations II, vol. 3845, pp 43-54, Sep. 1999.
[**6**] P. Moulin and J. A. O’Sullivan: “Information-theoretic analysis of information hiding”, Sep. 1999.
[**7**] J.K. Su and B. Girod: “Power-spectrum condition for energy efficient watermarking”, Proc. IEEE on Image Processing, ICIP ’99, Japan, Oct. 1999.
[**8**] J.J. Eggers, J. K. Su and B. Girod: “A blind watermarking based on structured codebooks”, Proc. IEEE on Secure Images and Image Authentication, UK, pp4/1-4/6, April 2000.
[**9**] Min Wu, Edward Tang,: ”Data Hiding in Digital Binary Image”, IEEE Workshop, 1998.
[**10**] M. Wu, Liu.: “Digital Watermarking Using Shuffling”, ICIP,1999.
[**11**] Ingemar J. Cox, Matthew L. Miller, Jeffrey A. Bloom: “Digital Watermarking”, 2001, Ch. 4., bp85.

Optimizing the Embedding Scheme of Image Watermarking in the Frequential Field for both robustness and imperceptibility

Hanène TRICHILI[(1)], Mohamed Salim BOUHLEL[(1)], Bassel SOLAIMAN[(2)] and Lotfi KAMOUN[(1)]

[(1)]LETI – Laboratory of Electronic and Information Technologies
National Engineering School of Sfax (ENIS)
PB W, 3038 Sfax, TUNISIA

[(2)]ITI – Department of Image and Information Processing
High National School of Telecommunications of Bretagne (ENST-Br)
Brest, FRANCE

hanene_trichili@yahoo.fr medsalim.bouhlel@enis.rnu.tn
basel.solaiman@enst-bretagne.fr lotfi.kamoun@enis.rnu.tn

Summary:
Existing watermarking schemes try, in general, to maximize the robustness or to reduce the signature visibility. In this paper, we present two new approaches in the embedding scheme that release both of these constraints. In one hand, we assure a great robustness, on the other hand, we guarantied the imperceptibility of the embedded mark. Both of these approaches represent the new steps added to the classic embedding scheme of image watermarking in the frequential field. This will characterize the object of the present paper where we present these ameliorations with the obtained results.
keywords: watermarking, Image, DCT, Robustness.

1. Introduction

With the recent growth of networked multimedia systems, techniques are needed to prevent the illegal copying, forgery and distribution of digital images. It is also desireable to determine where and by how much the multimedia file has been changed from the original. One way to improve one's claim of ownership over an image, is to place a low-level signal directly into the image data. This signal, known as a digital watermark, uniquely identifies the owner and can be easily extracted from the image. Our goal has been to develop a robust digital watermark scheme for images.
In this paper, we present a new approach of image watermarking in the frequential field. It is based on two steps that allocate to obtain both a great robustness and a great imperceptibility of the embedded mark. We have to precise in this step, that the embedded mark will be different from the classic mode of embedding signatures in the known watermarking schemesIn fact, in our proposed method, we'll not embed the mark itself. We'll embed the ratio between the original image and the mark.

2. Method Principle

the proposed method of image watermarking is based on the classic scheme of embedding a mark in the frequential field using the additif scheme. The extracting scheme is non blind one. The proposed method will modify the embedding scheme.
At a first step, we'll try to carry out a sorting between the elements of the original image and that of the embedded mark in order to optimize their correspondance. On the other hand, we'll try to embed their ratio instead of embedding the mark in the image. At this stage, we have to optimise by choosing which ratio to embed (the ration between the mark and the image or the inverse). We have so to choose between embedding the ration image/mark or mark/image.
This last modification on the embedding scheme will maximize the robustness of the watermarking action. In fact, when retrieving the embedded "mark", the hacker can't discover the real mark because the found "mark" is the ration and not the real one.
The first modification that concern sorting the elements of the image and that of the mark between the embedding scheme is a pre-step in the embedding scheme. Its objective is to minimize the mark perceptibility. In fact, when proceeding with this method we'll be sure that the elements of the mark won't influence that of the original image. They will be corresponded and have the same magnitude order.

2.1 Perceptibility Minimization: Arrangement procedure and blocks rebuilding:

In this paragraph, we propose to arrange the mark pixels and that of the original image in order to minimize its imperceptibility when inserted on the image. In fact, given the image to watermark and the mark to embed, we decompose the original image and the embedded mark into 8x8 blocks and we apply on them the DCT operation. At this step, we obtain two matrixes of N*N values, that designate respectively an image block and a mark block. These matrixes will be transformed on vectors of n*n columns. A sorting operation of every block elements will be effected in order to classify them in a increasing order for the image elements and a decreasing order for the mark ones. An indices table will be established in order to assist the block rebuilding operation in the extracting scheme.

2.2 Robustness Maximization: Optimizing the ratio between the image and the embedded mark:
In this step, we propose to optimise the embedded ratio by effecting a comparison between the PSNR when inserting the ration image/mark and that when inserting the ratio mark/image.

2.2.1 1st method : Ratio: Signature / Image
The signature (Wi) will be on this method a vector of elements that represent the ratio of the Image/signature. This vector will be sorted and arranged.

2.2.2 2nd method : Ratio: Image /Signature
The signature (Wi) will be in this method a vector containing the ratio signature/image.

3. Watermarking Steps:
3.1 Embedding Step
In this step, we'll try to correspond to each element of the vector representing the sorted original image, its homologue in the vector representing the mark to embed by applyin,g the following formula:

$$y_i = x_i(1+\alpha w_i)$$

with :
y_i DCT coefficient of the watermarked image.
x_i DCT quantified coefficient TCD of the original image
α : Visibility coefficient.
w_i : The mark to embed.

When finishing from the association between the image pixels and those of the mark, come the embedding step. In this step, the embedding scheme will be modified because we'll insert the the ration instead of inserting the mark.
The resulting vector will have the same size of that of the original image.

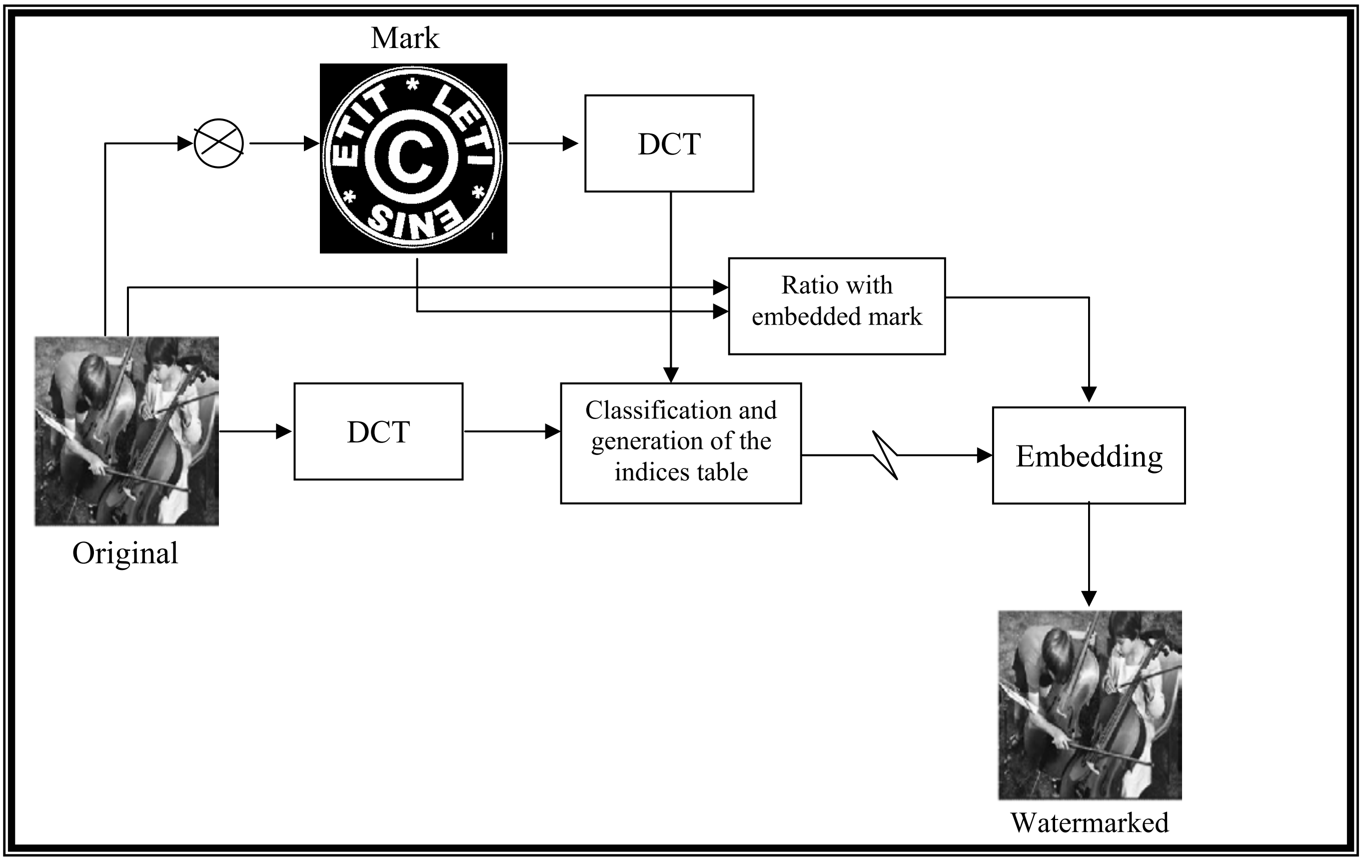

Figure 1: Proposed Embedding Scheme

3.2 Extracting Step :
This step is very important in the image watermarking process. It allows extracting the introduced signature and demonstrate the effectiveness of the used method. This can be done by the quality of the obtained image after mark extraction and by comparing the extracted signature with the original one.
Detection Scheme: The developed scheme in the detection process is based on a sequence of the inverse of the operations adopted in the embedded process. In fact, having the original image and the watermarking one, we apply the DCT on each one of them. The next step try to substrate the transformed coefficients of the watermarked image from the original one. The extracted mark will be the ratio between the mark and the original image.

4. Results & Evaluation

The attacks
The essential objective of our method is to obtain a procedure both robust and with imperceptible mark.

For this, we have developed a test procedure based on a success of different attacks: JPEG compression, Gaussian noise, Speckle noise, Cropping, Rotation, histogram equalisation, …). For each attack, we evaluate the quality of the watermarking process by measuring the PSNR between the original image and the watermarked attacked one.

Original Image and signature:

Original Signature

Original Images

➢ ***1***

1st Stage: optimising the ratio between the Image and the Signature:

inserting image / signature	**inserting signature / image**
	
PSNR = 12.661	PSNR = 78.801
	
PSNR = 12.567	PSNR = 80.854
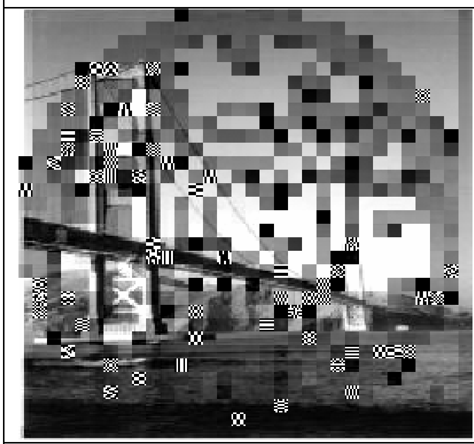	
PSNR = 12.306	PSNR = 78.892

	
PSNR = 14.461	PSNR = 78.736

Interpretations:
When trying to insert the ratio signature/image and image/signature we have conclude that the last method decrease the PSNR and the image quality.

So that, it will be necessary to choose the first ratio :signature/image. The PSNR with this embedding type will increase and exceed in all cases 78db.

➢ *2nd Stage:* **Robustness Test of the approach: Signature/ Image**

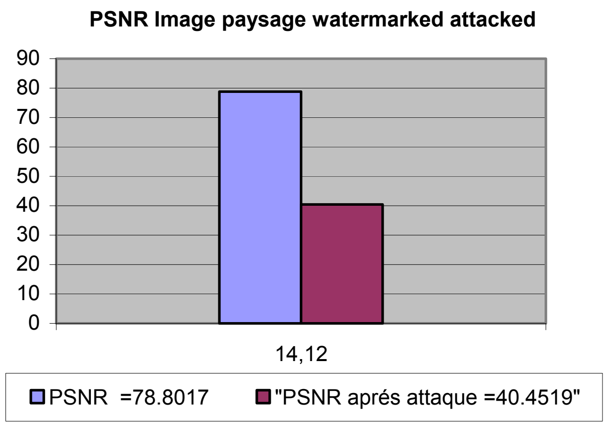

Image watermarked attacked by additive noise	**Evaluation de la robustesse pour le bruit additif**

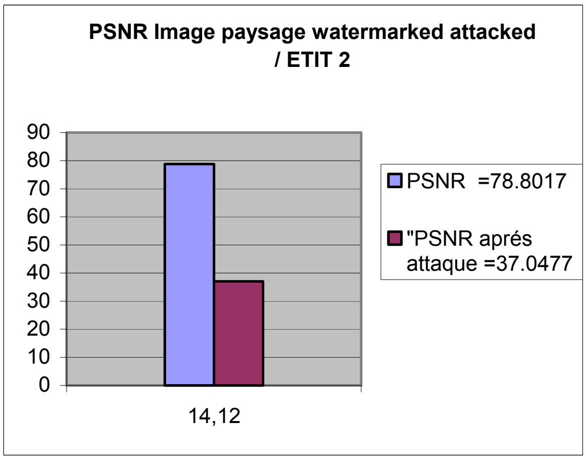

Image watermarked attacked by gaussian noise	**Evaluation de la robustesse face à l'attaque bruit gaussien**

Image watermarked attacked by cropping

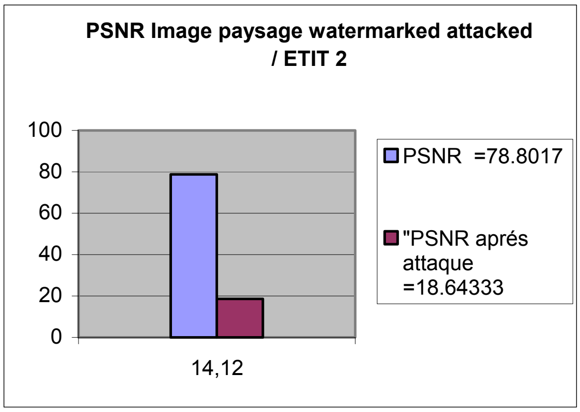

Evaluation of the robustness after a cropping

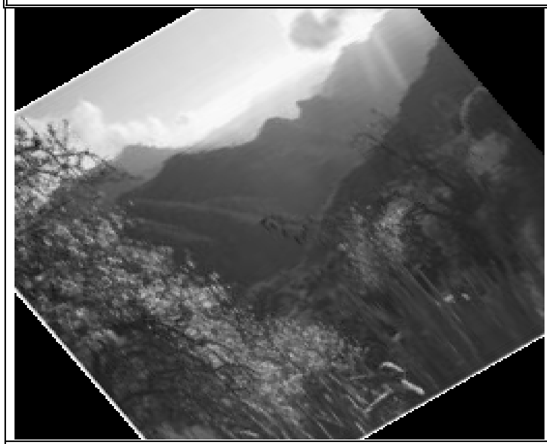

Image watermarked attacked by rotation

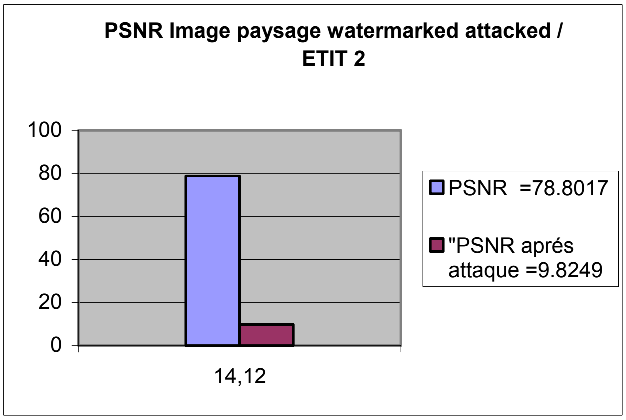

Robustness Evaluation after a rotation

Image watermarked attacked by histogram equalization

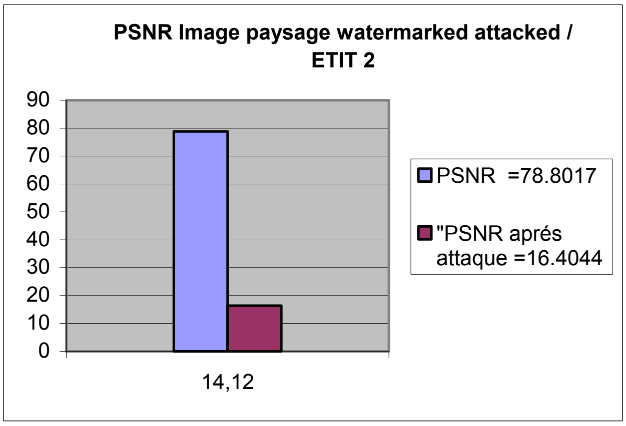

Robustness Evaluation after an histogram equalization

5. Conclusion

This paper present a new method of image watermarking in the frequential field by adding some modifications in its embedding scheme. These modifications have allowed us to obtain a robust watermarking algorithm in the frequential field having both the advantages of the robustness and the invisibility of the embedded mark. A robustness test have been done and have demonstrate the efficacy of the proposed method.

6. References

[ALA 00] A.M.Alattar. "Smart images using digimarc corporation's watermarking technologie. Proc. SPIE, pp 264-273, Janvier 2000.

[BAR 99a] M.Barni, F.Bartolini, V.Capellini, A.Lippi and A.Piva, "A DWT-based technique for spatio-frequency masking of digital signatures". In P.W.Wong and Edward J.Delp, ISET/SPIE's 11^{th} annual symposium, Electronic Imaging'99 : Secutity and watermarking of multimedia content II,Vol 3657 of

SPIE proc, pp.31-39, San Jose, California USA, Janvier 1999.
[BAR 99b] M.Barni, F.Bartolini, A. Derosa and A.Piva, "capacity of watermarking channel : How many bits can be hidden within a digital image ?", In Proc. SPIE, pp 437-448, Janvier 1999.
[BAS 00] P.Bas, "Méthodes de tatouage d'images fondées sur le contenu", Thèse, INPG, directeur de thèse : J.M.Chassery, Octobre 2000.
[BOR 99] A.Bors and I.Pitas, "Image watermarking using DCT domain constraints", In Proc. ICIP, Vol 3, pp.473-480, Trieste 1996.
[BOU 02b] M.S.Bouhlel, H.Trichili and L.Kamoun, "New approach for watermarking medical images with patient information", Scientific Medical Journal. ISSN 1110-5607. Juillet 2002.
[BRU 95] O. Bruyndonckx, J.-J. Quisquater, and B. Macq. Spatial method for copyright labeling of digital images. In *Nonlinear Signal Processing Workshop*, pages 456-459, Thessaloniki, Greece, 1995.
[COH 99] G.Cohen, S.Encheva, and G.Zémor, "Protection des droits d'auteur pour des données numériques". Technical report, École Nationale Supérieure des Télécommunications, Juin 1999.
[COX 97b] I.J. Cox, J.Kilian, T. Leighton, and T.Shamoon. "Secure spread spectrum watermarking for multimedia". IEEE Transactions on Image Processing, Vol 6, N°12, pp.1673-1687, 1997.
[COX 99] I.J. Cox, M.L. Miller, and A.L. McKellips. "Watermarking as communications with side information". Proceedings of the IEEE, Special Issue, "Identification and protection of multimedia information". July 1999.
[COX 97a] J. Cox and Matt L. Miller, "A review of watermarking and the importance of perceptual modelling". In Proc.of Electronic Imaging '97*,* Fevrier 1997.
[CRA 98] S.Craver, N.Memon, B-L.Yeo, "Resolving Rightful Ownerships with Invisible Watermarking Techniques : Limitations, Attacks and Implications", IEEE Journal on selected areas in communications, Vol. 16, N° 4, Mai 1998
[DAV 99] F.Davoine, P.Bas, P-A.Hebert and J-M.Chassery, "watermarking et résistance aux déformations géométriques", In Coresa'99, Institut EURECOM, Sophia Antipolis, France, Juin 1999.
[DEL 99] E.J.Delp, R.B.Wolfgang and C.I.Podilchuk, "Perceptual watermarks for digital images and video", Proceeding of IEEE, Vol 87, N° 7, pp.1108-1126, Juillet 1999.
[HAR 99a] F.Hartung and M.Kutter, "Multimedia watermarking techniques", Proc of IEEE, Vol 87, N° 7, pp 1079-1107, Juillet 1999.
[HAR 99b] F.Hartung, J.K.Su and B.Girot, "Spread spectrum watermarking : Malicious attacks and counter attacks, Proc of SPIE : Security and watermarking of multomedias contents, Vol 3657, pp.147-158, San Jose CA, Janvier 1999.
[HER 99] J.R. Hernández and F.P.González. "Statistical analysis of watermarking schemes for copyright protection of images". Proceedings of the IEEE, Special Issue,"Identification and protection of multimedia information". July 1999.
[KOC 95] E. Koch and J. Zhao. "Towards robust and hidden image copyright labelling". In IEEE Workshop on Nonlinear Signal and Image Processing, pp. 452-455, 1995.
[KUT 98] M.Kutter, "Watermaeking resisting to translation, rotation and scaling", In Proc of SPIE : Multimedia systems and appliocations, Vol 3528, pp.423-431, Boston, Novembre 1998.
[PET 98a] F.A. P.Petitcolas, R.J.Anderson, and M.G. Kuhn. "Attacks on copyright marking systems". In Second workshop on information hiding, pp.218-238, 1998.
[PET 99] F.A.P.Petitcolas, R.J.Anderson, and M.G.Kuhn. "Information hiding-a survey". Proceedings of the IEEE,Special Issue, "Identification and protection of multimedia information". July 1999.
[PIV 97] A.Piva, M.Barni, F.Bartolini and V.Capellini, "DCT based watermark recovering without restoring to the uncorrupted original image", In Proc ICIP, pp 520-523, 1997.
[REY 02] C.Rey and J.L.Dugelay, "an overview of watermarking algorithms for image authentification", Technical Report, Institut EURECOM, Sophia Antipolis, France, 2002.
[TIR 99b] R.Schyndel, A.Z.Tirkel and C.F.Osborne, "A digital watermark", In IEEE, ICIP'94, Vol 2, pp 86-90, Austin (TX), USA, Decembre 1999.
[TRI 02a] H.Trichili, M.S.Bouhlel, N.Derbel et L.Kamoun, "Vers le Tatouage Des Images Médicales Pour Le Télédiagnostic", 3ème Rencontres Institutionnelles : Rhônes Alpes/ Tunisie (RIRAT'02), Tozeur Tunisie, 21-22 mars 2002.
[TRI 02b] H.Trichili, M.S.Bouhlel, N.Derbel et L.Kamoun, "Tatouage d'images par étalement du spectre : Etude, évaluation et amélioration", 2èmes Journées Scientifiques des Jeunes Chercheurs en Génie Electrique et Informatique (GEI'2002). Hammamet, Tunisie, 25-27 mars 2002.
[TRI 02c] H.Trichili, M.S.Bouhlel, N.Derbel et L.Kamoun, "Contribution aux mesures efficaces de l'imperceptibilité du tatouage et nécessité de l'introduction d'un masque psychovisuel", 2èmes Journées Scientifiques des Jeunes Chercheurs en Génie Electrique et Informatique (GEI'2002). Hammamet, Tunisie, 25-27 mars 2002.
[TRI 02d] H.Trichili, M.S.Bouhlel, N.Derbel and L.Kamoun, "A New Medical Image Watermarking Scheme for a Better Telediagnosis", IEEE Conference on Systems, Man and Cybernetics : SMC, Hammamet ,Tunisia, October 6-9, 2002.
[TRI 02e] H.Trichili, M.S.Bouhlel and L.Kamoun, "A review of image Watermarking Techniques : Applications, Properties and fields", Journal of Testing and Evaluation for Applied Sciences and Engineering, Published by ASTM International.

NOVEL AUDIO WATERMARKING TECHNIQUE BASED ON WAVELET TRANSFORM

Marwan M. Al-Akaidi
Faculty of Computing Sciences and Engineering
University of De Montfort
The Gateway, Leicester LE1 9BH,
United Kingdom
Email: mma@dmu.ac.uk

Mikdam A. T. Alsalami
Computer Science Department
Zarka Private University
PO Box 2000
Zarka 13110
Jordan
Email: mikdam@zpu.edu.jo

KEYWODS

Digital Audio Watermarking, Copyright Protection, Audio Signal Processing.

ABSTRACT

In this paper, a novel audio watermarking technique is proposed. This technique uses wavelet transformation to embed a watermark signal in wavelet domain. A novel technique is used to generate audio signal dependent watermark patterns. These patterns are scaled and filtered to ensure high fidelity. Correlation is used to detect the embedded watermark. Original audio signal is not required in detection process.

INTRODUCTION

Digital watermarking is the process of embedding an imperceptible message (watermark) into multimedia work. This message should be recoverable in detection stage to provide a proof for the ownership of copyright. The watermarking algorithm has to satisfy two conflicting conditions. First, the embedded watermark must introduce as less as possible distortion to the multimedia work. Second, the embedded watermark must be robust against removal process. A number of audio watermarking algorithms have been proposed. These algorithms exploit different techniques to realize these conditions. Embedding process can be classified according to the domain where the watermark is embedded. There are four domains for watermark embedding (Alsalami and Al-Akaidi 2003): time domain, frequency domain, compressed domain and wavelet domain.

In time domain watermarking, the watermark is embedded directly into digital audio signal (Bassia et al. 2001). No domain transform is required. Frequency domain watermarking techniques need to transform the audio signal to frequency domain where the watermark embedded (e.g. (Arnold 2000)). Fast Fourier Transform (FFT) or discrete Cosine Transform (DCT) can be used for this purpose. Other audio watermarking techniques hide the watermark in compressed audio (Neubauer and Herre 2000) to avoid going through costly decompressed and compress process to embed the watermark. Wavelet Transform is also used in audio watermarking to add the watermark in Wavelet domain.

The discrete Wavelet Transform (DWT) is a technique for extracting information about non-stationary signals like audio. It was developed as an alternative to the Short Time Fourier Transform (STFT) to overcome problems related to its time and frequency resolution properties. In Fourier Transform, the signal is expressed as infinite sum of a series of sine's and cosines. This sum is referred as A Fourier expansion. The problem with Fourier Expansion is that it has no time resolution. This means that although we might be able to determine all the frequencies present in a signal, we do not know when they are present DWT provides time-frequency resolution. In Wavelet Transform, signal is decomposed to two parts, approximation and details. Approximation part contains the low frequency components while the details part contains the high frequency components the approximation part can be decomposed again to low and high frequencies. Data obtained from these decompositions are called DWT coefficients. The original signal can be reconstructed by applying inverse DWT on the coefficients. More information about wavelet transforms can be found in (Daubechies 1992 and Burrus 1998).

Kim et al (Kim et al. 2002) proposed an audio watermarking technique using wavelet transform. Their technique uses patchwork algorithm to embed a watermark in wavelet domain by changing some statistical value related to the DWT coefficients. This technique modifies audio signal regardless the properties of audio signal being watermarked. By other words, the watermark signal is audio-independent and depends only on the watermarking key. Consequently, fidelity of watermarked audio might be seriously affected.

In this paper, a new technique for wavelet based audio watermarking is proposed. A novel technique is used to generate signal dependent watermark patterns in wavelet domain. Correlation is used to detect the embedded watermark pattern. Unwatermarked audio is not necessary in detection process.

The rest of this paper is organized as follows. The proposed embedding technique is explained in next section. Then the detection technique is shown. In Robustness Test section, some of attacks results are shown to demonstrate the robustness of the proposed technique. We conclude with conclusion and future work.

WATERMARK EMBEDDING

Audio signal is broken to blocks; each block is used to embed one watermark bit. Watermark embedding process consists of four stages. At the first stage, audio signal is decomposed using wavelet transform. The decomposed audio signal is used in second stage to generate a signal dependent watermark patterns using a novel technique used in this work. At the third stage the watermark is added into audio signal. And finally we reconstruct the decomposed audio signal to get the watermarked signal.

Suppose we have a watermark W = $\{w_1, w_2,\ldots,w_n\}$ where $w_i \in \{0, 1\}$, i = 1,2,…,n. each bit in the watermark W will be embedded in one audio block S. the embedding process will be parameterised by a watermarking key K_w. The four stages of watermarking will be performed as follows:

1. The signal S decomposed using wavelet transform to level k, so we have A_k, D_0, $D_1,\ldots,D_k$. The watermark will be embedded into approximation A_k and details D_k.

2. Two watermark patterns WA and WD are generated. First we compute the standard deviations of A_k and D_k, S_1 and S_2, respectively. Then two sets of indexes I = $\{i_1, i_2,\ldots,i_{n1}\}$ and J = $\{j_1, j_2, \ldots, j_{n2}\}$ are generated using the watermarking key K_w. Then after, the watermarking patterns WA and WD can be computed as follows:

   If watermark bit being embedded $w_i = 1$ then
   $WA (k_1) = S_1$
   $WA (k_2) = – S_1$
   $WD (k_3) = S_2$
   $WD (k_4) = –S_2$
   Otherwise
   $WA (k_1) = – S_1$
   $WA (k_2) = S_1$
   $WD (k_3) = – S_2$
   $WD (k_4) = S_2$

   Where $k_1$and $k_3 \in$ I and k_2 and $k_4 \in$ J.

3. The watermark patterns are added to A_k and D_k as follows:

   $A'_k = A_k + WA$
   $D'_k = D_k + WD$

4. The components of audio signal A'_k, D_1, D_2, …, D'_k are used to produce the watermarked audio by implementing inverse wavelet transform to reconstruct the signal.

Watermark patterns are generated depending on information extracted from audio signal being watermarked. This helps the watermark to be inaudible. Further shaping operations can be made. Watermark patterns can be scaled using audio signal itself ($WA = WA * A_k$ and $WD = WD * D_k$). Filtering the resulting watermark patterns shows very good results in maintaining watermarked audio signal fidelity. Simple smoothing filter can be useful for that purpose. Figure 1 shows watermark generating, scaling using audio signal and smoothing using third order moving average filter.

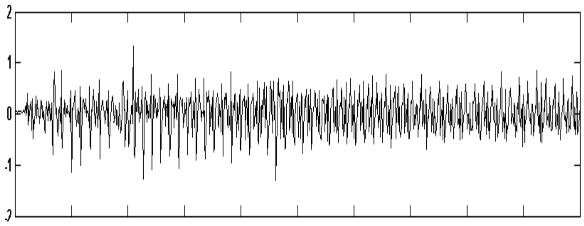

a. Original Audio Signal

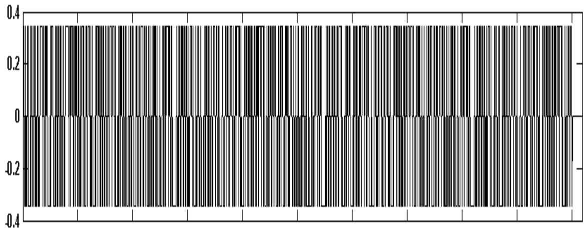

b. Original Watermark

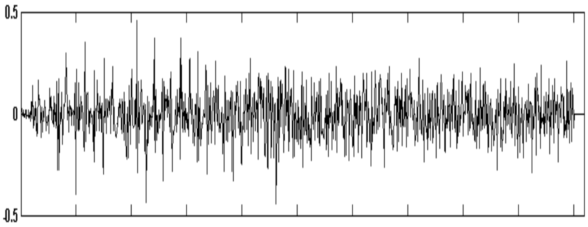

c. The Watermark after Scaling

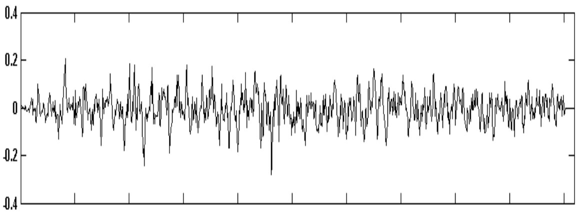

d. The Watermark after Filtering

Figure 1: Watermark Shaping

In order for the embedded watermark to be secure, watermarking key is used. Watermarking key is involved in generating two sets of indexes that are used to specify where the watermark will be buried. Parties those are interested in watermark removing will not be able to do so, as they don't know the location of the embedded watermark (they don't know the watermarking key).

WATERMARK DETECTION

Correlation is used in detection process. The watermarked audio is used to regenerate the watermark patterns and correlation is used to measure the similarity. First, audio signal is decomposed by wavelet transform, and then watermark patterns are computed and correlated. The following steps summarise detection process:

1. The signal S decomposed using wavelet transform to level k, so we have A_k, D_0, $D_1,\ldots,D_k$. The watermark will be detected in approximation A_k and details D_k.

2. Four watermark patterns (W_1, W_2, W_3 and W_4) will be computed. Patterns W_1 and W_2 are for 1 and W_3 and W_4 for 0. These patterns will be computed as bellow:

   S_1 = standard deviation of A_k
   S_2 = standard deviation of D_k

   $W_1 (k_1) = S_1$ & $W1 (k_2) = -S_1$
   $W2 (k_3) = S_2$ & $W2 (k_4) = -S_2$

   $W_1 (k_1) = -S_1$ & $W1 (k_2) = S_1$
   $W2 (k_3) = -S_2$ & $W2 (k_4) = S_2$

   Where k_1 and $k_3 \in$ I and k_2 and $k_4 \in$ J. J and I were generated using the watermarking key.

3. Correlation is used to detect the existence of the watermark.

   Let

   $$\text{corr}(W, X) = \frac{\sum_i w_i . x_i}{\sqrt{\sum_i x_i^2}} \qquad (1)$$

   represents a correlation function.

   Then we compute:

   $C_1 = \text{corr}(W_1, A_k)$
   $C_2 = \text{corr}(W_2, D_k)$
   $C_3 = \text{corr}(W_3, A_k)$
   $C_4 = \text{corr}(W_4, D_k)$

   C_1 and C_2 are used to measure the similarity between watermark patterns of 1 and the decomposed audio signal, and C_3 and C_4 are used to measure the similarity between watermark patterns of 0 and the decomposed audio signal. Each two values will be involved in computing two values CW_1 and CW_0 used in deciding the watermark:

   $CW_1 = C_1 . 0.7 + C_2 . 0.3$
   $CW_2 = C_3 . 0.7 + C_4 . 0.3$

4. The final decision can be made as follows:

   If $CW_1 - CW_2 < T$ then
   No watermark is embedded.
   Else if $CW_1 > CW_2$ then
   1 is embedded.
   Else
   0 is embedded.

Watermark patterns are regenerated from the watermarked audio signal without significant error. So, the unwatermarked audio is not necessary to be presented in detection stage. The watermark patterns must be shaped before correlation is made. The same way of embedding process shaping is used. The correlation result of approximation part is more significant than that of details part. That is because that the most significant components of audio signal lie in approximation. So that, the correlation result of approximation is weighted by 0.7, while 0.3 will weight the correlation of details.

Further criteria can be added to enhance watermark detection. In detection process four correlation values are computed. Two of them for the watermark 1 in approximation and details part and the other two for watermark 0. If the embedded watermark was 1 then both C_1 and C_2 must be greater than C_3 and C_4, respectively. Regardless that C_2 and C_4 do not have a significant difference. And the reverse must be happened in case that 0 is embedded. If that logic cannot be held, this leads us to conclude that no watermark is embedded that was just false positive detection. For example, if we have C_1 greater than C_3, but C_2 was less than C_4. It is clear that C1 and C_3 values indicate 1 is embedded in approximation but C_2 and C_3 values indicate that 0 is embedded. While the two comparisons indicate different watermark patterns, this means that no watermark is presented. For purpose of computing probability distribution function for watermarked and unwatermarked audio, detection values that do not satisfy the criteria above will be decreased by an amount **S**.

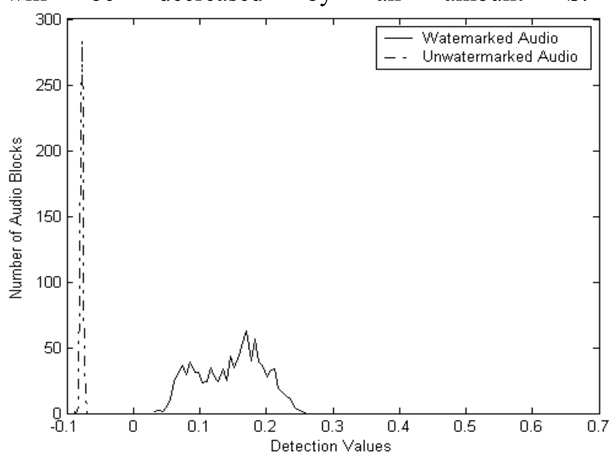

Figure 2: Probability Distribution for Detection Values of Watermarked and Unwatermarked Audio.

Figure 2 shows probability distribution function for the detection values computed from 1000 watermarked audio blocks and 1000 unwatermarked. Solid curve represents the probability distribution for detection values of watermarked audio while the dashed one represents the probability for detection values of unwatermarked audio.

The figure above gives us a clear idea about the performance of the proposed watermarking technique. The probability distribution of detection values of watermarked audio is isolated from that of unwatermarked. This enables the algorithm to detect the embedded watermark without false positive detection.

ROBUSTNESS TEST

The proposed watermarking algorithm has been subjected to a number of attacks in order to test its robustness. In this section we show some of the result we obtained from applying lowpass filter, high pass, filter, addition of random noise, and compression attacks. These results were as follows:

1. High pass filter attack: the cut-off frequency was 9 KHz. The affect of the attack can be demonstrated by showing probability distribution of 1000 high pass filtered watermarked audio as shown in Figure 3.

   The high pass filter does not have a serious affect on the watermarked audio, while it targets the high frequency components of the signal. That is because detection process considers only 30% of the correlation value of details part.

2. Low pass filter attack: the cut-off frequency was 200 Hz. The affect of the attack is shown in the Figure 4.

   As shown in Figure 4, the attack pushes down the curve of watermarked audio detection values distribution, but still we have the two curves isolated.

3. Addition of random noise attack: in this attack a random noise ranged from 0.01 to 0.1 (normalized values) is added to the watermarked audio. The affect is shown in Figure 5. The addition of random noise affects the fidelity of the watermarked audio, so we cannot consider it as an affective attack. On the other hand, adding a small amount of noise does not affect the watermark seriously.

4. Compression attack: MPEG III model is used to compress and decompress watermarked audio samples. The result of this attack is depicted in Figure 6. The watermark detector fails to detect the watermark in a very small number of audio blocks.

More attacks are conducting to proof the robustness of the proposed watermarking technique and very encouraging results obtained.

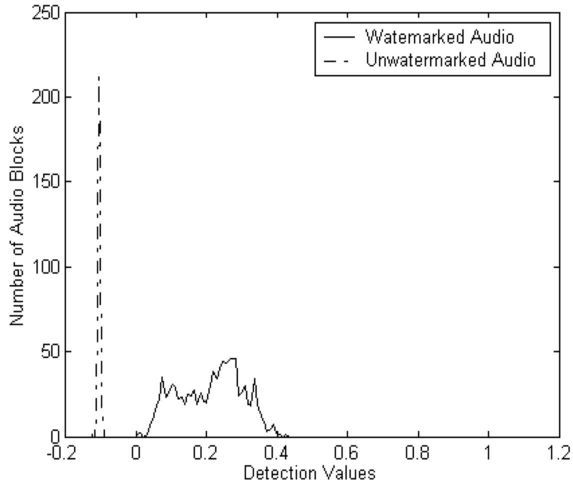

Figure 3: Probability Distribution for Detection Values of Watermarked after high pass filtering.

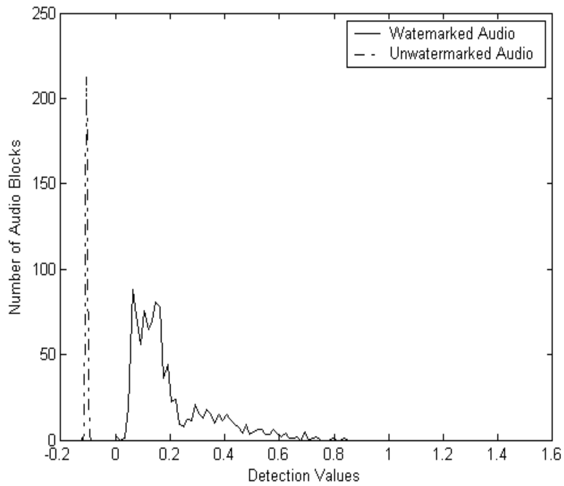

Figure 4: Probability Distribution for Detection Values of Watermarked after low pass filtering.

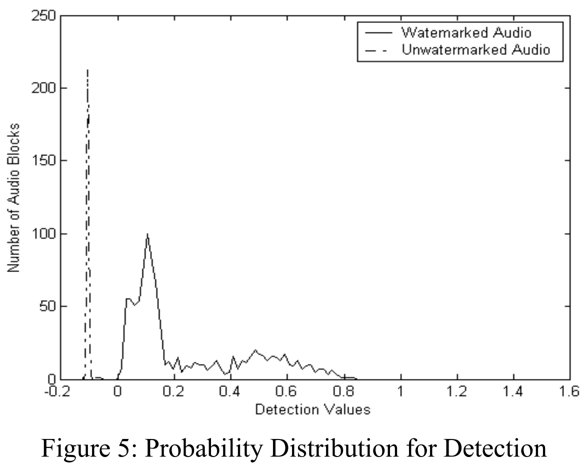

Figure 5: Probability Distribution for Detection Values of Watermarked after addition of random noise.

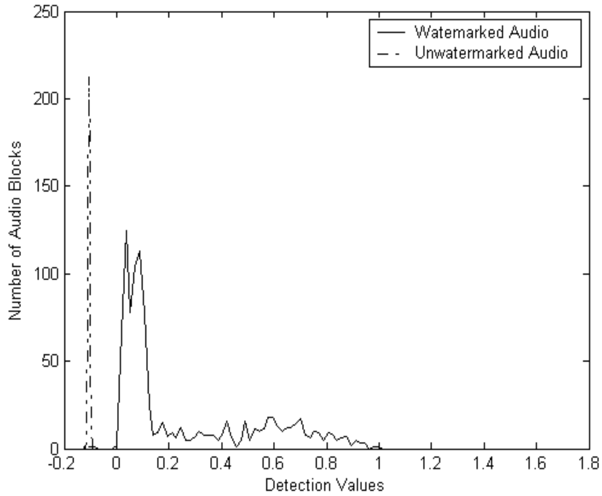

Figure 4: Probability Distribution for Detection Values of Watermarked after Compression Attack.

CONCLUSION AND FUTURE WORK

In this paper, a novel audio watermarking technique is proposed. This technique uses wavelet transform to embed a watermark in wavelet domain. We proposed a novel technique to generate audio signal dependent watermark patterns. These patterns are scaled using the audio signal itself and filtered by moving average filter to smooth the resulting watermark. Experiments show that the process of watermark patterns generation is able to produce a watermark signal that does not affect the fidelity of watermarked audio signal. Original audio signal is not required in detection stage, while the watermark patterns can be recomputed from the watermarked audio without significant error. The generated watermark patterns correlated to the audio signal to detect the existence of the watermark.

To test the robustness of the proposed technique, StirMark benchmark attacks (Steinebach, 2001) have been applied to a watermarked audio. Encouraging results are obtained and some of these results are shown in this paper. Further work is required to develop this technique to eliminate the need to the watermarking key in detection stage (Public key watermarking).

REFERENCES

Alsalami, M. and M. Al-Akaidi. 2003."Digital Audio Watermarking: Survey". *Proc. of EMS'2003*, Nottingham, UK, (Jun.), 543-556.

Arnold M. 2000. "Audio Watermarking: Features, Applications and Algorithms". *Multimedia and Expo. IEEE international Conference*. Vol. 2, 1013-1016.

Bassia, P., I. Pitas and N. Nikolaidis. 2001. "Robust Audio Watermarking in the Time Domain"", *IEEE Trans. On Multimedia*, Vol. 3, 232-241.

Burrus C., R. Gopinath and H. Guo. 1998."Introduction to Wavelets and Wavelet Transformations: A primer". Prentice Hall. NJ USA.

Daubechies I. 1992. "Ten Lectures on Wavelets", SIAM, Philadelphia.

Kim H., B. K. Lee, and N. Y. Lee. 2002. "Wavelet-Based Audio Watermarking Technique: Robustness and Fast synchronization". http://amath.kaist.ac.kr/research/paper/01-11.pdf.

Neubauer C. and J. Herre. 2000. "Audio Watermarking of MPEG-2 AAC Bitstream", *18th AES Convention*, Audio Engineering Society Preprint 5176, Los Angeles.

Steinebach M., F. A. P Peticolas, F. Raynal, amd J. Dittmann. 2001. " StirMark Benchmark: Audio Watermarking attacks". Proc. of Inter. Conf. on Information Technology: Coding and Computing.

Professor Marwan Al-Akaidi has joint the department of Electronic Engineering at De Montfort University since 1991 as senior lecturer. He is prompted to principal lecturer in 1997, in November 2000 he became a professor of Communication & signal processing. His main research interest is in the field of Digital Signal Processing & Digital Communications including Speech Coding, Processing, Recognition, Wireless and Multimedia Mobile communication. His high quality of research own him a contract with Nokia – Finland to work on project on "Speech for Mobil & Wireless Communication" and another project with Panasonic to work on "Speech Recognition for New Generation TV & Internet", recent contract with ATDI to work towards Radio Network Planning
In September 1999, Professor Marwan Al-Akaidi appointed as a Chairman for the IEEE UKRI Signal Processing Society and March 2000 the IEEE UKRI Conferences chair and in December 2000 appointed to join the board of IEEE Industrial relation. He has won the award of the IEEE UKRI in Recognition of Outstanding Leadership as a chapter chair for Year 2001 & 2002.
In January 2002 he is appointed as a Head of the School of Engineering & Technology which have 3 divisions (Engineering, Technology & Design) at De Montfort University. In the year 03 he has been selected to be included in Who's Who.

MIKDAM A. T. ALSALAMI was born in Iraq, obtained his BSc and MSc from university of Basrah in 1996 and 1999, respectively. He is a lecturer in Computer Science Department – Zarka Private University / Joradn and a part-time PhD student in De Montfort University / UK. His research areas include Information hiding, digital audio watermarking and cryptography.

SIMULATION
OF
NETWORKS
AND
COMMUNICATIONS

Cell Assignment Management Scheme in Hierarchical Cell Structure

O. Alani, M. Al-Akaidi
School of Engineering & Technology
De Montfort University
Leicester, LE1 9BH, UK,
Email: mma@dmu.ac.uk

Abstract

Hierarchical Cell Structure (HCS) or multi-tier has become a major trend in the design of 3G systems networks in order to support the high capacity demand required for multimedia traffic in 3G systems. In this type of network an efficient cell assignment scheme is required to improve the Quality of Service (QoS) of the system in terms of dropping probability, blocking probability, and channel utilisation.
In this paper we propose a new channel assignment scheme which exploits the delay insensitive property of the non real-time data service to admit users to the preferred cell layer. We believe the new scheme is anticipated to improve the QoS of the real-time voice users for both blocking probability and channel utilisation parameters.

1. INTRODUCTION

The 3G wireless network integrates different types of multimedia traffic such as voice, data, and compressed images and videos. The implementation of broadband features on the wireless medium is one of the most difficult encountered problems to handle, as a large bandwidth is required to offer such services with QoS similar to these of wired networks. Therefore a major trend in the design of wireless networks is to use Hierarchical (multi-tier) Cellular Structure (HCS). In HCS more than one cell's size type are employed to provide high coverage and capacity. Depending on the traffic density area, wireless cellular systems are partitioned into two cellular categories: small cells of a few hundred meters which is called microcells and larger ones called macrocells covering few kilometres area. Another category could be added to serve indoor users of an area as large as an office which is called picocells. Macrocells provide cost efficient coverage and are used in low density areas. On the other hand microcells are used to achieve high spot traffic in urban areas. There are two principal benefits of a two-tier design. The first is, if a macrocell covers an area, it is not necessary to cover the same area with a microcell. In rural areas with low overall demand and scattered high demand points, this means that fewer resources need to be spent on providing adequate service. Instead of covering the entire service area with microcells, a macrocell can be used in combination with microcells at high demand points. The second being if there are mobile phone's users that are travelling at high speeds, these users can be serviced by the macrocell and there by Reduce the need for handoff of the calls. When a handoff is avoided, the risk of call dropping due to channel shortage in the handoff service area is eliminated.

Trend in cellular networks is to shrink cell size in order to accommodate more mobile users in a given geographical area. This results in more frequent handoffs, and makes connection-level QoS more difficult to achieve. Some important connection-level QoS parameters are the probability of blocking newly-requested connections and the probability of dropping handoffs due to the unavailability of channels in the new cell, and channel utilization. Dropping a call in progress is generally considered to have more negative impact from users' perception than rejecting (blocking) a newly requested call. Therefore, one of the key design goals is to minimize the call dropping probability by giving priority to handoff calls. This, however, usually comes at the expense of high call blocking probability and potentially poor channel utilization by admitting less new calls; therefore there is a trade-off between these two probabilities. Basically, there are two ways to prioritise handoff calls for reducing dropping probability: guard channel and queuing. Many variation or combination of the above two schemes have been proposed [1-3]. Reserving a number of channels exclusively for handoff will improve dropping probability at the expense of higher new call blocking probability. Handoff queuing is an alternative scheme that employs a handoff queue for storing temporarily unacceptable handoff attempts. However dropping would not be totally eliminated due to the limited size of the handoff queue.

In order to achieve high QoS performance in terms of the aforementioned parameters within HCS environment good admission control and channel assignment policies should be utilised. These policies should be able to assign users to the appropriate cell layer such that minimum number of handoff occur and at the same time preserving good channel utilisation. Much works have been done regarding this issue. One method to do this is by classifying users according to their speeds so that fast moving users will be assigned to the macrocell layer while low speed and stationary users will be assigned to the microcell layer. The other method used in this respect is to transfer users between cell tiers in case of no channels available at the preferred tier, this is called *overflow* as shown in Figures 1, and 2.

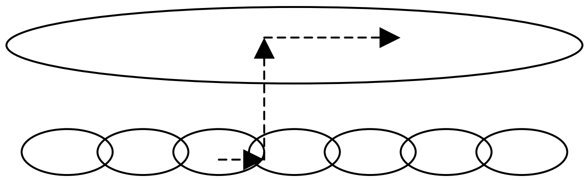

Figure 1. Call overflow

We have proposed a cell assignment management policy for HCS radio systems that aims to reduce dropping probability and at the same time preserving good channel utilisation by exploiting the time delay tolerance characteristic of the non real time users. In our policy, real time user that cannot find free channel at either cell layers can be admitted to the preferred tier by delaying a non real-time user. This paper is organised as follows: In section 2, the cell assignment policies in HCS in the literature are reviewed. In section 3, the new proposed scheme is presented, and the performance of the scheme is evaluated in section 4. Section 5 presents the conclusion.

2. HCS ASSIGNMENT POLICIES

To provide higher capacity in 3G systems, cells in hierarchical networks are being designed with smaller size. However such a trend may result in increased number of handoff requests and the corresponding increase in signalling load. Among the other problems raised in HCS that of how to assign a mobile to microcell or a macrocell has attracted a lot of interest [7-10]. Mainly there are two schemes for assigning calls to cell's layer in HCS these are: the overflow scheme and the speed-sensitive assignment. In the overflow scheme all types of traffic users will be assigned to a default cell layer (normally the lower layer). Calls that cannot find a channel at the default layer will be handed up (overflow) to the higher layer (the overlaying macrocell) as shown in Figure 1. The overflow could move in both directions i.e. from microcell level to macrocell level and vice versa.

On the other hand, in the speed-sensitive assignment scheme calls are required to be classified according to their speed. Moving fast or slow this decision will be made either by the mobile terminal which is able to evaluate its own speed, or by the base station which measures the dwell time of a mobile and compares it with a threshold [11-12]. If the dwell time of the mobile user lower than the microcell dwell time threshold, this user will be considered fast user and assigned to the macrocell layer otherwise it is considered as slow user and assigned to the microcell layer. The threshold can be adjusted dynamically by either the network or by the mobile terminal.

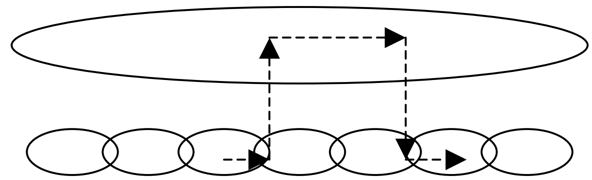

Figure 2. Two-way overflow

Only single type of service was considered in the above schemes that is real time voice service. We present our new scheme in the next section, which differs from these schemes by considering the non real-time service as well and exploiting the delay insensitive characteristic of this service to reduce dropping and blocking probability for the real time services.

3. THE PROPOSED SCHEME

A. System description

An FDD-WCDMA [13] system employing two-tier hierarchical cell structure is proposed in this paper. Therefore the resources in this system are the codes which in combination with the frequency band represent the user's channels. We have decided to consider one macrocell cluster overlaying N microcells and we consider a homogeneous cellular network. That means, all cells of the same hierarchical level are assumed statistically identical so that we can focus on one particular cell in each layer. Each macrocell can support C_o users while a microcell can support C_i users. Values of N, C_o and C_i are selected to meet the requirements of our system. Two types of users are defined according to their mobility: slow users such as pedestrian denoted as S, and fast users such as vehicles denoted as F. Classifying new arriving users as fast or slow is performed by the cellular system. We assume that new slow users and new fast users arrive according to Poisson process with mean arrival rate λ_s and λ_f respectively. The call holding time is defined as the time that a call would last if it could successfully complete without forced termination. The two mobility types have an exponentially distributed call holding time of $1/\mu_s$ and $1/\mu_f$ respectively. The call sojourn time represent how long a call can be maintained in a cell, it follows an exponential distribution with mean $1/\eta_{si}$ in the microcells and mean $1/\eta_{so}$ in the macrocells. For the fast users at the macrocell, sojourn time is also supposed to be exponentially distributed with mean $1/\eta_{fi}$ and $1/\eta_{fo}$ at the microcell.

Two classes of services are considered here: real-time voice service and non real-time data service. Data users are assumed to have only slow mobility with a rate of arrival according to Poisson process λ_d. Data traffic is buffered upon arrival to the microcell layer and they are served in a FIFO queuing discipline to fill their reserved capacity C_D. A data call can occupy an idle channel at the range (C_i-C_D), with pre-emption priority to the voice calls; the pre-empted data call will join the head of the buffer. The difference in the QoS requirements of the two classes will be exploited to favour the real time service when admitting users to the network as it will be shown next.

B. Scheme description

A new call that originated by a user will be assigned to microcell or macrocell depending on its mobility. We assume that knowledge of user mobility criterion is provided at the time of new call request [14]. Hence when a new connection arrives, it first declares its mobility criterion, and its class of service, to inform the network of the user class request. High bit rate data users require high transmission power for reliable QoS performance. Therefore we assume data service is only associated with slow users.

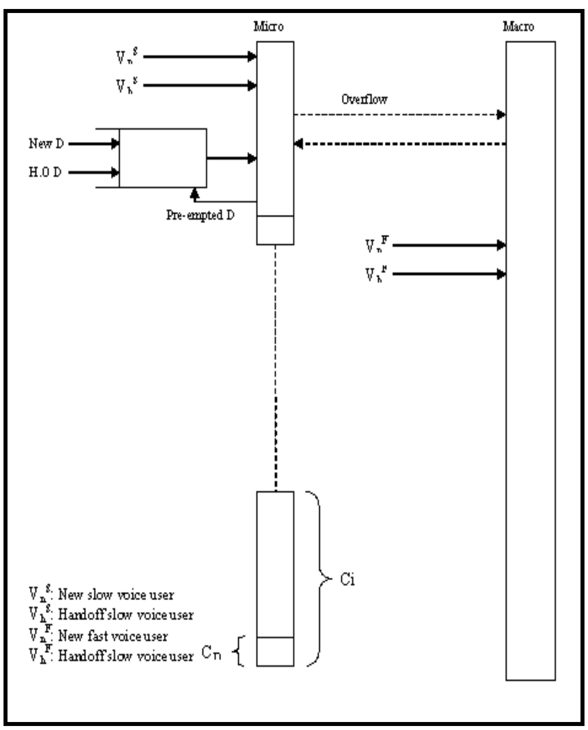

Figure 3. System model

A new call request of slow voice user, denoted as S type, is first served at the microcell level if there is idle channel. In case there is no idle channel available this request will be served by the overlaying macrocell level. Again if there is no channel available at the macrocell level the scheme will try to find data user at the microcell level that could be served at lower rate or even drop that user in order to accommodate for the voice user. The selection of data user for this purpose can be done based on different criteria such as selecting the one with highest transmission power or the one that is at the cell boundary or the one who is been connected for long time, etc. Finally if no such a user can be found the connection is blocked and cleared out. For handoff request the algorithm process in the same manner as for the new request. Slow data users type will arrive to a buffer of length L according to Poisson process. Data calls at the head of the buffer will be served at the microcell until these calls fill the channels reserved for them (C_D), after that they will wait to be served if there is available channel in the range of (C_i-C_D), as shown in Figure 3 otherwise if no idle channel available at this range the connection blocked and cleared out after waiting time t_d..

When a fast user denoted as F type, request a call, it will first served at the macrocell level if there is an idle channel. Otherwise the F type user will be assigned to the microcell level. If once more no channel available at the microcell the connection is blocked and cleared out. If an F type user is being served at the microcell level the scheme tries to move it back to the macrocell as it crosses the microcell boundary during handoff. If a channel is still not available at the macrocell level the F type user will continue on the microcell level if there is channel available. Otherwise it will be dropped and cleared out. The scheme works in the same way for the handoff request.

4. PERFORMANCE EVALUATION

Performance evaluation of our policy is carried out in terms of blocking probability for both voice and data compared with two other schemes: the first is the same proposed scheme but with only single type service, we denote this scheme as scheme I. The other scheme is the fixed resource allocation, denoted as scheme II In the fixed resource allocation scheme a fast user is assigned to the macrocell layer and it will be accepted if there is available channel, otherwise the call is blocked. New connection request or handoff request originates by slow moving user will be served at the microcell level. If there are no channels available the request will be either blocked or dropped whichever is applicable.

The simulation result for scheme I is shown in Figure 4. Blocking probability at both layers for the fast and slow voice calls is depicted.

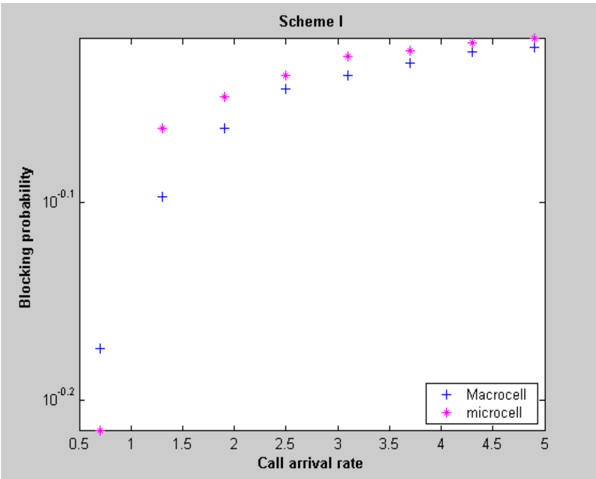

Figure 4. Blocking probability of Scheme I

Figure 5, shows the simulation result for scheme II in terms of blocking probability for voice calls at the macrocell and microcell layers. The result shows higher blocking probability than scheme I. this is expected result since scheme II does not allow overflow between layers.

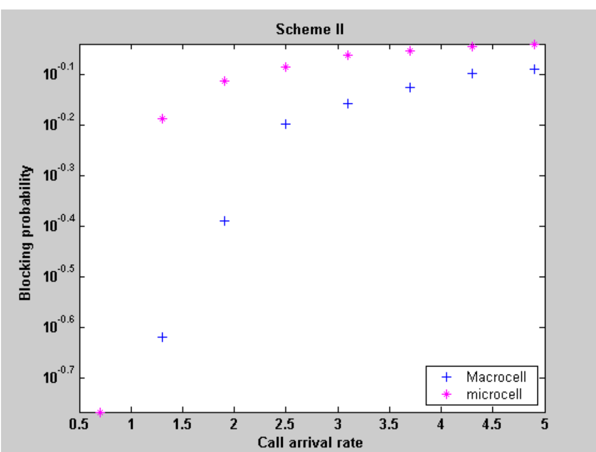

Figure 5. Blocking probability of Scheme II

Figure 6 shows lower blocking probability for the voice traffic in the proposed scheme. This is due to the introduction of data service introduced at the microcell layer. By pre-empting the data calls at the micocell the voice traffic experience a lower blocking probability at the expense of a greater time delay for the data service.

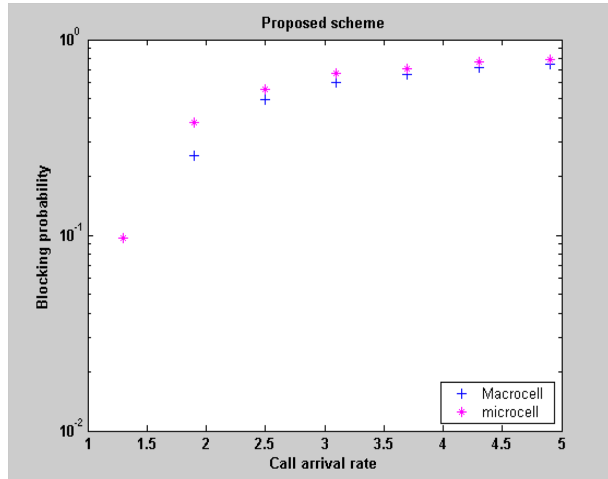

Figure 6. Blocking probability of proposed scheme

5. CONCLUSIONS

A cell assignment scheme for integrated voice and data services in which a pre-emption priority is given to voice over data is proposed in this paper. The performance of the proposed scheme in terms of blocking probability was compared with two other traditional schemes. The results show lower blocking probability of the voice traffic for the proposed scheme. This is due to the introduction of the pre-emption policy given to the voice traffic over the data traffic. Although not shown this improvement comes on the expense of longer delay periods of data traffic when the pre-emption policy is used.

Therefore there is always a chance to exploit the time insensitive delay of the non-real time data service to improve the QoS of the real time service. In practice there are many types of non real time service, such as interactive and background, hence the degradation in the QoS of the non-real time service cannot go on for long, and there should be an upper limit for this degradation. Furthermore some data services are considered as real time, such as streaming and conversational services, thus priority over these services are not allowed.

From the results and what have been said above we conclude that, the problem of achieving good QoS for all types of services supported in the 3G system simultaneously is not easy to achieve, however an algorithm that can achieve fair resource sharing to guarantee adequate QoS for all types of service is not difficult to attain.

Further work will be conducted to extend the scheme to include data service at the macrocell, and the ability of voice users to pre-empt data users at both cell layers.

REFERENCES

1- I. Katzela, M. Naghshineh "channel assignment schemes for cellular mobile telecommunication systems: a comprehansive survey, *IEEE Personal Communications* 3(3), 1996, 10-31.
2- L. Ortigoza-Guerrero, A Aghavami, A Prioretrised handoff channel allocation strategy for PCS, *IEEE Transactions on vehicular Technology* 48(4), 1999, pp 1203-1215.
3- Y.C. Kim, D. E. Lee, B. Mukherjee "Dynamic channel reservation based on mobility in wireless ATM*, IEEE communication magazine* 37 (11), 1999, pp 47-51.
4- T. Lu, J. Silvester, "joint admisiion/congestion control for wireless CDMA systems supporting integrated services", *IEEE J. Sel. Areas in Communications,* 16 (6), Aug. 1998.
5- S. J. Oh and K. Wasserman. "Dynamic spreading gain control and in multi-service CDMA networks" *IEEE Journal on Selected Area in Communications,*17 (5), May.1999.
6- S. Ramakrishna and J. Hotlzman. "A scheme for throughput maximisation in a dual class CDMA system" " *IEEE Journal on Selected Area in Communications,*15 (8), Oct.1997.
7- C. Mihailescu, X. Lagrange, D. Zeghlache, Analaysis of a two-layer cellular mobile communication system, *IEEE 47th Vehicular Technology Conference*, 1997, pp. 954-958.
8- Long-Rong Hu, S. Rappaport, Personal communication systems using multiple hierarchical cellular overlays*, IEEE Journal on Selected Area in Communications* 13(2), 1995, pp. 406-415.
9- W. Huang , V.K. Bhargava, Effects of user mobility on handoff performance in a hierarchical cellular system, Canadian Conference on Electrical and Computer Engineering, 1995, pp. 551-554.
10- W. Jolley, R. Warfield, modelling and analysis of layered cellular mobile networks, ITC-13,1991, pp.161-166.
11- C.W. Sung, W.S. Wong, "User speed estimation and dynamic channel allocation in hierarchical cellular systems", IEEE 47th Vehicular Technology Conference, 1997, pp. 91-95.
12- K.L. Yeung, S. Nanda, Optimal mobile-determined micro-macro cell selection, *IEEE PMRC,* 1995
13- 3GPP Technical Specification 25.213, "Spreading and modulation FDD".
14- S. Tabbane. "Location management methods for third generation mobile systems". *IEEE communication magazine,* 35(8), Aug.1997, pp.72-85.

ADAPTIVE EQUALIZATION FOR THE DOWNLINK OF SATELLITE MULTIPATH CDMA MOBILE SYSTEM

K. S. Rabayah
Arab American Univerisity-Jenin (AAUJ)
West Bank, Palestine
e-mail: said@aauj.edu
F. Petre*, L. Deneire*
*Interuniversity Micro Electronic Center (IMEC)
Kapeldreef 75, 75 B-3001 Leuven Belgium

ABSTRACT

In the forward link of synchronous DS-CDMA systems using orthogonal spreading codes (like TDMA/CDMA LEO satellite systems), the multipath propagation channel destroys the orthogonality of the spreading codes and therefore causes multi-user interference (MUI).

MUI can be suppressed by orthogonality restoring equalizers proposed in literature. However, many of these receivers can only deal with slow fading multi-path channels. To track fast fading multipath channels with reasonable complexity, compatible with mobile terminal design, the system may require a continuous training sequence (pilot). In this paper, we evaluate a pilot-aided adaptive fractionally-spaced chip equalizer receiver, that is suited for fast fading multipath channels. The continuous pilot signal that is provided in forthcoming third generation cellular and LEO satellite communication systems is exploited to continuously update the equalizer, using the simple NLMS adaptive scheme. Moreover, using the pilot signal for training and updating the equalizer coefficients at the symbol rate, enables a low complexity design, independent of the number of active users. This solution is therefore suitable for mobile terminals. We provide extensive simulations demonstrating that our equalizer leads to a significant performance enhancement and outperforms the RAKE receiver with prefect channel knowledge for a wide range of vehicle speeds and realistic satellite channel models.

1- INTRODUCTION

In the downlink of a code division multiple access (CDMA) system, users are multiplexed by use of orthogonal spreading codes. All user codes are transmitted over the same multi-path channel, which causes multiple user interference (MUI) by destroying the code orthogonality. The code orthogonality can be restored by equalization. For a mobile terminal, where power consumption and size are crucial, the equalizer must have a low computational complexity. Several adaptive algorithms with different levels of complexity have been proposed [1-6].

A low-complexity equalizer suitable for the downlink of a CDMA system was proposed in [7]. It is a pilot-aided adaptive fractionally-spaced chip equalizer, which exploits the presence of a continuous pilot signal. Either a normalized LMS or RLS algorithm can be used to train equalizer coefficients. Because the coefficients are updated at the symbol rate rather than the chip rate, the equalizer complexity is independent of the number of active users, and this solution is relevant for low power applications. The proposed receiver out-performs the RAKE receiver with prefect channel knowledge over a wide range of normalized Doppler spreads [7].

In this paper, the performance of this equalizer is further analyzed for the specific cases of a rural and urban satellite communication channel. In section 2, the equalizer structure is presented in detail. Section 3 describes the rural and urban channel models used in the simulations. The simulation setup is described in section 4, as well as the effects of multi-user interference (MUI), pilot power level, and terminal speed, which are considered independently. Finally, optimal equalizer parameters are determined for practical load scenarios in both rural and urban environments. Based on these results, a complete equalizer algorithm suitable for satellite communications is recommended. Finally conclusions are presented in section 5.

2-SYSTEM DESCRIPTION

A schematic diagram of the fractionally spaced chip (FSC) equalizer is shown in figure 1. The data model for the equalizer is detailed in reference [7]. The equalizer consists of two main parts: the adaptation part, and the equalization part.

The adaptation part adaptively updates the equalizer coefficients at the symbol rate instead of the chip rate which otherwise would be difficult to be employed in real implementations. Adapting the equalizer coefficients at the symbol rate was made

.

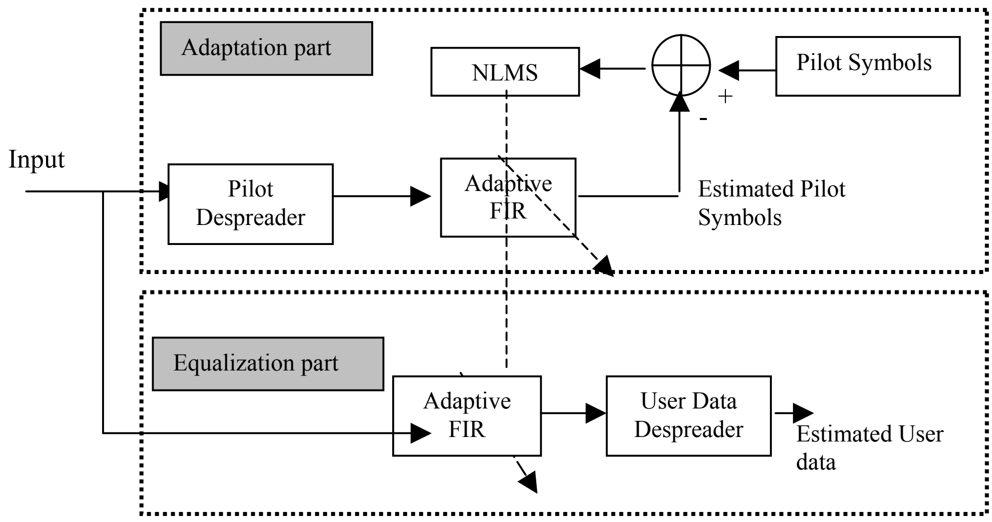

Figure 1: schematic diagram of the chip waveform equalizer

possible by reversing the order of the despreader and the FIR filter, as both of them are linear operations. The size of the equalizer (number of taps in the FIR filter, see figure 1), was optimized for both the rural and urban channel models, as will be shown in section 3. Due to the channel, the outputs of the despreader are correlated values. These values are then passed through the FIR filter, which coherently combines them to obtain an estimate of the transmitted pilot symbol.

In the equalization part, the coefficients generated by the NLMS algorithm are continuously and simultaneously employed to update another FIR filter in order to equalize the signal and restore orthogonality of the user codes, before despreading. The equalized chips are despread with the desired user code and fed to the detection device, to detect the transmitted symbols.

3-CHANNEL MODELS

We developed a tapped delay-line channel model whose parameters are determined by measurements reported in literature. The parameters are based on the wideband measurements performed for the satellite link of the third generation UMTS and IMT2000 at frequency of 2 GHz, collected by the DLR institute for communications in Germany [8,9] and adapted to the 20 GHz case. This adaptation is an educated guess based on newly reported measurements performed by the same institute at higher frequencies (40 GHz) [9]. From these measurements, we estimate the delay spread to be in the range of 100 nsec. In both rural and urban environments, the line of sight (LOS) case is modeled by Rice distribution, while the Non-line of sight (NLOS) case is modeled by Rayleigh distribution model. Typical channel parameters are given in table 1.

4- PERFORMANCE EVALUATION

In this section, the performance of the proposed receiver using the adaptive chip equalization is examined. Subsection 4.1 describes the simulation environment, and the subsequent subsections discuss the simulation results. The overall goal of this study is to investigate the performance of the adaptive equalizer in different reception conditions; ranging from a line of sight rural area, fixed mobile terminal, and clear weather condition to a non-line of sight urban area, rainy weather, and a mobile terminal at a maximum speed of 200 km/h.

4.1 Simulation Setup

We consider a CDMA downlink using QPSK modulation with K active users, each assigned a Walsh-Hadamard code of length N. The combined signal is then scrambled with long overlay PN Gold code. The signal is sampled at 4 samples per chip and filtered by a 30-tap square root raised cosine (SRRC) filter with a rolloff factor of 0.33.

The receiver consists of a matched SRRC filter of 30 taps, the FSE equalizer, despreader and data detector. The receiver performance was tested in a time-varying statistical channel generated using the parameters described in the previous section. In the upsampling case, the maximum excess delay is divided into time bins which equals to T-chip/sampling factor, and the multipath components within each time bin are unresolvable. We have assumed a stationary channel during the transmission period of one symbol, which

.

means that the channel coefficients do not change throughout that period. Perfect synchronization is assumed.

Chip rate of 20 Mchip/s, carrier frequency of 20 GHz, and different vehicle speed (0-200 km/hr) are used in simulation. As explained in section 2, a continuous pilot signal is used to train the equalizer coefficients. In order to ensure convergence, the error counting starts after reception of 500 symbols from the beginning of the transmission process. For each average probability of bit error (P_e), 50-100 channel iterations were considered, and in each iteration 10000 symbols are transmitted with independent channels for each symbol. SNR is given in terms of E_b/N_0, where E_b is the bit energy (i.e. half the symbol energy E_s) and N_0 is the noise power spectral density.

In order to eliminate any source of degradation in the equalizer BER performance, the adaptation parameter Δ of the LMS algorithm as well as the length of the equalizer have been optimized in advanced. The optimization is done for two loading scenarios; scenario 1(best case) and scenario 2 (the worst case), see table 2. The optimal Δ parameters ranged between 0.01-0.26 for the rural model, and 0.20-0.45 for the urban model. A one-tap equalizer was found to give the best results for the rural channel, while a 27-tap equalizer is needed in the case of the urban channel.

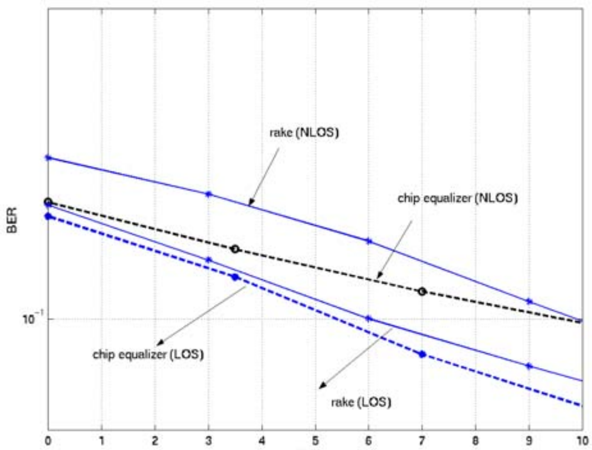

Figure 2: Equalizer performance for the urban channel using scenario 2 and terminal speed of 50 km/h.

4.2-Effect of Reception Environment

The equalizer performs sufficiently and equally well for both rural and urban channels as long as a direct line of sight is maintained. Better performance was achieved with LOS than NLOS for both channels. This is probably due to the fact that the received power from the first tap is substantially higher for the LOS with narrower amplitude distribution than the NLOS. Recall that the LOS uses Rice and the NLOS uses Rayleigh distribution, which undergoes wider amplitude variations. In both cases the chip equalizer performs better than the RAKE receiver.

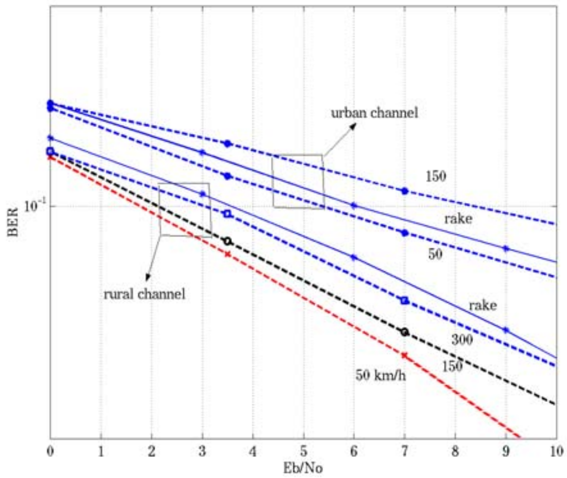

Figure 3: Equalizer performance for different terminal speeds for both channel models and using scenario 2.

Although the rural channel model is almost a perfect one with one strong and one very weak path (see table 1), the terminal speed does have a significant influence on the BER performance, as demonstrated by figure 3. For both channels, the performance degrades with higher terminal speed. The equalizer may lag behind channel variations at higher speeds, which gives rise to an enhancement of the residual error signal (MSE), and consequently resulting in performance degradation. The equalizer out-performs the rake receiver even at speed of 300 km/h.

4.3-Performance Under Interference

To examine the capability of the adaptive equalizer to combat multi-user interference (MUI), both rural and urban environments with a mobile receiver at a speed of 50km/h and equal power users were simulated. The equalizer uses the LMS adaptation scheme with the optimal values of Δ as has been found earlier.

The impact of multiple users depends highly on the channel, (see figure 4). In the rural case, multiple has a marginal negative effect on the BER performance (figure 4a). In contrast, the number of interfering users does substantially influence the BER performance for the urban channel model, (figure 4).

At about $6x10^{-2}$ BER, there is a 4 dB SNR degradation between a one user and a full load case.

.

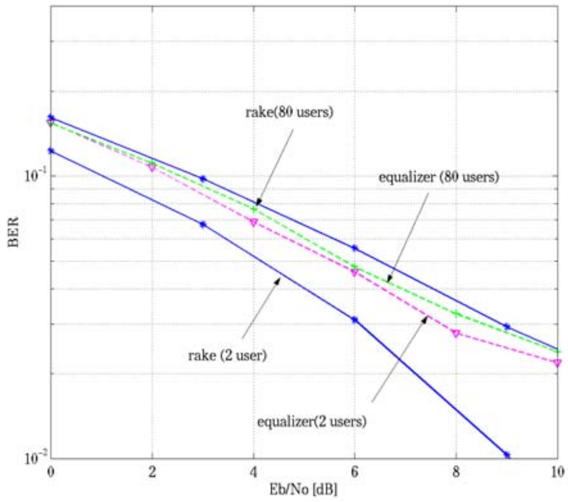

Figure 4: Error performance of the adaptive equalizer in the rural environments under MUI. Terminal speed of 50 km/h is used

In the rural case, the transmitted signals experience small amount of channel induced interference (ICI), and the orthogonality of the different user codes are maintained, therefore, de-spreading is sufficient to effectively eliminate the other user's signals. In contrast, for the urban channel model, the more interfering users, the more ICI and the harder it is for the equalizer to restore the code orthogonality and alleviate the MUI.

Compared to the rake receiver, the equalizer has exhibited less sensitivity to the MUI

4.4-Effect of Pilot Power

The BER performance analysis has shown a strong influence of the pilot power (with respect to the power of the desired user). Figure 5 shows the bit error performance for the urban channel at different pilot power levels. For both of the above BER curves, only two codes were transmitted: the desired user code and the code containing the pilot. No additional MUI was added to the signal. In the simulations, the pilot power level was set to 16 dB, 12 dB, 8 dB, and 0 dB below the desired user power level. The optimal performance is achieved when the pilot power is set equal to the desired user power.

This behavior can be explained by noting that in the case of the urban channel which contains spectral dips, equalizer coefficients will converge to different values for different pilot signal to noise ratios, because the effect of noise enhancement is more pronounced for low SNR than for high SNR. Therefore, the equalizer will minimize the mean squared error (MSE) for the pilot signal, but may not minimize it for the user signal when both signals are transmitted at different power levels. In order to ensure the coefficients minimize the MSE for both the user and pilot signals, the level of their power signals have to be equal. Since these power levels are almost never the same in the downlink of a practical CDMA system, this might be a drawback of this scheme. In such cases, channel estimation based equalization may be more appropriate.

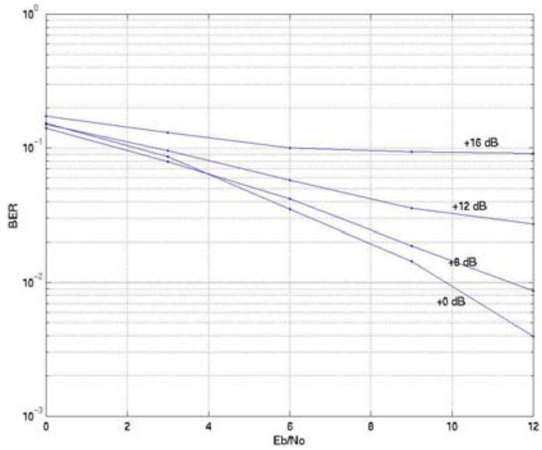

Figure 5: BER for pilot powers less than the desired user power (urban model)

Better performance is noticed for higher pilot power levels in the case of the rural channel, (see figure 6). This can be explained by noting that the rural channel has a flat frequency response. Thus, there is no noise enhancement and the equalizer coefficients converge to the optimal value for the pilot and user signal. Furthermore, the higher pilot power does not increase MUI as the signal received in the second path is so weak. Therefore, performance improves for higher pilot power levels.

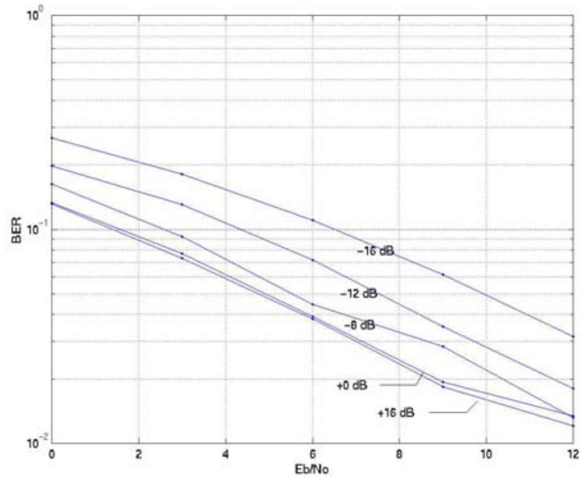

Figure 6: BER performance for increasing pilot powers (rural channel)

.

Table 1 channel parameters for the rural and urban environments

Tap number	tap delay [nsec]	Tap distribution	Parameter of amplitude distribution
Rural channel model			
1	0	LOS: Rice NLOS: Rayleigh	10logc [dB]= 6.3 10log P_m [dB]= -9.5
2	100	Rayleigh	10logPm [dB]= -24.
Urban channel model			
1	0	LOS: Rice NLOS: Rayleigh	10logc [dB]= 5.2 10log P_m [dB]= -12.1
2	60	Rayleigh	10logPm [dB]= -17.0
3	100	Rayleigh	10logPm [dB]= -18.3

Table2: the best the worst scenario used in the simulations

Scenario	User Power (dB)	Pilot Power (dB)	Interfering User Power (dB)	Percentage of codes used
1	-6.8	3.5	None	-
2	7.97	3.5	8.5	50

5- CONCLUSIONS

We have presented extensive results and analysis demonstrating the performance of the fractionally spaced chip waveform equalizer for CDMA downlink satellite system in real world scenarios. The BER results show the capabilities of this receiver in restoring orthogonality among the user signals and minimizing the effect of interference resulting from multipath. The analysis has shown a strong correlation between pilot power (with respect to the power of the desired user) and the equalizer BER performance. The best performance was achieved with the power of both the pilot signal and that of the desired user set equal, especially for a channel with nonlinear frequency characteristics. The simulation shows clearly that the rate of mobile channel changes is extremely important in terms of the degree to which an adaptive equalizer can improve system performance. The equalizer outperforms the RAKE receiver and mitigates MUI. The results presented are useful in predicting the equalizer specifications (the adaptation scheme, the size of the equalizer, the pilot power level) in different reception environments.

ACKNOWLEDGMENT

The experimental work has been carried out at IMEC Belgium and was partly supported by the European Space Agency, Noordwijk, The Netherlands, through contract 13781/99/NL/FM

REFERENCES

[1] M. L. Hong, U. Madhow, and S. Verdu, Blind adaptive multiuser detection IEEE Transaction on information theory, vol. 41, pp. 944-960, July 1995.

[2] N. Zecevic and J.H. Reed, Blind adaptation algorithms for direct-sequence spread-spectrum CDMA single-user detection, IEEE International VTC, May 1997, pp. 2133-2137.

[3] M. J. Heikkila, P.Komulainen, and J. Lilleberg, Interference suppression in CDMA downlink through adaptive channel equalization, IEEE VCT'99 vol. 2 pp. 978-982

[4] K. Hooli M. Juntti, M. Latva-aho, Multiple access interference suppression with linear chip equalizers in WCDMA downlink receiver, IEEE VCT'99 vol. 2 pp. 421-425

[5] A. Klein, Data detection algorithms specially designed for the downlink of CDMA mobile radio systems, IEEE VTC'97 vol.1 pp. 203-207

[6] I. Ghauri, D. Slock, Linear receivers for the DS-CDMA downlink exploiting orthogonality of spreading sequence, Asilomar Conference on Signal and computers vol. 1 pp. 650-654, November 1998.

[7] Frederik Petré, Marc Moonen, Marc Engels, Bert Gyselinckx, Hugo De Man, Pilot-aided adaptive chip equalizer receiver for interference suppression in DS-CDMA forward link, accepted for publication in VTC'2000-Fall, Boston, USA, September 2000.

[8] H. Bischl, A.J. Lutz, Wideband channel model for UMTS satellite, ETSI SMG5 (96) TD 007/96

[9] A.Jahn and M.~Holzbock, EHF-Band Channel Characterisation for Mobile Multimedia Satellite Services, Proceedings 48th IEEE Vehicular Technology Conference (VTC'98) ,1998, pp.209-212 and private communications.

[10] J. Proakis, Digital communications, McGraw-Hill, 3rd edition, 1995, pp. 642-648.

[11] T. Rappaport, W.Huang, and M. Feuerstein, IEICE Trans. Commun, vol. E76-B, NO.2 1993.

.

SIMULATION OF ADAPTIVE BEAMFORMING IN SMART ANTENNA SYSTEMS

Ebrahim Al-Ardi, Raed Shubair and Mohammed Al-Mualla
Etisalat College of Engineering
P.O.Box: 980, Sharjah, UAE
United Arab Emirates
E-mail: rshubair@ece.ac.ae

KEYWORDS
LMS Algorithm, Adaptive Beamforming, Smart Antennas.

ABSTRACT

Optimizing beam patterns of adaptive antenna arrays at the base station is essential for mitigating the interference and increasing the capacity of wireless networks. This paper presents a performance evaluation of the LMS algorithm used as an adaptive beamforming technique in smart antennas. This performance evaluation is carried out with respect to the antenna array parameters such as size of the array and its element spacing. The effect of incident signals in terms of their number and angular separation is also investigated. The performance evaluation study carried out in this paper helps in making the right choice of parameters leading to an optimal array design

INTRODUCTION

Beamforming is the process by which the information, obtained from the signals incident on an antenna array, are used to generate an optimum pattern which maximizes the radiated power towards the intended users and minimizes it, in the form of radiation nulls, towards the interferers. Estimating the directions of the desired users is a prior process to beamforming and is achieved by using high-resolution direction finding techniques (Schmidt R. 1986) and (Roy R. and Kailath T. 1989).

LMS ALGORITHM

By combining the signals incident on the linear antenna array and by knowing their directions of arrival, a set of weights can be adjusted to optimize the radiation pattern. The application of the LMS algorithm to estimate the optimum weights of an antenna array is widespread and its study has been of considerable interest (Godara L. 1997). The emphasis of previous work has been on the convergence behavior of such an algorithm rather than the effect of various parameters used in the design of the beamformer. Some of these parameters are related to the array structure in terms of its size and element spacing. Others are related to the incident signals including their number and angular separation.

The LMS algorithm involves the adjustment of a set of weights to minimize the difference between a reference signal and the antenna array output. The reference signal is used by the array to distinguish between the desired and interfering signals at the receiver (Winter J. 1984). The beamformer is visualized as an N-element linear array used to receive M signals, incident at angles $\varphi_1^d, ..., \varphi_M^d$ relative to the array axis, and m interfering signals incident at angles $\varphi_1^i, ..., \varphi_m^i$.

The total signal that is received by the linear array is expressed, in vector form, as:

$$\boldsymbol{u}(t) = \boldsymbol{x}^{\boldsymbol{d}}(t) + \boldsymbol{x}^{\boldsymbol{i}}(t) \tag{1}$$

where the signal vector $\boldsymbol{x}^{\boldsymbol{d}}(t)$, representing the desired signals, is given by:

$$\boldsymbol{x}^{\boldsymbol{d}}(t) = \sum_{k=1}^{M} \boldsymbol{A}^d(\varphi_k^d)\, \boldsymbol{s}_k^d(t) \tag{2}$$

where $\boldsymbol{s}^d(t)$ is an M×1 vector of source waveforms representing the reference or desired signals, and $\boldsymbol{A}^d(\varphi)$ is an N×M matrix formed by combining the array steering vectors, each of which corresponds to one direction of the incident signals. In a similar fashion, the vector $\boldsymbol{x}^{\boldsymbol{i}}(t)$, which represents the interfering signals, is expressed as:

$$x^{\boldsymbol{i}}(t) = \sum_{k=1}^{m} \boldsymbol{A}^i(\varphi_k^i)\, \boldsymbol{s}_k^i(t) \tag{3}$$

The output $\boldsymbol{z}(t)$ of the beamformer is then given by:

$$\boldsymbol{z}(t) = \boldsymbol{w}^{\mathrm{T}}(\mathrm{t})\ \boldsymbol{u}(t) \tag{4}$$

where $\boldsymbol{w}$ is a vector of the weights that need to be adjusted to optimize the radiation pattern. This is achieved by minimizing the difference between the beamformer output $z(t)$ and the reference signal $s^d(t)$. This difference is given by:

$$\varepsilon^2(n) = \left| z(n) - s^d(n) \right|^2 \tag{5}$$

Since the mobile environment is time-variable, the solution for the weight vectors must be updated continuously. Also, since the data required to estimate the optimal solution is noisy, it is desirable to use a technique which uses previous solutions for the weight vector to smooth the estimate of the optimal response and reduce the effects of noise (Liberti J. and Rappaport T. 1999). In the LMS algorithm, the weights are updated using the equation:

$$\boldsymbol{w}(n+1) = \boldsymbol{w}(n) + \mu\, \boldsymbol{u}(n)\, \varepsilon(n) \tag{6}$$

where $\boldsymbol{w}(n+1)$ denotes the weights to be computed at iteration $n+1$. μ is a positive constant that controls how fast and how close the estimated weights approach the optimal solution that minimizes the error $\varepsilon^2(n)$. The value of μ that shows stability and convergence of the algorithm should not exceed the following limit (Godara L. 1997) and (Liberti J. and Rappaport T. 1999):

$$0 < \mu < (1/Y) \tag{7}$$

where Y is the sum of the eigen-values of the correlation matrix $\boldsymbol{R}$ of $\boldsymbol{u}(t)$ which is given by:

$$\boldsymbol{R} = (\boldsymbol{u}.\boldsymbol{u}^H)/K \tag{8}$$

where K is the total number of iterations or samples taken for the incident signals.

RESULTS AND DISCUSSION

It has been noticed from our numerical results that sharper beams are directed towards the desired signals as more elements are used in the antenna array. Figure 1 shows that sharper beams are directed towards two desired signals incident at angles φ^d =60° and 120° if the number of elements of the antenna array is increased from N=5 to N=10.

Also, the spacing between the array elements d has an effect on the beamformer performance such that a very small or large spacing between the array elements can degrade the beamformer performance. It was observed from the extensive numerical experiments that an element spacing of 0.5λ is a good value. Figure 2 demonstrates the performance improvement of the beamformer if the spacing between the array elements is increased from 0.2λ to 0.5λ for three signals incident at angles φ^d =30°, 60° and 90° on a linear array of 8 elements.

By analyzing the effect of changing the number of incident signals on the antenna array, it was found that the performance of the beamformer degrades as more signals are incident on the antenna array. Figure 3 shows the performance degradation of a six-elements beamformer if the number of incident signals is increased from M=2 to M=5. Antenna arrays with more elements must be used to improve the beamformer performance as the number of incident signals increases.

Another parameter that affects the performance of the beamformer is the angular separation of the incident signals. Different numerical experiments showed that better results are obtained when the angular separation between the incident signals increases. Figure 4 shows that the main beams of the beamformer become sharper as the angular separation between two incident signals is increased from 20° to 80°.

Figure 5 also illustrates that with the same number of array elements (N=6 as an example), the beamformer cannot form sharp beams towards signals with grazing incidence, compared to signals that are closer to normal incidence. The number of array elements should be increased further to overcome this.

CONCLUSIONS

This paper studied the effect of the linear antenna array parameters in terms of its size and element spacing. It was found that the performance of the LMS beamformer improves as more elements are used in the antenna array. This improvement is seen in the form of sharper beams directed towards the desired users. By studying the effect of the spacing between the antenna elements, it was seen that using small or large spacing values could degrade the performance of the LMS beamformer. An element spacing value of 0.5λ was found to be a good value that ensures successful performance of the LMS beamformer. The effect of the incident signals on the antenna array has been studied too. It was concluded that the performance of the beamformer degrades as more signals are incident on the linear array. This can be alleviated by increasing the number of elements of the antenna array. It was also found that the performance improves as the angular separation between the incident signals increases. Moreover, it was noticed that increasing the number of elements of the antenna array ensures better performance towards signals with grazing incidence. Finally, it was observed that performance of the LMS beamformer improves as the *SNR* is made larger.

REFERENCES

(Godara L. 1997). "Application of Antenna Arrays to Mobile Communications, Part II: Beamforming and Direction-of-Arrival Considerations," *IEEE Proceedings,* Vol. 85, No. 8, 1195-1245.

(Liberti J. and Rappaport T. 1999). *Smart antennas for wireless communications.* Prentice Hall, New Jersey, USA.

(Roy R. and Kailath T. 1989). "ESPRIT – Estimation of Signal Parameters Via Rotational Invariance Techniques," *IEEE Trans. Acoustics, Speech, and Signal Processing,* Vol. 37, No. 7, 984-995.

(Schmidt R. 1986). "Multiple Emitter Location and Signal Parameters Estimation," *IEEE Trans. Antennas and Propagation,* Vol. 34, No. 2, 276-280.

(Winter J. 1984). "Optimum Combining in Digital Mobile Radio With Co-Channel Interference," *IEEE. Trans. Vehicular Technology*, Vol. 33, No.3, 144-155.

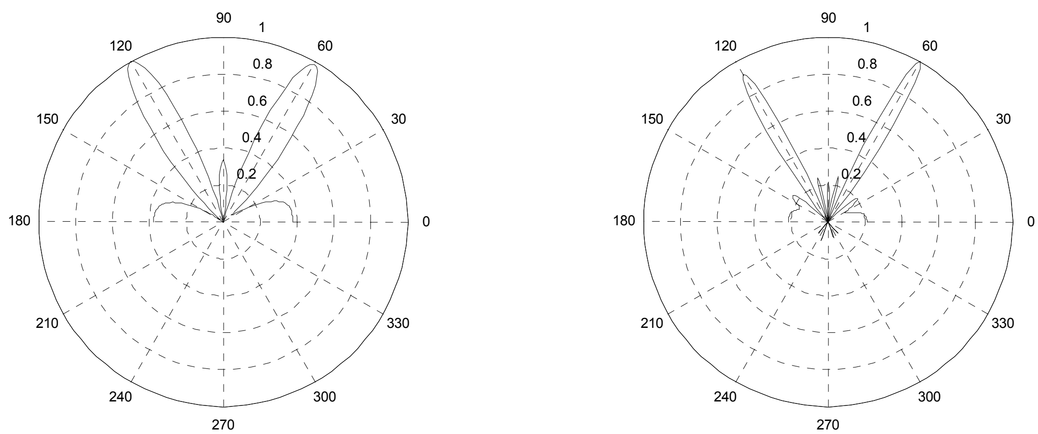

(a) N=5 (b) N=10

Figure 1: Effect of Increasing the Number of Elements of the Antenna Array on the LMS Beamformer (d=0.5λ, μ=0.001, *SNR* and *SIR* =20dB)

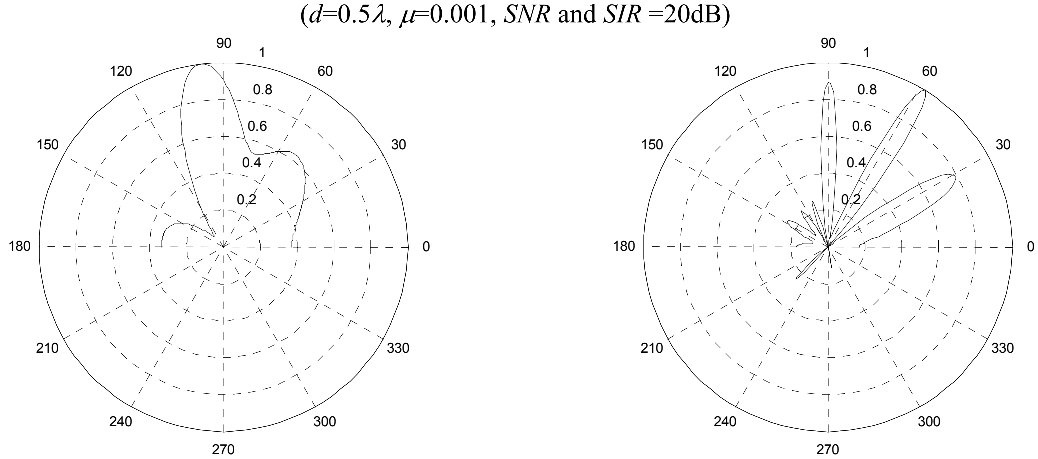

(a) d=0.2λ (b) d=0.5λ

Figure 2: Effect of the Spacing Between the Antenna Array Elements on the LMS Beamformer (μ=0.001, *SNR* and *SIR* =20dB)

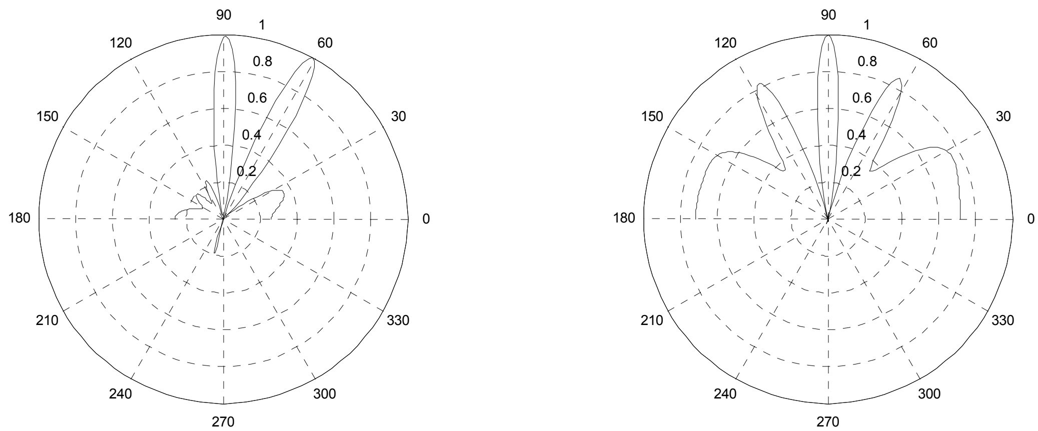

(a) M=2, φ^{d} =60° and 90° (b) M=5, φ^{d} =30°, 60°, 90°, 120° and 150°

Figure 3: Effect of Increasing the Number of Incident Signals on the LMS Beamformer (μ=0.001, n=1000, SNR and SIR =20dB)

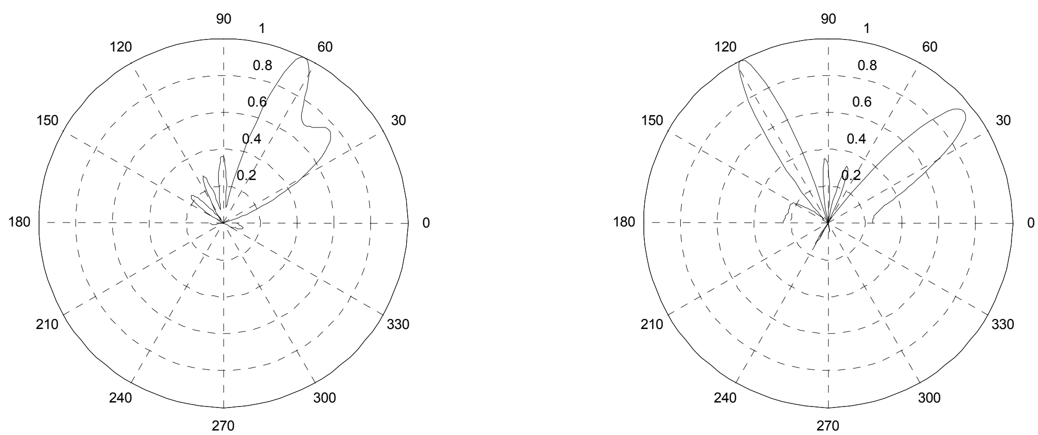

(a) ϕ_1=40°, ϕ_2=60° – angular separation=20° (b) ϕ_1=40°, ϕ_2=120° – angular separation=80°

Figure 4: Effect of Angular Separation Between the Incident Signals on the LMS Beamformer (N=6, M=2, μ=0.001, n=1000, SNR and SIR =20dB)

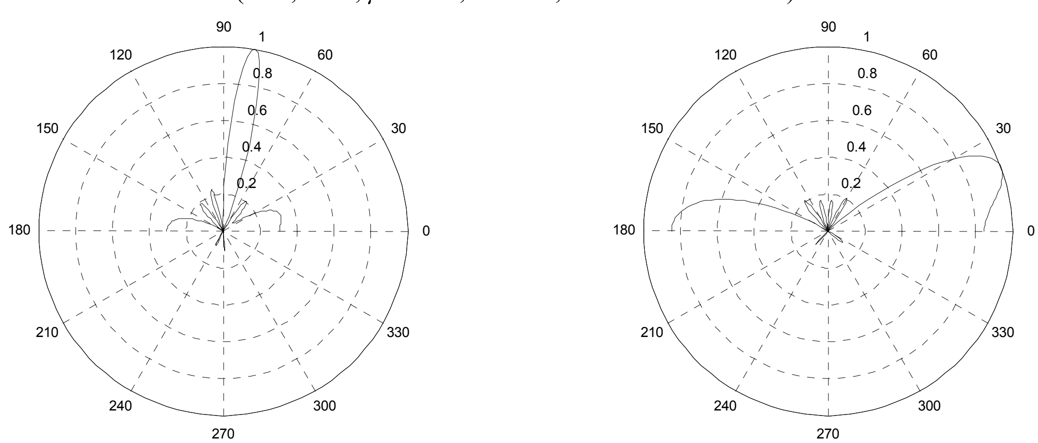

(a) φ^{d} =80° (b) φ^{d} =20°

Figure 5: Effect of Direction of Incidence on the LMS Beamformer (N=6, M=1, SNR and SIR =20dB)

LOWER ORDER BASED DS-CDMA RECEIVER OVER AWGN CHANNEL

Shihab A. Jimaa
Mohamed E. Jadah
Etisalat College of Engineering, Emirates Telecommunications Corporation, Sharjah, PO Box 980, Sharjah, UAE

Bayan S. Sharif
School of Electrical, Electronic, and Computer Engineering, University of Newcastle upon Tyne, Newcastle upon Tyne, NE1 7RU, UK

KEYWORDS
Equalization, Digital Communications, Adaptive Signal Processing, Non-Quadratic cost functions

ABSTRACT

This paper investigates the performance of using the lower order non-quadratic cost function adaptive algorithm (L*p*) in the adaptation of a non-linear receiver affected by Additive White Gaussian Noise (AWGN). The non-linear receiver comprises a feed-forward filter (FFF) with its taps updated by using the L*p* adaptive algorithm. The investigation includes the performance of the bit-error-rate (BER) using various cost functions and step-sizes. Computer simulation results indicate that the proposed receiver algorithm with the cost function of power 1.8 gives the best performance. Furthermore results show that the best value of the algorithm's step-size is 0.0005. Finally it is demonstrated that non-linear receivers adapted by the proposed algorithm will have better BER performance, in comparison with the NLMS adaptive receiver.

INTRODUCTION

Various adaptive MMSE receivers have been proposed for the detection of DS-CDMA systems. For AWGN channels, adaptive MMSE receivers were developed based on the standard MSE cost function [5], [7]. Demodulation of DS-CDMA signals is conventionally achieved with a matched-filter receiver, which exploits the low cross-correlation between signatures of different users. In most of DS-CDMA systems, transmitters send information independently resulting in users arriving asynchronously at the receiver. In such a system, signatures are unable to maintain their orthogonality resulting in multiple-access interference (MAI). Another major drawback associated with DS-CDMA is the near-far problem whereby a weak signal from distant user suffers from interference from a strong signal from a nearby user. The linear and non-linear MMSE detectors considered in [6] are single-user detectors in the sense that they demodulate the bit stream of one user at a time. So far, the Least-Mean-Square (LMS) algorithm, based upon $E[e^2(t)]$ has proved popular for many applications because of its simplicity and ease of implementation. However, many alternatives based upon non-mean-square-error cost functions can also be defined to improve the adaptation performance in specific statistical environments [1]- [3]. Hence the proposed receiver in this paper is based on using the lower order cost function, $E[e^p(t)]$, algorithm to update the tap coefficients of the feedforward filter. Extensive tests have been carried out to determine the best value of the proposed algorithm cost function's power and its step size.

SYSTEM MODEL

In this work, asynchronous DS-CDMA system with K active users has been considered. QPSK with symbol duration T_s is assumed while the chips of the spreading sequence have duration T_c. The unit-energy signature waveform of the kth user is given by:

$$s_k(t) = \frac{1}{\sqrt{T_s}} \sum_{j=1}^{N} \delta_k[j] \Psi\left(t-(j-1)T_c\right) \tag{1}$$

where $\delta_k[n] \in \{-1,+1\}$ is the nth chip of the k^{th} user and $N=T_s/T_c$ is the processing gain of the system. The chip waveform $\Psi(t)$ is zero for $t \notin (0,Tc)$. AWGN, resulting from receiver thermal noise, is considered. The DS-CDMA system model used in this paper is shown in Figure 1. The received signal from K users is represented as

$$r\ (t) = \sum_{k=1}^{K} r_k(t) + n(t) \tag{2}$$

where $r_k(t)$ is represented as

$$r\ (t) = \sum_{i=-\infty}^{\infty} d_k[i] ns_k[i] \tag{3}$$

where $d_k[i]$ is the i^{th} QPSK symbol of the k^{th} user, and $s_k[i]$ is the spreading sequence of the i^{th} QPSK symbol .

RECEIVER STRUCTURE

The proposed receiver model is shown in Figure 2. Assuming perfect estimation of the transmission time of each user, the signal to the input of the k^{th} user chip-match filter (CMF) is delayed by T_s-τ_k, and then sampled at $\Delta=T_c$. Without loss of generality, the user of interest is assumed as user number 1. The N taps of the FFF are arranged in a row vector α_l^T , and the input signal samples currently stored in the FFF are given by:

$$r_1(n) = [r(nT_s + T_c + \tau_1),...., r(nT_s + NT_c + \tau_1)]^T \tag{4}$$

The coefficients of FFF are defined in the vector α1. The soft-symbol estimate of the n^{th} QPSK symbol of the 1^{st} user is $\hat{d}_1[n] = \alpha_1' x_1[n]$ which in turn will be fed to the hard symbol decision to produce

$$\tilde{d}_1[n] = \mathrm{sgn}\left[\{\hat{d}_1[n]\}\right] \quad (5)$$

The MSE of the receiver at instant time n is given by:

$$\boldsymbol{\varepsilon_1} = E\{|\varepsilon_1[n]|^2\} = E\{|\tilde{d}_1[n]-\hat{d}_1[n]|^2\} \quad (6)$$

While the mean lower-order error (ML$_p$E) of the receiver at time n is given by:

$$\boldsymbol{\varepsilon_1} = E\{|\varepsilon_1[n]|^p\} = E\{|\tilde{d}_1[n]-\hat{d}_1[n]|^p\} \quad (7)$$

where p=1.8. The equalizer must be designed to adaptively compensate for the ISI introduced by the channel. While the NLMS adaptive algorithm, used here for comparison, is used to updates the equalizer as follows [4]:

$$\alpha_1[n+1] = \alpha_1[n] + \frac{\mu_{NLMS}}{\|r_1[n]\|^2+\gamma} r_1[n]\varepsilon_1^*[n] \quad (8)$$

The proposed Lp adaptive algorithm is used to update the equalizer as follows [2]:

$$\alpha_1[n+1] = \alpha_1[n] + p\mu_{Lp} r_1[n]\varepsilon_1^{*(p-1)}[n] \quad (9)$$

where μ_{NLMS} is the NLMS step size, μ_{Lp} is the Lp algorithm step size, and γ is a small positive constant used to ensure stability if the input signal power is low. It should be noted that the structure shown in Figure 2 is applicable to all other users.

L*p* ADAPTIVE ALGORITHM

The choice of a cost function is central to the design of adaptive algorithms using the method of gradient descent. Different cost functions lead to different algorithms [6]. Lp algorithm is based on a cost function with the error to the power p, where 1<p<2. The traditional quadratic cost function used in the NLMS algorithm is defined in Equation (6). A lower order algorithm Lp is derived from the LMS by using p=1.8 giving rise to a non-quadratic cost function. Justification of using this value of p will be given in the results and discussion section. Such a lower order cost function can be described as in Equation (7), and it is applied to the method of gradient descent using the iterative algorithm of Equation. (9).

RESULTS AND DISCUSSION

The proposed receiver is tested by means of simulations in an asynchronous system where the arrival time of the first ray of each user satisfies $\tau_k[1] \sim U(0,N)$. 31chip Gold sequences are used and the modulation scheme is QPSK. The channel considered here is AWGN channel. In this research it is assumed that we have 5 equal power users. All the performances shown in Figures 3-5 are obtained using the AWGN channel.

Firstly, it is demonstrated in Figure 3 the BER performance of the proposed lower order receiver for different values of p, where p is the power of the lower-order cost function. Several values of p were tested (1.2, 1.4, 1.6, and 1.8). It can be observed that the BER performance of the proposed receiver adapted by the Lp algorithm with p=1.8 achieve the best performance. In Figure 3 the value of μ_{Lp} equals to 0.0005. In Figure 4 the BER performance of the Lp adaptive receiver for various step-sizes are examined. It is clear that the Lp performance with μ=0.0005 performs better.

To highlight the advantage of using the lower-order algorithm, the BER plots in Figure 5 show that a 1 dB improvement can be achieved by using the Lp algorithm over AWGN channel compared to traditional NLMS.

CONCLUSIONS

This paper presents the computer simulation results of using the lower order algorithm as an alternative to NLMS over AWGN channel in the DS-CDMA receiver. The results show that improved BER performance could be achieved by using the Lp algorithm. Extensive computer simulation tests show that the best performance is obtained when the power (p) of the cost function is 1.8 and the step size is 0.0005. The proposed receiver structure using Lp adaptive algorithm provides a BER improvement of 1 dB compared to the NLMS adaptive algorithm over AWGN channel, albeit at similar computational complexity.

REFERENCES

[1] C. Rusu and C. F. N. Cowan. 2000, "Adaptive data echo cancellation using cost function adaptation, *Journal of Signal Processing, 80 (2000)*, pp. 2457-2473.

[2] S. A. Jimaa. 1999**,** "Adaptive Equalization Using Lower-Order-Cost-Function In The Presence of Co-Channel Interference", In *Proceedings of the IASTED International Conference on Modeling and Simulation - MS'99*, pp. 254-258.

[3] S. A. Shah and C. F. N. Cowan. 1995. "Modified stochastic gradient algorithm using nonquadratic cost functions for data echo cancellation," *IEE Proc., Vis. Imag Sig. Proc*., vol. 142, no. 3, pp. 187-191.

[4] S. Haykin. 1986, *Adaptive Filter Theory*, Englewood Cliff, NJ: Prentice Hall.

[5] S. L. Miller. 1995. "An adaptive direct-sequence codedivision-multiple-access receiver for multiuser interference rejection*,"* *IEEE Trans. Comms.*, vol. 43, pp. 1746-1755.

[6] S. S. Petsis, B. S. Sharif, C. C. Tsimenidis, and O. R. Hinton. 2003. "MMSE-based receivers for asynchronous DS-CDMA communication systems in the presence of double-spread multipath channels," *Accepted in the 10th IEEE international conference ICECS2003*, to be held in Sharjah, UAE, 14-17 December 2003.

[7] U. Madhow and M. Honig. 1994. "MMSE interference suppression for direct-sequence spread-spectrum CDMA," *IEEE Trans. Comms.*, vol. 42, pp. 3178-3188.

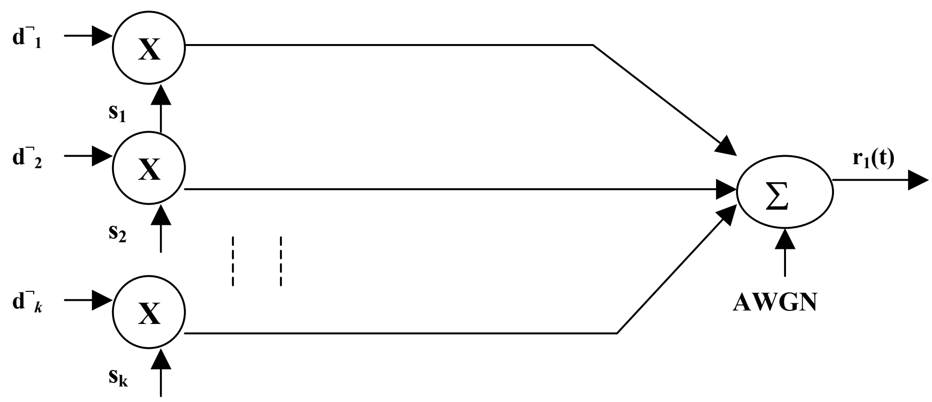

Figure 1: K Users CDMA System Model

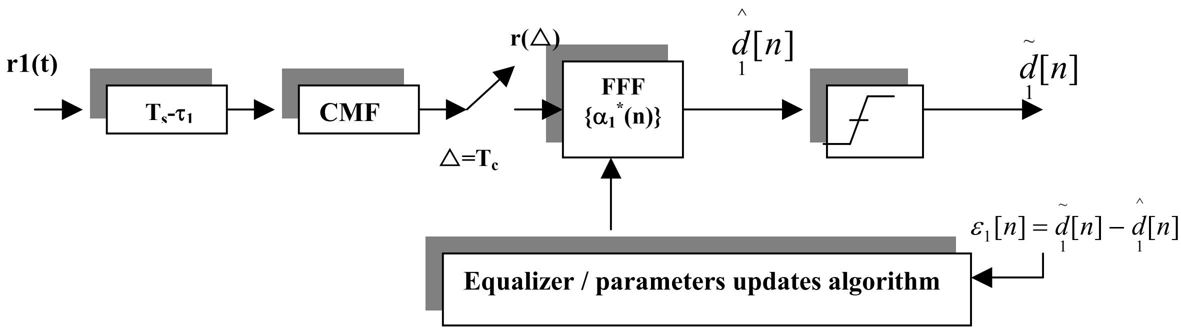

Figure 2: Receiver Structure

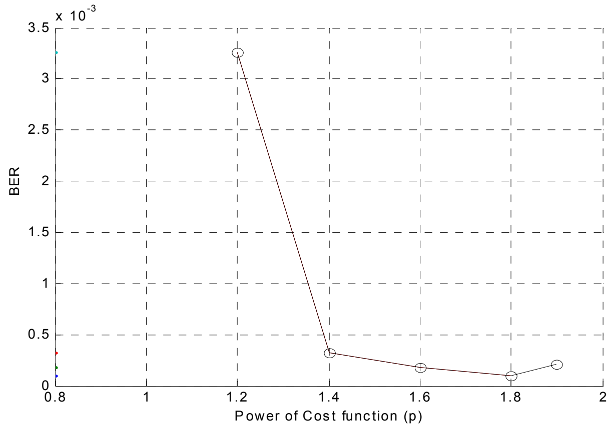

Figure 3: BER performance of the L*p* (step-size=0.0005) algorithm for various cost functions (SNR=5dB) over AWGN Channel

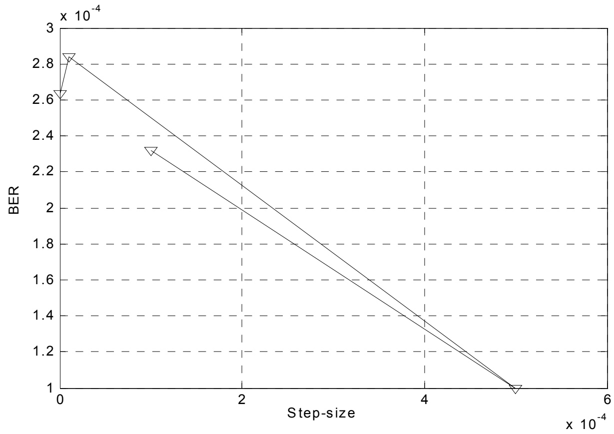

Figure 4: BER performance of the L*p* (*p*=1.8) algorithm for various step-sizes (SNR=5dB) using AWGN Channel

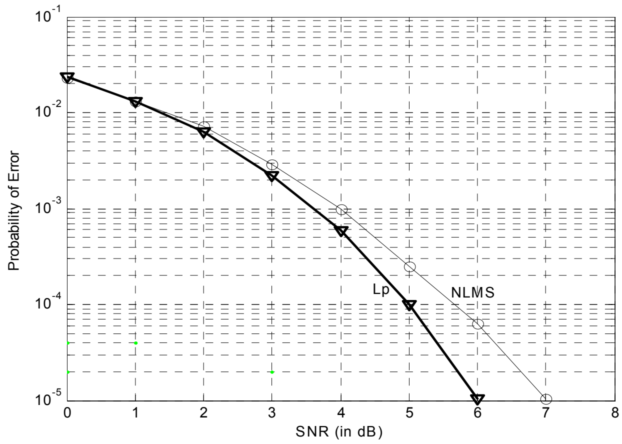

Figure 5: BER performance of the proposed algorithm (L*p*) and the NLMS algorithm over AWGN Channel

Product form Modelling of CAC In Cellular Mobile Networks

S. Al-hakeem and M. Woodward
Department of Computing,University of Bradford
E-mail:s.al-hakeem@bradford.ac.uk

Keywords:

Blocking, Call Admission Control, correlated routing, Independent routing, Prioritization.

Abstract:

This paper proposes call admission control (CAC) for wireless cellular mobile networks based on blocking mechanism. It is also intended to provide some basic concepts and notations for 3G mobile communication networks. These basics are the background for the proposed solutions and performance studies. The cellular concept, which resolves the basic problems of radio systems in terms of system capacity constraints, is also analyzed.

1 Mobile communication Systems Principles

A wireless access network provides wireless terminal within the service area with the possibility to reach information as well as other terminals. Ideally, the access network is an interface to global telephone and data communication networks. Communication can be initiated either from the wireless terminal or from within the fixed network. A terminal can then forward or retrieve information streams such as speech, sound, video, text, programs, or combinations thereof.

Service everywhere within a large geographical area can be a achieved by covering the area with many base stations. There is a limited area within which it is possible for mobile terminals to communicate with a specific base station. The maximum geographical area served by a base station is denoted a cell. Cells are usually designed to overlap so that an ongoing connection can be transferred from one base station to the next one (Thummler 2003). High level applications can use the information flow to provide, for example, a wide range of information and transaction based services. Since all applications can have very different requirements for the Quality of Service (QoS) and for the amount of bandwidth they use at any moment, it is crucial to have a mechanism that guarantees that all multiplexed connections on a link get the performance they negotiated with the network. The Connection Admission Control (CAC) is responsible for this task.

2 Call Admission Control CAC

The area of CAC is of vital importance, particularly for true Quality of Service traffic guarantees. There are a number of important issues that must be defined and addressed when developing a call admission algorithm for any network (J.R Moorman 2000). Many of these proposed CAC policies can be described as making admission decisions by comparing the resources required by an incoming connection request with the resources currently available in the network. In capacity-varying networks, a reduction in network capacity may affect connections in progress at that time. Under a CAC policy which considers only currently available resources, connections may be accepted prior to the known capacity change only to be dropped once the capacity decreases. A more intelligent CAC policy, aware of the upcoming capacity change, might block connections instead of accepting them and then dropping them. Dropping a connection is generally considered a less desirable result than blocking a connection request, since dropping a connection involves breaching QOS guarantees made upon connection acceptance, guarantees which were not made in blocking the connection request. So the CAC put limitation on the number coming from outside (new users) plus the number that can be accepted in term of the handover. Basically CAC for a mobile system will not allow more than a certain number of new users and handover into the system.

Based on the CAC function a connection request is progressed only when sufficient resources are available at each successive network element to establish the connection through the whole network based on its service category, traffic contract, and QoS and in order to maintain the agreed QoS of existing connections. Blocking mechanism introduced in our model will function as a CAC for the system.

3 Henderson And Taylor

Henderson and Taylor (Henderson and Taylor. 1990) proposed a way of finding a product form solution for a certain class of queueing networks. In their model, customers are also allowed to move simultaneously in batches. It is based upon the assumption that the state of the network behaves as an irreducible Markov Chain. They derived the equilibrium distribution in terms of the probability that a group of customers departing from a station is transformed into a new group of arriving customers. Henderson and Taylor consider the late arrival system. A similar method has also been published by Boucherie and Van Dijk (R.J Boucherie 1991).

If We consider an Open network of queues with nodes numbered 1,2,...,M. Customers enter the network from outside (which we usually consider as node 0), precede according to some routing regime through the network and eventually leave the system. The customers may be of different types which they may randomly change when entering a new node. The set

T of customer types is assumed to be finite. Denote $q(\mathbf{n},\mathbf{d})$ the probability that a batch of customers $\mathbf{d}$ depart just after the beginning of a slot, when the system is in state $\mathbf{n}$. These customers will join the nodes before the next time point with probability $p(\mathbf{d},\mathbf{a})$. the quantities $\mathbf{n},\mathbf{d}$,and $\mathbf{a}$ are vectors defined as follows:

- $n = (n(i,t), 1 \le i \le M, 1 \le t \le T)$ is the number of customers at each node in each class at a time point.
- $d = (d(0), d(i,t), 1 \le i \le M, 1 \le t \le T)$; $d(0)$: the batch of customers that enters the network from outside , $d(i,t)$: the batch of customers released from node i class t.
  d^+ indicates that all of the external arrivals are excluded.
- $\mathbf{a} = (a(0), a(j,s), 1 \le j \le M, 1 \le s \le T$; $a(0)$;represent the batch of customers that leave the network and $a(j,s)$ represent the customers that deposited at node j ,class s.The vector $\mathbf{a}^+$ is the restriction of $\mathbf{a}$ to the positions $(j,s), 1 \le j \le M, 1 \le s \le T$ which indicates that the departing customers from the network are not taken into account.

When $\mathbf{a}$ is deposited a new state $\acute{\mathbf{n}} = \mathbf{n} - \mathbf{d}^+ + \mathbf{a}^+$ is created at the next time point. Also it is assumed that $q(\mathbf{n},\mathbf{d})$ and $p(\mathbf{d},\mathbf{a})$ are such that $\mathbf{n}$ evolve as a discrete time Markov chain that is irreducible and positive recurrent and has state space Ω.
The essentials for the successful steady-state analysis are the following assumptions.

Assumption 1 There exist a non-negative functions $\Psi(.)$, and $\Xi(.)$ and $\Phi(.)$ is a positive function.These functions are related to the service and arrival distributions respectively. where examples of how to choose $\Psi(.)$,and $\Xi(.)$ to model a specific situations are given by (9). So the release probability q can take the form.

$$q(\mathbf{n},\mathbf{d}) = \frac{\mathbf{\Psi}(\mathbf{n}-\mathbf{d}^+)\Xi(\mathbf{d})}{\mathbf{\Phi}(\mathbf{n})} \tag{1}$$

Assumption 2 There exist a strict positive functions f and g such that f solves the following traffic equations for the batch movement systems $\Xi(\mathbf{d})f(\mathbf{d}) = \sum_{\mathbf{a}} \Xi(\mathbf{a})f(\mathbf{a})r(\mathbf{a},\mathbf{d})$ Now, define the routing chain on the finite set L of all transfer vectors to be the Markov chain which has transition probabilities $r(\mathbf{d},\mathbf{a})$.

$$r(\mathbf{d},\mathbf{a}) = \begin{cases} p(\mathbf{d},\mathbf{a}) & If\ q(\mathbf{n},\mathbf{d}) > \mathbf{0} \textit{ for some } \mathbf{n} \\ \delta_{\mathbf{d},\mathbf{a}} & \textit{otherwise} \end{cases}$$

Any vector that can be released or deposited is called a transfer vector. Next define the set $F = \{f(.), L \to R : f(\mathbf{d}) > \mathbf{0}\}$, where $\Xi(\mathbf{d})\mathrm{f}(\mathbf{d})$, $d \in L$, are an invariant measure for the routing chain.

if the function $f(\mathbf{d})$ which satisfies the above equation can be found, we will then proceed further to find a function $\mathrm{g}(\mathbf{n})$which satisfies the equation

$$\frac{\mathrm{g}(\mathbf{n})}{\mathrm{g}(\mathbf{n}-\mathbf{d}^+ + \mathbf{a}^+)} = \frac{f(\mathbf{d})}{f(\mathbf{a})} \tag{2}$$

as long as $q(\mathbf{n},\mathbf{d}).\mathbf{r}(\mathbf{d},\mathbf{a}) > \mathbf{0}$ is satisfied within the communication class.

With these Assumptions Henderson and Taylor give the equilibrium distribution as

$$\pi(\mathbf{n}) = \mathcal{K}\Phi(\mathbf{n})\mathrm{g}(\mathbf{n}) \tag{3}$$

where $\mathcal{K}$ is the normalising constant and $\Phi(.)$ is a function related to the service time of the network and $\mathrm{g}(\mathbf{n})$ is a function linked with the routing probabilities of the network.

4 Modified Henderson and Taylor Model

It is shown in (Woodward 1998) that the Henderson-Taylor model can be modified so that batches of customers released from node i,class t, denoted as $< i,t >$, have capacities that depend on the network state. This modification defines a vector $k_{n,d} = k_{n,d}(0), k_{n,d}(i,t), 1 \le j \le M, 1 \le s \le T$, where $k_{n,d}(0)$ is the maximum number of customers that can enter the network and $k_{n,d}(i,t)$ is the maximum number of customers that can be released from $< i,t >$ given the state $\mathbf{n}$ and the rest of the transfer vector $\mathbf{d}$. The form that $k_{n,d}(i,t)$ can take depends on the application and is discussed in (2). Then any $\mathbf{d}$ that can be released from state $\mathbf{n}$ must satisfy $d(0) \le k_{n,d}(0), d(i,t) \le k_{n,d}(i,t)\ \forall i,t,$

The remainder of this paper is concerned with showing how this basic product form network can be modified to model the features of a CAC for a cellular mobile system as previous described.

5 Blocking

The behavior of various systems, including communication and computer systems, as well as production and manufacturing systems, can be represented and analyzed through queueing network models to evaluate their performance. System performance analysis consists of the derivation of a set of figures of merit. This usually includes the queue length distribution and some average performance indices such as mean response time, throughput, and utilization (Balsamo 1998). Because of the system's resource constraints, realistic models should have finite capacity queues, i.e., the queue length cannot exceed a maximum threshold. When the queue length reaches this threshold, the queue is said to be full. Then any individual job that attempts to enter a full queue is not accepted and blocking arises (Balsamo 1998).

6 Blocking (Boucherie)

Networks of queues with blocking have proved useful in modelling computer systems, distributed systems, telecommunication systems, and flexible manufacturing systems. A queueing network with blocking is a set of arbitrary linked finite capacity nodes. Blocking arises because of the limitations imposed on the size of these nodes. That is, the flow of units through on node may be momentarily stopped if a destination node has reached its capacity. This type of blocking is not related to the notion of blocking in teletraffic, where an arriving unit is blocked, i.e. lost, if the node is full (R.J Boucherie 1992).

Queueing networks with blocking are, in general difficult to treat. Some exact closed-form results have been reported in the literature. However, closed-form solutions are not generally available. Most of the techniques, therefore, that are employed to analyze such queueing networks are based on analytic approximations, numerical analysis, and simulation. (R.J Boucherie 1991) impose some constraints on customer upon arrival to the station to show that the product form solution exists in their network even with blocking. It is simply a question of how to remove the right terms out of the global balance equation in order to simulate their blocking. Customers who upon arrival cannot enter a station will eventually return back and the transfer to which these customers belong will be taken as "never happen". As a consequence the state of the network remains unchanged. Only transitions which do not violate the constraints upon arrival are allowable to take place. It is based on the same idea for their minimal workload blocking in which a minimum number of customers must be retained in some stations after the departures and the anticipative minimal workload blocking whereas upon arrival certain conditions must be satisfied, otherwise the whole transition will not be allowed to go ahead. Henderson and Taylor (Henderson and Taylor. 1991) also adopted the same notion in showing that the system with correlated routing has also a product form solution (Pujolle 1995).

In ([Perros 1990) a survey of results was given for tow-node queueing networks with blocking. This is the simplest configuration of queueing networks with blocking, and it consist of two nodes linked in tandem, where the second node is always finite. The first node may not be finite. This model has been studied under a multiplicity of different assumptions regarding service time distributions, feedbacks and blocking mechanisms. A systematic presentation of the literature related to closed queueing network with blocking which consist of two or more nodes is given in (Onvural 1990).

7 Blocking Mechanisms

Various blocking mechanisms have been considered in the literature so far, These mechanisms arose of different studies of real-life systems. They are distinct types of models for blocking, a fact that may be easily missed by a reader unfamiliar with the subject. The most commonly used blocking mechanisms can be classified as follows.

7.1 Repetitive Service Blocking (RS)

A customer upon completion of its service at queue i attempts to enter destination queue j. If node j is full, the customer is looped back into the sending queue i, where it receives a new independent service according to the service discipline. Two different sub-categories have been introduced depending on whether the customer after receiving a new service, chooses a new destination node independently of the one that it had selected previously: 1. RS-RD (random destination) if a customer destination is randomly chosen at the end of each new service, whatever the previous choices; 2. RS-FD (fixed destination) if a customer destination is determined after the first service and cannot be modified.

7.2 Blocking Before Service (BBS)

a customer declares its destination node j before it starts receiving service at node i. If at that time node j is full, the service at node i does not start and the server is blocked. If a destination node j becomes full during the service of a customer at node i whose destination is j, node i service is interrupted and the server is blocked. The service of node i will be resumed as soon as a departure occurs from node j. The destination node of a blocked customer does not change. Two different subcategories can be introduced (Onvural 1990) depending on whether the server can be used as a service center buffer when the node is blocked: 1. BBS-SO (server occupied) when the server of the blocked node is used to hold a customer; 2. BBS-SNO (server is not occupied) when the server of the blocked node cannot be used to hold a customer.

7.3 Blocking After Service (BAS)

if a job attempts to enter a full capacity queue j upon completion of a service at node i, it is forced to wait in node i server, until the destination code j can be entered. the server of source node i stops processing jobs(it is blocked) until destination node j releases a job. Node i service will be resumed as soon as a departure occurs from node j. At that time the job waiting in node i immediately moves to node j. if more than one node is blocked by the same node j, then a scheduling discipline must be considered to define the unblocking order of the blocked nodes when a departure occurs from node j. First blocked First Unblocked is a possible discipline(Onvural 1990)which states that the first node to be unblocked is the one which was first blocked.

8 Some basic concepts

We define a node to consist of a queue served by a single server. (If a node consists of more than one server, then it will be specifically mentioned.) We well mostly deal with finite capacity nodes. We indicate such a node by the familiar figure shown below, where the circle indicates the server, And the rectangular with a finite number of positions indicates the finite capacity queue. It is assumed that there is a position in front of the server that is occupied by the unit currently in service. Thus, the maximum number of units that can be accommodated in this finite capacity node is equal to the maximum number units that can be accommodated in its queue plus the one in service. Whenever possible, the service rate will be indicated within the circle.

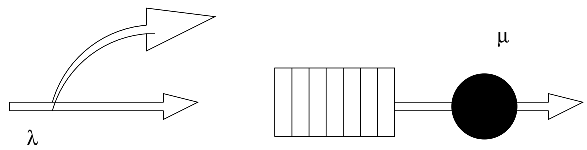

Figure 1: Finite Capacity Que

9 The model

We consider a cell as node with a finite buffer capacity. Three types of calls are assumed, namely, originating (abbreviated by letter O) calls, the hand-over (abbreviated by letter H) calls and call in progress or existing connections(abbreviated by letter E). Priority is given to E calls over H and O calls and the next priority has been given to H call over O calls. We are able to achieve the CAC algorithm within our frame work and still retain a product form solution for the model simply by putting restriction on the batch size. The model considers a finite set of nodes. Each node of the system has got a finite capacity C. The model proposed in this section concentrate on a single node or a cell. A connection can admit to the cell as a new call or as a handover or as an existing call.A priority check will run in the system depending on the batch size or number of arrivals. If there is enough capacity in the system and the new arrivals will not cause a buffer overflow the batch will be allowed into the cell other wise the batch will be blocked. The blocking will be depending on the batch size, the node spare capacity and the type of routing .We assume that different connection types tolerate call blocking differently. Moreover, generally blocking on-going handover calls is less tolerable than the blocking of new calls.There fore we suppose that the cell preserve some capacity for blocking sensitive connections and for handover connection.

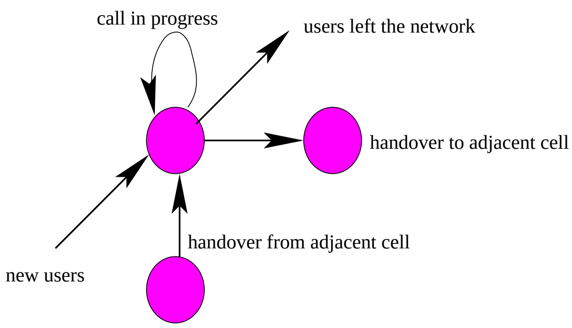

Figure 2: MCN Customers Routes

9.1 Independent routing

We consider a queueing network with arbitrary topology. Our model follow a RS-RD blocking mechanism. Basically we are stopping a batch of customers of being released from each que in the network. Because if we release this vector or this batch of customers it will cause a buffer overflow. If we release this batch we will set the relevant $\Xi(d)$ to zero. It means that this batch of customers will be retain to the que and continue to wait. In the next slot the service will be repeated and the batch will be serviced.

9.2 Correlated Routing

In the case of correlated routing if the vector released will cause a buffer overflow,it will be redirected to the same node, so that is equivalent to RS-FD blocking.In this case we have the option of fixing the destination.Because we direct the vector, the customers to any destination of our wish by making the routing probability equal to 1 as shown in figure 3. On the other hand some of these vectors will not cause any problem. In this case well assume that the system behaving as normal independent routing. Which means there is a probabilistically a chance of going to one node or another. In this contest it is RS-RD blocking. So it will depends on wether we are using entirely correlated routing or wether we are using a mixture of correlated routing and independent routing.

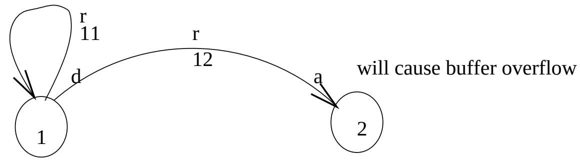

Figure 3: Blocking with Correlated Routing

10 Prioritization

Priority should be given to on going calls over both, the handover calls and new users calls. Furthermore, the next priority should be given to handover calls over new users calls.

10.1 The priority will be divided into three categories:-

Where $(n-d)$ is what left behind after the vector received the service and left the system. And $C-(n-d)$is the spare capacity which will be available in the system to receive arrivals.

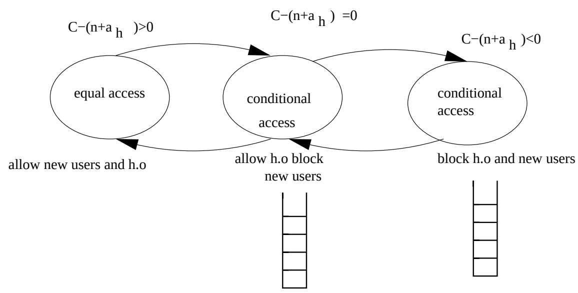

Figure 4: Priority Schedule

- $C-(n-d) \leq A$ As the spare capacity left is very limited. Priority will be given only to the ongoing calls and block the other the handover and the new users.
- $B > (C-(n-d)) \geq A$. As the spare capacity is more than the first stage. So handover calls are allowed and block new users calls.
- $B \leq (C-(n-d)) \leq C$ There is enough spare capacity to serve every user in the system. Handover calls and new users call are both allowed into the system.

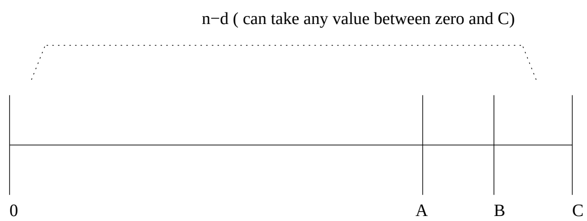

Figure 5: Spare Capacity Diagram

released vector $\mathbf{d}$								arriving vector $\mathbf{a}$							
$d(0)$	$d(1)$	$d(2)$	$d(3)$	$d(4)$	$d(5)$	$d(6)$	$d(7)$	$a(0)$	$a(1)$	$a(2)$	$a(3)$	$a(4)$	$a(5)$	$a(6)$	$a(7)$
1	0	0	0	0	1	1	1	0	1	0	0	0	1	1	1
								0	1	0	0	1	1	1	0
								1	1	0	0	0	1	1	0
								1	1	0	0	1	1	0	0

Table 1: The Released and Arrived Vectors

Example 1 *In this example we study Markovian queueing networks in which the routing characteristics have a particular form which leads to a product form stationary distribution for the number of customers in the various queues of the network. We show that if certain transitions are prohibited due to blocking conditions, then the form of the stationary distribution is preserved under a certain rerouting protocol. This example will illustrate the wide applicability of the model. In the case of a seven nodes cellular mobile communication network model. A vector* $\mathbf{d}$*will be released out of the central node. This vector suppose to arrive as* $\mathbf{a}$*to its destination. A correlated routing will be adapted in this example. A general assumption will be given to the value of* $\mathbf{d}$.

- $C-(n-d) \leq A$
  As mentioned earlier handover calls and new users calls have to be blocked at this stage. To achieve that vector $\mathbf{d}$ *will be forced to loop around it self by assigning the routing probability a value one* $r_{11} = 1$*.So non of the arriving vectors shown in table 1 will arrive to their destination.*

- $B \leq (C-(n-d)) \leq C$
  At this stage handover calls will be allowed and new users calls will be blocked. This will be achieved by putting $\Xi(a(0)) = 0$ *In this case the first tow arriving vector shown in table 1 will arrive to their destination without any problems. The other tow vectors will arrive to their destination as 01000110 and 01001100.*

- $B \leq (C-(n-d)) \leq C$
  *Both the handover calls and the new users call will be allowed.There should be no problems at this stage and the transfer vector **d** will be released and all the combinations of vectors **a** shown in table 1 should arrive to their destination safely.*

// It should be noted that all of these restrictions required to model the CAC can be incorporated either by setting the appropriate $\Xi(\mathbf{d})$to zero or by correlated routing. Both of these features can be incorporated in Henderson and Taylor's model without violating the product form result.

11 Conclusion

In this paper, we have proposed call admission control for wireless cellular mobile networks based on blocking mechanism. Blocking was achieved in the case of state independent routing as well as correlated routing. Prioritization of the calls in the system was discussed and the most priority was given to existing calls then handover calls and the last priority was given to the new users.

References

Henderson, W. and P. Taylor. 1990. ”Product-form in networks of queues with batch arrivals and batch services.” *Queueing Systems* 6, 71-88.

Henderson, W. and P. Taylor. 1991. ” Some new results on queueing networks with batch movement.” *J. appl. Prob* 28, 409-421

Moorman,J.R ; J.W. Lockwood and S. Kang. (2000). ”Real-time Prioritized Call Admission Control in a Base Station Scheduler.” *WOWMOM*.

Pujolle, G. 1995.” Product form in Discrete-time queueing networks: New issues.” *Laboratoire PriSM*, 148-153.

Perros,H.G. 1994. ” Queueing Networks with Blocking” *Oxford*.

Boucherie,R.J and N.M. Van Dijk. 1992. ”product-forms for queueing networks” *Phd. Thesis*.

Boucherie,R.J and N.M. Van Dijk. 1991. ”product forms for queueing networks with state dependent multiple job transitions.” *Adv. In appl. Probab*23, 152-187.

Thummler, A. 2003.” Stochastic Modelling and Analysis of 3G Moblie Communication Systems.” *Phd. Dissertation*, 15-20.

Woodward, M. 1998.” Product form solutions for discrete time queueing networks with bursty traffic.” *Electronic letters*17 ,1512-1514,

Balsamo, S. 1998.” A convolution algorithm for product-form queueing networks with blocking.” *Annals of Operation Research, Baltzer* 79 ,97-117, 1998.

Onvural,R.O. 1990.” Survey of closed queueing networks with blocking.” *ACM Computing Surveys (CSUR)* 22, 83-121, June 1990

[Perros,H.G. 1990.” Approximation Algorithms for the Analysis of Open Queueing Networks with Blocking.” *Chapter in: Stochastic Analysis of Computer and Communications Systems* ,451-498

Wireless Systems of the Future – Providing anywhere, anytime access to IT at an extraordinary high speed

A. Khan*, M. Al-Akaidi**, S. A. Khan*
**School of Engineering & Technology
De Montfort University, Leicester, LE1 9BH, UK
Email: mma@dmu.ac.uk
* COMSATS, Abbottabad, Pakistan

KEYWORDS
MIMO, SISO, WLAN, Communication

ABSTRACT

Multiple Input Multiple Output (MIMO) systems have evolved quickly to become one of the hottest research areas in wireless communication systems. By providing high capacities compared to their conventional Single Input Single Output (SISO) systems. In this paper we have reviewed the fundamentals of MIMO systems and explained why they became the researchers current attraction. We have simply explained the basic principles of MIMO systems, current challenges and limitations posed by developing them realistically.

INTRODUCTION

Basic purpose of the wireless communication system is to provide anywhere, anytime access to the user with the rest of the world. The current voice and low data services provided by the wireless devices is changing to advanced services of computer-data with Internet access, electronic mail, real-time image transfer, multimedia document transfer, mobile computing: telecommunications with mobility, video conferencing, video telephony: and audio/video-content with video on demand, infotainment, teleshopping, and value-added Internet services. For all these services systems supporting high data rate are essential.

Consequently many new mobile and Wireless Local Area Network (WLAN) standards are developed to provide high-speed access, supporting broadband services such as fast multimedia based applications, and Internet access. For example WLAN standards such as IEEE 802.11a and hiperlan/2 have the capability to provide wireless access with data rates up to 54 Mbps (Doufexi A.; S. Armour; M. Butler; A. Nix; D. Bull; J.McGeehan; and P. Karlsson. 2002)

Although much development have been made to increase the capacity of the systems but still multimedia based applications use several services like voice, audio/video, graphics, data and have e-mail services in parallel, which have to be supported by the radio interface. These high data rate requirements presents challenges to communication system researchers to find out new techniques that meet the current and future demands. One such breakthrough was first shown by J. Foschini in his papers (Foschini, G. J; and M. J. Gans. 1998; Foschini, G. J. 1996), where it was shown that data rates (i.e. capacity) could be improved dramatically of the system by changing conventional Single Input Single Output systems (SISO) to multiple Input Multiple Output (MIMO) systems. At no extra cost of power or spectral increase involved, which are the physical and/or the regulatory constraints.

In this paper research work done within the MIMO field to date i.e. transmission schemes for MIMO systems, space time codes and channel models are overviewed briefly with references to number of key papers and literature for all those who intend to study the area in depth. Finally paper concludes with future challenges within the area.

Format of the paper is: first of all basic principles of MIMO systems are discussed, then Space Time Codes used to increase the performance of MIMO systems are explained, after this briefly the channel models for MIMOs are overviewed, current challenges and limitations are discussed next, and finally the paper is concluded with future work and current challenges within the area.

BASIC PRINCIPLES OF MIMO SYSTEMS

MIMO systems are simply defined as: given an arbitrary wireless communication system, a link that has its transmitting end (Tx) as well as the receiving end (Rx) equipped with multiple antenna elements (Gesbert D; and J. Akhtar. 2002), as depicted in Figure 1.

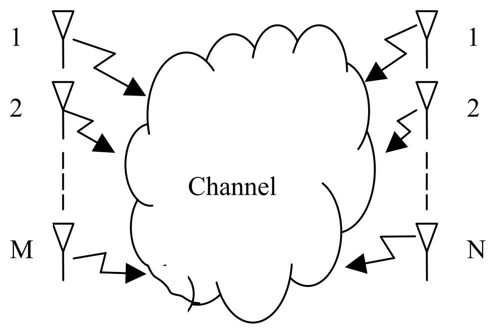

Figure 1: MIMO wireless system with M transmit and N receive antennas

Conventional wireless systems are mostly SISO systems, but some of them use multiple antennas at one end of the wireless link to achieve spatial diversity, and in the wireless terminology it is known as smart antennas (Gesbert D; and J. Akhtar. 2002). It was after the publication of two papers (Foschini, G. J; and M. J. Gans. 1998; Foschini, G. J. 1996), it was first shown that MIMO systems could provide higher capacity to the system at no extra cost of transmit power and spectrum. Actually MIMO is the extension of smart antennas, but are used in a different way. Smart antennas are used to add space-diversity, while MIMO systems are used to achieve greater capacity, and offer benefits that go beyond the smart antennas (Sheikh K; D. Gesbert; D. Gore; and A. Paulraj. 1999).

MIMO to gives greater Capacity

Channel capacity is defined as the maximum bit rate that could be transmitted over a channel, with arbitrarily low bit error rate. As a rule of thumb reported in (http://www.telenor.no/fou/ publisering /Not01 / nr5_2001.PDF) the average channel capacity of a MIMO system that uses n, number of antennas at both ends of a link is approximately n times higher than that of a SISO system for a fixed bandwidth and a fixed overall transmitted power. Good tutorial on the MIMO capacity gains over a SISO could be found in (Holter B. 2001). Here we will limit ourselves to the basic working principles of MIMO systems. Figure 2 shows one of the transmission scheme known as spatial multiplexing (SM) to achieve high data rates in MIMO systems. As shown in the figure high data rate is decomposed into three independent bit sequences (b_1, b_2 and b_3) which are then transmitted simultaneously using multiple antennas. Within the wireless channel simultaneous signals mix together because they all use same spectrum. Under rich multipath conditions signals could be recovered by first identifying the channel through training symbols and then separating the individual data streams. It is done in the same way as three unknowns are solved for three independent linear equations. Independency comes from a rich multipath channel, and is vital in order to separate the data bits. It is not the only way that MIMO systems could be used more generally transmission techniques of MIMO systems could be classified as one to improve the capacity (i.e. SM) and the other to improve spatial diversity (SD). Obviously performance of the system will be better if spatial diversity transmission schemes are used.

Performance of the multiplexing scheme however could be increased by jointly encoding the individual streams. If the level of joint encoding is increased then multiplexing scheme will tend to SD and multiple antennas will only be used to achieve SD (Gesbert D; M. Shafi; D. Shiu; and P. Smith. 2003).

Best transmission technique would compromise between the SM and SD. Schemes that allow to adjust and optimize joint encoding of multiple transmit antennas are called space time codes (STC) discussed in next section. A part from the SM and SD schemes there are hybrid techniques developed that switches between SM and SD over the time (Skjevling H; D. Gesbert; and N. Christophersen. 2003) to provide optimum results. For more details on SM and AD see (Zheng L; and D. N. C. Tse. 2003).

Space Time Codes

STC are the channel encoding techniques that jointly encode the individual streams in MIMO systems to achieve the compromise between the SM and SD (Lucent; Nokia; Siemens; and Ericsson. 2001). There exists quite a number of STC that could be classified as Space Time Trellis Codes (STTC), and Space Time Block Codes (STBC). STTC were shown to provide a diversity benefit equal to the number of transmit antennas without any loss in bandwidth efficiency. However STTC are complex and are computationally hungry. Problem of complexity was solved with the introduction of STBC, which only require a decoder that is much simpler and had linear operators at little loss of performance. Two of the most famous STBC codes to date are based on the work of Alamouti (Alamouti, S. M. 1998), and V-BLAST (Vertical Bell Labs Layered Space-Time) (Foschini, G. J. 1996). Alamouti based STBC are biased towards maximizing the diversity, on the other hand V-Blast achieves spatial multiplexing. A good paper summerizing the STBC could be found in (Naguib A; N. Seshadri; and R. Calderbank. 2000), and details on code construction in (Tarokh V; N. Seshadri; and A. R. Calderbank. 1998; Damen1, M. O; A. Tewfik;, and J. C Belfiore. 2002). Some work has also been done in the concatenation of conventional channel codes (e.g. RS, Hamming) with that of STC. It has been shown in (Berthet, A. O; and R. Visoz. 2003) that concatenation of codes gave better results.

MIMO Channel Modelling

To design a MIMO communication system and to predict its performance requires an accurate MIMO channel models. Channel models can be classified into number of ways as wideband models vs. narrowband models, field measurements vs. scatterer models, and non-physical models vs. physical models to name a few. Further details related to these classifications and different MIMO channel models could be found in the PhD thesis (http://www.s3.kth.se/~kaiyu/Licentiate.pdf), and standardised MIMO channel models for broadband wireless access and 3GPP (Lucent; Nokia; Siemens; and Ericsson. 2001) for mobile applications in IEEE 802.16 (http://standards.ieee.org).

Current challenges and Limitations

Real achievements of MIMO depends on the highly decorralated reception at the receiver antennas. That will result in independent set of linear equations at the receiver. Independent equations are solved to separate the mixed data due to simultaneous transmission using multiple antennas.

In MIMO terminology *rank* of the MIMO channel is define as the number of independent equations that could be received. The number of independent signals that one may safely transmit through the MIMO system is at most equal to the rank.

Therefore techniques are needed to achieve maximum decorrelated reception.

One way to achieve it is by spatially separating antennas at both ends of the link (http://www.telenor.no/fou/publisering/ Not01/ nr5_2001.PDF). However, for small handheld devices (e.g. mobile phones) the amount of antenna spacing that can be achieved is highly constrained.

Another problem of size, cost and power consumption of mobile terminal occurs while increasing the MIMO performance using STC. As good STC such as STBC providing simplicity in decoding are shown to be limited to the case of two transmit antennas, data rate or decoding simplicity must then be sacrificed if the number of antennas is increased. Hence new STC needs to be developed that are low in complexity and offer good performance.

Conclusion and Future Work

In this paper an overview of the emerging wireless technology i.e. MIMO communication systems using multiple transmit and receive antennas is presented. Channel capacity study using MIMO reveals that this technology is capable of providing greater advantages compared to that of conventional SISO systems at no extra cost of power and spectrum utilisation. Consequentially MIMO systems will enable high speed mobile Internet access, enhanced capacity wireless local loops, wireless high definition video transport, and other exciting opportunities. Such systems will be a key technology for future wireless systems, leading to higher capacity dimensions.

Whether we achieve this fully or at least partially in practice depends on the usage of transmit and receive signal processing techniques. Real success of MIMO depends on integrating this technique into the existing and future wireless standards. More future work is needed to find out new techniques that allow us to compromise between the SD, and SM, the optimum number of antennas required, antenna arrays spacing and their selection methods, therefore, further research in channel models of real environments is required so that benefits of MIMO and corresponding signal processing techniques could be exercised out realistically.

Finally we have concluded that it can be said that the MIMO systems will provide future communication systems at dramatically higher data capacities using the same bandwidth and transmit power as used today by a SISO systems. However, to date a lot of work needs to be carried out in practically implementing these systems to current as well as upcoming standards.

References

Alamouti, S. M. 1998 “A simple transmit diversity technique for wireless communications". *IEEE J. Sel. Areas Comm.*, vol. 16, pp. 1451-1458, (Oct).

Berthet, A. O; and R. Visoz. 2003. “Iterative Decoding of Concatenated layered Space-Time trellis Codes on MIMO Block fading Multipath AWGN Channel”. *IEEE Trans on Communications* vol. 51, no. 6, pp. 940-951, (June).

Damen1, M. O; A. Tewfik;, and J. C Belfiore. 2002. “A Construction of a Space-Time Code Based on Number Theory”. *IEEE Trans on Information Theory*, VOL. 48, NO. 3, (March).

Doufexi A.; S. Armour; M. Butler; A. Nix; D. Bull; J.McGeehan; and P. Karlsson. 2002. "A comparison of the HIPERLAN/2 and IEEE 802.11a wireless LAN standards". *IEEE Communications Magazine*, vol. 40, no. 5, pp. 172--180, (May).

Foschini, G. J; and M. J. Gans. 1998. “On limits of wireless communications in a fading environment when using multiple antennas". *Wireless Personal Communications*, vol. 6, pp. 311-335, (March).

Foschini, G. J. 1996. “Layered space-time architecture for wireless communication". *Bell Labs Technical Journal*, vol. 1, pp. 41-59, (Autumn).

Gesbert D; and J. Akhtar. 2002. “Breaking the barriers of Shannon’s capacity: An overview of MIMO wireless systems”. *Telektronikk. Telenor’s Journal*, (Jan).

Gesbert D; M. Shafi; D. Shiu; and P. Smith. 2003. “ From theory to practice: An overview of space-time coded MIMO wireless systems**".** *IEEE Journal on Selected Areas on Communications (JSAC),* vol 21.

Holter B. 2001. "On the Capacity of the MIMO channel- A Tutorial Introduction," *in Proc. of IEEE Norwegian Symposium on Signal Processing*, pp.167-172, Trondheim, Norway, (Oct.18-20).

Lucent; Nokia; Siemens; and Ericsson. 2001. "A standardised set of MIMO radio propagation channels," *3GPP TSG-RAN WG123*, vol. Jeju, Korea, (November 19-23).

Naguib A; N. Seshadri; and R. Calderbank. 2000. "Increasing data rate over wireless channels". *IEEE Signal Processing Magazine*, (May).

Sheikh K; D. Gesbert; D. Gore; and A. Paulraj. 1999. "Smart antennas for broadband wireless access". *IEEE Communications Magazine*, (Nov).

Skjevling H; D. Gesbert; and N. Christophersen. 2003. "Combiing Space Time Block Codes and Multiplexing in Correlated MIMO Channels: An antenna assignement strategy". *Proc. of Nordic Signal Processing Conference (NORSIG)*.

Tarokh V; N. Seshadri; and A. R. Calderbank. 1998. "Space-Time Codes for High Data rate wireless Communication: performance Criterion and Code Construction". *IEEE Trans on Information Theory*, vol. 44, No. 2. (March).

Zheng L; and D. N. C. Tse. 2003 "Diversity and Multiplexing: A Fundamental Tradeoff in Multiple-Antenna Channels". *IEEE Trans on Information Theory*, vol. 49, pp. 1073-1096, (May).

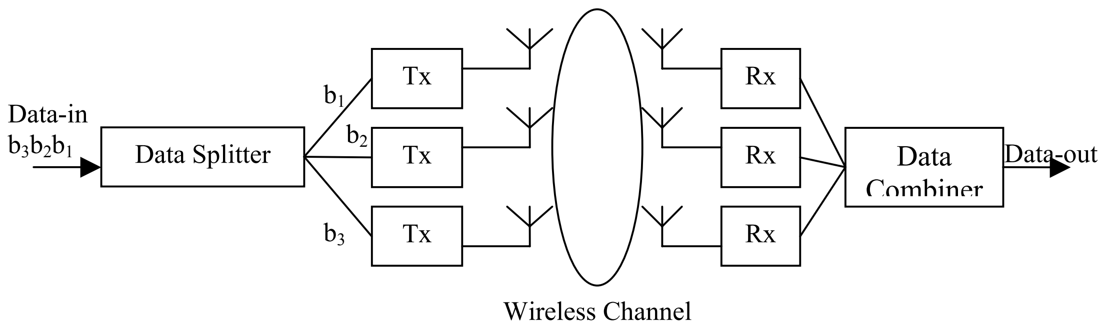

Figure 2: Spatial Multiplexing in MIMO systems

MODELLING AND SIMULATION FOR INDUSTRIAL APPLICATIONS

A Bi-LEVEL PETRI-NET BASED APPROACH FOR MODELING AND SCHEDULINF OF MULTIPURPOSE BATCH PLANTS

Mahsa Ghaeli
Department of Chemical Engineering,
Curtin University,
Bentley, WA, Australia

Parisa A.Bahri
School of Engineering,
Murdoch University
(Rockingham Campus),
Murdoch, WA , Australia

Peter Lee
Division of Science,
Engineering and Computing, Curtin University, Bentley, WA, Australia

KEYWORDS
Scheduling, Optimisation, Linear programming, Decision making, Operation research.

ABSTRACT

This paper presents a Petri net based approach for the modeling and scheduling of a multipurpose batch plant with the objective of maximizing profit.

The graphical and mathematical properties of Petri nets make them very practical in modeling of many chemical industries. The main aim of this paper is to present a Petri net model as an applicable tool for modeling and scheduling of multipurpose plants. This paper begins with a general description of the issues discussed later in the paper. It proceeds with giving some background to the concept of Petri nets. Then, a novel approach for achieving the best schedule of a multipurpose plant wile maximizing profit is presented. Finally, a case study is simulated in order to illustrate the effectiveness of the proposed approach.

INTRODUCTION

The Petri net model was first introduced by Carl Adam Petri in 1962 in his PhD thesis (Murata 1989). A Petri net is populated by four types of objects: Places, Transitions, Directed Arcs and Tokens. Each place represents a resource, while a transition illustrates an event. The availability of that condition is depicted by tokens. Directed Arcs are used to connect places (transitions) to transitions (places). Petri nets as a graphical and mathematical tool provides an applicable environment for the modeling and design analysis in many systems. As a graphical tool, it assists to visualize the complex systems similar to a flow chart. As a mathematical tool, Petri nets can be used to formulate and solve modeling, control and scheduling problems. Characteristics of Petri nets make it very practical for many industries.

The main benefit of Petri nets is that the same model can be used for the analysis of behavioral properties and performance evaluation, as well as for the systematic construction of discrete event simulators and controllers (Ghaeli et al. 2003).

Scheduling with the meaning of allocating jobs to resources is a very important issue in many chemical industries and has a direct effect on their efficiency. The optimization criteria, based on which the schedule is being defined, is different from one industry to the other and it can range from minimizing a makespan (the latest finishing time) to maximizing the facility utilization or profit. Recently, Timed Place Petri Net (TPPN) has been used for scheduling of multiproduct and multipurpose plants with the objective of minimizing the makespan (Ghaeli et al. 2003 ; Gu et al. 2001). This paper extends the application of TPPN to the modeling and scheduling of a multipurpose chemical plant with defined production time and the objective of maximizing profit. A case study is taken from Karimi (1991) in which the problem is to find the best schedule with the maximum profit based on the corresponding constraints. In order to solve this problem, first the example is modeled through TPPN. Then, an optimization algorithm is used to find the best production time for each product that maximizes the profit, given the specific total time. Finally, based on the optimal production time achieved in the optimization algorithm, the best schedule with the minimum total makespan is derived through the associated TPPN model.

The results are represented to demonstrate the validity of the proposed algorithm and the improvements made on previous work in this regard.

WHAT IS A PETRI NET?

A Petri-net is a particular kind of bipartite directed graph. Each Petri net is represented by Places, Transitions and Tokens, which are respectively illustrated by circles, bars and small dots. Places and transitions are connected through arcs. If there is a directed arc, which connects a place to a transition, then this place is an input for that transition and if the transition is connected to a place through a directed arc, this place becomes an output for that transition. Each place may potentially hold zero or a positive number of tokens, pictured by small dots. The distribution of tokens in places is referred to as the marking. The transition's firing renders the tokens being redistributed, resulting in a new marking. The places are used to show the condition or the availability of the resources when they contain one or more tokens. These resources can be either a machine or raw material. The transitions represent the start or completion of an activity (operation) and they are depicted by empty rectangles or solid bars. To demonstrate the dynamic behavior of the system, tokens are introduced, in which they allow one to visualize the flow of the materials through the firing of the transitions in each state.

The model specifies which resources should be shared and also defines the precedence relations between activities (Zhou 1993). In order to create a Petri net model, first the activities and required resources for each activity should be identified. Second, for each activity (O_{ij}), one place one place should be assigned to show the status of the associated activity, for example p_{ij} shows the processing of product i in unit j. The start (t_{sij}) and stop (t_{fij}) points of this activity are shown by two transitions at the two sides of the place, as illustrated in Figure 1. Third, by considering the precedence relationships between activities, they should be connected together, in which the final point of one activity will be the start of the other activity, as shown in Figure 2. Fourth, the resources (including the shared ones) should be connected to the associated activity by using arcs. This is shown in greater detail through case study.

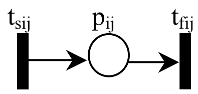

Figure 1: processing activity O_{ij}

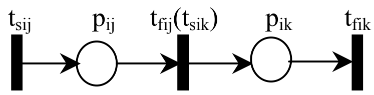

Figure2: processing activity O_{ij} and processing activity O_i

A Petri net is executed by firing the enabled transitions. A transition is enabled when each of its input places is marked with at least one token. When a transition fires, a token of the input places associated to the transition is removed and added to the output places of the following transition.

In order to extend the application of the Petri net to the complex systems, several types of Petri nets have been developed. One example is the timed Petri nets (Ramchadani 1974) , which has many applications in chemical plants. Usually the evaluation of a plant is done based on the production time. Time can be introduced into the Petri nets by relating it to either the places or transitions. If the time is associated with the transitions, the Petri net is called Timed Transition Petri Net (TTPN) and if the time is introduced to the places, it results in Timed Place Petri Net (TPPN) (Ghaeli et al. 2003).

SCHEDULING OF A MULTIPURPOS BATCH PLANTS WITH THE OBJECTIVE OF MAXIMIZING THE PROFIT

Nowadays, scheduling is a very common issue in almost all the industries. Moreover, finding the best way of assigning different jobs to different processing units does not only optimize the utilization of the resources but also improves economy. This confirms the reason that finding a good method for scheduling has become a very significant concept in most industries. Usually, scheduling of a plant is done for a specific period of time; this time can be varied from one week to one year and it depends on the planning of the plant.

Characteristics such as liveness, boundness, reversibility and mutual exclusion make Petri nets a very useful model for application in chemical industries. TPPN has been recognized as a promising tool for modeling and scheduling of these industries. One good feature of Petri nets is that the same model can be used for modeling and scheduling of the plant and the schedule can be observed step by step as the products pass through the processing units. Each time the sequence of firing transitions defines the route of the schedule.

In this paper an endeavor has been made to extend the application of Petri nets to a multipurpose batch plant with the objective of maximizing profit. To solve this, the problem is divided into two parts, which includes first, applying an optimization algorithm and second, employing a Petri net based scheduling algorithm to find the best schedule with the minimum total makespan. The following algorithm shows the sequence of these steps.

Step 1: Using the optimization algorithm to find the best production time for a defined total time
Step 2: Modeling of the plant using TPPN
Step 3: Finding a schedule by firing of the transitions in a Petri net model
Step 4: If the production time of any unit is bigger than the available total time go to step7
Step 5: If the total time is bigger than the makespan go to the step 7
Step 6: Update the makespan
Step 7: Check if assessing of all the schedules have not been finished go to step 3
Step 8: End

The optimization algorithm, used in this paper, is Newton Raphson and is implemented in the C language (Lawrence et al. 1997). The best time for each product within a defined total time is resulted from this algorithm. These results are then assigned to the places in the Petri net model to be used in the second part. In this part, each schedule is derived based on the sequence of firing transitions and the optimum time achieved from the optimization algorithm. Branch and bound search methods is used to find the optimal schedule. To reduce the number of searches, heuristic method is used to eliminate the unnecessary branches. As soon as the time of the unit exceeds from the defined total time, or the total time/the total remaining time becomes bigger than the current total makespan, further search of that branch stops and the assessment of another branch begins. Every time, the total makespan is updated by the smaller one. This search is repeated until the assessment of all branches is completed and the optimal schedule with the minimum total makespan is achieved.

The optimal schedule is the one with the minimum total makespan, which results in the maximum profit of the corresponding industry in a defined total time. The smaller the total makespan, the shorter the delay is between the processing of the products, which results in a better usage of resources over the long term.

CASE STUDY

To show the capability of the proposed algorithm, the method has been tested against a case study by Karimi (1991), which is a multipurpose plant with 3 products and 2 processing units. There are two ways to produce the first two products and three ways to produce the third product and the total available time is 700 hours. All the information about the batch sizes, profit and maximum and minimum demand of each product has been written in Table 1. The aim of this problem is to find the optimal schedule with the maximum profit. In the original example, the processing time for each product has been given but not the processing time in each unit. In order to solve this problem with the proposed method, the time that each product spends in a unit should be given. Both optimization and scheduling algorithms are implemented in Visual C++ 6.0 on a PC/Pentium 4.

Solution: The TPPN model of this example is shown in Fig3. After formulating the optimization algorithm and the related constraints, the following results have been achieved for the optimal production time:

Product1 with the first route : 116.6
Product1 with the second route : 125.0
Product2 with the first route : 227.4
Product2 with the second route : 264.2
Product3 with the first route : 340.2
Product3 with the second route : 310.7
Product3 with the third route : 355.9

Then based on the above results, the optimal time that each product should spend in each unit for the available total time of 700 hours is calculated (Table 2) and assigned to the places in the TPPN. These times are passed to the scheduling algorithm to define the optimal schedule with the minimum total makespan. The resulting Gantt Chart is illustrated in Fig 4.

Table 1: The data for the case study

Product Routes		Units		Batch Data			Demands		Profit
Product Name	Route No.	Task 1	Task 2	Batch Size	Time of Task 1(h)	Time of Task 2(h)	Min (Mg)	Max (Mg)	$/kg
A	1	3	5	2500	4.2	2.0	100	150	1.0
	2	2	4	2000	3.0	2.4			
B	1	3	5	1670	3.0	1.8	250	300	0.8
	2	2	4	1330	2.0	2.0			
C	1	1	-	500	3.2	-	150	200	0.5
	2	2	-	1000	4.9	-			
	3	3	-	1500	6.4	-			

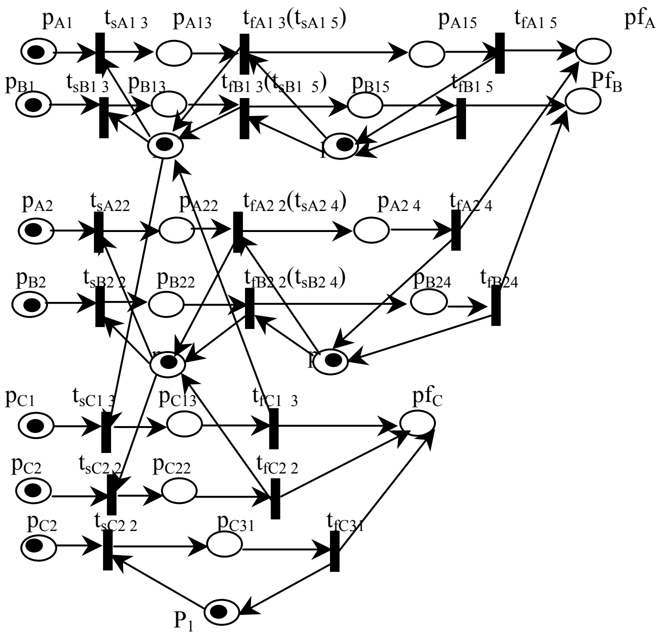

Figure 3: The TPPN Model of the Case Study

Table 2: The Data for The Case Study

Product Routes		Units		Time	
Product Name	Route No.	Task 1	Task 2	Time of Task 1(h)	Time of Task 2(h)
A	1 2	3 2	5 4	113.4 120.0	54.0 96.0
B	1 2	3 2	5 4	225.0 262.0	135.0 262.0
C	1 2 3	1 2 3	- - -	352.0 308.7 339.2	- - -

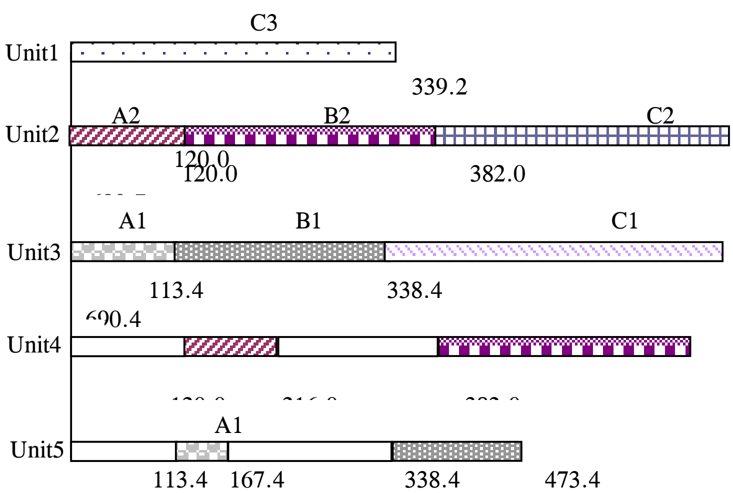

Figure 4: The Gantt Chart of the best schedule of the case study

Karimi(1991) has solved this problem by manually dividing it into several campaigns in which the resources have not
any relations to each other. Then the LP solver in GAMS is used to find an optimal solution. The Petri net model is eligible to recognize the units with no relations and there is no need to determine the campaigns.

CONCLUSION

Finding a schedule, which satisfies all the constraints related to the processing of the products in chemical industries and leads to maximum profit, is one of the most important considerations in these industries.

Petri nets as a modeling tool has become a new horizon for easing the scheduling in many industries. The graphical characteristic of Petri nets helps the designers to better understand and formulate the scheduling problems.

This paper has shown that modeling a multipurpose batch plant by TPPN facilitates scheduling and simulation of the plant. The applicability of the developed algorithm to chemical industries is illustrated through a case study. The simulation and scheduling results are also presented.

REFERENCES

Ghaeli, M., Bahri, P.A., Lee, P. and Gu, T. (2003). "Petri-Net Based Formulation and Algorithm for Short Term Scheduling of Batch Plants", Revised version submitted to *Computers and Chemical Engineering*, (August 2003).

Gu, T., Bahri, P.A. (2001). "A survey of Petri net applications in batch processes", *Computers in Industry*, **47**, 99-111, (2001)

Karimi, I. (1991). "Production Planning in Multipurpose Batch Plants", *Chemical Engineering Optimization Models with GAMS*, **6**, (1991).

Lawrence, C., Zhou, J.L., Tits, A.L. (1997). " User's Guide for CFSQP Version 2.5: A C Code for Solving (Large Scale) Constrained Nonlinear Satisfying All Inequality Constraints", TR-94-16r1, (1997)
Murata, T. (1989) "Petri nets: Properties, Analysis and Applications", IEEE, **77**, (1989).
Ramchandani, C. (1974). "Analysis of Asynchronous concurrent systems by timed Petri nets", MIT MAC-TR-120, (1974)
Zhou, M. (1993). "Petri Net Synthesis for Discrete Event Control of Manufacturing Systems", Kluwer Academic Publishers, (1993)

Prototype Simulation of Contactless Diameter Measurement of Metal Bars and Tubes

Dr. Tahseen RAFIK[1], Klaus NEUMANN[2], Ivan JORDANOV[3] and Taher GALOUZ[1]
[1]School of Product and Engineering Design,
University of Wales Institute, Cardiff, Cardiff, UK
[2]Physics Department, Loughborough University, Loughborough, UK
[3]De Montfort University, Milton Keynes, UK

KEYWORDS
Quality Control, Contactless Diameter Measurement, Automation.

ABSTRACT

This paper discusses a prototype simulation of Contactless Diameter Measurement System. The Contactless Diameter Measurement is a technique used for measuring the diameter of a conductive material with circular cross section area (e.g., wires, bars, nails, tubes etc) without making any physical contact with the material itself. This measuring system could be useful as a Quality Control monitoring system to detect fluctuations in the diameter of manufactured wires, bars or nails without disrupting the manufacturing process. The simulation has involved the design, construction and testing of a prototype system to extract a relation between the diameter of different metals, both solid bars and hollow tubes, and its response to stimulating signals. Results of simulation proved the feasibility of the system in detecting any fluctuations in the diameters of metal bars and tubes.

INTRODUCTION

In manufacturing, measuring the diameter of a metal products with circular cross-section area is considered to be one of the most important quality control activities. This includes the manufacturing of wires, nails, metal tubes and many more. Using manual measuring technique in such situation is impractical because it is slow and time consuming. Many attempts have been made to automate the monitoring of the diameter of manufactured wires without disrupting the manufacturing process but these systems are either complicated to set-up or very expensive [Arque, 1972].

In the last three decades, a method was developed in solid state physics research to measure the resistivity of material knowing its dimension without making physical contact with the material itself. It was mainly developed for solid state physics research and manufacturing. The principle of this technique is based on applying a pulsed magnetic field to the sample. This will cause eddy currents to be generated on the sample the amount of which depends on the resistivity of the material and its dimension. By picking up the field that these currents generate and analyse the signal, the resistivity of the material can be extracted if the dimension of the sample is known [Schippan, 1997, Bean, 1976].
This research is based on the idea of using the principle of the contactless measurement of electrical resistivity for developing contacless diameter measurement. We are suggesting using the same principle of contactless resistivity measurement but instead of measuring the resistivity of the sample knowing its dimension, we are investigating the possibility of measuring the dimension knowing the metal resistivity.

PROTOTYPE SYSTEM'S SIMULATION

The prototype system operates by applying high current pulses to the excitation (primary) coil. These pulses will create a pulsating magnetic field, which in turn, causes eddy currents to flow in the sample. The field of these currents is picked by a pick-up coil placed too close but not in contact with the sample. The signal from the pick-up coil is then applied to a PC-controlled digital storage scope, which sample the signal and pass it to the PC for storage and further processing. Then the simulation will start and the final results will be shown in different graphs.

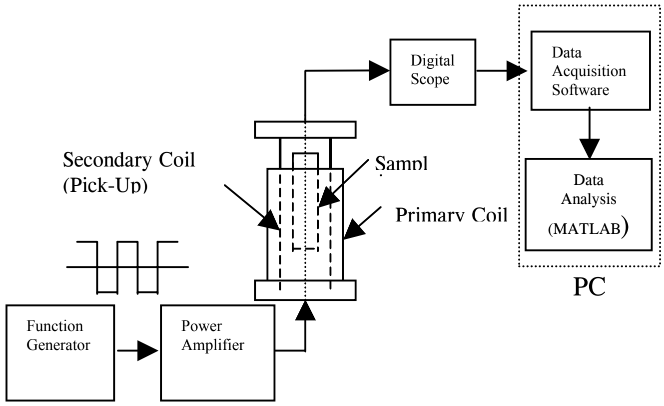

Figure 1: Prototype Simulation System for Contactless Diameter Measurement

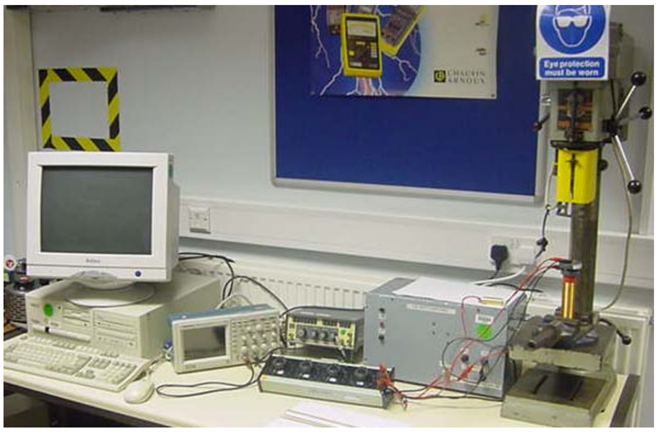

Figure 2: Photograph of the prototype System.

Figure 1 shows the block diagram of the prototype simulation of contactless diameter measurement system and figure 2 shows a photograph of the system. The prototype system consists of the following main parts:

- Signal Generator to supply a square wave.
- A power amplifier to amplify the square wave signal.
- An excitation coil (primary coil) to provide the pulsed magnetic field (Figure 2a).
- A secured sample holder to hold the sample securely in its place while the experiment is carried out (Figure 3b).
- A pick up coil to pick the signal generated by the eddy currents flowing in the sample (Figure 2b);
- A PC-controlled data capture system.

The simulation is carried out firstly with no sample in the sample holder. The signal obtained from this test (figure 4) is used as a reference for the further processing when a sample is inserted in the sample holder.

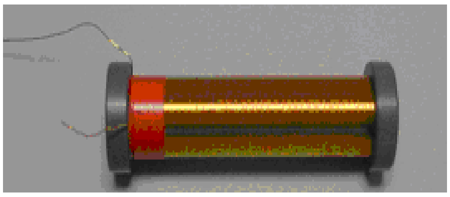

Figure 3a: Excitation Coil (Primary)

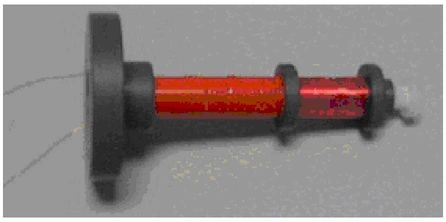

Figure 3b: Sample Holder and Pick-up Coil

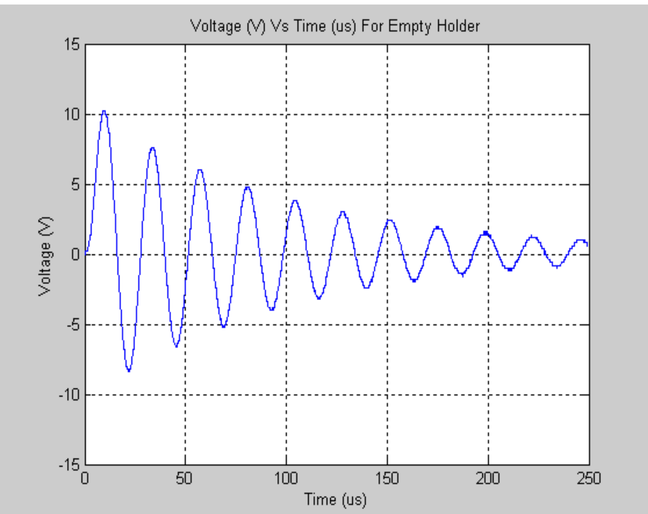

Figure 4: the results of the pick up coil with No Sample

Two processing methods were simulated to extract a relation between the picked-up signal and the diameter of the samples. These are:

1. Direct Processing of Time Domaim Signal

The peak voltages and their corresponding times are recorded for each sample. A constant is then calculated by referring these peaks to their corresponding no sample peaks using the following equation:

$$C_i = \left(\frac{1}{t}\right) \ln\left(\frac{P_i^{\,0}}{P_i^{\,k}}\right) \qquad (1)$$

Where,

C_i Is the Calculated constant for each peak or dip,

t Is time (ms),

P_i^0 Is Peak or dips value when there is no sample,

P_i^k Is Peak or dips value when there is a sample,

k Is sample number from 1 to 5 and

i Is Peak or dip Number from 1 to 8

2. Convolve the No-sample Signal with Sample Signal

In this method we convolved the signal with no sample with the signal when a sample is inserted in the sample holder. The typical result of convolution is shown below.

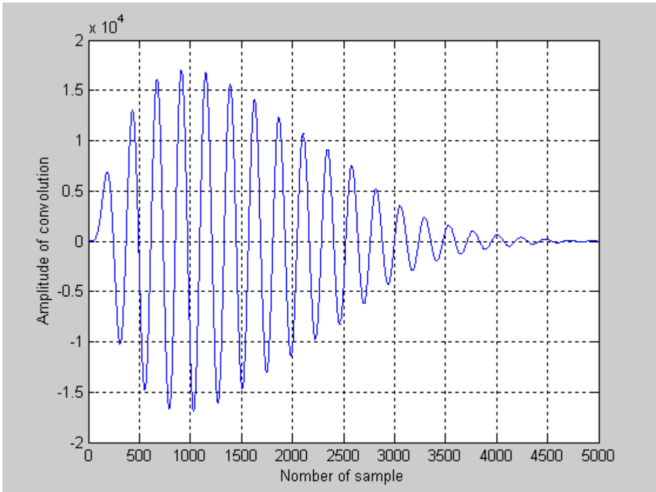

Figure 5: Result of Convolution.

We then search for the maximum value of this result and relates it to the diameter of the sample.

SIMULATION

The two methods described above have been simulated using Matlab. The following samples were used:

Table 1: Diameters of the Selected Samples

Sample type	**Diameter (mm)**				
Brass samples	3.60	4.00	4.70	5.28	6.28
Aluminium samples	3.65	4.00	4.78	5.66	6.28
Aluminium tube	2.75	3.17	3.91	4.73	5.52
Brass tube	2.45	3.20	4.00	4.77	6.40

SIMULATION RESULTS

The relationship between the diameter and the calculated average constants is shown in Figures below. It is clear from the figures that there is a strong direct relationship between the diameter and the processed signal parameters.

Aluminium Bar Samples (Method 1)

Figure 6a below shows the simulated relation between the diameter of brass bars and the calculated constant using method 1. The relation is approximately a straight line (R^2=97%).

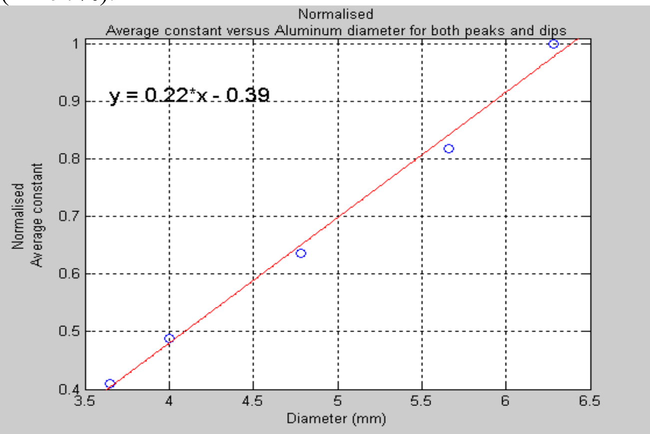

Figure 6a: Calculated Constant Vs Diameter for Aluminium Bars (Method 1).

The equation of the model is:

$$C_{i_{av}} = 0.22 * \left(D_{i_{AL}}\right) - 0.39$$

Where,

$D_{i_{AL}}$ Is the Diameter of the Aluminium sample

$C_{i_{av}}$ Is the Average constant calculated, from equation 1

The Sum of Squares Error of the model is,

$$SSE = 0.001346$$

The standard error of the estimate in the linear model fitting the five given give data points is,

$$\text{SEE} = \sqrt{\frac{SSE}{5}} = 0.016$$

The calculating correlation coefficient

$$R^2 = 0.97$$

Aluminium Bar Samples (Method 2)

Figure 6b shows the simulated relation between the diameter of brass bars and the maximum amplitude of the convolution function (Method 2). This result relation is approximately a straight line (R^2=99%).

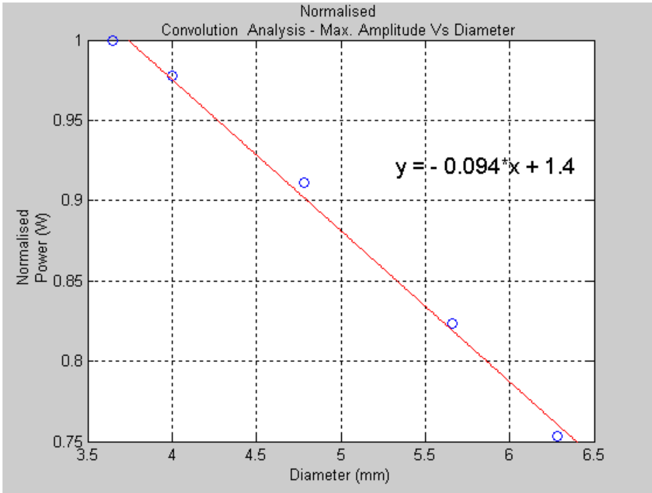

Figure 6b: Relationship between the Aluminum diameter and the maximum amplitude of convolution (Method 2)

$$V_{i_{AL}} = -0.094 * \left(D_{i_{AL}}\right) + 1.4$$

$D_{i_{AL}}$ Is Diameter of the Aluminium sample

$V_{i_{AL}}$ is Amplitude, from the convolution of data Aliminium sample

The Sum of Squares Error of the model is,

$$SSE = 0.0002787$$

The standard error of the estimate is: in the linear model fitting 5 give data points is,

$$\text{SEE} = \sqrt{\frac{SSE}{5}} = 0.0075$$

The calculating correlation coefficient is

$$R^2 = 0.9944$$

Aluminium Tube Samples (Method 2)

Figure 6c shows the simulated relation between the diameter of aluminium tubes and the maximum amplitude of the convolution function (Method 2).

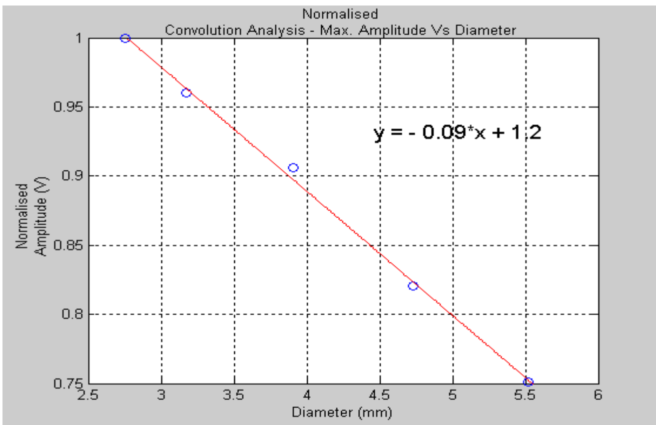

Figure 6c: Diameter Vs. Max. Amplitude for Aluminium tube Samples

Brass Bars Samples (Method 1)

Figure 7a shows the relation between the diameters of brass samples and the average calculated constant from the pick-up signals. Again a clear and measurable relation is demonstrated.

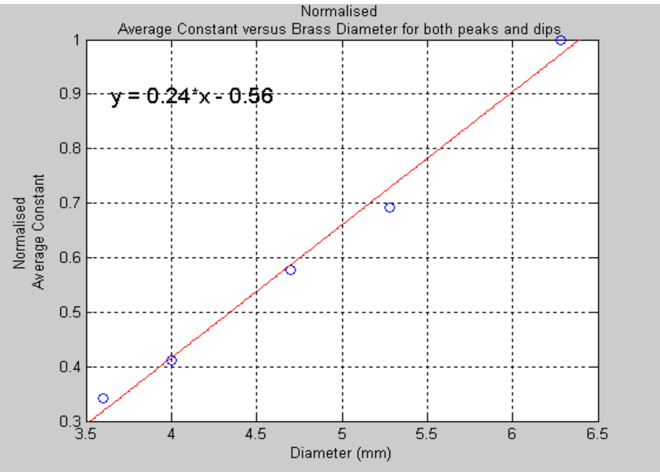

Figure 7a: Calculated Constant Vs Diameter for Brass Bars (Method 1).

The equation of the model is:

$$C_{i_{av}} = 0.24 * (D_{i_{Br}}) - 0.56$$

The standard error of the estimate in the linear model fitting the five given give data points is,

$$SEE = 0.023$$

The calculating correlation coefficient

$$R^2 = 0.97$$

Brass Bars Samples (Method 2)

Figure 7b shows the relation between the diameters of brass samples and the maximum amplitude of the convolution function.

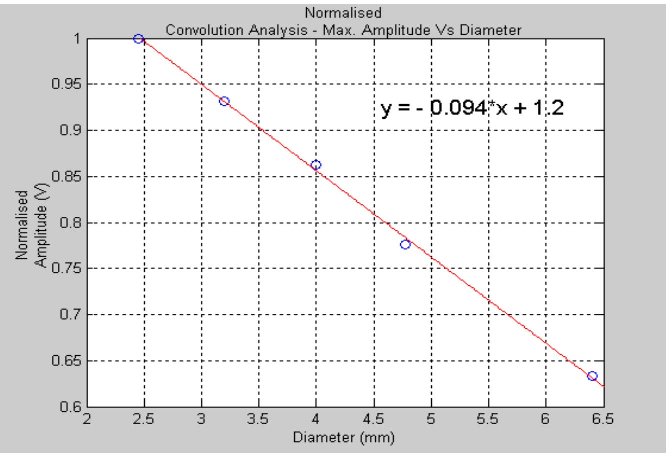

Figure 7b: Maximum Convolution Vs Diameter for Brass Bars (Method 2).

The equation of the model is:

$$V_{i_{Br}} = -0.09 * (D_{i_{Br}}) + 1.2$$

The standard error of the estimate in the linear model fitting the five given give data points is,

$$SEE = 0.005$$

The calculating correlation coefficient

$$R^2 = 0.996$$

Brass Bars Samples (Method 2)

Figure 7c shows the simulated relation between the diameter of brass tubess and the maximum amplitude of the convolution function (Method 2).

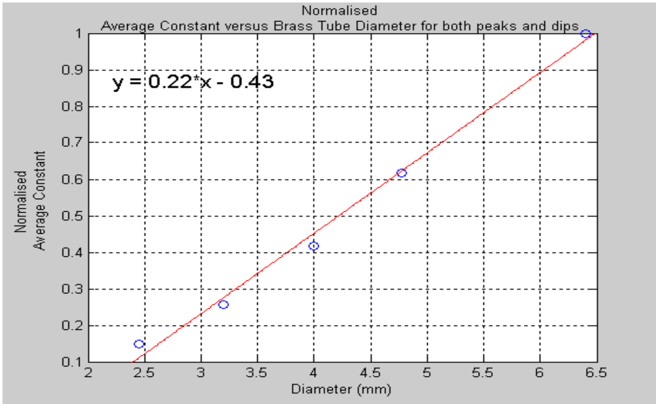

Figure 7c: Diameter Vs. Max. Amplitude for Brass tube Samples

Brass Bars with Different Diameters (Method 2)

Another simulation was carried out to test the resolution of the system by modeling diameter changes of brass bars as shown in figure 8 below.

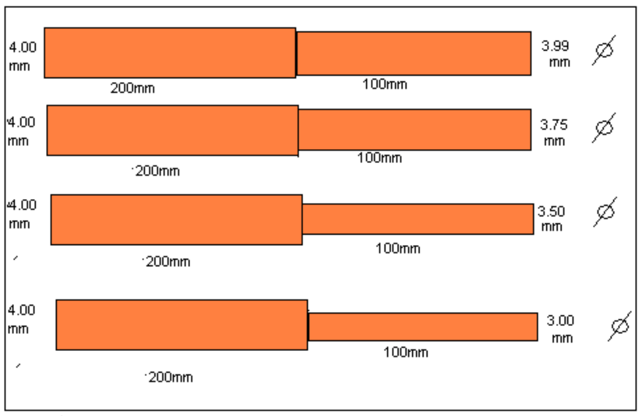

Figure 8: Brass Bars with diameter changes.

The results of this simulation using Method 2 is shown in figure 9. It is clear that the system was able to detect the diameter changes very accurately.

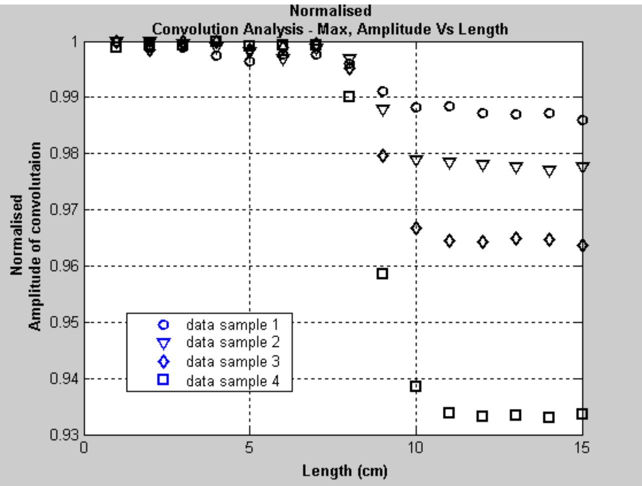

Figure 9: Results of simulating diameter changes of brass bars.

CONCLUSION

The prototype system for studying the feasibility of measuring the diameter of metallic materials with circular cross sectional area has been designed and built. The simulation of the output from the prototype systems has been developed and analysed. The prototype is based on the well-developed principles of contactless resistivity measurement commonly used in solid-state physics. The results obtained proved the feasibility of measuring the diameter of the sample without making physical contact with it.

REFERENCES

ARQUE, H, Callarotti and Schmidt P. 1972, "Theory of the measurement of thickness and conductivity of cylindrical shells by an inductive method", J. Applied Physics.

BEAN, DeBlois and Nesbitt 1976 "Eddy-current Method for measuring the resistivity of metals", J. Applied Physics.

JIEPING, Liu, 2002 "Active views on quality control in automated manufacturing" IEEE. USA. 3, pp 1617-31.

SCHIPPAN, F. 1997. "The Contactless Measurement of Electrical Resistivity", Master thesis, Physics Department, Loughborough University, Loughborough, UK.

ZHANG GY, 2002, "The measurement and control of diameter in large-scale part processing" Journal of materials processing technology, Switzerland, 129, pp1-3.

SIMULATION AND MODELLING OF LAYERED FLUID FLOW IN A RECTANGULAR MICROCHANNEL

Manisah Aumeerally and Renate Sitte
School of Information Technology
Gold Coast Campus
Griffith University PMB50
Gold Coast Mail Centre
Queensland 9726, Australia
E-mail: m.aumeerally@griffith.edu.au

KEYWORDS
Computer-aided design (CAD), MEMS, microfluidics

ABSTRACT

In this paper, we present the modelling of the flowrate of a rectangular microchannel using an electrical network. The aim of this study is to produce a fast first approximation of the flowrates of microchannels to be incorporated into microfluidic devices. It contributes to the physical component of our Virtual Reality-prototyping CAD tool for MEMS, with emphasis on fast calculations for VR representations. In our model, the flow is segmented into layers. The velocity of each layer is determined by solving numerically the Navier-Stokes equation and applying the no-slip boundary condition. The resistances of the layers are obtained from the velocity profile of the flow. The electrical network model is implemented in Matlab Simulink. The results are compared with finite element model software (ANSYS) and experimental data.

INTRODUCTION

The microchannel is an essential constituent of microfluidic devices such as chemical analysis systems, liquid dosing systems, biochips etc. Due to its manufacturing process, which employ IC technology, rectangular and square channels are relatively easier to produce than circular ones. The flowrate delivered by a microchannel is an important parameter.

MEMS design is costly because it is a lengthy and tedious process, especially the fine-tuning of the geometric sizes, which are critical for the correct functioning of the device and its manufacturability. For a micropump, this involves lengthy hours of finite element analysis (FEA) calculations just to get the approximate geometric dimensions of the structures. In our work, we try to shorten this time drastically, by producing fast first order approximations that lead to the approximate design of the device. From then on, fine-tuning is not only faster but cheaper, because less prototypes need to be built. For a more efficient prototyping phase, a cyclic sequence of steps of first order approximation modelling, followed by animated time scaled VR simulations, followed by re-adjustments of the geometry, helps to drastically reduce the cost and time for MEMS design.

In (TBendib et al. 2001) an approximation is made for rectangular microchannel of aspect ratio close to 1 by replacing the diameter of a circular channel by an equivalent hydraulic diameter. This technique however is subject to errors of order 10 to 20% (Sharp et al. 2002).

Electrical equivalent circuit has been used in the modeling and simulation of microchannels in micropumps as in (Morris and Forster 2000) and (Voigt and Wachutka 1998). In (Morris and Forster 2000), the concept of electrical equivalent circuit is applied to the whole microchannel. In (Voigt et al 1998) the channel is divided into small slices of equal length and each is described by an RLC circuit.

In our paper, the electrical circuit concept is applied to layers of fluid within the channel, so that the different flowrates can be visualized and the transient flow at the entrance of the channel can be demonstrated. The error for the flowrate is less than 10%.

Our aim is to apply a fast approximation technique in order to obtain the microchannel dimensions for a specific flow characteristics and to visualize this flow.

We solve the Navier-Stokes equation numerically to obtain the velocity profile. From here we determine the equivalent resistances and inductances. We also use the velocity profile obtained from the numerical solution to calculate the flowrate directly without the use of the electrical model.

LAYERED FLOW MODEL

Fluid flow in MEMS is laminar and characterized by low Reynolds number (Re). The flowrate is an important parameter for fluid flow in a microchannel. The concept of hydraulic diameter is traditionally used to characterise ducts with a single length scale. The hydraulic diameter D_H is defined as in (White 1994):

$$D_H = \frac{4 * w * h}{2(w+h)} \qquad (1)$$

where w is the width and h is the height of the cross-section of the channel. With the hydraulic diameter, the flowrate for a rectangular channel can be approximated using:

$$Q = \frac{1}{32}\frac{wh}{\mu l}\Delta P D_H^2 \qquad (2)$$

where ΔP is the pressure difference, l the length of the channel and μ is the dynamic viscosity of the fluid.

For circular microchannel the velocity is derived from the Navier-Stokes equation in cylindrical coordinates, which is easily solved analytically (Aumeerally and Sitte 2003). In what follows we present the numerical calculation for the derivation of the equivalent resistance for a rectangular channel.

To determine the equivalent resistance for laminar viscous flow in a rectangular microchannel, a numerical approach is required. The Navier-Stokes in cartesian coordinates reduces to (Panton 1984):

$$\frac{\partial^2 u}{\partial y^2} + \frac{\partial^2 u}{\partial z^2} = \frac{1}{\mu}\frac{\partial P}{\partial x} \qquad (3)$$

By substituting the following variable into equation (3):

$$u^* = \left[\frac{\mu}{\left(\frac{A^2}{4}\right)\left(-\frac{dP}{dx}\right)}\right]u \qquad (4)$$

we obtain the poisson's equation:

$$\frac{\partial^2 u^*}{\partial y^2} + \frac{\partial^2 u^*}{\partial z^2} = -1 \qquad (5)$$

where A is the length of the cross-section and B is the width of the cross-section of the channel.

Equation (5) is discretized using finite differences and the Dirichlet boundary condition is used. It is assumed that the no-slip boundary condition applies at the walls, where the velocity of the fluid is equal to zero. The program is written in MATLAB 6.5 and iterated 250 times with step-size 0.7 and error tolerance 0.001. The velocity profile is shown in Figure 1.

The average velocity $\bar{u}$ is Q/area, where Q is the volumetric flowrate. Using equation (4):

$$Q = \frac{dP}{dx}\frac{1}{\mu}\int_0^B\int_0^A u^* dydz \qquad (6)$$

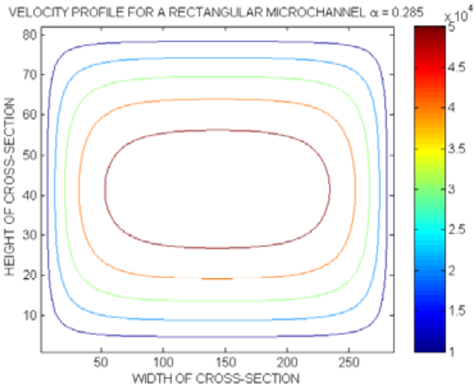

Figure 1 Velocity Profile for the Microchannel

For the lumped-element model of the mechanical effect of Poiseuille flow, using e→V convention, the resistance is given by (Senturia 2001):

$$R = \frac{across}{through} = \frac{\Delta P}{Q} \qquad (7)$$

Substituting equation (7) into equation (6), the resistance is given by:

$$R = \frac{\mu l}{\int_0^B\int_0^A u^* dydz} \qquad (8)$$

where μ is the viscosity of the fluid and l is the length of the microchannel.

To determine the resistances of each layer, the cross-sectional area is divided into 3 equal parts. The denominator in equation (8) is calculated using trapezoidal rule. The limits of integration depend on the cross-sectional area of each layer. The code is implemented in MATLAB 6.5.

ELECTRICAL CIRCUIT MODEL

To represent the flow of the different layers in the channel, we use parallel circuit components. The idea is to incorporate the whole as a Simulink model into our MEMS CAD prototyping tool, where Simulink provides a convenient design interface.

In our model, the current represents the volume flow, the voltage is the pressure difference, the resistance represents the viscous forces, and the inductance depends on the mass of the fluid.

The resistance is given by equation (8) and the inductance (L) is given by (Morris and Forster 2000):

$$L = \frac{\rho l}{S} \tag{9}$$

where ρ is the density of the fluid, l is the length of the microchannel and S is the cross-sectional area.

A branch consisting of a resistor and inductor in series represents each layer of the fluid. For the 3 layers of fluid, the model is given by Figure 2.

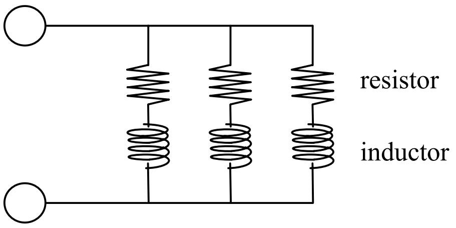

Figure 2 Three Layer Fluid Model

SIMULATION OF FLOW

Fluid entering a channel undergoes a period in which the velocity profile changes in the streamwise direction. For pressure-driven flow in a slot (Poiseuille flow), the profile is initially flat with the center slightly lower as shown in Figure 3. Further in the slot, the profile eventually reaches a parabolic shape and is fully developed. (Panton 1984)

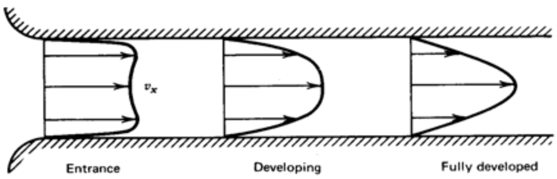

Figure 3 Velocity Profile for Poiseuille Flow

A step-function input represents the pressure increase at the microchannel inlet. For each branch of the RL circuit in Figure 2 the current is given by the equation (Ong 1998):

$$i(t) = \frac{1}{L}\int_0^t (V - iR)dt \tag{10}$$

where V is the voltage increase, i is the current, L the inductance and R the resistance. The integral equation (10) is implemented in Simulink (©Matlab) as shown in Figure 4.

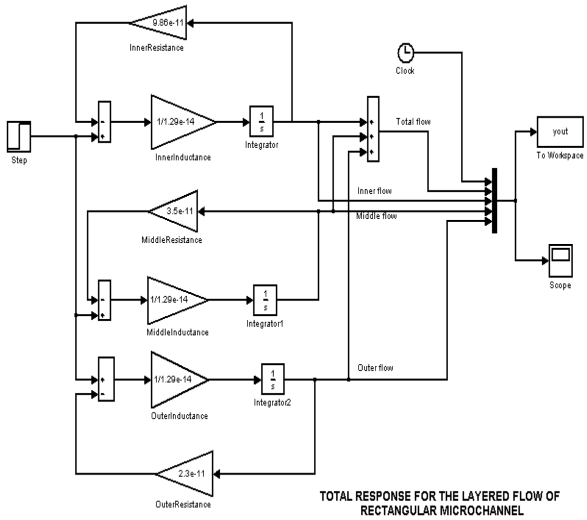

Figure 4 Simulink Model for the Total Response of the Flow to the Increase in Pressure

In Figure 5, the topmost curve is the response for the microchannel as a whole, the second curve from the top is the response for the innermost fluid layer, the third curve shows the response of the middle fluid layer and the lowest curve shows the response of the outermost fluid layer. The innermost fluid layer has the fastest flowrate while the outermost layer, which is closest to the walls of the channel has the slowest flowrate. From the results of the calculations the total flowrate is 5.13e8 $(\mu m)^3$/s, the innermost layer is 2.72e8 $(\mu m)^3$/s, the middle layer is 1.79e8 $(\mu m)^3$/s and the outermost layer is 0.64e8 $(\mu m)^3$/s.

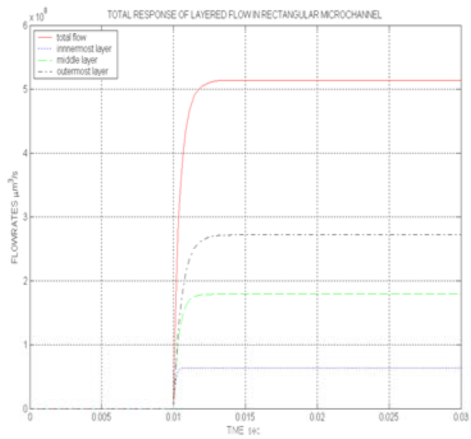

Figure 5 Total Response to Increase in Pressure

The transient part of the response is a very small portion of the total time. For the total flow, the transient time is 8.5 ms, the inner layer is 9.3 ms, the middle layer is 6.1 ms and the outer layer is 2.4 ms. The outermost layer, nearest to the walls, achieves its steady state much faster than the innermost layer. Initially the viscous shear stress affects mainly the particles of the fluid near the wall. Further into the channel, more particles away from the walls are affected as the pressure decreases and the velocity increase is slowed down. The innermost layer reaches its steady state at a longer time than the outermost layer. The response shown in Figure 5 reflects the transient behavior of the flow at the entrance region and the steady state flow in the fully developed region .

VALIDATION AND DISCUSSION

We use the experimental data from (Park et al 2003) to validate the total volumetric flowrate obtained from Simulink. The rectangular microchannel has a length of 48050 μm, height 57 μm and width 200 μm. A pressure difference of 6250 Pa is applied across the channel. The working fluid is deionized water at 25.5°C at which the density is 996 kg/m^3 and viscosity is 0.0009 Pa.s. The mass flowrate is 0.5 mg/s.

The experimental volumetric flowrate is compared with the total flowrate obtained from our Simulink model and an error of 2.19% is obtained. (See Table 1) The total flowrate is also calculated by using the hydraulic diameter concept as given in equations (1) and (2) above. This gives an error of 19.32%.

Table 1 Comparison of Total Flowrates between Simulink Model, Hagen-Poiseuille Approximation and Experimental Data for Rectangular Microchannel

	Rectangular microchannel		
	Simulink Model	**Experimental**	**% difference**
Total flowrate	5.13e8	5.02e8	2.19
	Hagen-Poiseuille D_H approximation	**Experimental**	
Total flowrate	4.05e8	5.02e8	19.32

To validate the flowrates of the layers of fluid, a finite element model of the microchannel is created using ANSYS. Meshing is done using Fluid element 141 and the axial velocities for the laminar flow of water in the channel is obtained. This is shown in Figure 6.

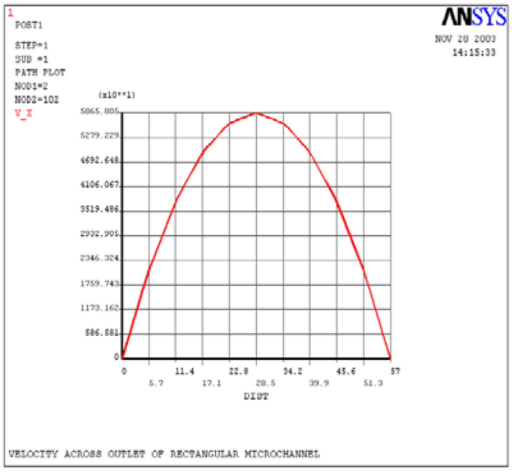

Figure 6 Velocity Across the Outlet for a Rectangular Microchannel (α=0.285) using 2D Analysis in ANSYS

From Table 2 and Table 3 it can be seen that, as expected, the flowrates for the innermost layer is the fastest. The flowrate is dependent on the cross-sectional area and the average velocity of the fluid. In this analysis the areas of the layers are made equal so the flowrates are dependent on the velocity only. When we compare our numerical calculation using Matlab, with our Simulink-electrical, the error is between from 0.18% to 0.79%. When we compare our numerical calculation with the ANSYS finite element model, an error range of 24.7% to 44.7% is obtained. It should be noted that ANSYS simulations may have an error of up to 20%. A chart comparing the values obtained using the 3 techniques is shown in Figure 7. The total flowrate obtained using our Simulink model gives much lower error.

Table 2 Comparison between Simulink Model and Numerical Calculation using Matlab

Flowrates	**Rectangular microchannel**		
	Numerical Model	**Simulink Model**	**% difference**
Outermost layer	0.634e8	0.639e8	0.79
Middle layer	1.782e8	1.795e8	0.73
Innermost layer	2.718e8	2.723e8	0.18

Table 3 Comparison between Simulink-Electrical Model and ANSYS of Flow Rates for Rectangular Microchannel

Flowrates	**Rectangular Microchannel**		
	Simulink Model	**ANSYS**	**% difference**
Outermost layer	0.64e8	0.85e8	24.7
Middle layer	1.79e8	1.22e8	46.7
Innermost layer	2.72e8	1.88e8	44.7

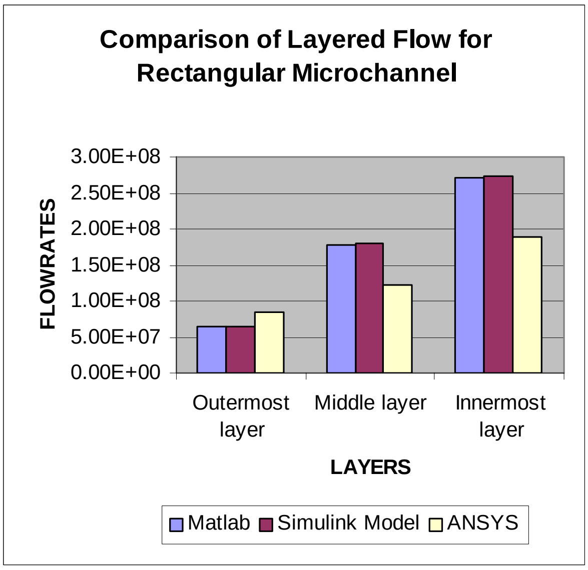

Figure 7 Comparison of Layered Flow Rates using the Simulink Model, Matlab and ANSYS Calculations

CONCLUSION

In this paper we calculated the layered flowrates of fluid in a rectangular microchannel using the velocity profile obtained through numerical methods using Matlab. We also presented an electrical model for the flowrates of the different layers of fluid, with the purpose to be built in our MEMS CAD prototyping system for fast calculations in virtual reality visualizations. Our electrical equivalent model incorporates the entrance effect of the microchannel and it demonstrates the transient flow when the velocity is changing as well as the steady flow when the velocity reaches a steady state. The simulations were implemented in Simulink and the results, i.e. the errors, were compared with the numerical calculations using Matlab as well as with finite element model using ANSYS.

The electrical model provides a fast first approximation of the flowrate. There are no physical modeling or meshing to be done. Despite this, the errors obtained are below 10%. The electrical network concept of parallel branches of resistances and inductances provides a suitable model for the flow rate of a liquid in laminar flow in a rectangular microchannel. Future work in validation with other experimental data needs to be carried out.

REFERENCES

Bendib, S.; O. Français; P. Tabeling and W. Hervé. 2001. "Analytical Study and Characterization of Microchannel and Passive Microdiode." *12th Micromechanics Europe workshop MME2001*. (Cork, Ireland, Sept 16-18).

Sharp, K.V.; R.J Adrian.; J.G. Santiago; and J.I. Molho. 2002. "Liquid Flows in Microchannels." In *The MEMS Handbook*, M. Gad-el-Hak (Ed). CRC Press, London.

Morris, C. and F.K.Forster. 2000. "The Correct Treatment of Harmonic Pressure-Flow Behavior in Microchannels." *Microelectromechanical Systems (MEMS)*, ASME, vol.2, 473-479.

Voigt, P.; G. Schrag; and G. Wachutka. 1998. "Microfluidic System Modelling using VHDL-AMS and Circuit Simulation". *Microelectronics Journal 29,* 791-797.

White, F.M. 1994. Fluid Mechanics 3rd Edition. McGraw Hill, New York.

Aumeerally,M and R. Sitte. 2003. "Modelling of Layered Fluid Flow in a Circular Microchannel." *Proceedings of the 2003 European Simulation and Modelling Conference.* (Naples, Italy, Oct 27-29). 458-462.

Panton, R.L. 1984. Incompressible Flow. John Wiley & Sons, USA.

Senturia, S.D. 2001. "Microsystem Design." Kluwer Academic Publishers, USA.

Ong, C-M. 1998. Dynamic Simulation of Electric Machinery using MATLAB^R/SIMULINK. Prentice-Hall, New Jersey.

Park, H.; J.J. Pak; S.Y. Son; G. Lim; and I. Song. 2003. "Fabrication of a Microchannel Integrated with Inner Sensors and the Analysis of its Laminar Flow Characteristics." *Sensors and Actuators A,* vol 103, 317-329.

SYSTEMS SIMULATION

LOCALLY WEIGHTED REGRESSION FOR DESULFURIZATION INTELLIGENT DECISION SYSTEM MODELING

Hiphung Leung
Yingsong Huang
Changxiu Cao
College of Automation, Chongqing University,
ShaPingba Dist. Chongqing,
P.R. China
E-mail: hhleung@vtc.edu.hk, huangys128_cn@yahoo.com.cn, cxcao@cqu.edu.cn

KEYWORDS
Locally weighted regression, locally weighted learning, desulphurization, intelligent decision system, genetic algorithm.

ABSTRACT

Locally weighted regression (LWR) is a memory-based learning method that performs regression around a point of interest which is useful for learning the rule of complex phenomena and system. This paper surveys the possibility of using locally weighted regression for modeling the desulphurization intelligent decision system in metallurgical process and proposes a hybrid algorithm by combining LWR with the Genetic Algorithm (GA) to determine the bandwidth of LWR adaptively. The proposed algorithm proves to be effective and practicable in its application.

INTRODUCTION

Locally Weighted Learning is a kind of lazy learning. This type of learning forms a local model around a point of interest whereby only training data that are “local” to that point would be used in handling any query, instead of a global model. After answering the query, the local model is discarded. A new local model is hence created to answer each query. This has an advantage in avoiding the difficulty of finding an appropriate structure for a global model, especially for some complex nonlinear system. Different models for different queries could also be constructed in enabling the improvement of performance. This method provides an approach to learning models of complex phenomena, dealing with large amounts of data, training quickly, and avoiding interference between multiple tasks during control of complex systems. It is therefore an effective way for intelligent decision system modeling in complex industrial production processes.

The desulphurization in steel-making process is a very complex and severe nonlinear system. It is extremely difficult to find a globally optimal model for the system. Artificial Neural network, which is robust to errors in the training data, has traditionally been applied to construct the prediction control model. Such technique focuses on selecting the right structure to overcome the local optima or over fitting problems which is in fact rather difficult to achieve. In addition, even the well defined neural net lacks the generality for its application.

The Locally Weighted Learning method seems a promising solution to the afore-mentioned engineering project, where the nonlinear global model could be transferred to various relatively linear local models. It is true that the computational cost of Locally Weighted Learning is a little higher; however, the linear parametric estimation process during lookup is still fast enough for the production prediction in certain desulphurization process.

There are several types of Locally Weighted Learning methods, such as K-Nearest Neighbor, Weighted Average and Locally Weighted Regression. Nevertheless, extensive research on the Locally Weighted Regression was conducted for deriving the desulfuration model. Although this method has been proved to be effective and widely used in robot control, limited work was done to improve it for the intelligent decision system modeling with satisfactory results.

The object of this paper is to find an optimal Locally Weighted Regression method for the desulfurizer prediction control model. Some basic concepts of Locally Weighted Regression were briefly reviewed followed by the introduction of the Genetic Algorithm to optimize the bandwidth. In the last section, the improved algorithm is tested by comparing it with the BP neural network for predicting the weight of desulfurizer .

LOCALLY WEIGHTED REGRESSION

Locally Weighted Regression is derived from standard linear regression. This algorithm fits a surface to “local” points using distance-weighted regression. In nonlinear system, it is extremely difficult to provide the global model accurately. Therefore, the simple linear model to local patches instead of the whole region of interest was used.

The locally weighted regression can be regarded as a type of function approximation method. Considering the following functions:

$$F(x) = w_0 + w_1 a_1(x) + \cdots + w_n a_n(x) \qquad (1)$$

$a_i(x)$ is the i^{th} attribute of pattern x.

A local model was being used in trying to find the best approximation for the function output *F(x)*. By redefining the error criterion of traditional linear regression, the local model was used to fit nearby points well, with less concern for distant points:

$$E(x_q) = \frac{1}{2}\sum_{x \in D}(f(x) - F(x))^2 K(\frac{d(x_q, x)}{\sigma}) \quad (2)$$

D is the k nearby patterns set of query point x_q, and *f(x)* is the output value of each training pattern in the training cycle. $K(\cdot)$ is a kernel function, which is used to calculate a weight for the data point from the distance. Typically, we use Gaussian function:

$$K(d) = e^{-d^2} \quad (3)$$

σ is the bandwidth that is very important for the performance of LWR and will be optimized in the latter part of this paper. $d(x, y)$ is the distance function to calculate the distance between the query point x_q and each data point x. A typical distance function is the Euclidean distance function, to be used in this paper:

$$d(x_q, x) = \sqrt{(x_q - x)^T (x_q - x)} \quad (4)$$

In order to speed up the training cycles, the clustering analysis was introduced to decrease the size of training set nearby the query point. A kind of K-Means algorithm is applied before the Locally Weighted Regression to find the nearby pattern set D of the query point. When constructing the model, only the training data in the set D is used instead of the whole data in the instance space. Because these patterns belong to the nearest clusters to the query point, the influence of other data on the local model could hence be omitted.

The best estimate $E(x_q)$ in Equation (2) will minimize the cost $E(x_q)$ by the gradient descent method

$$\frac{\partial E}{\partial w} = 0 \quad (5)$$

According to the least mean square (LMS), the following training criterion could easily be obtained:

$$\Delta w_i = \eta \sum_{x \in D} K(d(x_q, x))(f(x) - F(x))a_i(x) \quad (6)$$

D is the pattern set near the query point x_q and η is the learning rate.

After obtaining the weight w_i, the function output could be estimated accordingly:

$$f(x_q) = w_0 + w_1 a_1(x_q) + \cdots + w_n a_n(x_q) \quad (7)$$

$a_i(x_q)$ is the i^{th} attribute of query point x_q.

GENETIC ALGORITHM FOR OPTIMIZING THE BANDWIDTH

The bandwidth parameter σ defines the range over which generalization is performed. Increasing the bandwidth σ means further away data points get an opportunity to influence the query. As the σ goes to infinity, the prediction tends to become the global average. This is a very important parameter for the performance of the local model. If the bandwidth is too large, the training accuracy is unsatisfactory. On the other hand, if it is too small, the problem of over fitting occurs.

Typically, there are two ways to determine this important parameter:

1. Fixed Bandwidth Selection: since σ is a constant, the training process deals with constant data shape. It is the easiest and most convenient way to adjust the radius of the kernel function. Its performance is however unsatisfactory for nonlinear system.

2. Nearest Neighbor Bandwidth Selection: σ is calculated to be the distance between the query point and the k^{th} nearest data point. The radius expands or decreases according to the density of "local" data. This method has proved to be very effective in many applications; however, the constant k appears to be difficult to be optimized for each query model, as compared to the Fix Bandwidth Selection, especially for the severe nonlinear system with much noisy data.

The above-mentioned techniques are not desirable for the current mission in the model of desulphurization, because the process is severely nonlinear. It is hence proposed to adopt Genetic Algorithm (GA) to optimize the bandwidth σ in the current research work.

GA is a global optimal algorithm based on the evolution theory and uses a process of variation and selection to search for the whole parameter space. It can hence be used to optimize many traditional algorithms to improve their performance. To this end, the possibility of combining the GA with Locally Weighted Regression was explored.

Coding Method

To initialize the bandwidth σ population, a set of chromosomes (bandwidth) $\sigma_1, \sigma_2, \ldots, \sigma_{30}$ are generated randomly and then encoded to binary strings. The length of chromosome was set to 10 and the population size is set to 30.

Fitness Computation

The fitness function can be defined as:

$$Fitness = \frac{1}{(f(x) - F(x))^2} \quad (8)$$

f(x) is the calculated output of the model and *F(x)* is the expected output of the model

The proposed GA algorithm would maximize the fitness function by genetic operations, i.e. minimizing the error between *f(x)* and *F(x)*, until the fitness reaches the threshold or the genetic operations are executed for the maximum number (N) of iterations. In our experiment, N is set to 100.

Genetic Operations

The genetic operation process consists of the following steps:

1. Based on the notion of survival of the fitness, a new population was formed with the roulette wheel selection method used. Such a technique is based on fitness proportionate selection. The fitness of each chromosome was calculated by using the equation (8). According to its value, the selection proportion was determined for the current candidate chromosome in the population. The survival was selected depending on the selection proportion.

2. The offspring was created by applying genetic operators as crossover and mutation.

In crossover operation, substrings from pairs of individuals were wrapped to form new pairs of individuals. It was a probabilistic process that had exchanged information between two parent chromosomes for generating two child chromosomes. The crossover is the most important operator to obtain the better individual from the current generation, which means to explore the new searching space to find the better solutions. There are normally three crossover operators: single-point crossover, two-point crossover and uniform crossover, in which the third crossover operator has stronger searching ability and can keep the diversity of the population for overcoming the premature problem effective. Therefore, in the proposed algorithm, we adopt the uniform crossover with fixed crossover probability: $p_c = 0.68$.

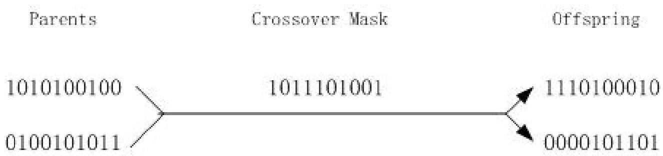

Figures 1: Crossover Operation

The crossover mask is generated randomly in every crossover operation.

In mutation, randomly selected bits in an individual string were inverted (0 to 1 or 1 to 0). The mutation can preserve the diversity of the population. In the algorithm, each chromosome adopts a fixed mutation probability: p_m=0.065

The last generation of the GA provides the solution of the bandwidth. Because the fitness function minimizes the error, elitism at each generation is implemented by preserving the best chromosomes. The last solution would hence be the optimized bandwidth for the query.

Since the GA had consulted the whole feature space for the optimized σ in each query, and different query combined with different σ, the result is therefore better than those obtained from the fixed method and nearest neighbor method. Although it appears that the GA is relatively time-consuming; however, bandwidth σ can also be calculated in advance of the queries and store with the data points, if the computation time are strictly concerned, and of course the expense is the a little of fall of the prediction accuracy. Taking into the fact of the corresponding long duration in the desulfurization process, it is considered to be suitable for the decision support in the production, even if the GA is applied in each query.

DESULFURIZATION MODEL WITH LOCALLY WEIGHTED REGRESSION

The following factors are selected as the input features of the model:

1. The weight of hot iron water (WI)
2. The content of sulphur in the iron water(SI)
3. The target of the desulphurization process (TI)

The output of the model was the weight of desulprizer (WD).

The structure of the model is shown in Figure 2

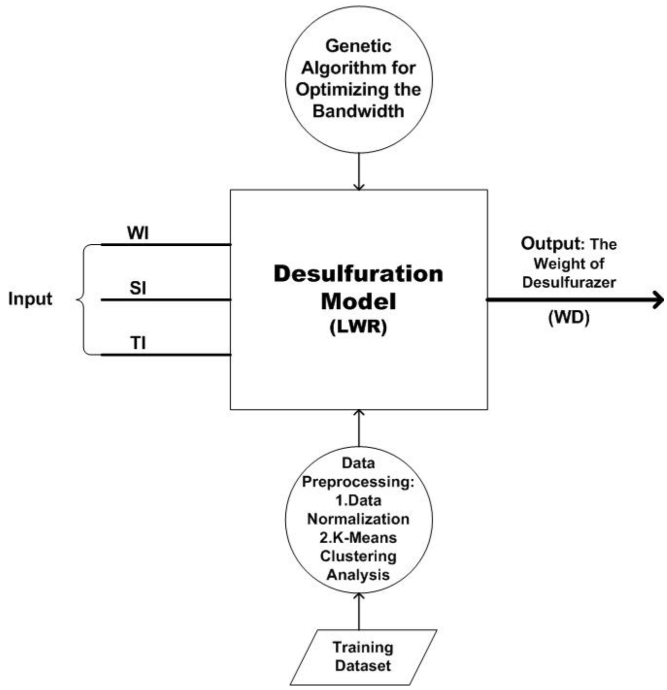

Figures 2: The Structure of the Model

Data Normalization

In the desulphurization model, the range of each input and output attribute varies greatly. For example, the WI attribute ranges from 70 ton to 150 ton, with the SI ranges from 0.020 to 0.2. Therefore, it is necessary to normalize each attribute to prevent those with initial large range from out weighing attributes with initial smaller range

The z-score normalization was adopted. The values for an attribute were normalized basing on the mean and standard deviation of such attribute. A value v of attribute X is normalized to v' by computing

$$v' = \frac{v - \overline{X}}{\sigma_x} \quad (9)$$

where $\overline{X}$ and σ_X are the mean and standard deviation of the attribute X respectively

This method of normalization is especially useful when the outliers dominate the traditional Min-Max normalization. So, it is very suitable for the desulphurization in which there is much industrial noisy data.

Cluster Analysis
To decrease the computational cost of locally weighted regression, the feature space, to the data, nearby the query point was confined by using K-Means algorithm.

1. Randomly select k of the objects in the formation of x_i (WI, SI, TI). Each of the selected objects initially represents a cluster center ($c_0, \ldots, c_k$). In this model, after analyzing the data set and experiment, $k = 50$ was chosen.

2. Each of the remaining objects was assigned to a similar cluster basing on the distance between the object and the cluster center. Here, the Euclidean distance was used.

3. The mean of each cluster was computed to find the new center c_i for each cluster.

$$c_i = \frac{1}{M_i} \sum x_i \tag{10}$$

M is the size of cluster i *and* x_i is the object in the cluster

The three steps cycle, until the cluster center c_i converged. The cluster analysis only needs to be done once before the LWR modeling. After the clusters are created, the centers and the cluster information would be stored for the later modeling. Such a technique could determine the points for regression by only simply comparing the distance between the centers and input data, and then load the points in selected clusters to the memory, which can save enormous computation time and memory.

Experimental and Model Prediction Results

The locally weighted regression combined with GA as mentioned above was applied to the desulphurization model. The dataset was retrieved from the metallurgical industrial database of a large national steel corporation of China located in Siechuen, from May to October, 2002. After the data cleaning, more than 8000 items of data were divided into two sets: two third of the original dataset was used for training with the remaining for testing.

The experiment was based on two modeling method: LWR with GA method and BP neural network. The experiment results are shown and compared in Table 1.

Table 1 the Comparison between BP Neural Network and LWR

Modeling Algorithm	MAX ERROR(kg)	Mean ERROR(kg)	Prediction Accuracy
BP Neural Network	692	212	48.1%
LWR with GA method	221	71	81.5%

The LWR with GA method: cluster number K=50, bandwidth population size of σ is 30, chromosome length l=10, crossover probability $p_c = 0.68$, mutation probability $p_m = 0.065$, maximum iteration $N = 100$, learning rate $\eta = 0.0014$. BP neural network: 3 layer neural network, the input layer: 3 neurons, the hidden layer: 35 neurons, the output layer: 1 neuron, learning rate: $\eta = 0.008$.

The above table shows that the LWR with GA method outperforms BP neural network in the prediction results. Its prediction error and accuracy are both much better than BP neural network.

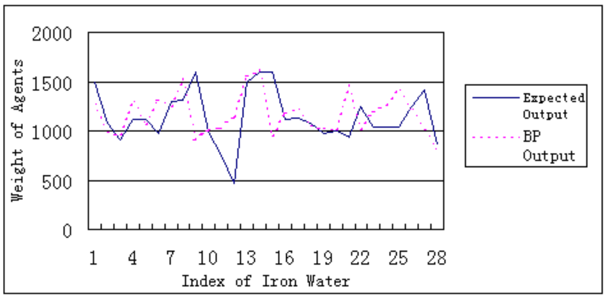

Figures 3: The Prediction Results of BP Neural Network

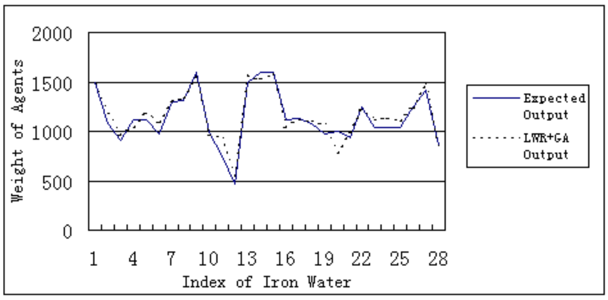

Figures 4: The Prediction Results of LWR with GA Method

Figure 3 and Figure 4 indicate that the proposed algorithm produces the more accurate prediction to the desulphurization process than the traditional BP neural network. The BP neural network performs well in the situation in which there are abundant clean training data, but will fail in dealing with some edge data that do not appear frequently, i.e. scarce data, in particular, with some noise data, such as index 12 in Figure 3. This is also a big challenge to many current modeling and data mining algorithm. On the contrary, the LWR with GA method performs very well for almost the whole range of data.

The optimized bandwidth in each new query will find the suitable data points dynamically for each regression and obtain the best prediction result. From the machine learning point of view, the locally weighted regression which belongs to lazy learning can choose a new hypothesis based on the training data near the query points each time, i.e. utilizes many different local linear functions to form its implicit global approximation to the sever nonlinear target function. In contrast, BP neural network which is a kind of eager learning method must commit to a single hypothesis covering the entire data space. So, the former can effectively uses a richer hypothesis space than latter and achieve better result.

Besides the experiment of model prediction accuracy, the computation time is also tested and compared for evaluating the proposed hybrid algorithm.

Table2: The Comparison of Computation Time between BP Neural Network and LWR

Modeling Algorithm	Training Time (sec.)	Prediction Time (sec.)	Overall Time(sec.)
BP Neural Network	35	<1	<36
LWR with GA method	190		190

The BP neural network known as the eager learning clearly defines the training stage and prediction stage. It commits to the network structure and weights at the training time. This period would be much longer than the prediction stage and would be even longer if there is more training data, however, once the network is set up, the prediction is very fast, and can be an approximately real time prediction.

On the contrary, the LWR is a lazy learning algorithm which defers the training process until prediction happens, i.e. when each new query is encountered. So, this proposed hybrid algorithm deem the training process and prediction process as an integrated one. Consequently, the computation time is much longer than the BP neural net in prediction under the current situation. However, because the desulphurization process and many other metallurgical industrial processes require long time (>900s) and the prediction accuracy is more important for such processes, the proposed hybrid algorithm can be applied successfully to such areas or decision support.

Judging from the above analysis, the LWR with GA method outperforms the traditional neural network. The prediction results are satisfactory and in accordance with the actual metallurgical industrial process.

CONCLUSION

This paper has studied an improved Locally Weighted Regression method combining the Genetic Algorithm to learn intelligent decision support models for control. By means of GA, the bandwidth σ is optimized globally and the performance of locally weighted regression is improved. This method is useful and applicable for modeling some rigorous nonlinear system in global area but linear in local area, which is very common in the steel-manufacturing industrial production process. The implementation of the improved method proves to be effective and superior to the traditional neural network.

One of the drawbacks of the proposed algorithm is its relatively high computational cost in each query. It still needs a more efficient way to speed up the data search process and GA process to fit the real-time control for very large dataset.

ACKNOWLEDGEMENTS

This work is partly supported by the National Ministry of Education Doctor Research Fund (98061117) and Chongqing Application Basic Research Project Fund (7369).

REFERENCES

Atkeson, C.C et al. 1997. "Locally Weighted Learning". *Artificial Intelligence Review special issue on Lazy Learning*. 11, 11-73.

Atkeson, C.C., et al. 1997. "Locally Weighted Learning for Control". *Artificial Intelligence Review*. 11, 75-113.

Cai Tianyou.1999. "Endpoint Prediction of Basic Oxygen Furnace Steel Making Based on RBF Neural Network". *The Chinese Journal of Nonferrous Metal*. Vol.9, No.4 (Dec), 868-872.

Huang Yingsong, et al. 2002. "Desulphurization Prediction Model Based On GRBF Neural Network". *Computer Engineering and Application*. Vol. 24, 218-220.

Maulik, Ujjwal, et al 2000. "Genetic Algorithm-Based Clustering Technique". *Pattern Recognition*. 33, 1455-1465.

Rui Qing, et al. 1998. "The Simulation Research of the Ping-Pong Orbit Prediction by LWR". *Robot*. Vol.20, No.5 (Sep.), 373-377.

Shi Zhizhong. 2002. *Knowledge Discovery*, Tsinghua University Press.

Tao Yun. et al.2000. "Steel Making BOF Model Based on GAs and RBF Neural Network". *Journal of System Simulation*. Vol.12, No.3 (May), 241-244+277.

Wang Yongji and Tu Jan. 1998. *Neural Network Control*. China Machine Press.

AUTHOR BIOGRAPHY

HIPHUNG LEUNG was graduated from Coventry University of United Kingdom and has involved in tertiary technical education for over twenty years; currently works as a Chief Industrial Training Officer responsible for the training policy of his locality. His research interest includes data-mining, modeling and control system.

YINGSONG HUANG was born in SiChuan Province, P.R.China and went to Chongqing University in 1996, where he obtained M.S in 2003 and B.S. in 2000 respectively in the College of Automation. His research interest includes data mining, control systems design and modeling and machine learning.

CHANGXIU CAO is the Professor in Automation of the College of Automation of the Chongqing University. His research interest lies in the areas of Data-warehousing, data-mining, simulation and modeling.

A Simulation-Based Fault Injection Technique For Simulating Bit Flip Error in VHDL Models

Haissam ZIADE
Lebanese University
Faculty of Engineering I
Tripoli – Lebanon
hziade@ul.edu.lb

Rafic AYOUBI
University of Balamand
Faculty of Engineering
Tripoli – Lebanon
rafic@balamand.edu.lb

Amer HELWANI
Lebanese University
Faculty of Science III
Tripoli – Lebanon
ahelwani@ul.edu.lb

Abstract*: Fault injection has become an important method for experimentally validating the dependability of computer systems. Several efforts have been made to develop techniques for injecting faults into a system prototype or model. Most of the techniques fall into three essentials categories: hardware-based fault injection, software-based fault injection and simulation-based fault injection. More recently, several authors proposed to apply fault injection early in the design process. The main approach consists in injecting the faults in high-level models (most often, VHDL models) of the circuit or system Also, at the present time, it is generally accepted that the occurrence of transient faults in memory elements, commonly knowing as Single event Upset or Bit Flip, are the potential threat of the reliability of integrated circuits operating in radiation environment. Then this paper presents a new simulation-based fault injection technique for injecting bit flip errors in VHDL models.*

Keywords: Fault tolerance, fault injection, fault simulation, VLSI circuits, fault injector, VHDL fault models.

1. Introduction on Simulation-based Fault Injection

Simulation-based fault injection [1,7] involves the construction of a simulation model of the system under analysis, including a detailed simulation model of the processor in use. It means that the errors or failures of the simulated system occur according to predetermined distribution. The simulation models are developed using a hardware description language such as the Very high speed integrated circuit Hardware Description Language (VHDL). Faults are injected into VHDL models of the design and excited by a set of input patterns. It is important to note that VHDL constitutes a privileged language to comply with the goals of fault injection for the following reasons:

- Its widespread use in detailed design.
- Its inherent hierarchical abstraction description capabilities.
- Its ability to describe both the structure and behavior of a system in a unique syntactical framework.
- Its recognition as a viable framework for developing high-level models of digital systems.
- Its recognition as a viable framework for driving test activities.

An elementary fault injection *experiment* corresponds to one simulation run of the target system during which any number of faults can be injected on single or multiple locations of the model and at one or several points in time during the simulation. A series of experiments consists of a sequence of elementary fault injection experiments.

Several techniques have been proposed in the past to efficiently implement simulation-based fault-injection. Two main categories can be identified: those that require modification of VHDL code and those that use the built-in commands of the simulator.

A first approach, based on *VHDL code modification*, modifying the system description by the addition of a dedicated fault injection components called *saboteurs* or the mutation of existing component descriptions in the VHDL model which generates modified component descriptions called *mutants*. So that faults can be injected where and when desired, and their effects observed, both inside and on the outputs of the system.

A *saboteur* is a component added the VHDL model for the sole purpose of fault injection. It is inactive during normal system operation, while altering the value or timing characteristics of one or more signals when active, i.e when a fault is being injected. Saboteurs are inserted, in series or in parallel, either interactively at the schematic editor level or manually/automatically directly into the VHDL source code. Serial insertion, in its simplest form, consists of braking up the signal path between a driver (output) and its corresponding receiver (input) and placing a saboteur in between. In its more complex form, it is possible to break up the signal paths between a set of drivers and its corresponding set of receivers and insert a saboteur. For parallel insertion, a saboteur is simply added as an additional driver for a resolved signal (signal that have many drivers - signal sources – provided that a resolution function is supplied to resolve the values generated by the multiple sources into a single value). Saboteurs can be used to model most faults and to simulate environmental conditions such as noise or ESD. However, because they have no input pattern discrimination, saboteurs cannot model faults below the gate level of abstraction.

A *mutant* is a model which contains dormant code blocks within the normal gate description. These blocks of code are activated by injecting faults, altering the operation of the logic device itself. Because the fault response is generated internally within the model, any level of abstraction for fault injection is possible. However, the use of mutants requires that the original gate models be replaced by the new mutant models.

This method main advantage is its complete independence on the adopted simulator, but it normally provides very low performance, due to the high cost for modification and possibly recompilation for every fault.

A second approach uses modified simulation tools (built-in commands of the VHDL simulators), which support the injection and observation features. This approach normally provides the best performance (does not require the modification of the VHDL code), but it can only be followed when the code of the simulation tools is available and easily modifiable, e.g., when fault injection is performed on zero-delay gate-level models. Its adoption when higher-level descriptions (e.g., RT-level VHDL descriptions) are used is much more complex. The applicability of these techniques depends strongly on the existing (commercial) simulators and on the functionality of their commands. Two techniques based on the use of simulator commands have been identified: VHDL signal manipulation (faults are injected by altering the value of the signals that are used to link the components that made up the VHDL model, this is done by disconnecting a signal from its driver(s) and forcing it to a new value) and VHDL variable manipulation (faults are injected into behavioral models by altering values of variables defined in VHDL processes).

A third approach relies on the simulation command language and interface provided by some specific simulator. The main advantage of this approach lies in the relatively low cost for its implementation, while the obtained performance is normally intermediate between those of the first and second approaches. It must be noted that it is now increasingly common for the new releases of most commercial simulation environments to support some procedural interface, thus allowing an efficient and portable interaction with the simulation engine and with its data structures. Several approaches have been presented for speeding up the simulation process.

Fault injection techniques are compared in terms of fault modeling capacity, effort required for setting up an experiment and simulation time overhead.

Mutants offer the highest fault modeling capacity of the fault injection techniques presented, Saboteurs are generally less powerful, signal manipulation is suited for implementing simple fault models and variable manipulation offers a simple way for injecting behavioral faults.

The effort for setting up an experiment is small using signal and variable manipulation, as modification of the VHDL model is not required. More effort is needed for mutants and saboteurs (creation/generation, inclusion in the model, recompilation of the VHDL model).

The simulation time overhead imposed by signal and variable manipulation is only due to fault injection control, as the simulation must be stopped and started again for each fault injected. It is important to note that the simulation time overhead imposed by saboteurs and mutants depends on: amount of additional generated events, amount of code to execute per event and the complexity of the fault injection control.

When considering a series of fault injection experiments, two ways can be distinguished: one way is to generate a new configuration for each fault location (this requires recompilation of the VHDL model for each fault location and may also require manual intervention to start up a simulation using the new model), another way is to generate only one configuration in which all required fault are included and then activate these one at a time (this may increase the simulation time). Thus, there is a trade-off between the overhead in simulation time and the overhead in compilation time.

This technique supposes that the model is an accurate representation of the actual system under analysis. Its benefits are:

1) Simulated fault injection can support all system abstraction levels - electrical, logical, functional, and architectural. It provides the maximum flexibility in terms of supported fault models.

2) Not intrusive.

3) Full control of both fault models and injection mechanisms.

4) Low cost computer automation; Does not require any special-purpose hardware.

5) It provides timely feedback to system design engineers.

6) Fault injection experiments are performed using the same software that will run in the field. Simulated fault injection can normally be rather easily integrated into already existing design flows.

7) Maximum amount of observability and controllability. Essentially, given sufficient detail in the model, any signal value can be corrupted in any desired way, with the results of the corruption easily observable regardless of the location of the corrupted signal within the model. This flexibility allows any potential failure mode to be accurately modeled.

8) Allows performing reliability assessment at different stages in the design process, well before than a prototype is available.

9) Able to model both transient and permanent faults.

10) Allows modeling of timing-related faults since the amount of simulation time required to inject the fault is effectively zero.

Their drawbacks are:

1) Large development efforts

2) Time consuming (experiment length) : being based on the simulation of the system in its fault-free version as well as in the presence of the enormous number of the possible faults.

3) Model are not readily available; rely on model accuracy

4) Accuracy of the results depends on the goodness of the model used.

5) No real time faults injection possible in a prototype.

6) Model may not include any of the design faults that may be present in the real hardware.

Examples of these tools are:

- VERIFY, VHDL-based Evaluation of Reliability by Injection Faults Efficiently developed at University of Erlangen-Nurnberg, Germany [2].
- MEFISTO-C, A VHDL-based Fault Injection Tool developed at Chalmers University of Technology, Sweden [3].
- HEARTLESS, Hierarchical Register-Transfer-Level fault-Simulator for permanent and tranSient faults [4].
- GSTF, A VHDL-based Fault Injection Tool [5] developed by Fault Tolerance Systems Group at the Polytechnic University of Valencia, Spain.
- FTI, A Fault Tolerance Injection tool [6], developed at universidad Carlos III de Madrid in Spain.

2. Our proposed approach

We propose the use of VHDL simulators to perform fault injection campaigns of SEU faults. A characteristic of SEUs is that they are random events and thus they may occur at unpredictable times. For example, they may corrupt the content of a processor register during the execution of an instruction. In this paper we focused on the fault model called *upset* or *bit-fli*p, which results in the modification of the content of a storage cell during program execution. Possible fault locations are thus flip-flops, general purpose registers, control registers and every registers not accessible through the processor instruction set, and embedded memories such as register file and caches. Despite its relative simplicity, the bit-flip is widely used in the Fault Tolerance community to model real faults since it closely matches real faulty behavior. We adopt the classification of fault effects presented in [8]:

- *Silen*t: the output of the faulty system matches that produced by the fault-free system; moreover, the state of the faulty system matches that of the fault-free one.
- *Laten*t: the output of the faulty system corresponds to the fault-free one, but the faulty and fault-free system states at the end of the experiment do not match. The fault is still active in the system and may produce wrong outputs in the following clock cycles.
- *Failur*e: the output of the faulty system does not match that of the fault-free one.
- *Detecte*d: the fault is detected by some error detection mechanism existing in the system.

Our approach relies on the simulation command language and interface provided by some specific simulator. The main advantage of this approach lies in the relatively low cost for its implementation. It must be noted that it is now increasingly common for the new releases of most commercial simulation environments to support some procedural interface, thus allowing an efficient and portable interaction with the simulation engine and with its data structures.

3. Conclusions and future work

Simulation-based fault injection allows early evaluating the system dependability when only a model of the system is available. Moreover, it is very flexible in terms of fault model since any fault model can potentially be supported and faults can be injected in any module of the system. Also, this technique allows a high degree of versatility by injecting multiple bit-flips errors in the circuit memory elements. The major drawback of this approach is the high CPU time required for fault injection campaigns. Reducing this time is the principal problem of this technique. For this kind and for speeding-up the process,, the approach proposed in this paper show a very interesting alternative based on randomly injection technique

Acknowledgements

This work is supported by the Lebanese university research program and the French/Lebanon CEDRE program. We would like to acknowledge the support of all these organizations for their help and contributions.

References

[1] E. JENN, M. Rimen, J. Ohlsson, J. Karlsson and J. Arlat " Design guidelines of a VHDL-based simulation tool for the validation of fault tolerance " in Proc. 1st ESPRIT basic research project PDCS-2 open workshop, LAAS/CNRS, Toulouse, pp 461–483, September 1993

[2] V. Sieh, O. Tschäche, and F. Balbach, "VERIFY: Evaluation of Reliability Using VHDL-Models with Embedded Fault Descriptions", in *Proc. 27th Int. Symp. On Fault-Tolerant Computing (FTCS-27)*, Seattle, WA/USA, pp 32-36, June 1997

[3] P. Folkesson, S. Svensson, and J. Karlsson, "A Comparison of Simulation Based and Scan Chain Implemented Fault Injection", in *Proc. 28th Int. Symp on Fault-Tolerant Computing (FTCS-28)*, Munich, Germany, pp 284-293, June 1998.

[4] C. Rousselle, M. Pflanz, A. Behling, T. Mohaupt, H.T. Vierhaus "A Register-Transfer-Level Fault Simulator for Permanent and Transient Faults in Embedded Processors", DATE 2001 Conference, Munich, Germany, 2001

[5] J. C. Baraza, J. Gracia, D. Gil and P. J. Gil " A prototype of a VHDL-based fault injection tool ", DFT 2000 Conference, pp 396–404, October 2000.

[6] L. Entrena, C. López, E. Olías, "Automatic Generation of Fault Tolerant VHDL Designs in RTL", FDL (Forum on Design Languages), Lyon/France, September 2001.

[7] M.-C. Hsueh, T. K. Tsai, R. K. Iyer " Fault injection techniques and tools "IEEE Computer, Vol. 30, No. 4, pp 75-82, April 1997.

[8] B. Parrotta, M. Rebaudengo, M. Sonza Reorda, M. Violante, *New Techniques for Accelerating Fault Injection in VHDL description*s, IEEE Int. On-Line Testing Workshop, 2000, pp. 61-66

ENERGY SYSTEMS SIMULATION

The Synchronous Rotation of AC Machines

Dr. Ali S. Al-akayleh
Department of Electrical Engineering
Al-Balqa' Applied University,
Tafela - Jordan.
E-mail: ali_alakayleh@yahoo.com,
Fax: (++962) 5-2250033, Tel: (++962) 77-774254

Keywords: Synchronous rotation, Induction machines, Electrical shaft, Electromagnetic shafts, Equalizing current.

1. Introduction

All systems alternate and change constantly to improve their performance and enhance their compatibility. As a result of this, amongest these systems are the systems of synchronous rotation which are known as the systems depending on their work on the equality of the speeds of all motors taking part. The performance of these systems is very much related to synchronic capability, which is the ability of system motors to function synchronically regardless the load on the working shaft of each motor. The more the difference amongest loads, the more the synchronization power of the system. Having what was mentioned above in mind, any change or improvement of the system should take into consideration the synchronization ability in addition to performance factors.

The systems of synchronous rotation are most used in cranes, cutting tool machines and lifting machines as well as dryers in cement and potash factories. The synchronized ability differs according to the connection which links up the motors in the system. If the connection is direct mechanical one, then, the synchronized ability is finite, if, however, the connection is non mechanical, the synchronized ability depends on the connection kind. Later, is a discussion of the synchronized systems, which are mechanically misconnected. The most popular synchronized systems are the synchronous drive system set up with synchronous auxiliary machines and the synchronous slip-ring drive system with two motors having a common rheostat in the circuit with electrical shaft (Carlo,2000).

Given in figure (1), a drive scheme set up with two auxiliary synchronous machines SM1 and SM2, each being directly coupled to the respective main drive motor, namely, M1 and M2. The system serves to maintain shafts I and II running in synchronism.
When the drive motor M1 carries a greater load than drive motor M2, the rotor of the first auxiliary machine begins to lag behind the rotor of the second auxiliary machine by a displacement angle equal to θ. Due to the angular displacement θ, which arises between the rotor electric motive force E.M.F of both machines, an equalizing current will flow between the rotor windings and, thus, will produce a generator torque in auxiliary synchronous machine SM2 and a motor torque in machine SM1.

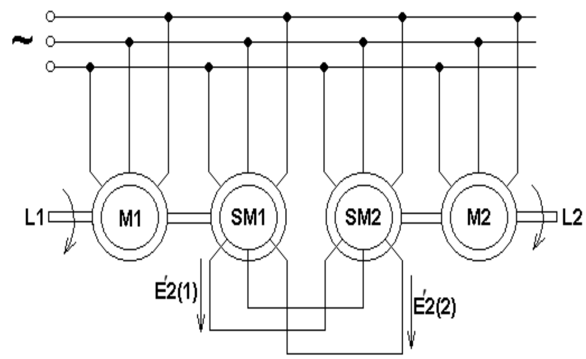

Fig.1. The system of synchronous rotation with synchronous auxiliary machines.

The torque developed by the auxiliary machines is found from the following equation:

$$T_{sm} = k\, E_s \sin\theta \qquad (1)$$

Where : k-coefficient and E_s-the synchronizing E.M.F.

The synchronizing E.M.F in this equation is a function of the speed and at $\omega = 0$ it will equal zero. At low speeds, the auxiliary synchronous machines will produce a low E.M.F and, hence, only a small synchronizing torque. This is a serious drawback, which limits the cases where such a system may be applied.

A system of synchronous drive with slip-ring motors connected to a common rheostat may consist of two or more motors as shown in figure (2) which, illustrates a system with two slip ring motors, both of which have their stator windings connected to the same AC supply circuit, while their rotor windings are connected in parallel to the same rheostat. These two motors have no mechanical coupling. For stable operations this system requires both motors to have identical performance characteristics.

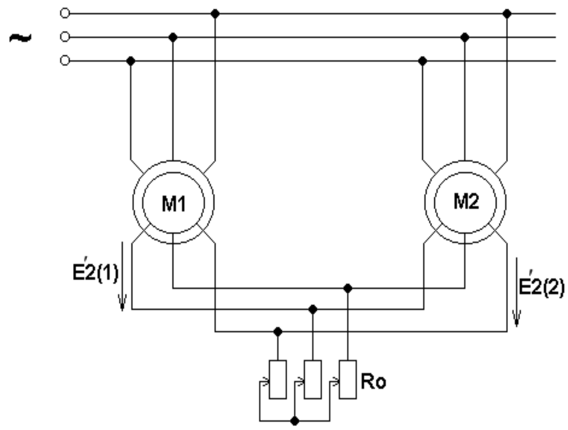

Fig. 2. The system of synchronous rotation with electrical shaft.

As long as the displacement angle θ, remains equal to zero, the currents flowing in both rotor windings will remain equal.

The total current, which is the sum of the two working currents, will flow through the rheostat. If the loads on the motor shafts are unequal, a part form the working currents flowing from the rotor circuit into the rheostat, an equalizing current will be setup, passing only through the rotor circuit and passing the rheostat. Accordingly, one may consider the torque developed by each motor as the sum of the working and equalizing torques.

As shown in figure (2), we can represent the E.M.F in the rotor circuit as following:

$$E'_{2(1)} = I'_{21} [Z_{21} + R_o] + I'_{22} R_o \quad (2)$$
$$E'_{2(2)} = I'_{22} [Z_{22} + R_o] + I'_{21} R_o \quad (3)$$
$$\Delta E = E'_{2(2)} - E'_{2(1)} \quad (4)$$

Where:
$E'_{2(1)}$, $E'_{2(2)}$: The rotor E.M.F in the first and second motors.
Z_{21}, Z_{22}: The total rotor resistance in the first and second motors.
I'_{21}, I'_{22}: The rotor current in the first and second motors.
R_o: The common resistance of the common rheostat.
ΔE: The resultant E.M.F in the rotor circuit.
Going over these equations, it's clearly shown that the synchronized ability depends mostly on the value of R_o, since having this resistance to vanish means the vanishing of the mutual influence amongst the main motors coils, and on the other hand its increase means the increase of the resultant E.M.F, ΔE.
The equality of the loads on the main motors abolish this resistance whatever its value is and makes it a useless element of the system. Having this piece of information in mind, before the R_o value is determined the difference amongst motors loads should be known so that it would be easy to choose the suitable value of R_o, which can ensure a high synchronized ability which eventually enables the system to stay within the range of high synchronized ability with acceptable energy factors.

2. The system of synchronous rotation with Electromagnetic Working Shaft.

The above mentioned systems of synchronous rotation are characterized with simplicity in structure and performance as well as their ability to work with high synchronized potentials, while the dark side of these systems is that firstly they have a working motor constantly regardless the need of the system to the synchronous rotation. Secondly, the fact that the full dependence on the common resistance reduces the efficiency of the system. In addition to the mentioned points the phases of rotors of main motors must be at the same angle position to protect the system from the vibrations that might occur.

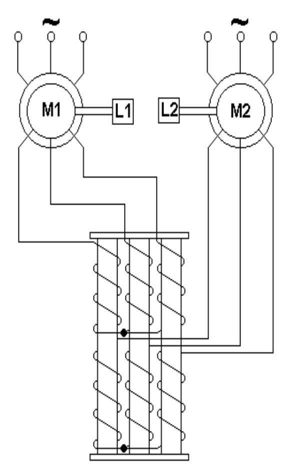

Fig. 3. The system of synchronous rotation with electromagnetic working shaft.

We suggest a new type of connection of synchronous rotation, which presents the synchronous drive system with electromagnetic working shaft E.M.W.S. this system is shown in figure (3). This type works on the principle of electromagnetic transformation of energy. In this type each motor of the system has a wounded rotor coil in steel cylinder which is very similar to the transformer connections, where the primary coils are connected to one motor and the secondary to the other. This type of connection will make a common inductive resistance and this system will change its own resistance in accordance with the change of the current flowing in its coils.

The elements of this shaft, coils and steel structure dimensions must be chosen depending on the characteristics and the demands of the synchronization of working equipment.
When the electric currents flow inside the inductive resistance from both sides, and electromagnetic connection is generated between them, the main motors' coils falls under a correspondent and continuous influence of the power where a change in one current of any of the motors leads to a change of the current motor in the other.

In case of equality of loads, the electric currents moving inside the inductive resistance are also equal in quantity and opposite in direction. The electromagnetic fields generated in those rotors are equal in quantity and opposite in direction, and that's how the electromagnetic connection is absent amongest the coils while the motors work independently. If the loads are different, then the electric currents and the electromagnetic fields will also change which will lead to an electromagnetic connection amongest the inductive resistances of rotors coils. The electromagnetic field generated from the motor coils with the greatest load will be greater than the electromagnetic field generated of the motor coils with less load. As a result of this, back E.M.F will be generated in the motor which carries the least load which will lead to reduce the speed of this motor, until it leads to equality of speeds in both motors.

3. Mathematical derivation of equations of the system with E.M.W.S.

To derive equations of this type of systems it's possible to use the simplified equivalent circuit given in fig 4.

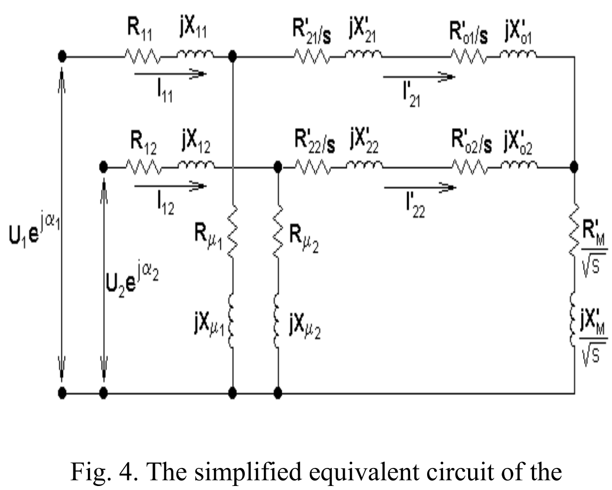

Fig. 4. The simplified equivalent circuit of the system with electromagnetic shaft.

Where $U_1e^{j\alpha1}$, $U_2\,e^{j\alpha2}$- Stator phase voltage in the first and second motors.

I_{11}, I_{12}: stator phase current in the first and second motors.
I'_{21}, I'_{22}: referred rotor current in the first and second motors.
R_{11}, R_{12}: stator resistance in the first and second motors.
X_{11}, X_{12}: stator inductive reactance in the first and second motors.
R'_{21}, R'_{22}: rotor resistance in the first and second motors.
X'_{21}, X'_{22}: rotor inductive reactance in the first and second motors.
$R_{\mu1}$, $R_{\mu2}$: Resistance of the magnetizing branch in the first and second motors.
$X_{\mu1}$, $X_{\mu2}$: Inductive reactance of the magnetizing branch in the first and second motors.
R'_M, X'_M: Resistance and inductive reactance of the magnetizing branch of the inductive rheostat.
R'_{01}, R'_{02}: Inductive rheostat resistance in the first and second motors.
X'_{01}, X'_{02}: Inductive rheostat reactance in the first and second motors.
S – Slip

Using superposition principle we can write the equations of voltages as following:

$$U_1 = I_{11}[(R_{11} + R_{\mu1}) + j(X_{11} + X_{\mu1})] - I'_{21}[R_{\mu1} + jX_{\mu1}]$$
$$U_2 = I_{12}[(R_{12} + R_{\mu2}) + j(X_{12} + X_{\mu2})] - I'_{22}[R_{\mu2} + jX_{\mu2}] \quad (5)$$

and

$$\left[I_{11}\left(R_{\mu1}+jX_{\mu1}\right)-I'_{21}\left[\left(\frac{R'_{21}+R'_{o1}}{s}\right)+j\left(X_{\mu1}+X'_{21}+X'_{o1}\right)\right]\right]e^{j\alpha_1} = \frac{R'_M+jX'_M}{\sqrt{s}}\sum_{i=1}^{n}I'_{2i}\,e^{j\alpha_i}$$

$$\left[I_{12}\left(R_{\mu2}+jX_{\mu2}\right)-I'_{22}\left[\left(\frac{R'_{22}+R'_{o2}}{s}\right)+j\left(X_{\mu2}+X'_{22}+X'_{o2}\right)\right]\right]e^{j\alpha_2} = \frac{R'_M+jX'_M}{\sqrt{s}}\sum_{i=1}^{n}I'_{2i}\,e^{j\alpha_i} \quad (6)$$

Where: n – the amount of AC motors contributed in the system.

If we give the stator, rotor and magnetic branch impedances the symbols Z_1, Z_2, and Z_M and taking into consideration that the R_μ value is very small relative to the X_μ we can neglect R_μ value in equation number (5), then equation number (5) will be.

$$U_1 = I_{11}Z_1 - I'_{21}X_{\mu1}$$
$$U_2 = I_{12}Z_2 - I'_{22}X_{\mu2} \quad (7)$$
$$\left[I_{11}\left(jX_{\mu1}\right)-I'_{21}\,Z_2\right]e^{j\alpha_1} = Z_M\sum_{i=1}^{n}I'_{2i}\,e^{j\alpha_i}$$

$$\left[I_{12}\left(jX_{\mu 2}\right)-I'_{22}\,Z_2\right]e^{j\alpha_2}=Z_M\sum_{i=1}^{n}I'_{2i}\,e^{j\alpha_i} \qquad (8)$$

Where:

$Z_1 = R_1 + j(X_1 + X_\mu)$; $Z_2 = [(R'_2 + R'_o)/s] + j(X_\mu + X'_2 + X'_o)$; $Z_M = (R'_M + jX'_M)/\sqrt{s}$

In this system the rotors of both AC motors traveling at the same speed and in the direction of stator field rotation. Consequently when the rotor of the first motor is lagging from the rotor of the second motor in the angle equals α then, the E.M.F of the first motor will lead the E.M.F of the second motor at the same angle.

If we put the displacement angle α in the place of stator voltage, then the stator voltage to the first AC motor will lead the stator voltage to the second AC motor at the same angle α as its seen in equation (8).

After some simplifications, we can come up with stator and rotor currents.
The rotor current of the first motor will be:

$$I'_{21}=\frac{jX_\mu\left[X_\mu^2+Z_1\left(Z_2+Z_M(2-\sum_{i=1}^{n}e^{-j(\alpha_i-\alpha_1)})\right)\right]}{\left[X_\mu^2+Z_1\left(Z_2+2Z_M\right)^2+\left(X_\mu^2+Z_1Z_2\right)\right]^2} \qquad (9)$$

To simplify the rotor current calculation we can neglect the stator resistance R_1, then the rotor current of the first AC motor will be

$$I'_{21}=\frac{U_1}{2}\left[\frac{2-\sum_{i=1}^{n}e^{j(\alpha_i-\alpha_1)}}{Z}+\frac{\sum_{i=1}^{n}e^{j(\alpha_i-\alpha_1)}}{Z+2Z_M}\right] \qquad (10)$$

Where:

$Z = [(R'_2 + R'_o)/s] + j(X_1 + X'_2 + X'_o)$

In this system the main relationship to analyze the work can be considered as torque characteristics. According to [Dimentberg et.al 2001], the rotational torque of the first motor will have the form:

$$T_1 = mU/2\omega_o\,[I'_{21} + I'_{21}] \qquad (11)$$

Where,

$$\dot{I}'_{21}=\frac{U_1}{2}\left[\frac{2-\sum_{i=1}^{n}e^{-j(\alpha_i-\alpha_1)}}{\dot{Z}}+\frac{\sum_{i=1}^{n}e^{-j(\alpha_i-\alpha_1)}}{\dot{Z}+2\dot{Z}_M}\right] \qquad (12)$$

And

$$\dot{Z}=\left[\left(\frac{R'_2+R'_o}{s}\right)-j(X_1+X'_2+X'_o)\right]$$

$Z'_M = (R'_M - jX'_M)/\sqrt{s}$

Substitute the values of I'_{21} and I'_{21} in the equation number (11) and taking into consideration that

$$\frac{e^{j\alpha}+e^{-j\alpha}}{2}=\cos\alpha \quad and \quad \frac{e^{j\alpha}+e^{-j\alpha}}{2j}=\sin\alpha$$

We find that

$$T_1=\frac{mU_{ph}^2}{2\omega_o}\left[\frac{\left(\frac{R_2'+R_o'}{s}\right)(1-\cos\Delta\alpha)}{\left(\frac{R_2'+R_o'}{s}\right)^2+(X_1+X_2'+X_o')^2}+\frac{\left(\frac{R_2'+R_o'}{s}+\frac{2R_M'}{\sqrt{s}}\right)(1+\cos\Delta\alpha)}{\left(\frac{R_2'+R_o'}{s}+\frac{2R_M'}{\sqrt{s}}\right)^2+\left(X_1+X_2'+X_o'+\frac{2X_M'}{\sqrt{s}}\right)^2}+\left\{\frac{\left(X_1+X_2'+X_o'+\frac{2X_M'}{\sqrt{s}}\right)}{\left(\frac{R_2'+R_o'}{s}+\frac{2R_M'}{\sqrt{s}}\right)^2+\left(X_1+X_2'+X_o'+\frac{2X_M'}{\sqrt{s}}\right)^2}-\frac{(X_1+X_2'+X_o')}{\left(\frac{R_2'+R_o'}{s}\right)^2+(X_1+X_2'+X_o')^2}\right\}+\sin\Delta\alpha\right] \qquad (13)$$

From formula (13), we can see that, the rotor current and torque of second AC motor can be determined similar to the first AC motor, having only one difference, which is the displacement angle of each rotor.

If we know that $T_m = (mU^2_{ph}) / (2\omega_o X_k)$, $S_m = R'_2/X_k$, and represent all parameters of system through X_k, after some transformations and simplification we can come up with new equation of speed – torque characteristics of two motors coupled with electromagnetic working shaft in relative units as following.

Where:
$K_1 = R'_o/X_k$, $K_2 = R'_M/X_k$, $B_1 = X'_o/X_k$, $B_2 = X'_M/X_k$, $X_k = X_1 + X'_2$; $\Delta\alpha = \alpha_2-\alpha_1$

$$T_1^*=\left[\frac{\left(\frac{Sm}{s}+\frac{K_1}{s}\right)(1-\cos\Delta\alpha)}{\left(\frac{Sm}{s}+\frac{K_1}{s}\right)^2+(1+B_1)^2}+\frac{\left(\frac{Sm}{s}+\frac{K_1}{s}+\frac{2K_2}{\sqrt{s}}\right)(1+\cos\Delta\alpha)}{\left(\frac{Sm}{s}+\frac{K_1}{s}+\frac{2K_2}{\sqrt{s}}\right)^2+\left(1+B_1+\frac{2B_2}{\sqrt{s}}\right)^2}\right]+\left[\frac{\left(1+B_1+\frac{2B_2}{\sqrt{s}}\right)}{\left(\frac{Sm}{s}+\frac{K_1}{s}+\frac{2K_2}{\sqrt{s}}\right)^2+\left(1+B_1+\frac{2B_2}{\sqrt{s}}\right)^2}-\frac{(1+B_1)}{\left(\frac{Sm}{s}+\frac{K_1}{s}\right)^2+(1+B_1)^2}\right]\sin\Delta\alpha \qquad (14)$$

The speed – torque characteristics of this type of synchronous systems will be built, taking into consideration that we use two AC motors Ak – 51/4 type with the following parameters:

$P_n = 2.8$ KW ; $R_1 = 1.92\ \Omega$; $n_o = 1500$ RPM; $R'_2 = 3.12\ \Omega$; $\tau_n = 0.78$; $X_1 = 3.49\ \Omega$;cos $\varphi_n = 0.82$; $X'_2 = 3.43\ \Omega$; $X_\mu = 71.3\ \Omega$; $R_\mu = 2.42\ \Omega$

The curves are built according to the different K_2 Value as shown in figure (5), which depends on inductive rheostat parameters. With increasing K_2 values the starting torque of the system will be less, which will help the system in soft starting with working equipment(Sagetov et.al 1986).

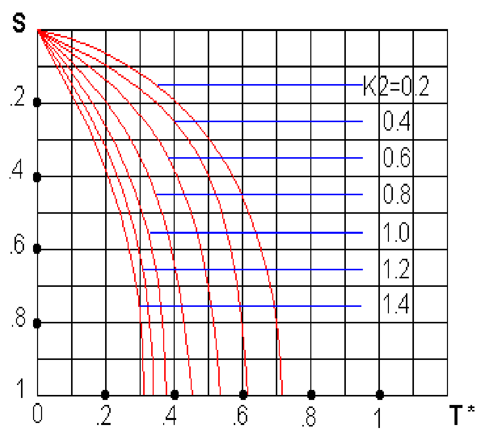

Fig. 5. Slip-torque characteristics of the system with E.M.W.S.

Construction of the angle-torque characteristic of the system is shown in figure (6), where T^*_1 – the torque of the first AC motor and T^*_2 the torque of the second motor.

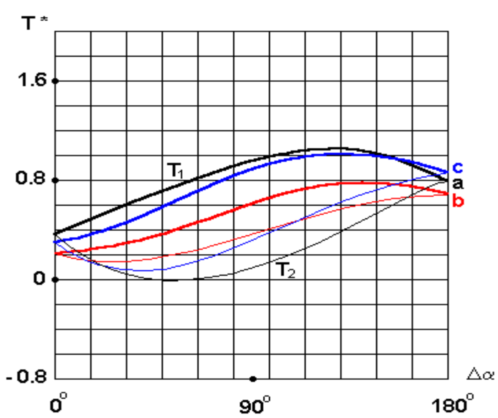

Fig. 6. The angle-torque characteristics of the system with E.M.W.S.

Conclusions:

The most important advantage of the system with E.M.W.S. is that, there is no need to position each rotor winding axis with respect to the axis of the stator field at the same position in both machines. That is because the main role in synchronization in the system with E.M.W.S. plays the mutual magnetic flux between the rotors windings of both machines, and not the resultant E.M.F. as in the systems with E.M.W.S. Consequently, the system with E.M.W.S. can reverse without the need to stop the motors rotation.
Another important advantage of the system with E.M.W.S. is that, the system needs not insert additive resistance to start the system, because the inductive reactance can change it's value according to the current flow through it.

The use of systems of synchronous rotation with E.M.W.S. makes synchronous systems work with better indications of synchronization and with wide range of different loads, where $\Delta\alpha$ can reach 90°. In the other side, the most important disadvantage of the systems of synchronous rotation with E.M.W.S. is the low power factor as the result of the high value of the resistance of common rheostat.

<u>References</u>

Carlo Cecat " Position control of the induction motor using a passivity – based controller". *IEEE – Industry applications, vol.36, N05, September \ October 2000*

Dimentberg M , Cobb E, Mensching Y. "Self-synchronization of transient rotation in multiple shaft systems" *.Journal of vibration and control, Feb 2001, vol. P221*.

Sagetov P., Kim B., J. Tashkenbaev " The regulation of many motors electric drive systems with high synchronization. Moscow" *Energy and atom publishers ,1986.*

SIMULATION MODELLING OF THE MARINE STEAM TURBINE

Marijo Orsulic
Ante Munitic
Josko Dvornik
University of Split
Maritime Faculty of Split
Zrinsko-Frankopanska 38
21000 Split, Croatia
e-mail: amunitic@pfst.hr, josko@pfst.hr

KEYWORDS
System Dynamics, Modelling, Steam turbine, Continuous and discrete simulation and heuristics optimization

ABSTRACT

Simulation Modelling, together with System Dynamics and intensive use of modern digital computer, which mean massive application, today very inexpensive and in the same time very powerful personal computer (PC-a), is one of the most suitable and effective scientific way for investigation of the dynamics behaviour of non-linear and complex: natural, technical and organization systems.
The methodology of System Dynamics (Prof dr. J. Forrester – MIT), e.g. relatively new scientific discipline, in former educational and designer practice showed its efficiency in practice as very suitable means for solving the problems of management, of behaviour, of sensibility, of flexibility and sensibility of behaviour dynamics of different systems and processes.
System Dynamics computer simulation methodology have been used from 1991 to 2003 for modelling of dynamics behaviour of the large number of non-linear ship electrical, thermo-dynamical, hydraulically, mechanical and pneumatically systems. This methodology is used by students as a material for graduate these at Maritime faculty Split. Investigation of behaviour dynamics of the ship propulsion system, as one of the complex, dynamics, non-linear and technical system, requires application of the most effective modelling methods.
The aim of this paper is to show the efficiency of the application of the System Dynamics Simulation Modelling in investigation of behaviour dynamics, one of the complex marine system and process i.e. “steam – turbine”. Steam turbine shall be presented with mental-verbal, structural and mathematical-computing models, and will simulate working process of turbine.

SYSTEM DYNAMICS SIMULATING MODELLING OF THE STEAM TURBINE

The steam turbine working process is the conversion of water steam energy to mechanical energy converted to trust on the propeller. Therefore, turbine is subjected to various loads transmitted from the propeller. The steam turbine working system can be derived into two parts: regulating valve and nozzle ring steam space that can accumulate steam energy and rotational part that accumulate kinetic energy.
Steady state for the first part can be derived:

$$G_T - G_m = 0 \tag{1}$$

G_T - Turbine steam flow rate, [kg/s]
G_m - Regulating valve steam flow rate, [kg/s]

Dynamical state for the first part is defined by this equation:

$$(G_m - G_T)dt = dG_1 \tag{2}$$

G_1 - Steam quantity accumulated in steam space [kg/s]
Opening or closing regulating valve can change quantity of steam accumulated in the steam space part.
Concerning G_m, G_T, G_1, and functional dependencies of each parameters and stated variables, each function increment can be calculated.
If those functions are derived in Taylor series and literalized using relative values, then the first differential equation for the first part is defined according to [4]:

$$T_2 \frac{d\psi_1}{dt} + \psi_1 = K_0\psi_0 + K_4\mu \tag{3}$$

Where are:
T_2 - Time constant of the steam space [s]
ψ_1 - Relative value of the steam pressure increment in the steam space;
ψ_0 - Relative value of the steam pressure increment before regulating valve;
μ - Relative value of regulating valve opening change;
K_0, K_4 - Gain coefficients;

Steady state for turbine and propeller shaft revolution can be defined:

$$M - M_r = 0 \tag{4}$$

Transient state for the other part of the turbine system can be represented by this equation:

$$J\frac{d\omega}{dt} = M - M_r \tag{5}$$

M - shaft torque transmitted by steam turbine [Nm]

M_r - Resistance propeller shaft torque which is defined as load moment [Nm]
J - Moment of inertia of the rotating parts [kgm^2]

Using the same procedure as for deriving equation (3) differential equation is defined which represents part of the turbine system, which accumulates kinetic energy:

$$T_1 \frac{d\varphi}{dt} + \varphi = K_1\psi_1 + K_2\psi_2 - K_3\alpha \qquad (6)$$

Where are:
T_1 - Time constant of rotating parts [s]
φ - Relative increment of turbine shaft angular velocity
φ_2- Relative pressure increment in main condenser
α - Relative turbine load change
K_1, K_2, K_3 - Gain coefficients

System dynamics structural model of the steam turbine:

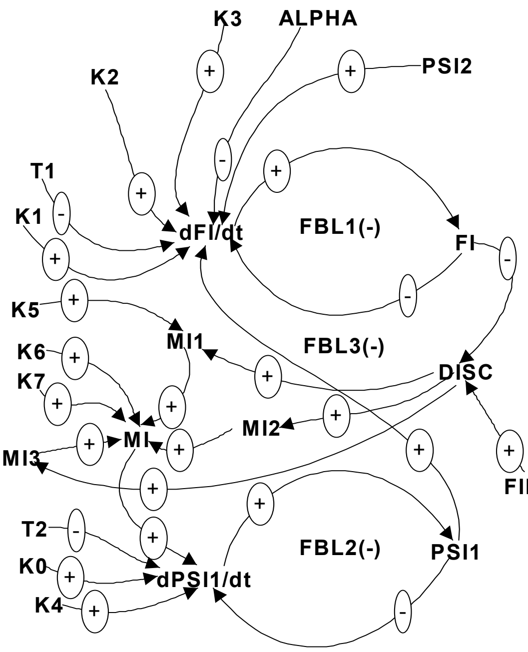

Figure 1. System Dynamics Structural Model of the Steam turbine

In the structural model (Figure 1.) are determined three self-regulating (-) dominated Feed Back Loops (FBL1, FBL2 and FBL3.), with a lot of cause-consequences links (CCL). We could present them on the this "short" symbolic version:

-FBL1(-): dFI/dt(+)=>FI(-)=>dFI/dt
-FBL2(-): dPSI1/dt(+)=>PSI1(-)=dPSI1/dt
-FBL3(-): FI(-)=>DISC(+)=>MI(+)=>
dPSI1/dt(+)=>PSI1(+)=>dFI/dt(+)=>FI

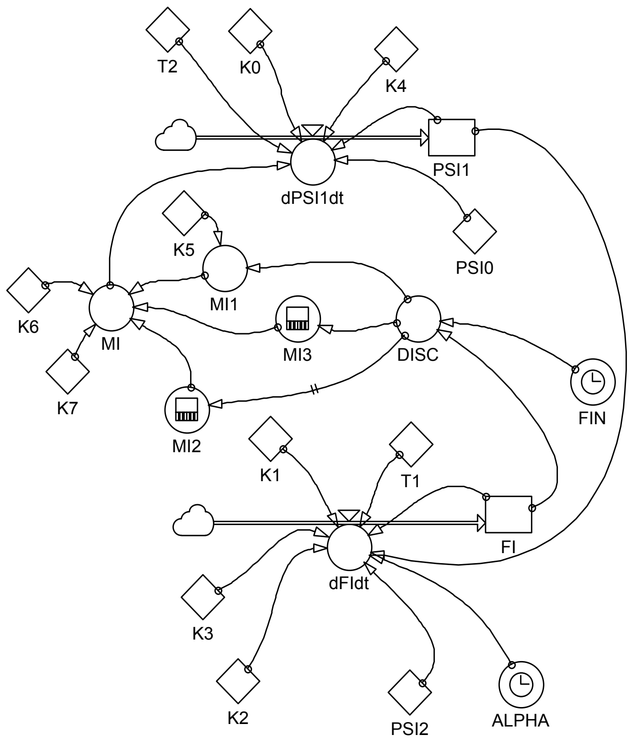

Figure 2. System Dynamics Structural FlowDiagram of the Steam Turbine and PID Regulator in the PowerSim Symbols

SIMULATION RESULTS

About simulation scenario:
The mixed scenario has been implemented in the computer simulation models of the steam turbine and PID regulator: Steam turbine with PID regulator starts in TIME = 0 and FIN = .05; TIME = 20 and FIN = .05+.45 = .50; and TIME = 40 and FIN = .05+.45+.5 = 1 (100%).
relative turbine load change ALPHA starts in TIME = 60 and ALPHA = .05; TIME = 100 and ALPHA = .05+.45 = .50; and TIME = 140 and ALPHA = .05+.45+.50 = 1 (100%)

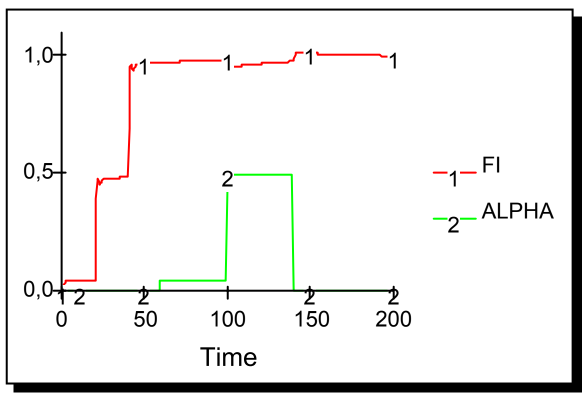

Figure 3. Relative increment of turbine shaft angular velocity and Relative turbine load change

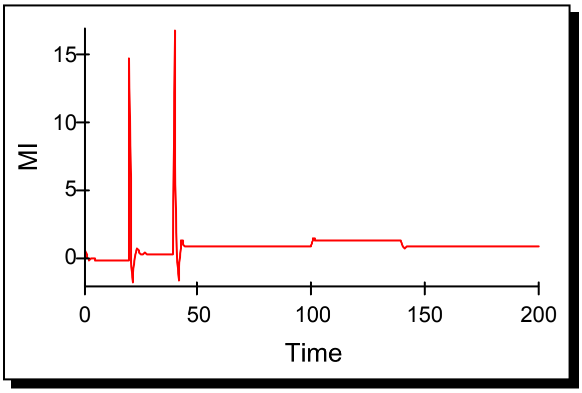

Figure 4. Relative value of regulating valve opening change

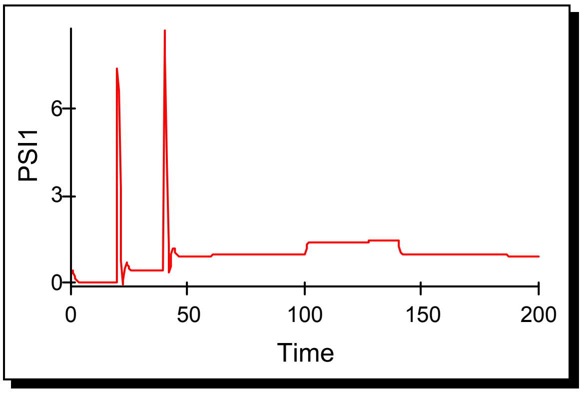

Figure 5. Relative value of the steam pressure increment in the steam space

CONCLUSION

Quality and economical steam turbine functioning depend on many parameters such as steam pressure before and after the regulating valve, condenser pressure, etc. Since successful turbine functioning depends on a large sequence of various parameters this problem should be solved systematically. Using system dynamics, in this paper the complexity of steam turbine dynamics system behaviour has been partially presented. The system dynamics mathematical model, dynamics continued computer simulation model and structural dynamic model of the steam turbine and automatic PID-regulator are presented. Therefore interaction links between each parameter and variables can be analysed. A simulation model is used to enable optimisation of all parameters of the steam turbine system and transient and steady state simulation according to the stated scenario. The most difficult operation conditions here can be investigated even in reality are not physically possible.

The authors suggest the use of this modelling approach in designing, for the engineering educational processes as well, which will allow an active and creative participation of students. This method is, therefore, expected to be economical in organising the educational process.

REFERENCES

Forrester, Jay W. 1973/1971. "Principles of Systems", MIT Press, Cambridge Massachusetts, USA,

Munitic, A., Milic M. and Milikovic M. 1997. "System Dynamics Computer Simulation Model of the Marine Diesel-Drive Generation Set", *Proceeding of World Congress on Scientific Computation, Modelling and Applied Matematichs*, Berlin,

Munitic, A. 1989. "Computer Simulation with Help of System Dynamics", BIS, Croatia,

Richardson, George P. and Pugh III Aleksander L. 1981. "Introduction to System Dynamics Modelling with Dynamo", MIT Press, Cambridge, Massachusetts, USA,

Miler, J., 1955, (in Croatian), "Parne i plinske turbine", Zagreb, Croatia,

Нелепиhа, P. A., 1975, "Abtоматиэадия cчдобыx эhepгетическиx чctahobok", Moskva, Rusia,

Munitic, A., et al.. 2002. "System Dynamics Modelling of Complex Electro Mechanical System", *IASTED,AMS 2002,* Cambridge, USA,511-515.

Munitic A., Antonic R., Dvornik J., 2003., "Computing simulation and heuristic optimization of ship anchor arrangement", *Proceeding of ICCC'03*, SLOVAK, 353-357

Munitic A., Antonic R., Dvornik J., 2003., "System dynamics simulation modeling of ship-gas turbine generator", *Proceeding of ICCC'03,* SLOVAK, 357-360

Munitic A., Orsulic M., Dvornik J., 2003, "Computer Simulation of Complex Ship System "Gas turbine.Sysnhronous Generator" *Proceeding of ISC 2003,* Valencia, Spain, 192-197.

BIOGRAPHY

MARIJO ORSULIC received his B.Sc, M.Sc. and Ph.D. in mechanical engineering from Faculty of Mechanical Engineering University of Rijeka in 1968, 1984 and 1988 respectively. He is currently an associative professor at University of Split, College of Maritime Studies. He is author or co-author of a number of bibliographical units (scientific and professional conference and journal papers, research projects, text books, etc.). His research interest is in Marine Engineering, auxiliary marine engines and technical mechanics theory and practise.

COMPUTING SIMULATION OF THE MARINE DIESEL ENGINE START UP SYSTEM

Marijo Orsulic
Ante Munitic
Josko Dvornik
University of Split
Maritime Faculty of Split
Zrinsko-Frankopanska 38
21000 Split, Croatia
e-mail: amunitic@pfst.hr, josko@pfst.hr

KEYWORDS
System Dynamics, Modelling, Asynchronous motor, Start up system and Ship/s piston compressor.

ABSTRACT

System dynamic simulating modelling is one of the most appropriate and successful scientific dynamics modelling methods of the complex, non-linear, natural, technical and organisational systems. Investigation of behaviour dynamics of the ship/s propulsion system as one of the complex, dynamic, non-linear technical systems requires application of the most efficient modelling methods.
Marine Diesel engine start up system, which it is consisted of ship/s piston compressor and its driving electric motor, i.e. in this case asynchronous motor, shall be presented in the System Dynamics modelling approach in POWERSIM simulation symbolic and language. System dynamic models are essentially continuous models since the realities have been demonstrated by a set of non-linear differential equation, i.e. "equations of conditions", however they are at the same time discrete ones because their principle time interval calculation i.e. (discretisation) sampling "DT" is determined in full compliance with (Sampling Theorem) by Shannon and Koteljnikov.

SYSTEM DYNAMICS MODELLING OF THE DIESEL ENGINE START UP SYSTEM

The system is made up of several complex sub systems which as a whole forms complete start up system. In this short paper it is impossible to present complete system. System is consisting of compressor with propulsion and air reservoir, the parts that will be presented in our model.
Complete model (27 equations) of the asynchronous motor has been presented in IASTED 1998, Pittsburgh, USA [9] and M. Jadric and B. Francic, *Dinamika elektricnih strojeva,* (Manualia Universitatis Studiorum Spalatiensis Graphics, Zagreb, Croatia, 1996) [3].
Basic equations of the piston compressor condition are:

$$\frac{d\omega}{dt} = \frac{Mem - Mkom}{Mt} \qquad (1)$$

$$Mkom = \frac{G \cdot Wk}{\omega} \qquad (2)$$

$$W_k = \frac{n \cdot R \cdot T_1}{(n-1) \cdot \eta}\left[1 - \varepsilon^{\frac{n-1}{n}}\right] \qquad (3)$$

$$\frac{dG}{dt} = G_{kom} - G_{zup} \qquad (4)$$

$$G_{kom} = \frac{V \cdot P_2}{R \cdot T_2} \qquad (5)$$

$$V = 0{,}42 \cdot \frac{d^2 \cdot \pi}{4} \cdot s \cdot 6 \cdot c \cdot 1{,}3 \qquad (6)$$

Mt- system inertia moment (kgm^2)
Mem- electric motor moment (Nm)
Mkom- compressor moment (Nm)
ω **-** compressor shaft speed of rotation (1/s).
G – suction air mass flow (kg/s)
Wk – compression work (J/kg).
V – cylinder volume (m^3)
v – specific air volume (m^3/kg).
n – polytropic compression coefficient
R – gas constant for air
Ti – initial air temperature
$\varepsilon -$ compression stage
$\eta -$ compressor efficiency ratio.
Vkom – compressor air volume delivery (m^3/s),
Gkom – compressor capacity (kg/s),
Gzup – air mass for starting (kg(s),
P_2 – pressure at the end of compression (N/m^2),
T_2 – temperature at the end of compression (K).
d - engine cylinder diameter (m),
s – piston stroke (m),
c – number of cylinders,
6 – number of startings,
1,3 – 30% is taken exceeding calculated value.
Air receiver capacity depends on whether the engine is reversing or non-reversing and thus the air receiver capacity for reversing engines shall be calculated for 12 starting and for non-reversing ones the capacity shall be calculated for 6 starting only.
At one starting air shall be supplied to the cylinder at 1/3 to1/2 piston stroke, therefore the air receiver volume is approximately to equation 3.

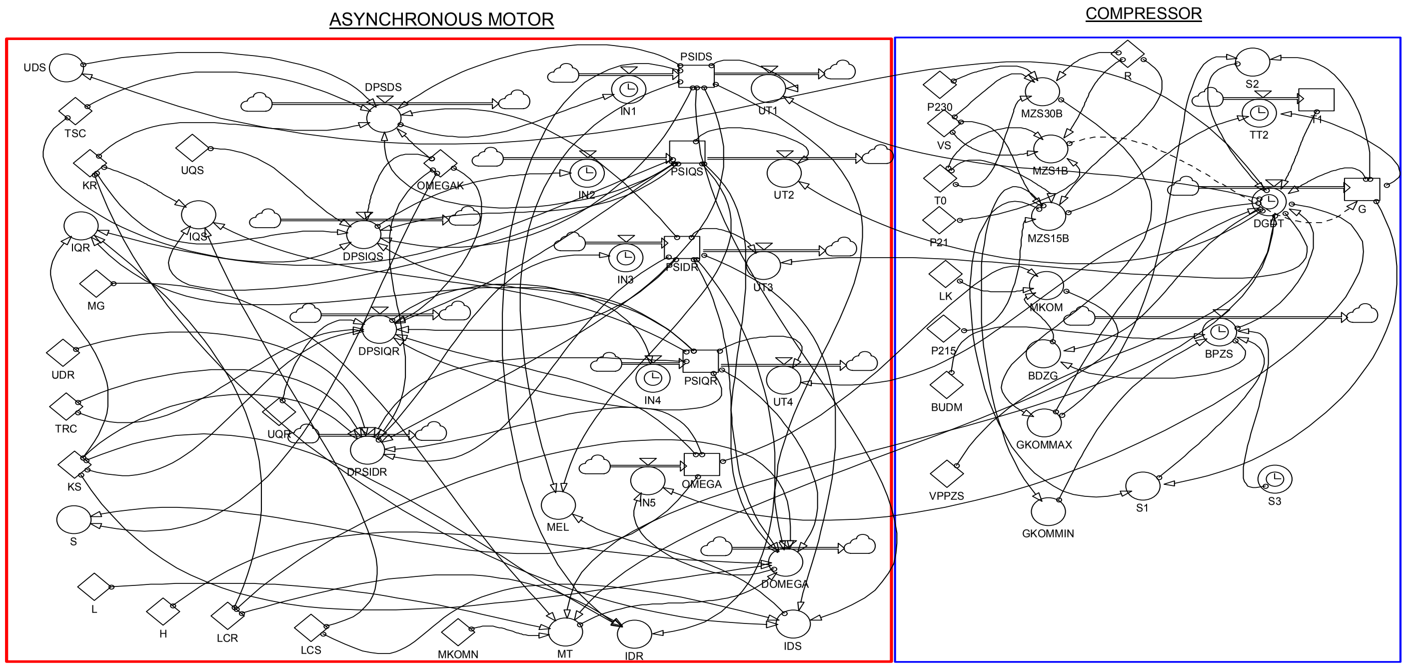

Fig.1. Global system dynamic model of driving system for piston compressor driven by asynchronous motor in POWERSIM symbols

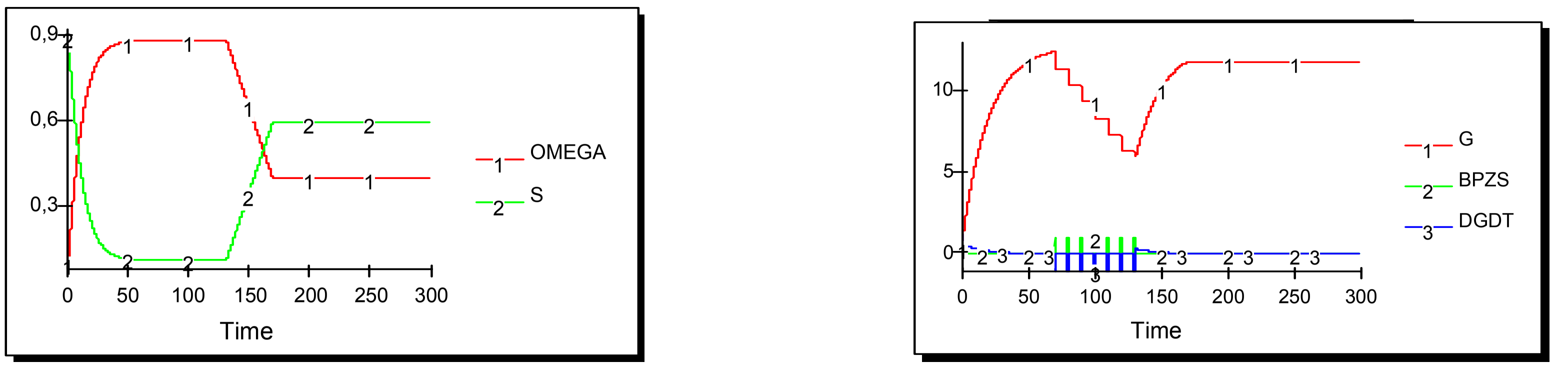

Fig.2. Angle speed, asynchronous motor slip and air mass condition in air receiver, air quantity speed variation and air consumption speed

Mental-verbal model, structural and flow diagram has been presented in IASTED MS 2003 [11].

COMPUTING SIMULATING MODEL OF THE MARINE DIESEL ENGINE START UP SYSTEM IN POWESIM SIMULATION SYMBOLICS

Complete continuity diagram of the dynamic shown in Fig.1.
Scenario of driving dynamics of the piston compressor driven by asynchronous motor includes I charging, I discharging, II charging and II discharging of the air receiver.
Graphical figure of the simulation results are presented on figure 2, 3.

Simulation Comment:
Diagrams point at the validity of dynamical behaviour of the present driving system and therefore it may be concluded that the piston compressor may be appropriately driven by a heavy asynchronous motor, complying with its specific requirements.

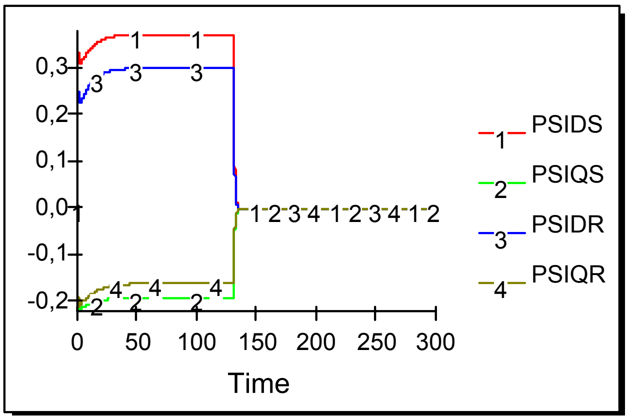

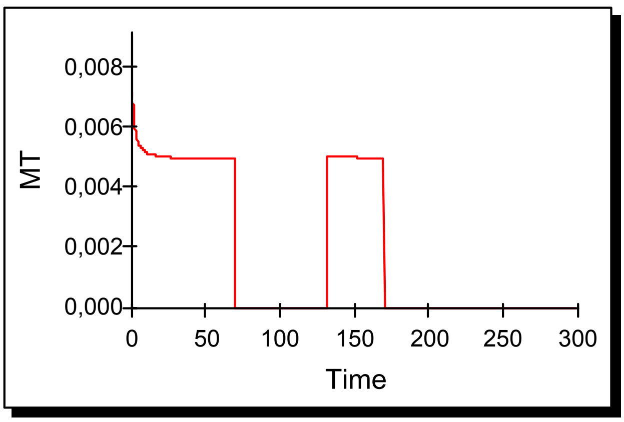

Fig.3. Stator and rotor linkage fluxes of asynchronous motor and load torque.

CONCLISION

The application of System Dynamics Simulation Modelling Approach of the complex marine dynamic processes, which the authors, together with their graduate students, carried out at the Maritime Faculty University of Split - Croatia eleven years ago, revealed the following facts:

l. The System Dynamics Modelling Approach is a very suitable software education tool for marine students and engineers.
2. System Dynamics Computer Simulation Models of marine systems or processes are very effective and successfully implemented in simulation and training courses as part of the marine education process.

REFERENCES

Forrester, Jay W. 1973/1971. "Principles of Systems", MIT Press, Cambridge Massachusetts, USA,

Munitic, A., Milic M. and Milikovic M. 1997. "System Dynamics Computer Simulation Model of the Marine Diesel-Drive Generation Set", *Proceeding of World Congress on Scientific Computation, Modelling and Applied Matematichs*, Berlin,

Jadric, M. and Francic, B., 1996., "Dinamika elektricnih strojeva", Manualia Universitatis Studiorum Spalatiensis Graphics, Zagreb, Croatia,

Munitic, A. 1989. "Computer Simulation with Help of System Dynamics", BIS, Croatia,

Richardson, George P. and Pugh III Aleksander L. 1981. "Introduction to System Dymanics Modelling with Dynamo", MIT Press, Cambridge, Massachusetts, USA,

Munitic, A., 1989, "Application Possibilities of System Dynamics Modelling", *Proceeding of SCS Western Multiconference*, San Diego, California, USA,

He:eB4ha, P. A., 1975, "Abtomat4⊥a∗4β cP∗ob∴ix ⊥hepηet4Peck4x Pctahobok", Moskva, Rusia,

Munitic, A.,Kuzmanic, I.,Krcum, M.,1998., "System Dynamic Simulation Modelling of the Marine Synchronous Generator", *Proceeding of Modelling and Simulation Conference, IASTED*, Pittsburgh, 372-375.

Munitic, A., et al.. 2002. "System Dynamics Modelling of Complex Electro Mechanical System", *IASTED,AMS 2002,* Cambridge, USA,511-515.

Munitic, A., Kulenovic, Z., Dvornik, J., 2003., "Computing Simulation of Driving System- "Ship/Piston Compressor-Electric motor", *IASTED MS 2003*,California, USA, 515-520.

Munitic, A., Kulenovic, Z., Dvornik, J., 2003, "System Dynamics Optimization of the ship piston compressor with electric drive", *TMT 2003,* Barcelona, Spain, 1085-1088,

Munitic A., Antonic R., Dvornik J., 2003., "Computing simulation and heuristic optimization of ship anchor arrangement", *Proceeding of ICCC'03*, SLOVAK, 353-357

Munitic A., Antonic R., Dvornik J., 2003., "System dynamics simulation modeling of ship-gas turbine generator", *Proceeding of ICCC'03,* SLOVAK, 357-360

Munitic A., Orsulic M., Dvornik J., 2003, "Computer Simulation of Complex Ship System "Gas turbine.Sysnhronous Generator" *Proceeding of ISC 2003,* Valencia, Spain, 192-197.

SIMULATION
IN
INFORMATION
PROCESSING

HIDDEN DATA EXTRACTION WITHOUT ORIGINAL HOST

Nidhal Abdulaziz
Department of Computer Science
University of Wollongong in Dubai, UAE
Email: nidhal@uow.edu.au

K. Khee Pang
Dept of Elect & Comp Systems Eng
Monash University, Victoria, Australia
Email: khee.pang@monash.edu.au

Abdullatif Glass
Department of Planning and Training
Technical Studies Institute, Abu-Dhabi, UAE
Email: aglass@ieee.org

ABSTRACT

A robust data hiding technique for embedding images in images has been proposed. A key component of this scheme is the use of channel codes for encoding the signature image coefficients before inserting them into the host image wavelet coefficients. The hidden data can be recovered without the original host image. Experimental results show that this method is robust to lossy image compression.

INTRODUCTION

Much of the prior work in signature authentication and in data hiding assumes that the host source is available. The host signal serves as a major noise source in the detection of the watermark. Hence, the knowledge of host signal characteristics will definitely enhance detection performance. In this paper we propose an approach to signature recovery that does not require knowledge of the original host by using the discrete wavelet transform. This kind of watermarking is referred to in the literature as *blind watermark detection*. In this case, the interference from host image exists even when there is no noise from processing and other attacks. The most difficult problem associated with blind watermark detection in the frequency domain is to identify the coefficients that have been modified and the embedded watermark values. Since the non-marked (original) image is no longer available at the decoder, it is impossible to determine the position of the coefficients that has been marked. To get around the problem, the mark is always inserted in a predefined set of coefficients. In this paper, we develop a blind watermark detection algorithm by selecting specific coefficients and replacing them with the channel coded indices of the watermark. The choice of the subbands for embedding hidden data is of important significant and this will be explained in the next Section. Examples of methods that do not require the original host data for signature recovery include [Marvel et al. 1998], [Piva et al. 1998], and [Pereira et al. 1999]. The main contribution here is a technique that has the potential for embedding a significant amount of data, which can then be recovered without any additional knowledge of the host.

The proposed embedding and extracting methods utilize the discrete wavelet transform (DWT) domain. The DWT has good energy compaction properties and it is playing an important role in compression standards such as JPEG2000 and MPEG-4. For this reason it has been used in our data embedding research.

The next section explains the embedding approach for the wavelet coefficients. Sections 2 and 3 discuss embedding and extraction techniques. Experimental results are given in section 4 and conclusions in section 5.

EMBEDDING TECHNIQUE

We now focus on the issue of choice of subbands for embedding hidden data. In general, hiding data in the lower subbands has several advantages. The nature of current compression algorithms favors better preservation of the lower frequency data than high frequency data. Insertion of information in the lower bands, therefore, does not lead to easy destruction of the hidden information or to any significant change in the coding efficiency. On the other hand, insertion of data in the higher bands has the advantage that it does not degrade the host image quality significantly. Examples of such operations include low pass filtering for image enhancement and JPEG lossy compression. A disadvantage, on the other hand, is that distortion to the host image introduced by embedding in the lower bands may be perceptually more severe than other bands.

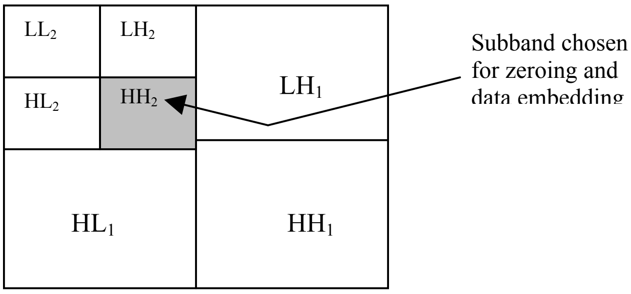

Figure 1: Subband chosen for zeroing and data embedding.

Moreover, as has been pointed earlier, the host image in data hiding serves as a major noise source in blind watermark detection, and the interference from host image exists even when there is no noise from processing and other attacks. In such a case marking only mid-band coefficients will reduce the interference from host image. This results from the observation that low-band coefficients generally have much higher power than the mid-band coefficients [Abdulaziz and Pang 2000]. Therefore, in order to obtain a tradeoff between perceptual invisibility and robustness to image processing techniques, the lowest subband coefficients are skipped and the watermark is inserted into the intermediary frequency coefficients.

Similar proposals for blind watermarking have been found, in [Barni, et al. 1998], [Herrigel, et al. 1998], and [Wu, et al. 1999] for embedding in the discrete cosine transform (DCT) domain using spread spectrum watermarking, and in [Chae and Manjunath 1999], for embedding in the wavelet domain. Like in [Barni, et al. 1998], our algorithm chooses the medium frequency range of the spectrum of the transform coefficients but unlike [Barni, et al. 1998], our algorithm has the ability to hide large number of data bits and casts the watermark in the DWT domain. This is due to the use of different techniques in the embedding process. For example, vector quantizer is used to compress the signature image, and channel codes to eliminate the errors introduced due to compression and noise attacks.

Further, noting that natural images typically have very low energy in the higher bands, we find that for most images, zeroing out some or all of the coefficients in one or more of the high subbands introduces a very low mean square error, and affects detail only hardly noticeable in the perceptual sense. Therefore, if the hidden data is embedded on the zeroed coefficients, the extraction process only needs to use the zero-vector as its estimated base for decoding the noisy vectors it receives. In practice, the exact coefficients that are zeroed out and subsequently used for embedding, are either predetermined, or selected in a pseudo-random manner using a key, or selected image-adaptively based on stable features of the host frame.

The scheme implements a two-stage wavelet transform decomposition of each image is made, and the hidden data is embedded in the coefficients of the middle subband, after zeroing. The DWT decomposition scheme used is shown in Figure 1. A two-stage Haar wavelet transform decomposition of host image is made, and the hidden data is embedded in the coefficients of the shaded HH_2 subband, after zeroing. Figures 2 and 3 show a schematic diagram for the embedding and extraction mechanism outlined above. The steps in embedding are:

1 The signature coefficients are vector quantized. The quantized coefficients are encoded using channel codes [Abdulaziz and Pang 2001].
2 The signature codes are then appropriately scaled by the factor α.
3 The selected host coefficients are then replaced by the scaled signature codes and combined with the original (unaltered) DWT coefficients.
4 The merged coefficients are then inverse transformed to give an embedded image.

The choice of the vector quantizer affects the quantity and quality of embedded data. Choice of the scale factor α depends on the application. A large value of α results in a more robust embedding at the cost of quality of the embedded image, i.e., there could be perceivable distortions in the embedded image. A smaller α may result in poor quality recovered signature when there is a significant compression of the embedded image.

To increase the security of the embedding, an encryption key could be used to pseudo-randomly shuffle the coefficients in the subband chosen for embedding before grouping them into n-dimensional vectors. The encryption key base shuffling introduces an additional layer of security apart from the security enforced by the already immeasurable variability in the source and channel codebooks chosen. It is practically impossible for unauthorized persons who know the algorithm, to pirate the hidden information, without knowledge of the source codebook, the channel codebook, or the encryption key. In our experiments shown in section 4 however, we didn't implement the encryption key for simplicity reasons.

EXTRACTION TECHNIQUE

Figure 3 shows the block diagram of the decoder without the host image. Signature extraction follows an inverse sequence of operations. The received embedded image is first DWT and the modified coefficients are identified. By appropriately scaling the coefficients corresponding to the signature data, the codes representing the signature data are recovered. To recover the original data a soft-decision decoding using Viterbi algorithm is implemented. Finally, the signature image is obtained from the source codebook of the vector quantizer.

IMPLEMENTATION AND EXPERIMENTAL RESULTS

This section provides simulation results to demonstrate the performance of the proposed technique. We specifically make use of the Haar wavelet transform for all

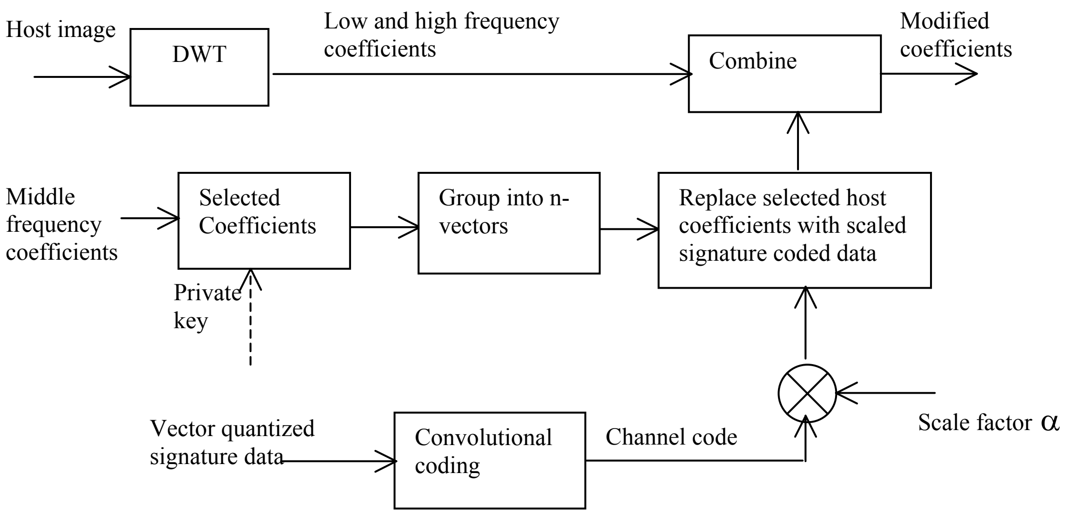

Figure 2: Schematic block diagram of the encoder.

simulation. We took the gray image of *Elaine* of size 512 x 512 and watermarked it with watermark image of *Bird* of size 128 x 128. The watermark is inserted into the DWT of the host image as explained in Section 1. A fixed scale factor α of 10 was used throughout the experiments.

The resulting watermarked signal is distorted using JPEG compression and noise addition. The watermark was then extracted without knowledge of the host image and compared with the original watermark to measure robustness and detection capability of the technique.
The embedding was implemented using vector quantizer to compress the signature images of *Bird* to one fourth of its original size. The indices obtained are then channel coded using convolutional code of rate 2/3 before embedding into the host DWT coefficients. The host image of *Elaine* was transformed to the wavelet domain using 2 levels of Haar wavelet transform and the coefficients of the subband HH_2 are zeroed to allow the insertion of the channel coded signature symbols.

Figure 4 shows the host image of *Elaine* and the watermarked image of *Elaine* with a signature gray image of *Bird*. This embedding results in one-sixteenth-size signature image. The PSNR of the watermarked *Elaine* image is 36.81 dB. Figure 5 shows the PSNR of the recovered *Bird* image for different JPEG compression. Here the PSNR of the extracted *Bird* image is compared to the original watermark image of *Bird*, higher values would be obtained if it has been compared to the compressed one.

CONCLUSIONS

In summary, we have proposed a robust data hiding technique for embedding images in images. A key component of this scheme is the use of channel codes for encoding the signature image coefficients before inserting them into the host image wavelet coefficients. The hidden data can be recovered without the original host image. Experimental results show that this method is robust to lossy image compression. Similar results can be obtained for concatenated and turbo codes. However, only convolutional codes is shown in this paper.

REFERENCES

Abdulaziz, N., and K. Pang. 2000. "Performance Evaluation of Data Hiding System Using Wavelet Transform and Error-Control Coding" IEEE International Conference on Image Processing 2000 (ICIP 2000), 10-13 September 2000, Vancouver, Canada, vol. I, pp. 605-608.

Abdulaziz, N., and K. Pang. "Coding Techniques for Data Hiding in Images" The Sixth International Symposium on Signal Processing and its Applications ISSPA 2001, 13-16 August 2001, Kuala-lumpur, Malaysia, pp.170-174.

Barni, M., Bartolini, F., Cappellini, V., and Piva, A. "A DCT-Domain System for Robust Image Watermarking", Signal Processing (Special Issue on Watermarking), vol. 66, no. 3, 1998, pp. 357-372.

Chae J. J. and Manjunath, B. S. "A Technique for Data Hiding and Reconstruction without Host Image," SPIE, Electronic Imaging 99, Security and watermarking of Multimedia Content, January 1999, San Jose, California.

Herrigel, A., O'Ruanaidh, O. J., Petersen, . H. , Pereira, S. and Pun, T., "Secure Copyright protection Techniques for Digital Images," Second information Hiding Workshop, 1998.

Marvel, L. M., Boncelet,Jr., C. G., and Retter, C. T., "Reliable blind information hiding for images," Proceedings of Second International Workshop, IH'98, Portland, Oregon, USA, April 1998.

Pereira, S. O'Ruanaidh, J. K., and Pun, T., "Secure robust digital watermarking using the Lapped Orthogonal Transform", Proceedings of SPIE, Security and Watermarking of Multimedia Contents, Electronic Imaging'99, San Jose, CA, Jan 25-27 1999, vol. 3657.

Piva, A., Barni, M., Bartolini, F., and Cappellini, V., "Threshold selection for correlation-based watermark detection," Proceedings of COST 254 Workshop on Intelligent Communications, L'Aquila, Italy, June 4-6, 1998, pp. 67-72.

Wu, M. Yu, H. H. and Gelman, A., "Multi-Level Data Hiding for Digital Image and Video," SPIE Photonics East'99, Boston, 1999.

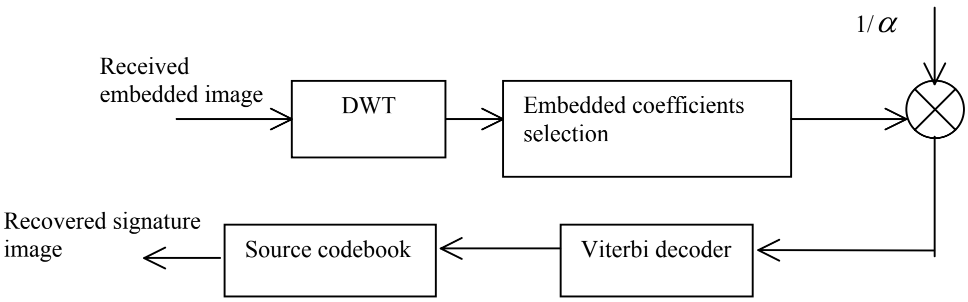

Figure 3: Block diagram of the signature extraction.

(a) (b)

Figure 4: Original and watermarked images of *Elaine*, (a) original image of size 512 x 512, (b) watermarked image with *Bird* image as watermark.

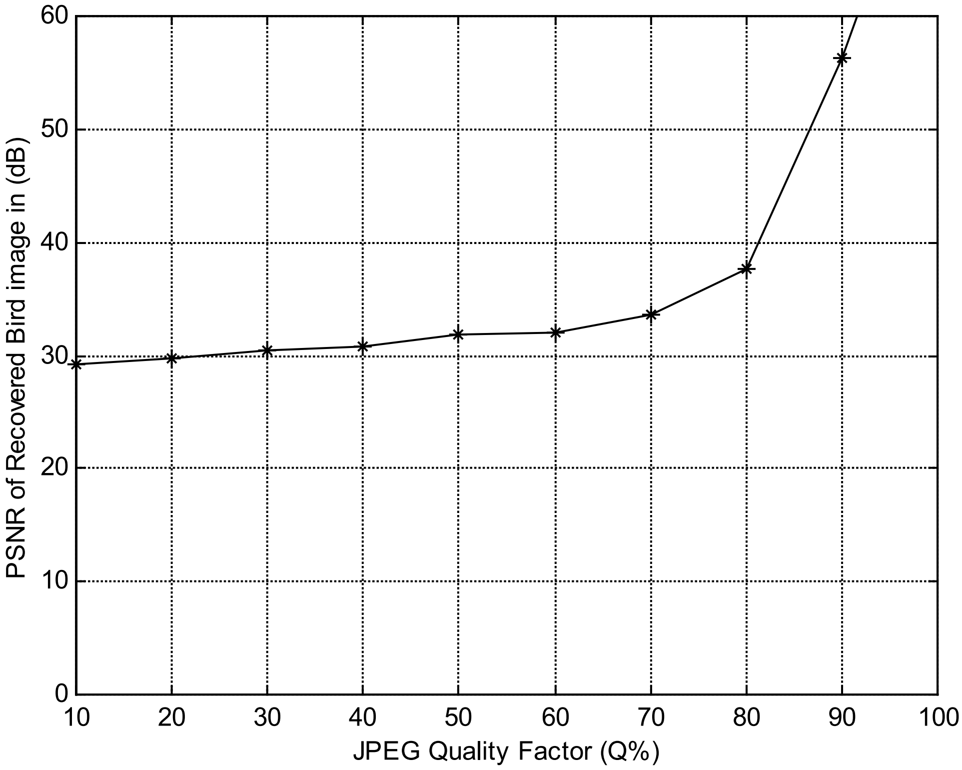

Figure 5: PSNR of recovered *Bird* image watermark for different JPEG compression. The host is *Elaine* image**.**

CELLULAR AUTOMATA EQUIVALENT TO DIL SYSTEMS

Alfonso Ortega, Abdel Latif Abu Dalhoum, Manuel Alfonseca
Escuela Politécnica Superior
Universidad Autónoma de Madrid
Campus de Cantoblanco
28049 Madrid, Spain
E-mail: { Alfonso.Ortega, Abdel.Latif, Manuel.Alfonseca}@ii.uam.es

KEYWORDS

Cellular automata, Lindenmayer systems, parallel derivation grammar, theoretical computer science, formal languages.

ABSTRACT

The authors of this paper have formally tackled the simulations of Lindenmayer systems by cellular automata and vice versa, that is, designing Lindenmayer systems that simulate a given cellular automaton and designing cellular automata that simulate a given Lindenmayer system. While the first direction has been totally covered, we have only simulated D0L systems before now. This paper describes an algorithm to build one-dimensional cellular automata that simulate any (k, l) DIL system, i.e. context sensitive deterministic Lindenmayer systems.

INTRODUCTION

DIL SYSTEMS

L-Systems (Lindenmayer 1968) are parallel derivation systems. A (k, l) DIL system is a context sensitive Lindenmayer system, with an alphabet (a finite non empty set of symbols) a set of production rules and an initial string or axiom. The rules determine the only way that each symbol of the alphabet can be replaced by a word, depending on the sub strings of k and l symbols currently extant to its left and to its right. The size of the context is the same for every rule. To complete the context of symbols too close to the beginning or the end of the string, a symbol that does not belong to the alphabet is used as a filler (g in this paper). The following is the formal definition for (k, l) DIL systems we will be using:

A (k, l) DIL system is a four-fold (Σ,P,g,ω) where Σ is the alphabet, $g \notin \Sigma$ is the filler symbol, $\omega \in \Sigma^+$ is the axiom and P is a set of production rules $P \in \Sigma^k \times \Sigma \times \Sigma^l \rightarrow \Sigma^*$ such that:

1. If $\omega_1 a \omega_2 \rightarrow \omega_4 \in P$ then if
    - $\omega_1=\omega_1' g \omega_1''$ for some ω_1', $\omega_1'' \in (\Sigma \cup \{g\})^*$, then $\omega_1' \in \{g\}^*$.
    - $\omega_3=\omega_3' g \omega_3''$ for some ω_3', $\omega_3'' \in (\Sigma \cup \{g\})^*$, then $\omega_3'' \in \{g\}^*$.
2. $\forall \omega_1 a \omega_3 \rightarrow \omega_4 \mid \omega_1 a \omega_3 \in (\Sigma \cup \{g\})^k \times \Sigma \times (\Sigma \cup \{g\})^k \wedge \omega_1$ and ω_3 satisfy the two conditions in point 1, $\exists! \omega_4 \in \Sigma^* \mid \omega_1 a \omega_3 \rightarrow \omega_4 \in P$.

In deterministic L-systems each word has a single possible derivation. This characteristic allows defining an homomorphism of languages (h) to formalize the derivation process. $h^i(\omega)$ is the word obtained after i derivations and $h^0(\omega)=\omega$ is the axiom.

CELLULAR AUTOMATA

A cellular automaton (Neumann 1966) (CA) is a set of finite deterministic automata distributed along a regular grid. The inputs of the automata are the sets of states of their neighbors; the neighborhood is the same along the grid.

A one-dimensional CA is a linear chain of automata. One-dimensional CA can be formalized as follows (Ortega 2000):

Given a set E, a one-dimensional grid on E is a function $G:Z \rightarrow E$ where G[i] or G_i is the element of E at the i^{th} position in the grid. A one-dimensional neighborhood V is a pair (k, N) where

- $k \in N$ is the number of neighbors of every automaton in the grid.
- $N \in Z^k$ is a vector of k integer offsets. Given the index of a position in the grid, each offset points to a different neighbor of the automaton in this position.

A one-dimensional deterministic cellular automaton is the six-fold (G,G_0,V,Q,f,T) where

- G is a one-dimensional grid of automata.
- Q is the finite and non-empty set of possible states of the automaton in the grid.
- G_0 is the initial configuration.
- $V=(k,N)$ is a one-dimensional neighborhood.
- $f:Q\times Q^k\rightarrow Q$ is the transition function that assigns the next state to each automaton in the grid, depending on its actual state and the states of its k neighbors.

SIMULATIONS BETWEEN L SYSTEMS AND CA

Different aspects of the relationship between L Systems and Cellular Automata have been explored: (Koza 1993) the structural similarities between both formalisms have been underlined. In (Stauffer and Sipper 1998a-b) CA equivalent to the turtle graphic interpretation of some self-replicating L systems were built.

The authors have previously studied the possibility of simulating CA's by means of L Systems (Alfonseca et. al. 2003). In the opposite direction, an algorithm is proposed to build cellular automata to simulate D0L systems (Abu Dalhoum et al. 2003). In this paper we extend this algorithm to DIL systems.

Other authors have previously tackled the design of cellular automata equivalent to L systems. In (Terrier 1991) it is shown that there exist interactive one-dimensional cellular automata able to generate signals with frequencies equal to the growth functions of D0L systems. These cellular automata are designed by means of sets of signals able to solve the problem. Signals in one-cellular cellular automata are widely studied in (Mazoyer and Terrier 1999).

In a similar way, we design linear cellular automata equivalent to given L systems, but our approach differs in several main features: first, our cellular automata are not interactive, no input is needed apart from the initial configuration; second, we are not interested in the growth functions but in the generation of the same languages, that is, our cellular automata generate the same words and in the same order as the L systems; third, although a description of the behavior of our cellular automata in terms of signals is also possible, we are mostly interested in the explicit definition of the whole cellular automata and finally, we simulate L systems more general than D0L.

THEOREM

Given a (i, j) DIL system S, there is a one-dimensional cellular automaton $A_{S,n}$ that simulates the n first derivations of S, for all n.

INFORMAL PROOF

Our proof is constructive, so we propose an algorithm to build the one-dimensional cellular automaton. A formal proof is available but, for clarity and space reasons, the algorithm will be described by means of examples.

In the previous work mentioned before, the authors have shown that, for every D0L system S_d, there exists a one-cellular automaton A_d that simulates its first n derivations. Each cell in A_d grid is associated to a symbol of the words derived by S_d (symbols < and > mark the word's ends) and several signals (<, >) are used to insert new symbols (if needed) in a given position after applying a derivation rule, and ($\leftarrow$, $>_{\leftarrow}$, $<_{\leftarrow}$) to shorten the words (if needed) when λ rules are used. Each A_d state had two components: one for the current cell symbol and other for signals and sub strings that are being displaced in the derivation process.

To handle the context, a new component is added to $A_{S,n}$ states: initially each symbol in the axiom equals its own context information and the filler (g) is used as marker context. Provided that the automaton simulates sequentially (from left to right) the parallel derivation process, the context must be maintained during the whole derivation, to correctly apply context sensitive rules. Thus, some mechanism must be supplied to keep the context information while symbols are displaced to the left when λ rules are applied, and to set the right context information after finishing the whole derivation. It will be shown in the following examples that a new symbol (◊') and a new signal ($◊'_{\leftarrow}$) suffice for the latter situation.

Let us consider the following (1,1)DIL system

$$S=\{\{A,B\}, \{AAA\rightarrow AA, AAB\rightarrow BA, BAA\rightarrow BA, BAB\rightarrow AB, gAA\rightarrow B, gAB\rightarrow A, AAg\rightarrow B, BAg\rightarrow A, xBy\rightarrow\lambda\ \forall x,y\in\Sigma\}, AAA\}$$

The axiom (and every word in the language of S) is represented as follows

g > >	A A ◊	A A ◊	A A ◊	g < <

That is: every marker cell has the filler (g) as context information; cells associated to symbols have an empty displacing substring (◊) and the symbol itself as context information.

The first step is sending the signal < from the right end until it reaches the first symbol, which is then replaced by its production rule [1] gAA→B (the rule context is highlighted). The displacing substring >B indicates this situation

g > >	A A ◊	A A ◊	A A <	g < <

…

g > >	A[1] A <	A A <	A A <	g < <
g > >	A A >B	A A <	A A <	g < <

The first symbol in the displacing substring is in its final position, so it can be removed. However, a new symbol is needed to show that the context (A) is not the right one (B). Symbol ◊’ is used rather than ◊ to distinguish between these circumstances. At the same time [2] the next cell can apply its own rule, AAA→AA, whose right hand side is added to the remainder of the displacing substring (λ, in this case). This process is repeated until the right marker is reached (in [3] the rule AAg→B is applied). The filler remains unchanged. So the displacement to the right finishes and the signal $◊_{\leftarrow}$’ is sent to the left to make each cell writing the correct context and replacing symbol ◊’ by ◊ to finish the derivation.

g > >	A B ◊’	A[2] A >AA	A A <	g < <	g < <
g > >	A A ◊’	A A ◊’	A[3] A >AB	g < <	g < <
g > >	A B ◊’	A A ◊’	A A ◊’	g < >B	g < <
g > >	A B ◊’	A A ◊’	A A ◊’	g B ◊’	g < <
g >	A B	A A	A A	B B	g <

>	◊’	◊’	◊’	$◊_{\leftarrow}$’	<

…

g > >	B B ◊	A A ◊	A A ◊	B B ◊	g < <

This configuration is associated with h(ω), that is, the first word derived from the axiom. The second derivation starts immediately in the same way. Rule xBy→λ means that symbol B must be erased from the string. When this rule is applied [4], all the symbols to its right must be displaced one position to the left, because the displacing substring of B’s left neighbor has no symbol. Signal ← is sent to the right end while each symbol is displaced. Each cell traversed by the signal is marked with symbol $<_{\leftarrow}$. Context information must be handled carefully because it must be kept unchanged until the whole derivation finishes. If the context information were simply displaced to the left towards the cell that contained the deleted B, the context would become “gAABg” rather than “g***B***AABg,” which is the correct one. To avoid this mistake, the context of B’s left neighbor is “added” to B’s context as shown in the example [5]. When signal ← reaches the right end, it rebounds (turned to $<_{\rightarrow}$) until the cell that contained the deleted symbol, and in its way changes all symbols $<_{\leftarrow}$ to the marker < [7].

g > >	B B ◊	A A ◊	A A ◊	B B <	g < <

…

g > >	B[4] B <	A A <	A A <	B B <	g < <
g > >	B[5] B ←	A A <	A A <	B B <	g < <
g > >	BA A $<_{\leftarrow}$	A A ←	A A <	B B <	g < <

…

g > >	BA A $<_{\leftarrow}$	A A $<_{\leftarrow}$	B B $<_{\leftarrow}$	g[6] < $<_{\rightarrow}$	g < <
g > >	BA A $<_{\leftarrow}$	A A $<_{\leftarrow}$	B B $<_{\rightarrow}$	g[7] < <	g < <

…

g > >	BA[8] A <	A A <	B B <	g < <	g < <

Notice that the context is correctly kept (gBAABg) during the deletion of symbol B and hence [8], the rule BAA→BA can be correctly applied. Notice also that, when a cell has a string as its context information, the symbol itself (the current content associated to the cell) is located at the rightmost position of the context. Derivation process continues (AAB→BA [9]) as explained before, until the application of the rule xBy→λ [10]. In this case, no symbol must be displaced to the left, because there are symbols enough to compensate for B's deletion.

g > >	BA A >BA	A A <	B B <	g < <	g < <
g > >	BA B ◊'	A[9] A >ABA	B B <	g < <	g < <
g > >	BA B ◊'	A A ◊'	B[10] B >BA	g < <	g < <
g > >	BA B ◊'	A A ◊'	B B ◊'	g < >A	g < <

At this moment, signal ◊$_{\leftarrow}$' is sent to the left to update the context information and the word $h^2(\omega)$ is obtained. The CA automaton is ready for a new derivation.

g > >	BA B ◊'	A A ◊'	B B ◊'	g A ◊'	g < <
g > >	BA B ◊'	A A ◊'	B B ◊'	A A ◊$_{\leftarrow}$'	g < <

...

g > >	B B ◊	A A ◊	B B ◊	A A ◊	g < <

Other examples show different cases that must be also taken into account.

In the next example, string gBBABBg is used as axiom with the same set of production rules as in the previous system. After applying rule xBy→λ, the leftmost symbol B* is deleted in a similar way as in the first example. Notice that the correct context (gBBABBg) is kept unchanged. The rule xBy→λ is applied again [11] to delete the second symbol B. Notice that the context remains unchanged and rules BAB→AB [12] and xBy→λ [13] can be applied

G > >	B* B ◊	B B ◊	A A ◊	B B ◊	B B ◊	g < <

...

g > >	BB[11] B <	A A <	B B <	B B <	g < <	g < <
g	BB	A	B	B	g	g

> >	B ←	A <	B <	B <	< <	< <

...

g > >	BBA A <$_{\leftarrow}$	A A ←	B B <	B B <	g < <	g < <

...

g > >	BBA[12] A <	B B <	B B <	g < <	g < <	g < <
g > >	BBA A >AB	B[13] B <	B B <	g < <	g < <	g < <
g > >	BBA A ◊'	B B >B	B B <	g < <	g < <	g < <

At this point a new situation appears: xBy→λ must be applied at the fourth cell [14] and no symbol is propagated from its right (◊' is the third cell's displacing sub string), the derived string is shorter, and the fourth cell's context must accumulate the fifth cell's context. So the whole context (gBBABBg) remains correct until the derivation finishes. Notice that the right marker is displaced to the fourth cell with a displacing substring (<$_{\rightarrow}$) that indicates that the shortening has ended. The only possible context for a cell that contains a marker is the filler g. So g must be copied [16] even if no ◊$_{\leftarrow}$' displacing substring is present. After several steps, the CA shows h(ω)=AB, the first word derived from the axiom.

g > >	BBA A ◊'	B B ◊'	B[14] B ←	g < <	g < <	g < <
g > >	BBA A ◊'	B B ◊'	Bg[15] < <$_{\rightarrow}$	g < <	g < <	g < <
g > >	BBA A ◊'	B B ◊$_{\leftarrow}$'	g[16] < <	g < <	g < <	g < <

...

g > >	A A ◊	B B ◊	g < <	g < <	g < <	g < <

The CA is now ready for a new derivation.

In the next example, string gBBBg is used as the (1,1)DIL's axiom. The reader can verify that, after several steps, the first symbol B is deleted by accumulating its right context information

g > >	B B ◊	B B ◊	B B ◊	g < <

...

g > >	BB B $<_{\rightarrow}$	B B <	g < <	g < <

The second B symbol is also deleted in a similar way.

g > >	BBB B $<_{\rightarrow}$	g < <	g < <	g < <

And, finally, when the last B is deleted, the empty word is obtained.

g > >	BBB B ←	g < <	g < <	g < <
g > >	BBBg < $<_{\leftarrow}$	g < <	g < <	g < <
g > >	g < <	g < <	g < <	g < <

CONCLUSIONS AND FUTURE RESEARCH

In this paper we present the following formal description of the CA ($A_{S,n}$) that simulates the first n derivations of the given (k,l)DIL system $S=\{\Sigma,P,\omega\}$.

$$A_{S,n}=(G_{S,n},G_{0S,n},V_{S,n},Q_{S,n},f_{S,n},T_{S,n,})$$

Where

- $G_{S,n}$ is an infinite one-dimensional grid of automata.

- $Q_{S,n} = \{ (\text{cntxt, symbol, dsplcmnt}) \mid \text{cntxt}\in\{g\}\cup\{\alpha\gamma|\alpha\in\Sigma^*,\gamma\in\{g\}^*\wedge|\alpha\gamma|\leq \max_{i\in\{0,\ldots,n\}}\{|h^i(\omega)|\}\}, \text{dsplcmnt}\in\{<, \leftarrow, <_{\leftarrow}, <_{\rightarrow}, \Diamond, \Diamond', \Diamond_{\leftarrow}'\} \cup \{>\alpha|\alpha\in\Sigma^* \wedge |\alpha| \leq \max_{A\in\Sigma}\{|\rho(A)|\} \times \max_{i\in\{0,\ldots,n\}}\{|h^i(\omega)|\}\} \text{ symbol}\in\Sigma\cup\{<,>\}\}$

- $G_{0S,n}$ is defined as follows:

$$G_{0S,n}[i]=\begin{cases}(g,>,>) & \text{if } i<0\\ (s,s,\Diamond) & \forall i\in[1,|\omega|],, s=\omega[i]\\ (g,<,<) & \text{otherwise}\end{cases}$$

- $V_{S,n}=(l+k+1,\{-1,-(l-1),\ldots,-1,0,1,2,\ldots,k-1,k\})$.

- $f_{S,n}:Q_{S,n}\times Q_{S,n}{}^{l+k+1}\rightarrow Q_{S,n}$ is the transition function informally described in the previous section. The table with the whole definition is omitted for space and comprehensibility.

The two following conditions on the components of $Q_{S,n}$ are essential for the correctness of our proof, because they ensure that the set of states is finite, and hence, the cellular automaton $A_{S,n}$ is well defined

- $|\alpha\gamma| \leq \max_{i\in\{0,\ldots,n\}}\{| h^i(\omega) |\}$ for the context, because the maximum context that can be collected in a cell is the largest word derivable in n steps.

- $|\alpha| \leq \max_{A\in\Sigma}\{ | \rho(A) | \} \times \max_{i\in\{0,\ldots,n\}}\{| h^i(\omega) |\}$ for the displacing substring, because each cell can be displaced to the right at most $| \rho(A) |$-1 symbols (one of them is deleted from the displaced substring, because it is in its final position) and $\max_{i\in\{0,\ldots,n\}}\{| h^i(\omega) |\}$ is the length of the largest word derivable in n steps.

The authors plan to extend this result to an infinite number of derivations and more complex types of L system (L systems with extensions and Lsystems with tables) in order to get a general result.

REFERENCES

Lindenmayer, A. 1968. “Mathematical Models for Cellular Interactions in Development”, *J. T. Biol*. 18, 280-315 (1968)

Neumann, J. von. 1966. *Theory of self-reproducing automata*, edited and completed by A. W. Burks (University of Illinois Press, Urbana, IL, 1966).

Ortega, A. 2000. *Equivalencias entre algunos sistemas complejos: fractals, autómatas celulares y sistemas de Lindenmayer*, phD thesis ETSI UAM

Koza, JR. 1993. “Discovery of Rewrite Rules in Lindenmayer Systems and State Transition Rules in Cellular Automata via Genetic Programming”, *In Proceedings of SPF-93*.

Stauffer, A. and Sipper, M. 1998. “On the relationship between cellular automata and L-systems: The self-replication case” *Physica D* 116, p.71-80.

Stauffer, A. and Sipper, M. 1998 “L-hardware: Modeling and implementing cellular development using L-systems”, in: D. Mange and M. Tomassini, ed., *Bio-inspired Computing Machines: Toward Novel Computational Architectures* (Presses Polytechniques et Universitaires Romandes, Lausanne, Switzerland, 1998) 269-287.

Alfonseca, M.; Ortega, A. and Suárez, A. 2003 “Cellular automata and probabilistic L systems: An example in Ecology”, In *Grammars and Automata for String Processing: from Mathematics and Computer Science to Biology, and Back*. C. Taylor and Francis Publishers.

Abu Dalhoum, A.; Ortega, A. and Alfonseca, M. 2003: “Cellular autómata equivalent to D0L systems”, in press.

Terrier, V., *Temps réel sur automates cellulaires*, Ph. D. Thesis, LIP ENS Lyon, 1991

Mazoyer, J. and Terrier, V. 1999. “Signals in one-dimensional cellular automata”, *Theoretical Computer Science* 217 53-80

SIMULATION AND PERFORMANCE COMPARISION OF INTEGER MULTIPLIER ALGORITHMS

Mahmoud A. Al-Qutayri   Hassan R. Barada   Ahmed Al-Kindi

Etisalat College of Engineering
P.O.Box 980, Sharjah, UAE
maq@ece.ac.ae

Keywords: simulation, performance analysis, software, emulation, processors,.

ABSTRACT

The goal of this paper is to compare and study the performance of some of the major integer multiplication algorithms. This is achieved through a simulation environment that at this stage implements five major multipliers in C++ programming language. The environment is a flexible one and has a well-designed user interface that makes it suitable for educational use. The multipliers are Hennessy multiplier, scaling accumulator multiplier, carry save multiplier, ripple carry array multiplier and Wallace tree multiplier. The environment enables the user to emulate the multipliers for various data inputs.

INTRODUCTION

The integer multiplication process is an important operation that is heavily used in various computation fields such as image processing and digital signal processing. Multiplication algorithms fall into two broad are categories: signed and unsigned. In the signed category the binary numbers to be multiplied are assumed to be signed. An example of this type is the Booth multiplier. The second category uses unsigned numbers and encompasses two sub categories: array multipliers (Pezaris 1971, Pekmestzi 1999, Hoffman 1968) and tree multipliers (Bickerstaff et al. 1995, Song et al. 1991, Wallace 1964). The array multipliers include scaling accumulator multiplier and carry save array multiplier. The tree ones include computed partial product multiplier and Wallace tree multiplier.

In this paper multiplication algorithms are compared in terms of performance or time complexity. Performance refers to the total number of clock cycles needed during the execution process of the multiplier. This in turns depends on the number of add and shift operation the algorithm consists of. This is also normally a function of the number of bits needed to represent the operands (i.e. n).

The time complexity of array multipliers is proportional to the operand word length (O(n)), but the time complexity of tree multipliers is proportional to the logarithm of the operand word length (O(log n)) (Koren 1998). The area complexity of both types of multipliers, when physically implemented, is proportional to the square of the operand word length ($O(n^2)$) (Schulte et al. 2000).

INTEGER MULTIPLICATION ALGORITHMS

The algorithms of the simulated multipliers are outlined in the subsections below.

Hennessy Multiplier

As shown in Figure 1, the Hennessy multiplier has regular structure (Patterson and Hennessy 1998). If the multiplier has length of n-bit, it will needs n-step to accomplish the multiplication process, where each step consists of add and shift operations or just an add operation depending on the content of the multiplicand (Patterson and Hennessy 1998). n-bit Hennessy multiplier requires n-bit adder. In 4-bit Hennessy multiplier, we need register called A, which is 4-bit and initialized to 0. The multiplicand is loaded to a register called M (4-bit). The multiplier is loaded to a register called Q (4-bit). A flip-flop C is also initialized to 0. The algorithm consists of steps where the number of steps needed equals to the multiplier length (4) in this example. In each step, the first bit in Q is checked. If it equals 0, combination CAQ is shifted to the right. If it equals 1 M is added to A, put the result is put in A and then the combination CAQ is shifted to the right. The previous process is repeated n times (4 in this example).

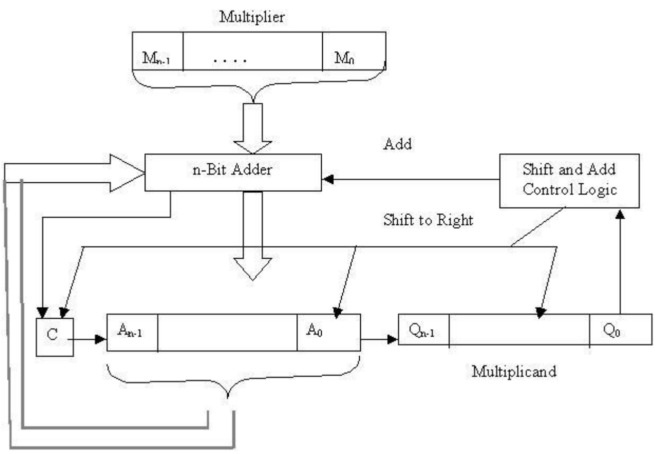

Figure 1: Architecture of Hennessy Multiplier

Scaling Accumulator Multiplier

The architecture of the Scaling Accumulator multiplier, with its regular structure, is shown in Figure 2. An n-bit scaling accumulator multiplier requires n steps to accomplish a single multiplication process, where each step consists of add and shift operation except the last step which just consists of an add operation [10]. It consists of 2*n-bit adder. 4-bit scaling accumulator multiplier takes the multiplier (4-bit) as parallel load and loads it to a register called M (4-bit).

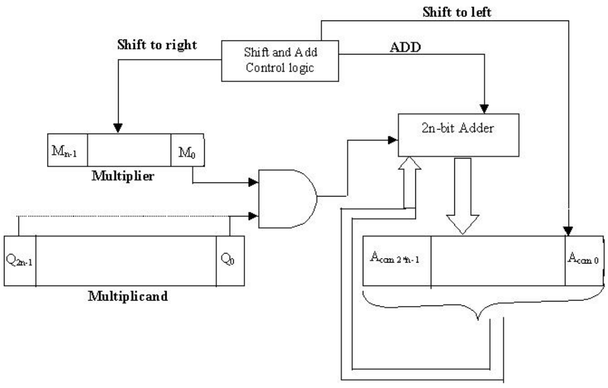

Figure 2: Architecture of Scaling Accumulator Multiplier

Ripple Carry Array Multiplier

The Ripple Carry Array multiplier, with its regular architecture, is shown in Figure 3. The number of steps that is required by n-bit multiplier is (3*n-4). The equation that represents the number of steps was inferred during the designing process of the multiplier by using the block diagram of 4-bit multiplier and extending it to multipliers of larger lengths then counting the number of steps for each multiplier. Each step consists of one or more full-add operations. All full-add operations that run at the same step must be executed in parallel. The number of full adders that are required by n-bit multiplier is (n*(n-1)).

Carry Save Array Multiplier

The architecture of carry save array multiplier is shown in Figure 4. It has a regular structure and the number of steps that are required by n-bit multiplier is (2n-2). This was inferred during the analysis process of the multiplier by using the block diagram of 4-bit multiplier and extending it to multipliers of larger lengths then counting the number of steps for each multiplier. Each step consists of one or more full-add operations. All full-add operations that run at the same step must be executed in parallel. The number of full adders that are required by n-bit multiplier is (n*(n-1)).

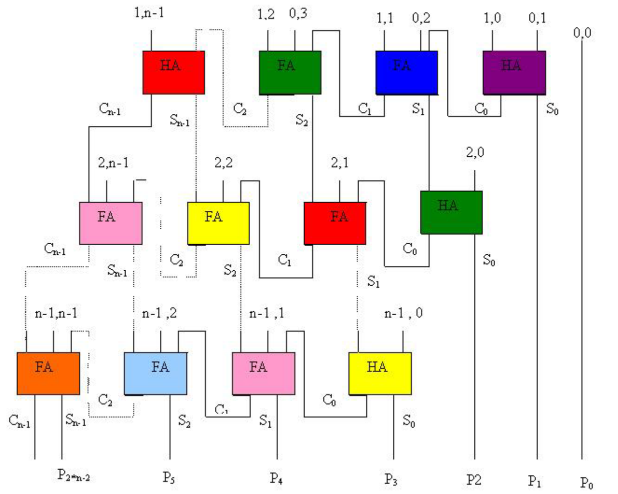

Figure 3: Architecture of Ripple Carry Array Multiplier

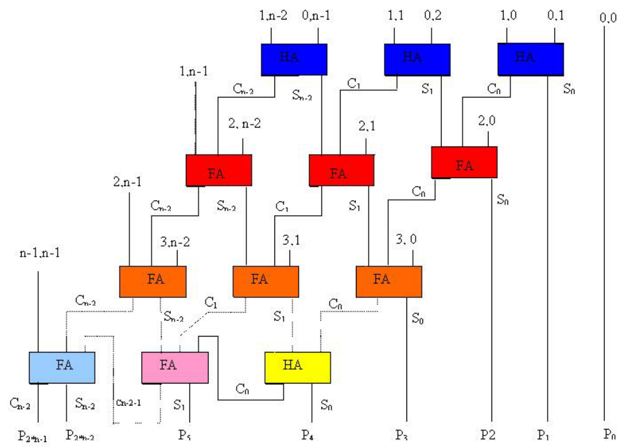

Figure 4: Architecture of Carry Save Array Multiplier

Wallace Tree Multiplier

A Wallace Tree multiplier has an irregular structure (Wallace 1964), see Figure 5, so for each multiplier of a specific length we need to have a specific design for its hardware circuit. The number of carry save adders needed by n-bit Wallace tree multiplier is proportional to the length of the multiplier (it equals n-1 if the multiplier has a length of 3*k where k=1,2,3,4,….). Wallace tree multiplier has an optimal speed as discussed in (Papadomanolakis 2001). For n-bit Wallace tree multiplier, the number of steps needed is $\lceil \log_{3/2}(n/2)+1 \rceil$ (Papadomanolakis 2001). Each step except the last step consists of one or more carry save add–operation. All carry save adders, which execute at the same step must be performed in parallel. The last step requires a parallel add operation.

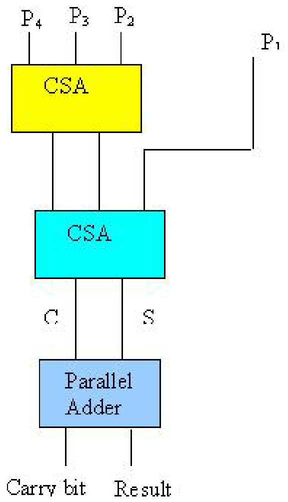

Figure 5: Architecture of Wallace Tree Multiplier

MULTIPLIERS SIMULATION ENVIRONMENT

A software environment that enables the simulation of the multiplication algorithms outlined in the previous section was implemented using C++ programming language. The system mainly has two interface windows. In the first window, which is the main one as shown in Figure 6, the user selects one of the five multipliers that have been implemented. Then the user is requested to enter the length of the multiplier. This must be an integer number between 1 and 128 for Hennessy, scaling accumulator, ripple carry array and carry save array multipliers. For Wallace tree multiplier, the user needs to enter the number 4 or the number 8. Finally the user is requested to enter the two operands of the multiplier in a binary form within the specified length.

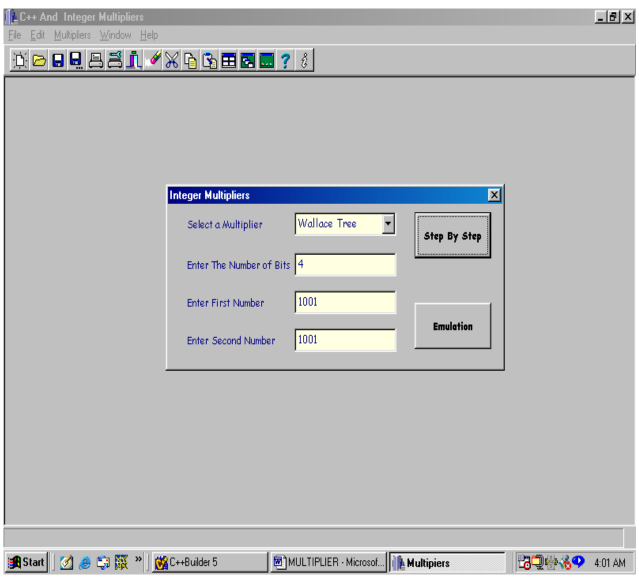

Figure 6: Main Simulation Environment Window

A second window, which is called the emulation window as shown in Figure 7, appears in the screen directly after the user finishes from entering the requested data requested in the main window. The emulation window emulates the multiplier selected by the user and provides the result of the multiplication process and the complexity (number of operations required by the multiplier with a specification of their types) of the multiplier. The emulation of the multiplier reflects the actual execution of the multiplier based on its architecture. Once the emulation of the multiplier is complete, the user returns to the main window.

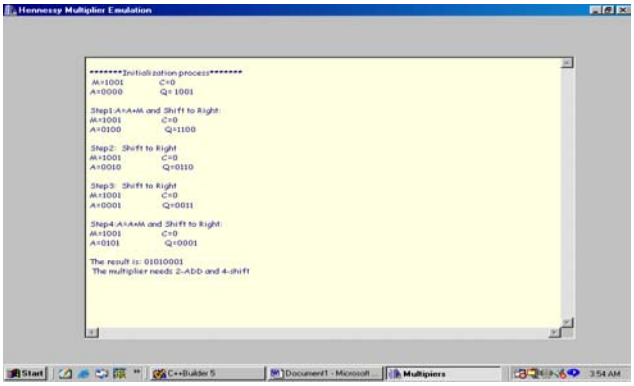

Figure 7: Emulation Window of the Multipliers Environment

Figure 7 shows the output of the software when Hennessy multiplier was selected with length of 4, the first number was 9 (1001_2) and the second number was 9(1001_2). The multiplier needs 4 steps (equals to the length of the multiplier), the first and the last steps each needs an add operation and a shift operation. The second and the third steps each needs just a shift operation. Figure 8 and Figure 9 show the emulation results of the 4-bit ripple carry array multiplier and 4-bit Wallace tree multiplier respectively.

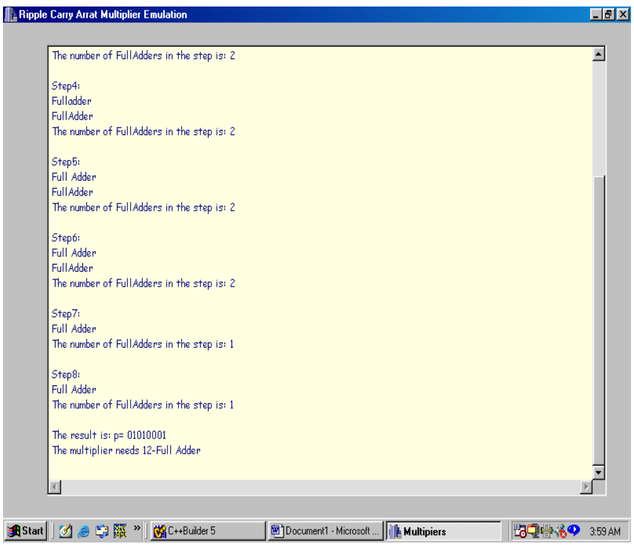

Figure 8: The Output of a 4-bit Ripple Carry Array Multiplier

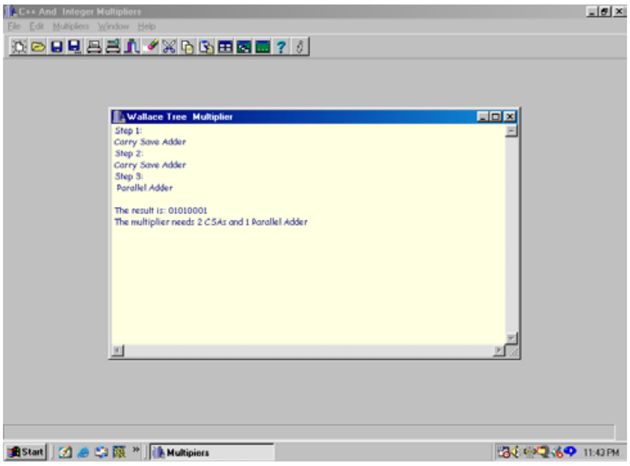

Figure 9: The Output of a 4-bit Wallace Tree Multiplier

CONCLUSIONS AND FURTHER WORK

The paper discussed the architecture and operation of five major integer multipliers. Namely Hennessy, scaling accumulator, ripple carry array, carry save array and Wallace tree. The paper showed the complexity of each multiplier and the implication on its performance. Wallace tree is the best in terms of the time complexity. Ripple Carry Array multiplier was faster than Hennessy multiplier when both of them were of length less than 4. Carry save array multiplier was faster than Hennessy multiplier. Ripple carry array multiplier is slower than carry save array multiplier.

The simulation environment described in the paper gives the user the ability to understand the multiplication process and assess the various algorithms. It also allows the user to emulate the multiplication of particular numbers and trace the execution process.

Some further enhancements will be introduced to the simulation environment as part of the future work. This will include real time measurements, graphical visualization of the multiplication process and introduction of additional multiplication algorithms.

References

Bickerstaff K., Schulte M.J. and Swartzlander E.E. Jr.. 1995. "Parallel Reduced Area Multipliers". *J.VLSI Signal Processing*, vol. 9 pp. 181-192.

Hoffman J.C. and Kitai R. 1968. "Parallel Multiplier Circuit", Electronic Letters, vol.4.

Koren I. 1998. *Computer Arithmetic and Algorithms*, Brookside Court Publishers.

Papadomanolakis K.S., Kakarountas A.P., Kokkinos V., Sklavos N., and Goutis C.E. 2001. "The Effect of Fault Secureness in Low Power Multiplier Designs." Proceedings of *IEEE International Workshop on Power And Timing Modeling, Optimization and Simulation*, 10.3, pp. 1-12.

Patterson D.A. and Hennessy J.L. 1998. *Computer Organization & Design: The Hardware/Software Interface*, Morgan Kaufman, USA, second edition.

Pekmestzi K.Z. 1999. "Multiplexer- Based Array Multipliers", *IEEE Trans. Computers*, vol.48, no. 1, pp. 15-23.

Pezaris S. D. 1971. "A 40 ns 17-bit Array Multiplier", *IEEE Trans. Computers*, vol. 20, no.40, pp. 442-447.

Schulte M.J., Balzola P.I., Akkas A., and Brocato R.W. 2000. "Integer Multiplication with Overflow Detection or Saturation", *IEEE Trans. Computers*, vol. 49, no. 7.

Song P.J. and Micheli G.D. 1991. "Circuit and Architecture Trade-Offs for High-Speed Multiplication". *IEEE J. Solid-State Circuits*, vol. 26, no. 9, pp. 1,184 -1,198.

Wallace C.S., 1964. "Suggestion for a Fast Multiplier", IEEE Trans. *Electronic Computers*, vol.3, pp.14-17.

http://www.andraka.com, last accessed 8/10/2003.

A GRAPHICAL ENVIRONMENT FOR SIMULATION OF C/PVM PARALLEL SOFTWARE ON A CLUSTER OF HETEROGENEOUS WORKSTATIONS

M.J. Zemerly
Etisalat College of Engineering
Department of Computer Engineering
PO Box: 980,
Sharjah
United Arab Emirates
Email: jamal@ece.ac.ae

T. Delaitre, G.R. Justo and S.C. Winter
University of Westminster,
Centre for Parallel Computing
115 New Cavendish Street,
London W1M 8JS
United Kingdom
Email: edpepps-all@cpc.wmin.ac.uk

KEYWORDS
Performance Prediction, Graphical Design, Simulation, Visualisation, Parallel Programming Environments, PVM.

ABSTRACT

This paper describes an environment for the design and performance prediction of portable parallel software. The environment consists mainly of a graphical design tool for building parallel algorithms, a commercial simulation engine, a CPU characterisation tool, a distributed debugging tool and a visualisation/replay tool. The environment is used to model a virtual machine composed of a cluster of heterogeneous workstations interconnected by a local area network. The simulation model used is modular and its components are interchangeable which allows easy reconfiguration of the platform. The model is validated using experiments on two parallel Givens linear solver algorithms with average errors of less than 10%.

INTRODUCTION

The rapid technological advances in high-speed networks and high-performance processors are making networks of computers an appealing vehicle for cost-effective parallel computing. However, the lack of parallel programming design tools and environment is delaying the widespread adoption of the use of networks in parallel computing (kacsuck et al. 1997, Pancake et al. 1995). In particular, there is a need for performance prediction tools, especially for clusters of heterogeneous workstations, to enable software designers to choose between design alternatives such as different parallelisation strategies or paradigms. A portable message-passing environment such as Parallel Virtual Machine (PVM) (Geist et al. 1994) permits a heterogeneous collection of networked computers to be viewed by an application as a single distributed-memory parallel machine.

Rapid prototyping is a useful approach to the design of (high-performance) parallel software in that complete algorithms, outline designs, or even rough schemes can be evaluated at a relatively early stage in the program development life-cycle, with respect to possible platform configurations, and mapping strategies. Modifying the platform configurations and mappings will permit the prototype design to be refined, and this process may continue in an evolutionary fashion throughout the life-cycle before any parallel coding takes place. The environment discussed in this paper is based on a rapid prototyping philosophy and comprises five main tools:

- **PVMGraph** (Justo 1996): A graphical design tool for designing of parallel PVM applications.
- **SES/Workbench** (SES Inc. 1996): A commercial simulation tool based on discrete-event simulation.
- **PVMVis**: A visualisation tool for animation of program execution using traces generated by the simulator and visualisation of platform and network performance measures and statistics.
- **Chronos** (Bourgeoi et al. 2000): A CPU characteriser tool for computational code based on basic operations in C to allow the simulator to predict the execution time of each block depending on the type of machine where the code is executed.
- **PVMDebug** (Audo 1998): A debugging tool based on the distributed debugging tool DDBG (Kacsuk et al. 1997) which provides debugging functionalities for distributed C/PVM programs.

Other tools used in the environment for integration purposes are:

- **Tape/PVM** (Maillet 1995): A trace instrumentation utility.
- **SimPVM** (Delaitre et al. 1997): A translator from C/PVM code to queueing network graphical representation.
- **C2Graph** (Schinkmann 1997): A translator from existing C/PVM parallel applications into PVMGraph graphical representation based on the SAGE++ toolkit (Bodin et al. 1994).

This paper describes the various tools within the environment and presents a case study for validation of the models used.

DESCRIPTION OF THE ENVIRONMENT

The design process using the environment starts with the graphical design tool (PVMGraph) by building a graph representing a parallel program design based on the PVM programming model. The graph is composed of computational tasks and communications. The tool provides graphical representation for PVM calls, which the user can select to build the required design.

The software designer can then generate (by the click of a button) C/PVM code (.c files) for both simulation and real execution. The environment also provides a tool to translate existing parallel C/PVM code into graphical representation suitable for PVMGraph.

In the simulation path each C/PVM source code file obtained from the PVMGraph is instrumented using the Tape/PVM trace pre-processor (Maillet 1995). The output is then parsed using Chronos (Bourgeoi et al. 2000) to characterise the code and insert special CPU execution time prediction call (*cputime*) calls at the end of each computational block. The instrumented C source files are translated using the SimPVM Translator (Delaitre et al. 1997) into a queueing network representation suitable for Workbench graph (.grf file). *SES/Workbench* translates the graph file into the Workbench object oriented simulation language called *SES/sim* (SES inc. 1996) using an SES utility (*sestran*). The *sim* file is then used to generate an executable model using some SES/Workbench utilities, libraries, declarations and the PVM platform model. The simulation executable code is run using three input files containing parameters concerning the target virtual environment (e.g. number of hosts, host names, architecture, the UDP communication characteristics and the timing costs for the set of instructions used by Chronos). The UDP model and the instruction costs are obtained by benchmarking (benchmarks are provided off-line) the host machines in the network.

The simulation outputs a Tape/PVM trace file and a statistics file about the virtual machine. These files are then used by the visualisation tool (PVMVis) to animate the program execution and visualise the performance of the system. The design can be modified and the same cycle can be repeated until a satisfactory performance is achieved.

In the real execution path the Tape/PVM pre-processor is used to instrument the C source files and these are then compiled and executed to produce the Tape/PVM trace file required for the visualisation/animation process. This step can be used for validation of simulation results but only when the target machine is accessible.

In the debugging mode, the user will be able to debug the loaded C/PVM application. The distributed debugging of the application is handled by controlling the execution of all the tasks using a textual window representing the code for each task. The textual window here is slightly different from that of the design and offers the user basic features of a debugging tool. PVMGraph, PVMVis and PVMDebug are incorporated within the same Graphical User Interface where the designer can switch between these possible modes. The following sub-sections describe in more detail the main tools within the environment.

PVMGraph

PVMGraph is a graphical programming environment to support the design and implementation of parallel applications. PVMGraph offers a simple yet expressive graphical representation and manipulation for the components of a parallel application. The main function of PVMGraph is to allow the parallel software designer or programmer to develop PVM applications using a combination of graphical objects and text. Graphical objects are composed of boxes which represent tasks (which may include computation) and arrows which represent communications. The communication actions are divided into two groups: input and output. The PVM actions (calls) are numbered to represent the link between the graph and text in the parallel program. Also, different types and shapes of arrows are used to represent different types of PVM communication calls. Parallel programs (PVM/C) can be automatically generated after the completion of the design. Additionally, the designer may enter PVM/C code directly into the objects. The graphical objects and textual files are stored separately to enable the designer to re-use parts of existing applications (Justo 1996).

PVMVis

The main objective of this tool is to offer the designer graphical views and animation representing the execution and performance of the designed parallel application. The animation is an event-based process and is used to locate an undesirable behaviour such as deadlocks or bottlenecks.

The animation view in PVMVis (see Figure 1) is similar to the design view in PVMGraph except that the pallet is not shown and two extra components for performance analysis are added: barchart view and platform view. The barchart view shows historical states for the simulation and the platform view shows some statistics for selected performance measures at the message passing layer, the operating system layer and the hardware layer.

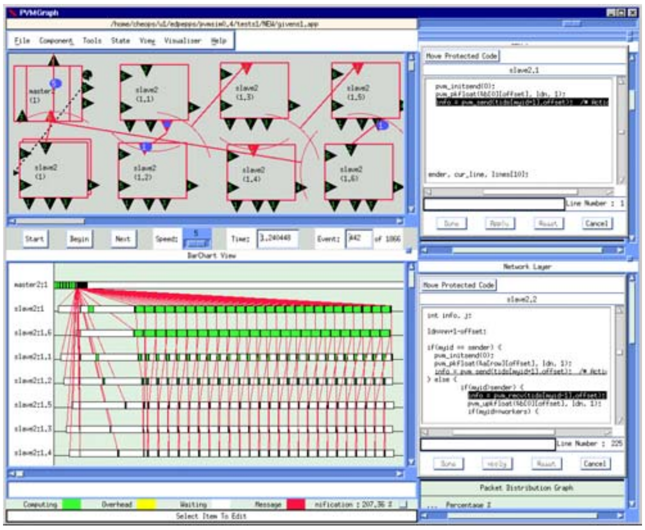

Figure 1: A screendump from the PVMVis.

PVMDebug

This tool is based on a Distributed Debugging tool DDBG (Kacsuk et al. 1997) which provides a set of debugging functionalities for distributed programs written in C/PVM.

In order to debug a distributed application and to control the execution of the distributed tasks, the debugger needs to know all PVM task identifiers (tids). During the execution, the graphical task objects in PVMGraph do not have their tids because their values change at each run.

Therefore, a debugging interface in the form of a wrapper program and a mapping table was developed to manage the link between the graphical objects and the PVM execution tasks. The wrapper program uses the on-line monitoring facility in PVM and collects the PVM events from the application and routes them to PVMDebug which manages the mapping list (Audo 1998).

Chronos

This tool estimates the time taken by computational blocks within a parallel algorithm. Chronos characterises a workload by a number of high-level language instructions (e.g. float addition) (Bourgeoi et al. 2000, Delaitre et al. 1997) taking into account the instruction and data caches effect. Assumptions have been made to reduce the number of possible machine instructions to 43. The costs associated with the various instructions are kept in a file in the hardware layer accessible by the SES utilities. These costs are obtained by benchmarking the instructions on different machines.

Chronos first parses an instrumented C/PVM program using the SAGE++ toolkit. In the second stage, Chronos traverses the parse tree using the SAGE++ library and inserts *cputime* calls with the number of machine instructions within each sequential C code fragment. A *cputime* function has a fixed number of parameters (a total of 31). This is different from the number of machine instructions because the instruction cache duplicates some of the instructions (hit or miss). Each parameter of the *cputime* function represents the number of times each instruction is executed within the code fragment. The last parameter determines whether the instruction cache is hit or miss for the fragment in question.

C2Graph

This tool is provided to allow existing C/PVM parallel code to be directly used within the environment rather than building the design from scratch. The C/PVM application files are first parsed using SAGE++ to get the .dep files. These files are then traversed by the C2Graph translator which also uses the SAGE++ library routines. The translator also takes into account the PVM calls in the original code and generates their corresponding graphical representation in the PVMGraph files. The translator then determines the master process, positions it with the other tasks by calculating appropriate coordinates for them in the PVMGraph screen, and writes the PVMGraph definition files (.def) for each task. The translator finally writes the application file (.app) required for PVMGraph.

SimPVM Translator

From PVMGraph graphical and textual objects, executable and "simulatable" PVM programs can be generated. The "simulatable" code generated by PVMGraph is written in a special intermediary language called SimPVM, which defines an interface between PVMGraph and SES/Workbench (delaitre et al. 1997).

To simulate the application, a model of the intended platform must also be available. Thus, the simulation model is partitioned into two sub-models: a dynamic model described in SimPVM, which consists of the application software description and some aspects of the platform (e.g. number of hardware nodes) and a static model which represents the underlying parallel platform.

The SimPVM language contains C instructions, PVM and PVM group functions, and constructs such as computation delay and probabilistic functions.

Simulation Model

The simulation model consists of the PVM platform model library and the PVM programs for simulation. The PVM platform model is partitioned into four layers: the message passing layer, the PVM group layer which sits on top of the message passing layer, the operating system layer and the hardware layer. Modularity and extensibility are two key criteria in simulation modelling, therefore layers are decomposed into modules which permit a reconfiguration of the entire PVM platform model.

A program generated by the PVMGraph tool is translated into the SES/Workbench simulation language and passed to its simulation engine, where it is integrated with the platform model for simulation. The message passing layer models a single (parallel) virtual machine dedicated to a user. It is composed of a daemon which resides on each host making up the virtual machine, a group server and the libraries (PVM and PVMG) which provide an interface to PVM services.

The main components in the operating system layer are the System Call Interface, the Process Scheduler and the Communication Module.

The hardware layer is comprised of hosts, each with a CPU layer, and the communications subnet (Ethernet). Each host is modelled as a single server queue with a time-sliced round-robin scheduling policy. The communications subnet is Ethernet, whose performance depends on the number of active hosts and the packet characteristics.

A CASE STUDY

A case study is presented here to illustrate the use of the environment. The case study selected is a communication intensive application based on two parallel Givens Linear Solver method developed in (Papay et al. 1996). The environment can help the designer to choose the best algorithm and to size the application by choosing the best number of processors. In this case study we also test the accuracy of the CPU characterisation toolset using the sequential Givens code.

Givens Linear Solver

The Givens linear solver can be represented in the form: $A\boldsymbol{x} = b$, where A is a non-singular square matrix, b is the right hand side vector and $\boldsymbol{x}$ is a vector of unknowns. The Givens transformation is defined by a 2×2 rotation matrix:

$$G = \begin{bmatrix} c & s \\ -s & c \end{bmatrix}$$

where $c^2 + s^2 = 1$. A Givens rotation is used to eliminate the elements of a vector or a matrix as follows:

$$\begin{bmatrix} c & s \\ -s & c \end{bmatrix} \times \begin{bmatrix} a \\ b \end{bmatrix} = \begin{bmatrix} r \\ 0 \end{bmatrix}$$

where

$$c = \frac{a}{\sqrt{a^2 + b^2}} \quad \text{and} \quad s = \frac{b}{\sqrt{a^2 + b^2}}$$

The Givens algorithm for solving a linear system with N equations can be decomposed into two computational stages. The first is the triangulation of the initial matrix, this stage is represented by the execution of the elimination block N times. The second stage is the substitution block which solves the triangular matrix.

Parallel Givens Algorithms

The triangulation stage, which is the time consuming part (with complexity of $O(N^3)$ as opposed to $O(N^2)$ for the back-substitution stage) is parallelised with two different parallelisation strategies termed collective and pipeline. The back-substitution stage is also programmed differently as will be seen later.

Both methods use at first block-row data decomposition, which divides the matrix horizontally and assigns adjacent blocks of rows to processors. The first step (A) in the collective method, all processors eliminate the required columns for their rows (except the first row for each processor) in parallel. Then to eliminate the columns of the first rows (step B), collective communication is used to collect the first rows from processors (rows are collected by the processor holding the corresponding row of the current eliminated column) and distribute the rows back. The back-substitution stage is started by the last processor and its results are broadcasted to other processors and then in a similar way all the processors solve their triangulated matrices in a back-pipeline way.

In the pipeline method the same first step A (as in method 1) is used. Here, instead of using collective communications to eliminate the columns of the first rows (step B in method 1), the row in question is passed from the sender to its neighbour to eliminate its column and then passed in a pipeline fashion through other neighbours until all the columns are eliminated. The last processor keeps the lines in a full matrix to be used in the back-substitution stage later on its own.

RESULTS AND DISCUSSION

The two methods were designed using the environment and results for both simulation and real execution (on a real network) were obtained. The network used for this algorithm consists of 3 Ultra-Sparc 10 machines with 300MHz, A Pentium II with 233 MHz, A Pentium 150MHz, A Super-Sparc 20 with 75 MHz and A Micro-Sparc 5 with 60 MHz. The mapping of tasks onto machines was done differently in the two algorithms based on a few simulation tests and the final optimal mapping only is used for the results shown here. The mapping for the machines was done in increasing power order (but giving priority to use the fastest machines if the number of processor is less than the total 7) for the pipeline method and in decreasing power order for the collective method.

The tests were done for problem sizes of 256 and 512 equations but for the 256 size we did not get any significant speedup relative to the fastest machine in the network as the algorithm is communication intensive and this will affect the performance of small problem sizes. Figure 2 shows the results for the simulation and real execution measurements (averages of 10 times taken at night) for both the collective and the pipeline methods.

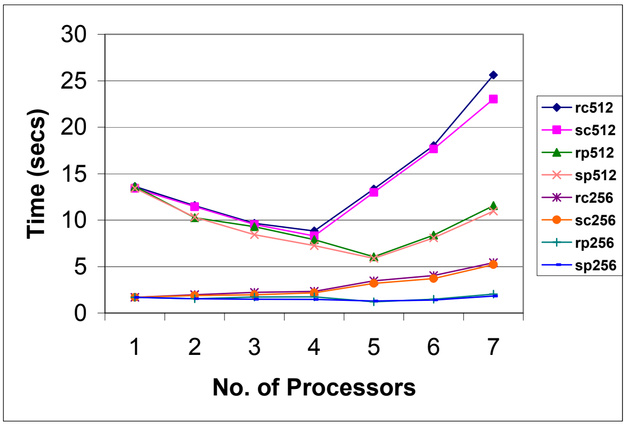

Figure 2: Comparison between Simulation (s) and Real (r) for Parallel Givens: Collective (c) and Pipeline (p)

The figure shows clearly that the measurements and predictions for both methods are in good harmony with maximum error well below 10% (except for one case for the collective algorithm with 7 processors, 12%). All the measurements including the benchmarks have been performed at night at low ambient network load and the standard deviation for all the measurements did not exceed 5% on any of the runs. As expected, the figure also shows the superiority of the pipeline algorithm over the collective algorithm even for small number of processors. Note that the machines are heterogeneous and adding more processors sometimes results in increasing the execution time rather than improving it. For the 512 problem size we obtained a speedup of 2 and 2.25 for 4 and 5 processors respectively for the pipeline algorithm. As expected, increasing the number of processors above 5 (4 for the collective) in both cases increases the execution time as the other processors (other than the UltraSparc and Pentium II 233 MHz) are considerably slower than the fastest four. Knowing that the pipeline algorithm is superior to the collective one, the user can then experiment with adding more powerful processors than available to see if better speedups can be obtained. Recent results obtained on a network of 12 Ultra-10 machines (faster than the ones used in the experiment here at 333 MHz) showed a superlinear speedup for the 512, 1024 and 2048 matrix sizes. This is an interesting case study since the superlinear speedup is mainly (if not wholly) attributed to the effect of cache with the Chronos tool may be able to detect during the simulation. However, prediction for these cases could not be performed due to lack of models for these new machines. This task could not be performed in time for this paper and is planned for the near future.

CONCLUSION

This paper has described an environment which is used to design and predict the performance of portable parallel software using C and PVM on a cluster of heterogeneous workstations. The environment supports graphical design, performance prediction through modelling and simulation, and visualisation of predicted program behaviour. The designer is not required to leave the graphical design environment to view the program's behaviour, since the visualisation is an animation of the graphical program description. It is intended that this environment will encourage a philosophy of program design, based on a rapid synthesis-evaluation design cycle, in the emerging breed of parallel program designers.

Success of the environment depends critically on the accuracy of the underlying simulation system. Preliminary validation experiments showed average errors between the simulation and the real execution of less than 10%.

An important direction of our work is to implement from scratch or to find another cheaper and readily available simulation engine for the environment as relying on an expensive commercial product such as SES, is having an impact on the usefulness and future deployment of the environment. SES offers many advanced features that exceed the requirements for this environment and hence can be substituted by a simpler tool. Another future direction is to generalise the simulation model and to extend it to support other platforms, such as MPI. Also, updating the environment with models of recent processors such as the Pentium IV is planned. An intelligent design assistant based on agent technology is also required to help beginners in parallel programming to choose between design alternatives and help with using the environment. Use of agent technology is currently being investigated.

ACKNOWLEDGMENT

This project was funded by an EPSRC PSTPA programme, Grant No.: GR/K40468 and also by EC Contract Numbers: CIPA-C193-0251 and CP-93-5383. The authors also wish to thank all students who implemented and successfully integrated various components of the environment at various times.

REFERENCES

Audo, A. 1998. Integration of the DDBG Distributed Debugger within the EDPEPPS Toolset, Technical Report, Centre for Parallel Computing, University of Westminster, UK, June

Bodin F. *et. al*. 1994. Sage++: An Object-Oriented Toolkit and Class Library for Building Fortran and C++ Restructuring Tools, Proc. 2nd Annual Object-Oriented Numerics Conf.

Bourgeoi, J.; F. Spies; M.J. Zemerly and T. Delaitre. 2000. "Chronos: A Performance Characterization Tool", The Journal of Supercomputing, Vol 15, No. 2, pp 123-140

Delaitre, T. *et. al*. 1997. Final Syntax Specification of SimPVM, EDPEPPS/22, Centre for Parallel Computing, University of Westminster, UK.

Delaitre, T. *et. al*. 1997. Final Model Definition, EDPEPPS/23, Centre for Parallel Computing, University of Westminster, UK.

Geist, A. *et. al.* 1994. PVM: Parallel Virtual Machine, MIT Press.

Justo, G.R. 1996. PVMGraph: A Graphical Editor for the Design of PVM Programs, EDPEPPS/5, Centre for Parallel Computing, University of Westminster, UK.

Kacsuk, P.; P. Dozsa and T. Fadgyas. 1996. Designing Parallel Programs by the Graphical Language GRAPNEL, Microprocessing and Microprogramming 41, 625-643.

Kacsuk, P. *et. al*.1997. A Graphical Development and Debugging Environment for Parallel Programs, Parallel Computing, 22:1747-1770.

Maillet, E. 1995. Tape/PVM: An Efficient Performance Monitor for PVM Applications: User Guide, LMC-IMAG, ftp://ftp.imag.fr/ in pub/APACHE/TAPE.

Pancake, C.; M. Simmons and J. Yan. 1995. Performance Evaluation Tools for Parallel and Distributed Systems, Computer 28, 16-19.

Papay, J.; M.J. Zemerly and G.R. Nudd. 1996. Pipelining the Givens Linear Solver on Distributed Memeory Machines, Supercomputer Journal 65, XII-3, pp 37-43.

Schinckmann, F.1997. Reverse Engineering Tools, EDPEPPS/36, Centre for Parallel Computing, University of Westminster, UK.

Scientific and Engineering Software Inc. 1996. SES/Workbench Reference Manual, Release 3.1.

A FRAMEWORK FOR MICROPROCESSOR EMULATION: MOTOROLA 68K MICROPROCESSOR AS AN EXAMPLE

Hassan Obaid Al-Muhairi, Hassan R. Barada and Mahmoud Al-Qutayri
Etisalat College of Engineering
P.O.Box: 980, Sharjah
United Arab Emirates
E-mail: maq@ece.ac.ae

KEYWORDS
Processor, environments, education, emulation, interactive.

ABSTRACT

This paper presents design methodologies and tools characterizing a computer-based learning environment developed for an introductory course in microprocessor programming. The environment emphasized the practical learning methodology to support the students in all phases of the learning process. Emphasis is specially placed on simulating the progressive process of microprocessor programming to stimulate the learners' activity and overcome some complexities intrinsic to this subject.

The paper discusses the design and implementation of an emulation software package targeted at the Motorola 68000 microprocessor. It focuses on the theoretical background and the technical implementation of the emulation framework and how this framework was used to develop an educational environment that provide a homogeneous and a seamless learning environment that help and enhance the learning process. The design methodology used in developing emulation framework discussed in this paper can be used to develop emulation software for other types of microprocessor systems.

INTRODUCTION

In computer science, the Church-Turing thesis [Copeland 1996a; Copeland 1996b] entails that any computer architecture can be emulated within any other. The thesis states in its simplest form that all effective mathematical computations or algorithms can be carried out by a Turing machine. In effect this leads to concluding that every computer program in any typical programming language can be translated into a Turing machine, and any Turing machine can be translated into most programming languages. Nowadays, the thesis is generally assumed to be true, and is also known as Church's thesis [Church 1936] (named after Alonzo Church) or Turing's thesis [Turning 1936] (named after Alan Turing).

In reality, it can be quite a complex process, particularly when the exact underpinnings of the system to be emulated are not documented (or not publicly available) and have to be deduced through reverse engineering. In addition, there is no timing constraints; if the emulator does not perform as quickly as the original hardware (which is usually true if: 1- the hardware is of largely different architecture 2- the hardware to be emulated is more advanced architecturally from the emulating system 3- the emulation framework is erratic), the emulated software may run much more slowly than it would have on the original hardware.

In simple terms, emulation is the process whereby the code (and therefore the programs) native to one type of computer are manipulated so that they can be run on another computer. This can be achieved in three theoretical approaches [Fayzullin 2002]:

- Dynamic Recompilation
- Static Recompilation
- Interpretation

Recompilation (also called binary translation) means that foreign machine code is changed into native machine code and then executed [Hookway and Herdeg 1997]. Dynamic recompilation means this is done in chunks at run time during the program execution, whereas static recompilation would involve translating the entire program before it beginning execution process [Altman and Ebcioglu 2000]. To increase speed, this technique can be combined with the static recompilation. So typically dynamic recompilation will statically recompile code upto the first subroutine call and maybe some other obvious subroutines before run time.

In Static Recompilation approach a program written in the code of the machine to be emulated is translated into the assembly code of the target machine. The result will be a usual executable file which can be ran on the target computer without any special tools. While static recompilation sounds very nice, it is not always possible. Static recompilation is very difficult, especially because it is never really apparent until code is run which parts of code represents instructions and which parts are data (e.g. graphics data). Secondly, program code can modify itself as it is run, and a static recompiler would some how have to foresee this. To avoid such situations, static recompiler can be combined with an interpreter or a dynamic recompiler. Besides the problem of running foreign machine code, an emulator also comes up against the fact that the code is expecting to run on a foreign machine. Code will expect to read and write to registers (specific memory locations) to achieve particular effects, and even perfectly recompiled code will not work if this does not happen [Bedichek 1990].

Interpretation means that the code is interpreted instruction by instruction at run time by some software, that is, the emulator. This is usually achieved by writing routines to perform the same operations as a machine code instruction, and this can be done in a high level language like C, or in assembly language.

In this approach the emulator reads the code to be emulated from memory byte by byte, decodes it, and performs appropriate commands on the emulated registers, memory, and I/O. The general algorithm for such emulator is:

```
while(CPUIsRunning)
{
  Fetch OpCode
  Interpret OpCode
}
```

For example, an interpretive emulator performs three main tasks in the emulation of a single 680x0 instruction. First, it must fetch the instruction from the 680x0 instruction stream. Second, it must decode the instruction and dispatch to a small semantic routine. Third, the semantic routine is responsible for carrying out the action of the original emulated instruction.

The benefits of this model include ease of debugging. A major drawback of this is the low performance. The interpretation takes a lot of CPU time and it may require a very fast computer to run the emulated code at an acceptable speed.

EMULATOR EXECUTION UNIT DESIGN

At the core of every microprocessor is a unit that is continually fetching instructions from memory, decoding them, and executing the The 16-bit MC68000 microprocessor is the result of the MACSS project (Motorola Advanced Computer System on Silicon), which begun in 1976 with the objective of developing a monolithic microprocessor whose performance would be based on the two main criteria of simplicity and orthogonality (that is, the internal registers would be general purpose with regard to addressing modes and instructions) [Clements 1990].

From the software point of view, the aim was to simplify programming by drawing upon the best of the modern programming techniques that enable the use of high-level languages. The first samples were offered to industry in 1979 with the majority of these aims having been realised. The only way to program the MC68000 microprocessor is through Assembly Language.

The MC68000 has the following general features [Motorola 1986]:

- CISC - Complex Instruction Set Computer architecture.
- 8 general-purpose 32-bit data registers (D0-D7).
- 8 general-purpose 32-bit address registers (A0-A7).
- 16-bit Status Register (SR) [which include 8-Bit Condition Code Register (CCR)]
- A7' is the stack pointer - user or supervisor.
- 32-Bit Program Counter (PC)
- 24 bits Address Bus
- 16 bits Data Bus
- 16 Mbytes linear addressing range (23 bit plus Upper and Lower data strobes for an effective 24 bit range).
- 56 Instruction types - over 1000 useful permutations are possible.
- Memory mapped I/O. (Peripheral registers addressed as memory).
- 14 Addressing modes on a contiguous address space (no segments).
- 5 Main data types. (Bit, Byte, BCD, Word and Long Word).
- Supervisor and User states. Stack Pointer A7 is set to User (USP) or Supervisor SP (SSP) by a bit in the status register.

Although the MC68000 is no longer in use, its derivatives has the same structure plus other added improvements. Therefore, when a student learns how to use that particular microcomputer, afterwards he is going to be able to program any derivative of the MC68000 family, with the little drawback that he has top take into consideration the changes from the MC68000.

EMULATOR EXECUTION UNIT DESIGN

At the core of every microprocessor is a unit that is continually fetching instructions from memory, decoding them, and executing the appropriate operation. Although modern microprocessors may have pipelines and multiple execution units, they are all still carry out the basic fetch, decode and execute loop. A block diagram of this loop is shown in Figure 1.

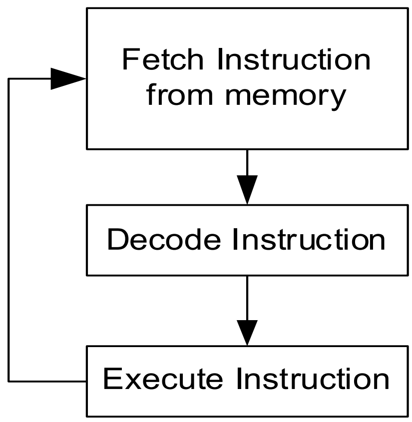

Figure 1: Execution Loop of a Microprocessor

In the MC68000 microprocessor the core code of the emulated execution unit follows the operations shown in this block diagram. It does have a prefetch buffer for instructions, but this is largely transparent to the programmer. Therefore, the prefetch buffer is not emulated. The high abstraction of the core execution unit implementation is illustrated in the following pseudo-code:

```
Loop Forever
      Get Instruction from Memory
      Update Program Counter
      Execute Instruction
End Loop
```

This pseudo-code provides an overview of the three main stages in the emulation engine. The most important stage is the execution stage where the 68k instruction is interpreted to the host machine instruction and executed. This interpretation has to take into account all the different instructions available in the instruction set of the machine to be emulated.

DECODING AND EXECUTING INSTRUCTION

Once an instruction has been fetched from memory, the operation and addressing modes of the instruction must be determined. The correct operation can then be carried out. This requires an understanding of the processor instruction format as explained below.

Instruction Format

A MC68000 instruction is made up of 16-bits, which is one machine word. Different parts of the instruction word, or fields, tell the instruction decoder what operation to carry out. For example, the least significant six bits almost always define the addressing mode used for an effective address operand. All instructions have a unique 'signature'; that is, part of the instruction word never changes regardless of the combination of addressing modes used. For example, a MOVE.L instruction always has 0010 in the first four bits of the instruction word. No other instruction word starts with the bit pattern 0010. Figure 2 shows this example, including the constant part of the instruction in bits 15 to 21, and the fields making up the addressing modes.

<table>
<tr><td>15</td><td>14</td><td>13</td><td>12</td><td>11</td><td>10</td><td>9</td><td>8</td><td>7</td><td>6</td><td>5</td><td>4</td><td>3</td><td>2</td><td>1</td><td>0</td></tr>
<tr><td colspan="4" rowspan="2">0010</td><td colspan="6">Destination</td><td colspan="6">Source</td></tr>
<tr><td colspan="3">Register</td><td colspan="3">Mode</td><td colspan="3">Mode</td><td colspan="3">Register</td></tr>
</table>

Figure 2: Example of Instruction Encoding for `MOVE.L`

Decoding the Instruction

The method that was considered for decoding the instruction was to check against each possible signature by applying the appropriate mask and comparing with the known signatures, for example:

```
If InstrWord And 0xF000 Equals
0x2000 Then
      ExecuteAddOp
Else If ... Then
      ExecuteOp
Else
      IllegalOpException
End If
```

If no match can be found, the illegal instruction exception is taken. The disadvantage of this approach is that the full code would be very complex. To find the correct instruction requires making a significant amount of comparisons for each instruction cycle. This would decrease the emulation speed. But the implementation of this method is uncomplicated and straight forward which made it an excellent choice considering the development schedule of the project.

The program is divided into two distinct and integrated modules; an application module that contains the text editor functionality and the assembler functionality, and another application module that contains the emulator.

68k editor & assembler module shown in Figure 3 allows the user to write his assembly program in a text editor with a graphical user interface that includes pull-down menus and buttons toolbars, file functionality like open, save and print, text editing functionality like cut & paste, and find & replace, a two-step ‘Undo’ functionality, and also a help menu.

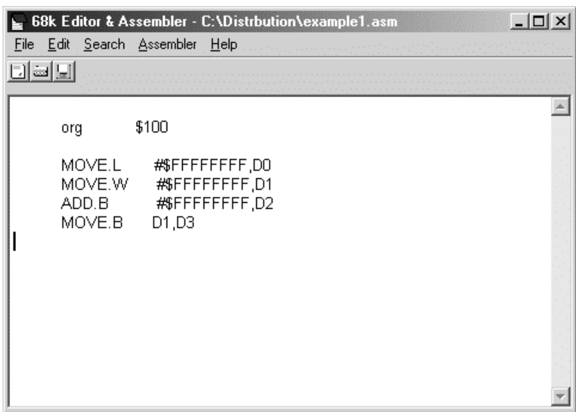

Figure 3: The Editor/Assembler Window

In the same module the user can assemble the program to produce a binary object code file and a listing file. If the assembler encounters a programming syntax error then the editor will indicate the line that has the error. In addition the program will indicate the type of the error encountered.

The user then can use the emulator module to run the correctly assembled program shown in Figure 4. This module contains a graphical environment that illustrates parts of the microprocessor internal architecture such as the data and address registers, a memory map, the program counter and others to help the user to get the picture of the inner working of the MC68000 microprocessor.

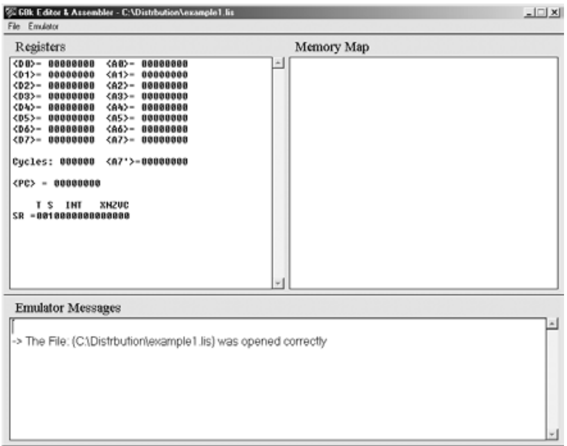

Figure 4: The Emulator Window

This module gives the user the ability to show the part of memory he wants in the memory map window. And allow the user to run the program in a single-step mode or run it in 'to the end' mode.

EDUCATIONAL BENEFITS OF THE EMULATION SYSTEM

Even though that the use of computer-based environments to help and improve learning and education is not new [Najjar 1996; Schodorf et al. 1996], it is a fact that the use of such technologies change the characteristics of the learning phases of the traditional education. Traditionally, technical education include concepts and theories presentation, explanation, verification of learning level and finally hand-on technical practice, of course, those steps can be maintained, and at the same time improved by using a computer-based learning (CBL) environments. CBL can enhance active learning, by making students the centre of the learning process, students can lead there own learning by building there own knowledge and skills using simulation-based instruction tools [Marcy and Hagler 1996].

Bormida et. al. [Bormida et al. 1997] classifies the instructional methodologies used in the computer-based educational tool into four categories:

1) Expositive methodology aims at presenting theories, concepts and other information using semi-interactive multimedia and hypertext enriched application.

2) Demonstrative methodology uses scripts underlying the schematics and algorithms to demonstrate their behaviour.

3) Interactive methodology encourages the student interactions with applications designed to practice and test his level of knowledge and technical skills.

4) Practical methodology allows students to design and analyze networks or algorithms, using custom-built general purpose simulators.

Following practical instructional methodology, we believe the only way to learn effectively a programming language is to use it to write programs. On this basis the Microprocessor emulator allow the students to write and run programs for the microprocessor taught in the university class: the Motorola 68000.

So the students will emphasize the functions which realize learn-by-doing concept. From our experience we found out that to improve the learning process in future versions, the overall interface will be refined, making it more user-friendly; the emulation kernel will be enlarged, including the I/O instructions to make it clearer. At last, besides the already existing help on-line, an additional online automated tutoring instruction can be added so that the learning process becomes completely computer-based. The instructor can write the instruction for each lab session beforehand, this way the ability of the student to detect and correct his programming mistakes will become completely transparent.

CONCLUSION

This paper introduced a generic emulation framework based on the interpretation architecture to emulate the 68k microprocessor. The interpretation framework helps in making the emulator development evolutionary, where simple features are added at the start and other features can be added or extended at a later stage of the development easily. In addition, because this framework uses the interpretation architecture, it can easily be modified and extended to accommodate other types of microprocessors

We believe the following missing features can be a valuable addition in the future: Proper memory mapping would need to be implemented to allow features such as serial IO and LCDs to be included. Given the current architecture of the application it would be relatively easy to add more instruction decoding/translating functionality. Once proper memory mapping is implemented, adding more devices would be quite straightforward due to the modularisation that memory mapping would provide. After implementing a basic form of IO, extending this would mostly involve developing and integrating a GUI widget. Emulating an LCD device would again be mostly GUI related.

REFERENCES

Altman, Erik R. and Kemal Ebcioglu. 2000. “DAISY Dynamic Binary Translation Software”, IBM T. J. Watson Research Center.

Bedichek, R. 1990. *Some efficient architecture simulation techniques*. In Proceedings Winter USENIX Conference, pp. 53—63.

Bormida, Giorgio D., Domenico Ponta, and Giuliano Donzellini. 1997. “Methodologies and Tools for Learning Digital Electronics”. *IEEE Transaction in Education*, Vol. 40, No. 4.

Church, A. 1936. *A Note on the Entscheidungsproblem*. Journal of Symbolic Logic, 1, 40-41.

Clements, Alan. 1990. *68000 Sourcebook*, McGraw-Hill. London, October.

Copeland, B.J. 1996. 'The Church-Turing Thesis'. In Perry, J., Zalta, E. (eds) *The Stanford Encyclopaedia of Philosophy*.

Copeland, B.J. 1996 “What is Computation?”, *Synthese*, vol. 108, pp. 335-359.

Fayzullin, Marat. 2002. "How To Write a Computer Emulator", *Computer Emulation Resources*, http://fms.komkon.org/EMUL8/HOWTO.html.

Hookway, Raymond J. and Mark A. Herdeg. 1997. "DIGITAL FX!32: Combining Emulation and Binary Translation", *Digital Technical Journal*, 9 (1).

Marcy, W. and M. Hagler. 1996. "Implementation Issues in SIMPLE Learning Environments." *IEEE Transaction on Education*, vol. 39, no. 3, pp. 423-429.

Motorola Microprocessor Inc. 1986. *MC68000 Family Programmer’s Reference Manual*, Fifth Edition, Great Britain, Motorola Inc.

Najjar, L. J. 1996. "Multimedia Information and Learning," *Journal of Educational Multimedia and Hypermedia*, vol. 5, no. 2, pp. 129-150.

Schodorf, J. B.; M. A. Yoder, J. H. McClellan, and R. W. Schafer, 1996. "Using Multimedia to Teach the Theory of Digital Multimedia Signals." *IEEE Transaction on Education*., vol. 39, no. 3, pp. 336-341.

Turing, A.M. 1936. *On Computable Numbers, with an Application to the Entscheidungsproblem*. Proceedings of the London Mathematical Society, Series 2, 42 (1936-37), pp.230-265. Available at http://www.abelard.org/turpap2/tp2-ie.asp. Last accessed: October 2002.

SIMULATION
IN
THE BUILT
ENVIRONMENT

EDUCATION – ORIENTED VISUALIZATION MODEL FOR BUILDINGS CROSS VENTILATION

Ahmed Mokhtar and Muqeem Khan
School of Architecture & Design
American University of Sharjah
P.O. Box 26666 Sharjah, United Arab Emirates
Email: mokhtar@aus.ac.ae mukhan@aus.ac.ae

ABSTRACT

We propose a tool to extract the cross ventilation of a building space using commercially available software, Maya and the power of Maya Embedded language (MEL). A graphical user interface enables students to investigate and explore the special configuration of building with reference of cross ventilation.

BACKGROUND

Cross ventilation is a natural technique used to provide thermal comfort to occupants of buildings. This technique is widely used in parts of the world where the climate is usually tempered.

A very simple example of cross ventilation is the movement of air that any car passenger feels when two opposite windows of the car are opened. If correctly designed – knowing that buildings have more complex spaces than cars – cross ventilation can save energy used to cool buildings through air conditioning systems. It also provides pleasing natural and variable wind speed to building occupants.

Architecture students need to learn how to correctly provide natural ventilation in their designs. This is not an easy task since many factors are involved in determining how the air moves inside a building when some of its windows are opened. These factors include:

- Wind direction.
- Wind speed.
- Building form.
- Building orientation relative to wind.
- Location of windows.
- Size and number of windows.
- Internal building obstacles such as wall and fixed furniture.

It is not adequate as well to just allow air to enter the building. The air should have reasonable wind speed in all areas where occupants are expected to be. Some bad designs can lead to the existence of large areas of some spaces with inadequate wind. Consequently thermal distress is to be felt by occupants of these areas.

THE NEED FOR A VISUALIZATION MODEL

Unlike many other engineering products, where a prototype model is built, tested and modified, buildings can only be examined after they are built. It is then too late to correct any design mistake. Therefore, architects depend on scaled models to simulate as close as possible the final product and test the design. The currently available approach for students as well as professionals to simulate cross ventilation is to build a small abstract physical model for the designed building and to put the physical model in a wind tunnel. Lines of smoke are passed in the wind tunnel to allow visualizing the behavior of wind in and around the building. While this approach can provide simulation with reasonable accuracy, it is rarely used and for several good reasons:

- Wind tunnels are expensive to build and take large space. Few universities around the world can afford having one.
- Building a physical model to test a design is a time consuming process, especially when small modifications need to be done to optimize the design. As a result, fewer options are examined and the study process is compromised.

With the continuous development in computer software capabilities, it seems that using them to overcome these difficulties in an appropriate new approach. If well designed, a computer tool can provide flexible, affordable and easy to use learning tool to help architecture students in understanding cross ventilation by testing alternative design configurations. This paper provides a model that use computer simulation capabilities to visualize the movement of wind through and around a building.

STRUCTURE OF THE VISUALIZATION MODEL

The proposed visualization model is built on the software Alias WaveFront “Maya”. Maya is commonly used in the film industry. It is capable of creating three dimensional models, render and animate them in a variety of fashions. Maya is been used to simulated physical phenomena such as wind movement through third party plug-ins and scripts.

Taking advantage of such capability, the proposed model in this project consists of the following five modules as shown in Figure 1:

1. The file transfer and translation module, which import, translate and rotate the selected DXF file from any digital modeling program. The DXF is to be generated by the student by using any three dimensional modeling software that s/he is familiar with. Maya provides translators for exporting and importing to various file formats. After importing 3d model into the environment Maya converts its texture information too. There may be some limitation while importing into Maya. Some

texture may not transfer or transfer with un-identified maps. In our case we do not need texture information of the model. So it was not important for a model to have correct texture information. Sometime, the file carry many nodes when transfer from DXF format. This was controlled by the script which selects and combines all the nodes into single node. This node can easily participate in the simulation process. When a user import a DXF model into Maya with "Import" button, the model will automatically be placed on the 0, 0, 0, coordinates. This should give user a clear view of the model and its orientation. The model can also be rotate arbitrarily by sliding the parameter on the Vent Tool. Once it is correctly placed at desirable position, simulation can be started. User will have all of the options to rotate and see deferent wind directions.

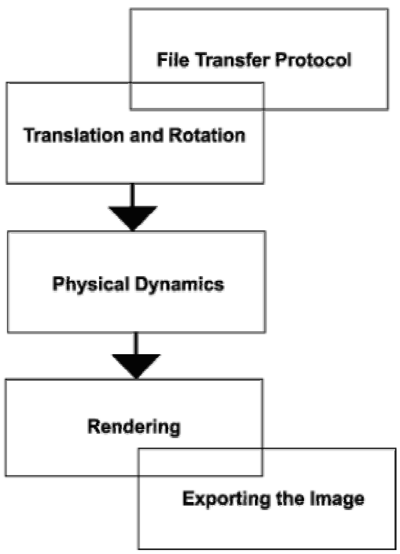

Figure 1: Structure of the Proposed Model

2. The Graphical User Interface (GUI) module, developed in MEL, Maya Embedded Language, which is designed to enable the user to pick a digital three dimensional computer model for the building under investigation. The module allows as well the user to rotate the building relative to wind direction. The user can also control the nature of the wind in terms of its speed and its collision to the walls (Figure 2). User can also control the collusion detail to investigate the precise simulation. We selected Maya for developing this tool as it provide a scripting language MEL (Maya Embedded Language). MEL provides the foundation for Maya. Nearly every feature of Maya's interface has been built upon MEL commands and scripts. Because Maya gives complete access to MEL itself, one can extend and customize Maya. With MEL, one can further develop Maya into a unique creative environment.

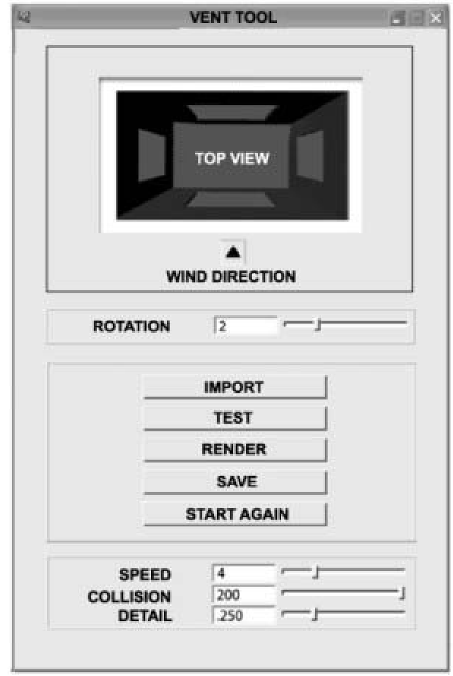

Figure 2: The Graphical User Interface Developed in MEL

3. Maya Fluid Dynamics module which create the physical simulation. Another reason to select Maya was its dynamics simulation capability. Maya introduces Fluid Effects, a major new dynamics and rendering technology that realistically simulates 2D and 3D atmospheric, pyrotechnic, space, and viscous fluid effects. One can use the Fluid Effects solvers to simulate these effects. With Fluid Effects provide a fully integrated solution to one of the most difficult challenges in the computer graphics industry-accurately modeling, animating, and rendering effects such as oceans, clouds, smoke, explosions, fire, comets, mud, and lava.

4. Maya rendering engine to render the scenes. We used Maya own rendering engine. Rendering is the final stage in the 3D CG (Computer graphics) production process. It pulls data together from every sub-system within Maya, interprets modeling construction histories, particle dynamics, and more. At the same time, it interprets its own data relevant to tessellation, texture mapping, shading, clipping, and lighting. Although there are other rendering options within Maya software but we found that Maya render was fine to get the desire results.

5. Exporting images to the required image file format.

CASE STUDIES

To test the potential of the model, several case studies were performed. The first case used a very simple building consists of one room with one window as shown in figure 3. The building orientation changes such as to make the window in one of three positions facing the wind, perpendicular to the wind, and opposite to the wind. Figures 3, 4, and 5 show snap shots from the animation generated by the model. It indicated that wind can hardly get into the room with on window. The same room is modeled but with two windows in adjacent walls. The building orientation changes to make one window facing the wind and the other window perpendicular to wind. Figure 6 shows the result where a pocket of almost stagnant air exists in the room. The same building is rotated 90° degree as in Figure 7. The figure shows that hardly any air is moving in the room.

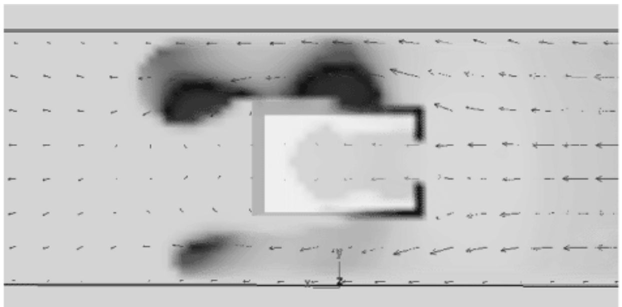

Figure 3: A Room with one Window Facing the Wind

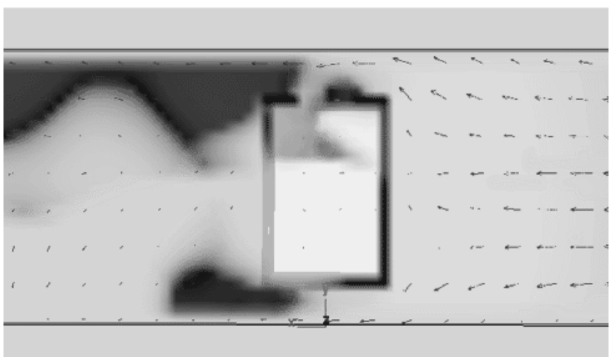

Figure 4: A Room with One Window Perpendicular to the Wind

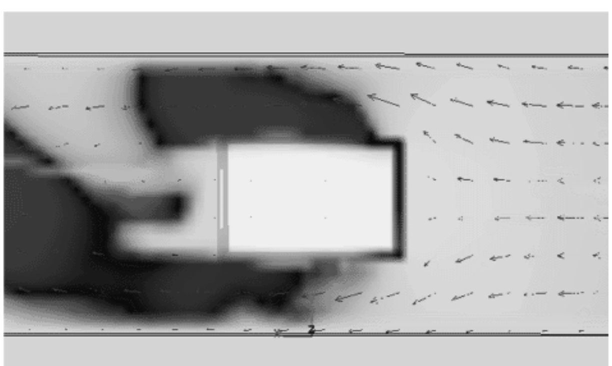

Figure 5: A Room with One Window Opposite to the Wind

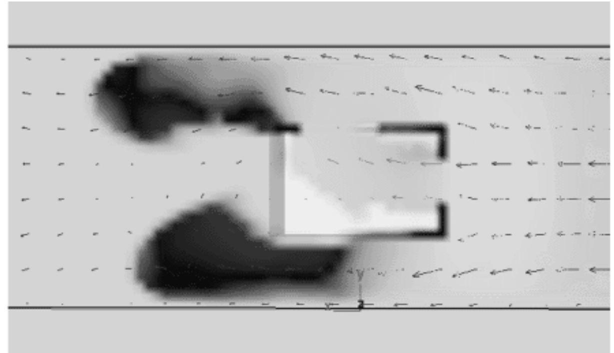

Figure 6: A Room with Two Windows, One of them is Facing the Wind

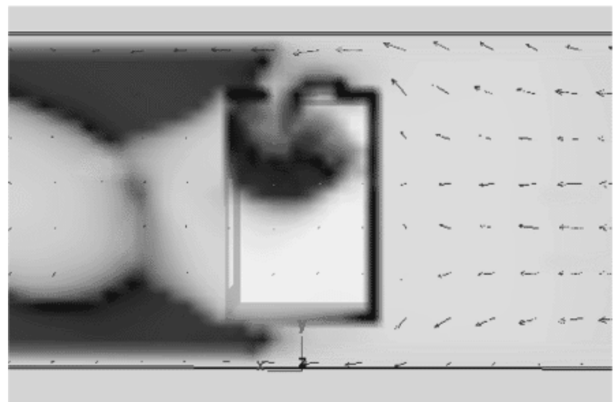

Figure 7: A Room with Two Windows, None of them is Facing the Wind

A more realistic building is treated in the model as shown in Figure 8. The figure shows the movement of wind within the building spaces. The figure clearly shows the capability of the model to let architecture students understand how cross ventilation is affected by the building design and the selection of windows' location. It worth noting that wind tunnel simulation will be valuable to make sure that the wind module used by Maya is an accurate one. The researchers plan to do this step in the near future.

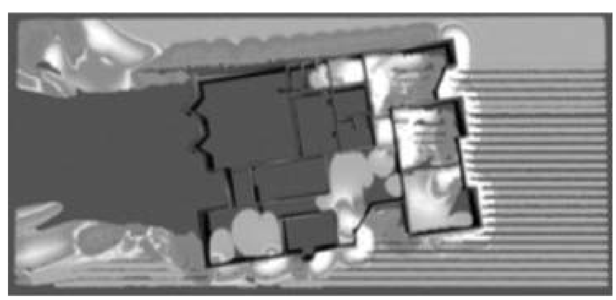

Figure 8: A Realistic Building is Tested in the Model

CONCLUSION

From the exploration experiment performed by the authors, it was clear that there is a great potential for using computer simulation in teaching architecture student the effect of design decision such as windows' location and orientation on natural ventilation in building. The ability of the model to evaluate simulated 3D building design is very beneficial to quickly test design alternative. The interface is designed to allow easy studying of the effect of various wind speed and orientation. The model still needs validation through a wind tunnel test or actual building cases.

BIOGRAPHY

AHMED MOKHTAR worked as an architect, contractor, and cross-disciplines design coordinator for various size buildings projects. Leaning towards the engineering aspects of buildings, Dr. Mokhtar earned both his Master and PhD degrees in Building Engineering from Concordia University, Montreal, Canada. Throughout his graduate studies and research work, he aimed at integrating architecture design with the design of various buildings systems; especially with the aid of computers. Dr. Mokhtar has numerous international and local publications ranging from the use of solar energy in design to the use of internet in design management. Before joining the American University of Sharjah, Dr. Mokhtar taught in Canada as well as in the USA where he was an assistant professor and the director of the Architectural Engineering program at Illinois Institute of Technology in Chicago. Current research interests focus on the development of local building codes as well as the use of information technology to improve building science educqation. Dr. Mokhtar is a founding member of the Architecture Engineering Institute, a member of the American Society of Civil Engineers, and a reviewer for the ASCE Journal of Architecture Engineering.

MUQEEM KHAN is an Assistant Professor of digital design at the School of Architecture and Design, American University of Sharjah. After Bachelor of Science in Industrial Design (1994) at Ohio State University, Columbus Ohio, he Obtained Masters of Arts in Industrial Design with the emphasis on computer graphics and animation from (ACCAD Advanced Computing Center for Arts and Design) and (Department of Industrial, Interior, and Visual Communication) (1996) at Ohio State University, Columbus Ohio. Muqeem worked with Walt Disney and Square USA (1996-2001) and produced the visual effects and animation for the movies Deep Rising, George of the Jungle, Flubber, Armageddon and Final Fantasy. His research interests are in teaching methodologies and computer graphic tools for designers and artists. Muqeem khan has published several articles and papers on the topics of design methodologies and computer graphics. His work can be seen at: http://www.muqeemkhan.com

MODELLING AND SIMULATION METHODOLOGY

ON EQUILIBRIUM PROBLEMS WITH TRIFUNCTIONS

Muhammad A. Noor
Etisalat College of Engineering
PO Box 980, Sharjah
United Arab Emirates
noor@ece.ac.ae

Khalida I. Noor
UAE University
Box 17551, Al Ain
United Arab Emirates
Khalidan@uaeu.ac.ae

KEYWORDS
Equilibrium problem, Variational inequalities, Models, Algorithms, Convergence.

ABSTRACT

Equilibrium problems are being used as mathematical model to study a wide class of unrelated problems in a unified and novel framework. In this paper, we introduce a new class of equilibrium problems, known as ϵ-equilibrium problems involving trifunction. This class of equilibrium problems include several classes of equilibrium problems and variational inequalities as special cases. We here use the auxiliary principle technique to suggest and analyze some iterative schemes for solving these problems. We prove that the convergence of the proposed methods requires only pseudomonotonicity, which is a weaker condition than monotonicity. Our results present a significant improvement and refinement of the previous known results in this field.

INTRODUCTION

Theory of equilibrium problems has appeared as an effective and powerful tool to investigate and study a large class of problems arising in finance, economics, network analysis, transportation, elasticity and optimization. This theory has witnessed an explosive growth in theoretical advances and applications across all disciplines of pure and applied sciences. This theory is rich source of mathematical structures and combines several interesting mathematical models both continuous and discrete. Equilibrium problems have generalized and extended in several directions using novel and innovative techniques both for the sake of generalization as well its applications in various disciplines. Motivated and inspired by the research going in this interesting and fascinating filed, we introduce and consider a new class of problems, called as ϵ-equilibrium problems with trifunction. This class is quite general than and flexible. As a result of this interaction, we have a variety of techniques to study the existence results for equilibrium problems. Equilibrium problems include variational inequalities as special cases. In recent years, several numerical techniques including projection, resolvent and auxiliary principle have been developed and analyzed for solving variational inequalities(Noor, 2003b). It is well-known and projection and resolvent type methods can not be extended for equilibrium problems.. To overcome this drawback, one usually uses the auxiliary principle technique (Glowinski et al. 1981). This technique has been used (Noor, 2003a, 2003b) to suggest and analyze a number of predictor-corrector and proximal methods for solving various classes classes of variational inequalities and equilibrium problems. We again use the auxiliary principle technique to suggest and analyze some proximal point methods for solving ϵ-equilibrium problems with trifunction. We study the convergence analysis of the proposed method under some mild conditions. Our results can be viewed as significant extension and generalization of the previously known results for solving classical variational inequalities and equilibrium problems.

PRELIMINARIES

Let H be a real Hilbert space, whose inner product and norm are denoted by $\langle .,. \rangle$ and $\|.\|$ respectively. Let K be a nonempty closed convex set in H. Let $T : H \longrightarrow H$ be a nonlinear operator. For given nonlinear function $F(.,.) : H \times H \times H \longrightarrow H$ and $\epsilon \in R$, an arbitrary vector, consider the problem of finding $u \in K$ such that

$$F(u, Tu, v) \geq \epsilon \|v - u\|, \quad \forall v \in K. \tag{1}$$

Problems (1) are called the *ϵ-equilibrium problems with trifunction.* For $\epsilon > 0$, problems (1) are called the *strong equilibrium problems* and for $\epsilon < 0$, problems (1) are called the *weak equilibrium problems.* It is clear that if $\epsilon = 0$, then problem (1) is equivalent to finding $u \in K$ such that

$$F(u, Tu, v) \quad \geq 0, \quad \forall v \in K, \tag{2}$$

which is the original equilibrium problem considered and investigated (Noor and Oettli, 1994).

If $F(u, Tu, v) = F(u, v),$, then problem (1) is equivalent to finding $u \in K$ such that

$$F(u, v) \geq \epsilon \|v - u\|, \quad \forall v \in K, v \tag{3}$$

which is called the ϵ-equilibrium problem considered and investigated (Noor, 2003b). Clearly for $\epsilon = 0$, problem (3) is equivalent to finding $u \in K$ such that

$$F(u,v) \quad \geq 0, \quad \forall v \in K, \tag{4}$$

which is the classical equilibrium problem introduced and considered by (Blum and Oettli, 1994) and (Noor and Oettli, 1994). Following (Blum and Oettli, 1994),one can easily show that several classical problems can be studied in the general framework of problems (1)- (4) such as:

i. general mathematical programming problem: $F(u, Tu, v) := f(v) - f(v)$.
ii. saddle point problem: $F(u, Tu, v) := h(u_1, v_2) - h(u_1, v_2)$, where $u = (u_1, u_2), v = (v_1, v_2)$.
iii. Nash equilibrium problem in a non-cooperatove game:

$$F(u, Tu, v) := \sum_{i \in I} \{f_i(u^i, v_i) - f_i(u)\}$$

where f_i is the loss function of player i and u^i is the vector obtained from u by deleting component i.
iv. The network equilibrium problems arise in applied contexts as urban transportation, energy distributions, electrical networks, telecommunication networks, computer networks and water resources planning etc. For simplicity and to convey an idea of the networks involved, we consider the predicted traffic flow on a congested transportation networks using the Wardrop's model of traffic equilibrium. The model (Giannessi, et al. 2001) is defined on a transportation networks $[N, A]$ with nodes N, and directed arcs A. Here

- I the set of origin-destination pairs (O, D)
- P_i the set of available paths for flow for (O, D)-pairs i,
- h_i the flow on path p,
- h the vector of $\{h_i\}$ with dimension $n_1 = \sum_{i \in p_i}$ equal to total number of (O, D)-pairs and path combination
- u_i an accessibility variable, shortest travel time for (O, D)-pairs i,
- u the vector $\{u_i\}$ with dimension $n_2 = |I|$,
- $D_i(u)$ the demand function for (O, D)-pairs $(i,), D_i : R^{n_2} \longrightarrow R$,
- $T_p(h)$ the delay time, or general disutility function for path p, $T_p : R^{n_1} \longrightarrow R$.
- If $x = (u, h) \in R^n$, where $n = n_1 + n_2$, we denote

$$\begin{aligned} f_p(x) &= T_p(h) - u_i, \text{ for } \quad p \in P_i \quad \text{and} \quad i \in I, \\ g_i(x) &= \sum_{p \in P_i} h_p - D_i(u), \quad \text{for} \quad i \in I, \end{aligned}$$

- $F(x) = (f_p(x), g_i(x) \quad p \in P_i, \quad i \in I$.

It is known that this transportation network problem is equivalent to the equilibrium problem (4) defined on $K = R^n_+$ with

$$F(x, y) = \langle F(x), y - x \rangle.$$

Definition 1
A function $f : K \longrightarrow H$ is said to be strongly convex, if there exists a constant $\beta > 0$ such that

$$\begin{aligned} f(u + t(v-u)) &\leq (1-t)f(u) + tf(v) \\ -t(1-t)\beta\|v-u\|^2, &\quad \forall u, v \in K, \quad t \in [0,1]. \end{aligned}$$

If the strongly convex function is differentiable, then

$$f(v) - f(u) \geq \langle f'(u), v - u \rangle + \beta\|v-u\|^2.$$

and conversely.
Definition 2
The trifunction $F(.,.,.) : K \times K \times K \longrightarrow H$ is said to be:
i. *jointly pseudomonotone,* if

$$F(u, Tu, v) \geq 0 \quad \Longrightarrow F(v, Tv, u) \leq 0, \quad \forall u, v \in K.$$

iii. *jointly hemicontinuous,* if the mapping $F(u + t(v-u), T(u+t(v-u)), v)$ is continuous, $\forall \in u, v \in K$, $t \in [0,1]$.

For $z = u$, partially relaxed strongly jointly monotonicity reduces to

$$F(u, Tu, v) + F(v, Tv, u) \leq 0, \quad \forall u, v \in K,$$

which is known as jointly monotonicity of the bifunction $F(.,.,.)$. It is known (Giannessi and Maugeri, 1995) that monotonicity implies pseudomonotonicity, but the converse is not true.

Lemma 1
Let the trifunction $F(.,.,.)$ be jointly pseudomonotone and jointly hemicontinuous. if the trifunction $F(.,.,.)$ is convex with respect to the third argument, then problem (1) is equivalent to finding $u \in K$ such that

$$F(v, Tv, u) \leq -\epsilon\|v-u\|, \quad \forall v \in K. \tag{5}$$

Proof
Let $u \in K$ be a solution of (1). Then

$$F(v, Tv, u) \leq -\epsilon\|v-u\|, \quad \forall v \in K, \tag{6}$$

since $F(.,.,.)$ is jointly speudomonotone.
Conversely, let $u \in K$ be a solution of (5). Then, $\forall u, v, \in K, t \in [0,1]$, $v_t = u + t(v-u) \in K$, since K is a convex set. Taking $v = v_t$ in (5), we have

$$F(v_t, Tv_t, u) \leq -\epsilon t\|v-u\|. \tag{7}$$

Now using the convexity of $F(.,.,.)$ with respect to the third argument and from (7), we have

$$\begin{aligned} 0 &\leq F(v_t, Tv_t, v_t) \\ &\leq tF(v_t, Tv_t, v) + (1-t)F(v_t, Tv_t, u) \\ &\leq tF(v_t, Tv_t, v) + t(1-t)\epsilon\|v-u\|. \end{aligned} \tag{8}$$

Dividing (2.8) by t, taking the limit as $t \longrightarrow 0$, and using the jointly hemicontinuity of $F(.,.,.)$, we have

$$F(u, Tu, v) \geq \epsilon\|v-u\|, \quad \forall v \in K,$$

the required (1). $\diamond$

Remarks
Problem (5) is known as the *dual ϵ-equilibrium problem with trifunction* . One can easily show that the solution set of problem (5) is a closed and convex set. Lemma 1 can be viewed as a natural extension of Minty's Lemma in equilibrium problems and variational inequalities (Noor, 2003b). This result is also very important in its own.

MAIN RESULTS

In this section, we suggest and analyze a proximal method for ϵ-equilibrium problems (1) using the auxiliary principle technique (Glowinski, et al. 1981) as developed (Noor, 2003a, 2003b).

For a given $u \in K$, consider the auxiliary problem of finding a unique $w \in K$ such that

$$\rho F(w, Tw, v) + \langle E'(w) - E'(u), v - w\rangle \geq \epsilon\|v - w\|, \quad \forall v \in K, \tag{9}$$

where $\rho > 0$ is a constant and $E'(u)$ is the differential of a strongly convex function $E(u)$ at a point $u \in K$. Problem (9) has a unique solution, since $E(u)$ is a strongly convex function. We note that if $w = u$, then clearly w is solution of the ϵ- equilibrium problem (1). This observation enables us to suggest and analyze the following iterative method for solving (1).

Algorithm 1
For a given $u_0 \in H$, compute the approximate solution u_{n+1} by the iterative scheme

$$\rho F(u_{n+1}, Tu_{n+1}, v) + \langle E'(u_{n+1}) - E'(u_n), v - u_{n+1}\rangle \geq \rho\epsilon\|v - u_{n+1}\|, \quad v \in K. \tag{10}$$

If $\epsilon = 0$, then Algorithm 1 reduces to the following iterative schemes for solving equilibrium problem (2).

Algorithm 2
For a given $u_0 \in H$, compute the approximate solution by the iterative scheme.

$$\rho F(u_{n+1}, Tu_{n+1}, v) + \langle E'(u_{n+1}) - E'(u_n), v - u_{n+1}\rangle \geq 0, \quad \forall v \in K,$$

If $F(u, Tu, v) = F(u, v)$, then Algorithm 1 collapses to the following iterative method for solving (3).

Algorithm 3
For a given $u_0 \in H$, compute the approximate solution u_{n+1} by the iterative scheme

$$\rho F(u_{n+1}, v) + \langle E'(u_{n+1}) - E'(u_n), v - u_{n+1}\rangle \geq \rho\epsilon\|v - u_{n+1}\|, \quad \forall v \in K,$$

which has been suggested and studied (Noor, 2003a).

We now study the convergence analysis of Algorithm 1 and this is the main motivation of our next result.

Theorem 1
Let $F(.,.,.) : K \times \times K \longrightarrow H$ be jointly pseudomonotone. If $E(u)$ is a differentiable strongly convex function with modulus $\beta > 0$, then the approximate solution u_{n+1} obtained from Algorithm 1 converges to a solution $u \in K$ of (1).

Proof
Let $u \in K$ be a solution of (1). Then

$$F(v, Tv, u) \leq -\epsilon\|v - u\|, \quad \forall v \in K \tag{11}$$

since $F(.,.,.)$ is jointly pseudomonotone.
Taking $v = u_{n+1}$ in (11), we have

$$F(u_{n+1}, T(u_{n+1}), u) \leq -\epsilon\|u_{n+1} - u\|. \tag{12}$$

Consider the function,

$$\begin{aligned} B(u, z) &= E(u) - E(z) - \langle E'(z), u - z\rangle \\ &\geq \beta\|u - z\|^2, \\ &\text{using the strongly convexity of } E. \end{aligned} \tag{13}$$

Combining (10), (12) and (13), we have

$$\begin{aligned} B(u, u_n) - B(u, u_{n+1}) &= E(u_{n+1}) - E(u_n) - \\ &\quad \langle E'(u_n), u - u_n\rangle + \langle E'(u_{n+1}), u - u_{n+1}\rangle \\ &= E(u_{n+1}) - E(u_n) - \langle E'(u_n) - E'(u_{n+1}), u - u_{n+1}\rangle \\ &\quad -\langle E'(u_n), u_{n+1} - u_n\rangle \\ &\geq \beta\|u_{n+1} - u_n\|^2 + \langle E'(u_{n+1}) - E'(u_n), u - u_{n+1}\rangle \\ &\geq \beta\|u_{n+1} - u_n\|^2 - F(u_{n+1}, Tu_{n+1}, u) + \epsilon\|u_{n+1} - u\| \\ &\geq \beta\|u_{n+1} - u_n\|^2. \end{aligned}$$

If $u_{n+1} = u_n$, then clearly u_n is a solution of the ϵ-equilibrium problem (1). Otherwise, the sequence $B(u, u_n) - B(u, u_{n+1})$ is nonnegative and we must have

$$\lim_{n\to\infty} (\|u_{n+1} - u_n\|) = 0.$$

Now by using the technique (Zhu and Marcotte, 1996), it can be shown that the entire sequence $\{u_n\}$ converges to the cluster point $\overline{u}$ satisfying the ϵ-equilibrium problem (1). $\diamond$

CONCLUSION

In this paper, we have shown that a number of problems arising in transportation, computer network and economics can be modeled in terms of equilibrium problems. We have suggested and analyzed some iterative schemes for solving these equilibrium problems. It is expected that the these new algorithms can be parallelized and will stimulate further research in this fast emerging field. The comparison of these new algorithms with other methods is open problem and is the subject of future research efforts.

REFERENCES

Blum, E. and W. Oettli. 1994 "From Optimization and Variational Inequalities to Equilibrium Problems." *The Mathematics Students 63,* 123-145.

Giannessi, F.; A. Maugeri; and P. M. Pardalos. 2001. *Equilibrium Problems: Nonsmooth Optimization and Variational Inequality Models.* Kluwer Academics Publishers, Dordrecht, Holland.

Giannessi, F. and A. Magueri. 1995. *Variational Inequalities and Network Equilibrium Problems.* Plenum Press, New York, N. Y.

Glowinski, R.; J. Lions,; and R. Tremolieres. 1981. *Numerical Analysis of Variational Inequalities.* North-Holland, Amsterdam, Holland.

Noor, M. A. 2003a."Multivalued General Equilibrium Problems." *Journal of Math. Anal. Applications 283,* 140-149.

Noor, M. A. 2003b."Theory of General Variational Inequalities." Preprint, Etisalat College of Engineering, Sharjah, UAE.

Noor, M. A., and W. Oettli. 1994. "On General Nonlinear Complementarity Problems and Quasi-equilibria." *Le Matematiche 49,* 313-331.

Zhu. D. L. and P. Marcotte. 1996. "Cocoercivity and its Role in the Convergence of Iterative Schemes for Solving Variational inequalities." *SIAM Journal on Optimization 6,* 714-726.

AUTHOR BIOGRAPHY

MUHAMMAD ASLAM NOOR received his M. Sc from Panjab University (Pakistan, 1967), M. Sc from Queen's University (Canada, 1971) and Ph.D from Brunel University (London, U. K. 1975). He became professor in 1985. He has taught several courses including variational inequalities, numerical analysis, finite element analysis, optimization and operations research in Iran, Pakistan, Saudi Arabia, Canada and UAE. He has published more than 300 research papers in international journals. He is a member of editorial boards of several scientific journals including Journal of Mathematical Analysis and Applications

DETERMINATION OF RAIN TYPE FROM TRMM SATELLITE OBSERVATIONS

K. Mubarak and A. M. Dawood
Communication Engineering Department
Etisalat College of Engineering
P. O. Box 980
Sharjah
UAE
E-mail: kmubarak@ece.ac.ae and dawood@ece.ac.ae

KEYWORDS
Wavelet, Satellite, Radar, Precipitation.

ABSTRCT

The TRMM satellite is dedicated to observing and understanding the impact of tropical rainfall. Two of the important products of the TRMM mission are classification of precipitation into convective and stratiform type as well determination of the height of the bright band. Currently TRMM uses an algorithm to arrive at these products based on a characterization of horizontal and vertical variability of reflectivity. This paper presents result of a new algorithm developed using wavelets transform. The algorithms for wavelet analysis based products of both convective/stratiform classification as well as bright band detection are described. The results obtained from wavelet algorithms are compared against both the current products as well as ground radar inferences. The results show that the wavelet-based analysis provides fairly accurate results for both convective/stratiform classification as well as bright band determination.

INTRODUCTION

The Tropical Rainfall Measuring Mission (TRMM) is NASA's first mission dedicated to observing and understanding tropical rainfall and its effects on global climate. The Precipitation Radar in TRMM is the first spaceborne instrument designed to obtain three-dimensional maps of precipitation reflectivity. Such measurements yield information on the intensity and distribution of rain, rain type, storm depth, and height of bright band. Rain can be classified as convective and stratiform rain regions that can be described by different mean vertical motion distributions and growth mechanisms [1][2]. Large horizontal reflectivity gradients, strong vertical motions, and high rainfall rate often characterize convective precipitation. Smaller horizontal reflectivity gradients, weaker vertical motions, and lower rain rate characterize stratiform precipitation. The presence of bright band typically indicates stratiform region.

Convective and stratiform rain regions have different heating profiles [3]. Therefore it is useful to partition the rainfall estimated from satellite radar into convective or stratiform components. Ideally, vertical motion data could be used to differentiate between convective and stratiform rainfall, but since such data is not available from space borne radar, other methods must be used. Several methods have been developed for convective/stratiform separation that use the radar reflectivity structure of precipitation [4][5][6]. All these methods were developed studying different types of spatial ariability in reflectivity. The objective of this study is to develop an information theoretic scheme using wavelet transform to characterize the variability in the reflectivity structure to determine convective/stratiform separation.

TRMM RADAR RAIN TYPE ALGORITHM

TRMM Precipitation Radar (PR) uses two different methods for classifying rain type; one is the vertical profile method (V-method) and the other is the horizontal pattern method (H-method). Both methods classify rain into three categories namely stratiform, convective, and other. TRMM PR algorithms classify rain type using combination of both H, and V-method. Further information about TRMM PR rain type algorithm can be found in [6]. V-method first tries to detect the existence of bright band by peak search on a vertical profile of reflectivity (Z). The analysis uses spatial filter, which is based on the second derivative of Z with respect to the range from the satellite. The bright band is detected when the profile has a clear peak and occurs at height within 2.5*km* of the ambient freezing height. Also the height of bright band must appear within 0.65*km* tolerance in the vertical plane and the value of the reflectivity decreases appreciably above the height of bright band. When bright band is detected, precipitation is classified as stratiform. When bright band is not detected, and if the maximum value of Z at a given angle bin exceeds 39 *dBZ* then rain type is classified as convective. The "other" type is defined as neither stratiform nor convective.

The H-method examines the horizontal pattern of Z at a given height. If the maximum of Z along the range for each antenna scan angle below freezing height exceeds a convective threshold or stands out against the background area then the pixel is judged as a convective center. Rain type for a convective center and for the pixels nearest to the convective center is convective. If rain type is not convective then the rain type is stratiform. The "other" type is meant for cloud echoes and noise.

WAVELET TRANSFORM ANALYSIS

Wavelet transform is a localized transformation in both space and frequency. Wavelet is used for scale decomposition [7]. Large scales can detect gross variations, whereas small scales can detect small variations. Due to the nature of the wide variability of space-borne radar measurements over both time and space, wavelet transform is well suited for this analysis. Multiresolution analysis computes the approximation and the details of signal at various resolutions. The original radar profile Z[n] is passed through a high pass filter (HPF) g[n] and a low pass filter (LPF) h[n], to yield

$$Z_{high}[k] = \sum_n Z[n] \cdot g[2k-n] \quad (1)$$

$$Z_{low}[k] = \sum_n Z[n] \cdot h[2k-n] \quad (2)$$

Where The HPF and LPF are related by:

$$g[L-1-N] = (-1)^n \cdot h[n] \quad (3)$$

And the result from the low pass filter goes to another level of decomposition and is repeated for many levels.

ALGORITHM

Wavelet transform method uses two steps for classifying rain type; first detect the bright band then classify rain type based on the wavelet variance of the vertical profile. A bright band can be seen as a singularity in the vertical profile from an information theoretic viewpoint. Singularity detection is done by choosing a wavelet to be equal to the first derivative of a smoothing function [8]. However this problem is complicated by changing vertical resolution of PR data as it scans off nadir. This problem is resolved by using different wavelet transforms each tuned for detecting the irregular shape of bright band at nadir, as well as off-nadir. The bright band is detected when the combined analysis of the details of both wavelet transforms have a clear peak. Several thresholds as well as slope from the peak are used to ensure that the singularity in the signal is not caused by local peaks or discontinuity of the signal. When bright band is detected, precipitation is classified as stratiform.

Wavelet transform has the ability to quantify variations at several scales. The convective storms contain spatial frequency components at several scales [9]. Haar wavelet transform is used to obtain the high frequency components from the vertical profile at different levels. The convective threshold index (CTI) for each profile is calculated from the variance of the details at different levels, as

$$CTI = \sqrt{\sigma^2(D_2) + \sigma^2(D_3) + \sigma^2(D_4) + \sigma^2(D_5)} \quad (4)$$

Where $\sigma^2(D_i)$ is the variance of the detail signal of the wavelet transform at level i. If the convective threshold index exceeds a value determined empirically then the corresponding profile is judged to be convective. Otherwise the rain type is classified as stratiform. $\sigma^2(D_1)$ is not used in the computation to avoid counting the natural sample-to-sample variability.

DATA ANALYSIS

Five cases (Aug. 1, Aug 26, 2001, Jan. 17, 2000 and Mar. 29, Aug 21, 1999) are analyzed. Comparisons between the wavelet transform method (WTM) and that of TRMM PR (2A23) algorithm [6] is done for all cases. For three of these cases ground radar decision (Houston, Melbourne, and Kwajalein) are used for cross validation. Fig 1 (a) shows the vertical section of the rain reflectivity along the direction of TRMM PR movement. Fig 1 (b), (c) show the rain type decision and bright band detection for WTM and 2A23. The data in this case has a low-level bright band level that the 2A23 algorithm failed to detect. This data was provided by Dr. Jun Awaka to test the detection of low-level bright band using the wavelet transform method. The WTM detects the bright band at off nadir as well as near nadir ray for low-level bright band. The current 2A23 method may overestimate convective region since it may fail to detect some bright band cases. Fig 2 shows the classification decision of Houston ground radar using 2A54 algorithm along with WTM and 2A23 rain classification. It can be seen qualitatively from this figure that WTM agrees better with the ground radar. It should be note that 2A23 uses both horizontal and vertical method to classify the rain type where as the WTM uses only vertical method to do that. There are small differences in the classification of the rain type between WTM and the 2A54 product due to the differences in the horizontal resolution between the ground radar and spaceborne radar. 2A23 in this case relied totally on the horizontal method.

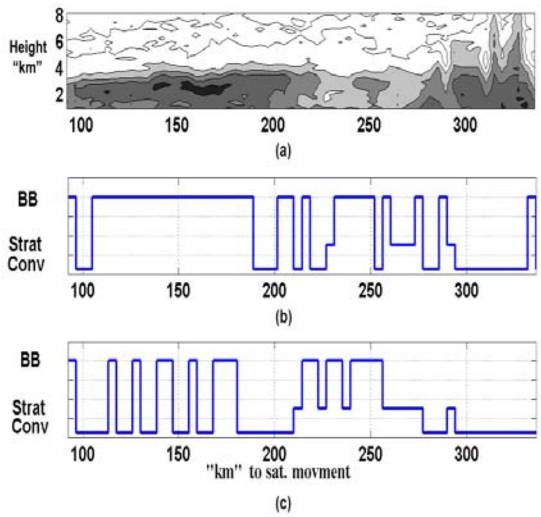

Figure 1: Case Study: August 26 2001 orbit 2880 (a) range profile; (b) WTM decision; (c) 2A23 decision.

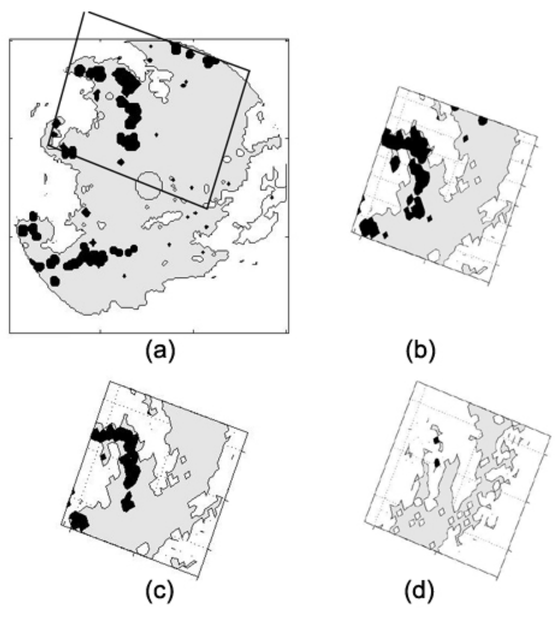

Figure 2: Case Study: March 29 1999 orbit 7679. (a) 2A54 decision map; (b) WTM decision map; (d) 2A23 decision map; (c) 2A23 (V-method) decision map; Black indicates convective region while gray indicates stratiform region.

These algorithms were evaluated on the five cases listed earlier through only two cases are presented. The results of the five case are summarized in Table 1 and 2. Table 1 shows the convective and stratiform rain type classification is in agreement between the WTM and the 2A23 algorithm, 81% of the time. The H-method used in 2A23 algorithm, which identified peaks and surrounding areas were labeled convective and all remaining points are labeled stratiform, is responsible for some of the differences in the comparisons with the WTM. Table 2 shows the bright band and no bright band flag decision of WTM and the 2A23 algorithms agree 77% of the time. 2A23 is the first generation of rain type algorithms and they have performed very well so far. The wavelet algorithms can be used in conjunction with current 2A23 algorithm to provide substantial improvements.

Table 1: Rain Classification Summary

Rain Type Method	Stratiform 2A23	Convective 2A23	Total
Stratiform WTM	68%	11%	79%
Convective WTM	8%	13%	21%
Total	76%	24%	100%

Table 2: Bright band summary

BB Method	BB 2A23	No BB 2A23	Total
BB WTM	41%	14%	55%
No BB WTM	8%	37%	45%
Total	49%	51%	100%

GLOBAL ANALYSIS

The procedure developed in this paper is extended to observations around the globe using TRMM data. In the monthly map plots, the data area is from 35N to 35S and from 180E to 180W. Hence, the plots are restricted to the latitudes of $\pm 35^o$ coinciding with converge of TRMM. The plot is of fairly high resolution since each pixel covers (0.5^o x 0.5^0) area. The resolution cells consist of 148 x 720 latitude-longitude elements. Fig. 3 (a) shows the monthly average of rain type estimated from TRMM for July, 2000 whereas Fig. 3 (b) shows the monthly average of rain type for July, 2000 by using the wavelet procedure. Table 3 shows the summary of global rain classification.

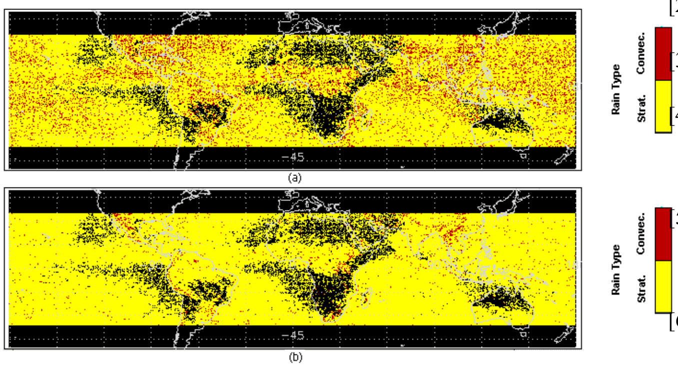

Figure 3: Monthly map of rain type for July 2000; (a) from TRMM; (b) from wavelet.

Table 3: Global Rain Classification Summary

Rain Type Method	**Stratiform 2A23**	**Convective 2A23**	**Total**
Stratiform WTM	86.34%	11.14%	97.48%
Convective WTM	1.13%	1.39%	2.52%
Total	87.47%	12.53%	100%

SUMMARY AND CONCLUSION

A precipitation type algorithm as well as bright band detection algorithm for TRMM PR using wavelet analysis is presented. The performance of wavelet transform to classify rain type is compared against the current algorithm used in TRMM spaceborne radar. Five cases are studied using data from the TRMM precipitation radar and three of those cases had coincident ground radar observations. The analysis comparing with ground radar inferences show that the WTM method provides an improvement over the current 2A23 for determining rain type. In addition the WTM algorithm showed excellent skill in detecting low-level bright band.

ACKNOWLEDGMENT

This research was supported by the NASA TRMM program. The authors acknowledge helpful discussion with Dr. V. Chandrasekar and Dr. Jun Awaka.

REFERENCES

[1] M. I. Biggerstaff, and R. A. Houze, Jr., "Midlevel vorticity structure of the 10-11 June 1985 squall line," Mon. Wea. Rev., 119, 3066-3079, 1991.

[2] H. G. Houghton, "On precipitation mechanisms and their artificial modification," J. Appl. Meteor., 7, 851-859, 1968.

[3] R. A. Houze, Jr., "Cloud clusters and large-scale vertical motions in the tropics." J. Meteor. Soc. Japan, 60, 396-409, 1982.

[4] M. Steiner, and R. A. Houze, Jr.,"Three-dimensional validation at TRMM ground truth sites: some earl results from Darwin, Australia. " Preprints, 26th Conference on Radar Meteorology, Norman, Oklahoma, 417-420, 1993.

[5] C. A. DeMott, R. Cifelli and S.A. Rutledge, "An improved method for partitioning radar data into convective and stratiform components. Preprints," 27th Conf. on Radar Meteorology, Vail, Colorado, Amer. Meteor. Soc. , 233-236, 1995.

[6] J. Awaka, T. Iguchi, and K. Okamoto, 1998 "Early results on rain type classification by the Tropical Rainfall Measuring Mission (TRMM) precipitation radar." Proc. 8th URSI Commission F Open Symp., Aveiro, Portugal, pp.143-146.

[7] I. Debouchi, "Ten Lectures on Wavelets", Capital City Press, 1992.

[8] S. Mallat, and W. L. Hwang, "Singularity detection and processing with wavelets," IEEE transactions on information theory, Vol.38, No.2, March 1992, 617-643.

[9] S. Al-Sowayan, and V. Chandrasekar, "Convective/stratiform classification from TRMM Precipitation Radar" Geoscience and Remote Sensing Symposium, IGARSS '01. IEEE 2001 International, Vol. 6, 2507 –2509.

NEURAL NETWORKS AND GENETIC ALGORITHMS

On the PID Control of a Temperature Regulation Process "Optimisation by Genetic Algorithms"

Houda Derbel[1,2]

[1]: Research Unit on Renewable energies and ELEctric Vehicles (RELEV)
Ecole Nationale d'Ingénieurs de Sfax, 3038, Sfax, Tunisie
[2]: Faculté des Sciences de Sfax, 3038, Sfax, Tunisie
Email. h.derbel@fss.rnu.tn

Abstract : *This work is aimed at looking into the control of a large scale nonlinear dynamical problem. The considered system is a blower controlled by a source of power placed at the input in front of a ventilator which is responsible of the propagation of the energy. Then, a PID regulator is optimised by genetic algorithms in order to obtain good performances.The obtained parameters are updated by a proposed procedure which gives best results. The implemented control system is then tested following a perturbation on the ambient temperature.*

Keywords : *Blower, PID Regulator, Genetic Algorithms, Parameter Optimisation.*

1. Introduction

Control of large scale systems is complex. In fact, the choice of the control is not evident. Moreover, the determining of the parameters of the chosen controller is very difficult.

A typical case of complex problems studied in this paper concerns the temperature regulation systems.

The aim of this paper is the determination of optimal parameters of a PID controller for a blower thermal system. The optimisation of such problem cannot be formulated as classical problems. In fact, the criterion is an implicit function of the optimisation variables. In order to overcome this comlexity, the use of genetic algoritms becomes very interesting.

This paper is organized as follows. Next section constitutes a brief description of genetic algorithms. In section three, the temperature regulation problem of the blower is formulated by a mathematical model. The unknown features are expressed by empirical formulmations. Section four presents the simulation results. A discussion on the optimisation procedure is briefly described; and an optimisation approach is then proposed in order to improve the optimal solutions given by genetic algorithms. At this level, the criterion is modified in order to get aperiodic dynamical behaviour of the closed loop blower system. The sensitivity with respect to environmental perturbations of the implemented PID control is tested.

2. A Brief Description of Genetic algorithms

Genetic algorithms are exploratory search and optimisation procedures. They derived from the principles of natural evolution and genetic population [2]. The basic concepts of genetic algorithms were developed by Holland [6], and subsequently in several research studies. Goldberg [5] provides recent comprehensive overviews and introductions to genetic algorithms. Genetic algorithms are iterative procedures in which a constant size of solution candidate population is maintained. The structure in the current population are evaluated, and on the basis of that evolution a new population of candidate solution is formed. In genetic algorithms, the solution structures are determined by genes presented in code terms. They are consisted on a number of chromosomes, for which, each one represents an individual. Genetic algorithms ensure the gradual increasing the fitness, through checking new solutions which are generated from old populations. Firstly, stochastic search processes play an important role in genetic algorithms (not deterministic processes as in many other optimisation methods). Secondly, genetic algorithms consider many points in a search space simultaneously, but only one point is considered in many other methods. Therefore, genetic algorithms have a low chance to converge to a local optimal solution (as in the case of classical methods). Thirdly, genetic algorithms do not require the structures, parameters or other information about the problem. Finally genetic algorithms work with a chromosome space which represents the search space. In the case of the basic genetic algorithms, solutions are represented as binary strings. There are three most commonly used operators: reproduction, crossover, and mutation.

3. Problem Formulation

Let's consider a fluid flow (air flow) in a blower whose axis is parallel to (ox).

Are considerd the following assumptions [1, 8, 9]:

1. In all points, the air speed direction is parallel to the (ox) axis. The magnitude of the mean speed v is practically constant. It is controlled by a ventilator placed in the input of the blower. Such ventilator ventilates an electrical resistance ensuring the propagation of the energy to the output of the blower. Let's consider $Q(t)$ the power consumed by the resistance. $Q(t)$ is the control input of the blower. The object of the process consists to regulate the temperature at the output of the blower.

2. The pressure gradient is so smaller in a such away that it can be considered that the energy exchange is done at a constant pressure.

3. The air temperature which depends on the three cartesian components will be considered as a function on x and t: $T = T(x, t)$.

4. Only conductive energy exchanges through the blower wall will be formulated. The axial conduction will be neglected [10].

The considered blower is a cylindrical volume whose axis is parallel to the (ox) direction. In order to develop a model of the blower describing the variations of temperatures inside the blower, we will quantify the space (only with respect to x-coordinates) in N cylindrical sections whose thikness is equal to Δx. Thus, we can write the following equations:

$$\begin{aligned} \rho_1 C_{p1} \Delta x \frac{dT_1}{dt} &= v(\rho_0 C_{p0} T_a - \rho_1 C_{p1} T_1) + Q \\ &\quad - \frac{2}{R} \times \frac{(T_1 - Ta)\Delta x}{\frac{1}{h_{f1}} + \frac{1}{h_a} + \frac{e}{\lambda_{p1}}} \end{aligned}$$

and for $i = 2$ to N:

$$\begin{aligned} \rho_i C_{pi} \Delta x \frac{dT_i}{dt} &= v(\rho_{i-1} C_{p,i-1} T_{i-1} - \rho_i C_{pi} T_i) \\ &\quad - \frac{2}{R} \times \frac{(T_i - Ta)\Delta x}{\frac{1}{h_{fi}} + \frac{1}{h_a} + \frac{e}{\lambda_{pi}}} \end{aligned}$$

with $T_0 = T_a$.

Because quantities ρ, C_p, h_f, λ_p and λ_f depend on the temperature, we notified: $\rho_i = \rho(T_i)$, $C_{pi} = C_p(T_i)$, $h_{fi} = h(T_i)$, $h_a = h(T_a)$, $\lambda_{pi} = \lambda_p([T_i + T_a]/2)$.

Identification procedures of parameters h_f, h_a, λ_p, λ_f, ρ and C_p give the following approximations [3, 4]:

$$\begin{aligned} C_p(T)\rho(T) &\approx 210496\ T^{-0.9097} \\ h(v,T) &\approx 143.9577\ v^{0.8}\ T^{-0.5855} \\ \lambda_p(T) &\approx 1.575 \times 10^{-3}\ T^{1.2076} \\ \lambda_f(T) &\approx 0.2673 \times 10^{-3}\ T^{0.8051} \end{aligned}$$

The following are the blower parameters: $R = 0.125m$: the radius of the base of the blower, $L = 1.2m$ its length; $e = 2cm$ the thikness of lateral sides, $v = 3m/s$ the air speed inside the blower, $v_a = 0.1m/s$ the air speed outside the blower, $N = 100$ sections, $T_a = 27°C$ the ambient temperature.

4. Simulation results

Let us consider $T = T_N$ the output temperature of the blower. In order to determine optimal values of PID parameters, we will consider the following criterion:

$$IAE \quad = \quad 10^{-3} \times \int_0^\infty |T - T_d| dt$$

where T_d is the desired temperature, and the IAE criterion correspond to the Integral of Absolute value of the Error.

The control output of the PID regulator is then expressed by:

$$u = Q = K_p(T_d - T) - K_d \frac{dT}{dt} + K_i \int_0^t (T_d - T) d\tau$$

for which parameters K_p, K_d and K_i will be determined by genetic algorithms.

The optimisation will be done in two steps. The first step uses genetic algorithms in order to localise optimal values of the PID regulator parameters. A second optimisation phase will be done by the use of an unidirectional optimisation procedure. This is done successively by:

1. the optimisation with respect to K_p and keeping K_d and K_i constants,

2. the optimisation with respect to K_i and keeping K_p and K_d constants,

3. the optimisation with respect to K_d and keeping K_p and K_i constants.

This procedure will be repeated until the convergence to the minimum is reached.

Proposed algorithm

The algorithm is then described as follows:

Note K_{po}, K_{io}, K_{do} the PID parameters giving the value of the criterion $IAE = J_o$ resulting from the genetic algorithm procedure.

1. Optimisation with respect to K_p for fixed values of K_d and K_i
   (a) Let: $K_{p1} = K_{po} - \Delta K_p$, $K_{p2} = K_{po} + \Delta K_p$, $K_i = K_{io}$ and $K_d = K_{do}$.
   (b) Evaluate the criteria:
      i. J_1 for K_{p1}, K_i and K_d
      ii. J_2 for K_{p2}, K_i and K_d
      iii. J_a for $K_{pa} = K_{p1} + \frac{1}{3}(K_{p2} - K_{p1})$, K_i and K_d
      iv. J_b for $K_{pb} = K_{p2} - \frac{1}{3}(K_{p2} - K_{p1})$, K_i and K_d
   (c) Compute $J_m = \min\{J_1, J_a, J_b, J_2\}$
   (d) If the minimum is J_1, let $K_{p2} = K_{pa}$ and $J_2 = J_a$
   (e) If the minimum is J_a, let $K_{p2} = K_{pb}$ and $J_2 = J_b$
   (f) If the minimum is J_b, let $K_{p1} = K_{pa}$ and $J_1 = J_a$
   (g) If the minimum is J_2, let $K_{p1} = K_{pb}$ and $J_1 = J_b$
   (h) Check if: $|K_{p2} - K_{p1}| < \varepsilon$ (the desired precision), if not, return to the step of the computation of the criteria J_a and J_b,
2. Let $K_{po} = \dfrac{K_{p1} + K_{p2}}{2}$
3. Optimisation with respect to K_i for fixed values of K_p and K_d
   (a) Let: $K_{i1} = K_{io} - \Delta K_i$, $K_{i2} = K_{io} + \Delta K_i$, $K_p = K_{po}$ and $K_d = K_{do}$.
   (b) Evaluate the criteria:
      i. J_1 for K_{i1}, K_p and K_d
      ii. J_2 for K_{i2}, K_p and K_d
      iii. J_a for $K_{ia} = K_{i1} + \frac{1}{3}(K_{i2} - K_{i1})$, K_p and K_d
      iv. J_b for $K_{ib} = K_{i2} - \frac{1}{3}(K_{i2} - K_{i1})$, K_p and K_d
   (c) Compute $J_m = \min\{J_1, J_a, J_b, J_2\}$
   (d) If the minimum is J_1, let $K_{i2} = K_{ia}$ and $J_2 = J_a$
   (e) If the minimum is J_a, let $K_{i2} = K_{ib}$ and $J_2 = J_b$
   (f) If the minimum is J_b, let $K_{i1} = K_{ia}$ and $J_1 = J_a$
   (g) If the minimum is J_2, let $K_{i1} = K_{ib}$ and $J_1 = J_b$
   (h) Check if: $|K_{i2} - K_{i1}| < \varepsilon$, if not, return to the step of the computation of the criteria J_a and J_b,
4. Let $K_{io} = \dfrac{K_{i1} + K_{i2}}{2}$
5. Optimisation with respect to K_d for fixed values of K_p and K_i
   (a) Let: $K_{d1} = K_{do} - \Delta K_d$, $K_{d2} = K_{do} + \Delta K_d$, $K_p = K_{po}$ and $K_i = K_{io}$.
   (b) Evaluate the criteria:
      i. J_1 for K_{d1}, K_p and K_i
      ii. J_2 for K_{d2}, K_p and K_i
      iii. J_a for $K_{da} = K_{d1} + \frac{1}{3}(K_{d2} - K_{d1})$, K_p and K_i
      iv. J_b for $K_{db} = K_{d2} - \frac{1}{3}(K_{d2} - K_{d1})$, K_p and K_i
   (c) Compute $J_m = \min\{J_1, J_a, J_b, J_2\}$
   (d) If the minimum is J_1, let $K_{d2} = K_{da}$ and $J_2 = J_a$
   (e) If the minimum is J_a, let $K_{d2} = K_{db}$ and $J_2 = J_b$
   (f) If the minimum is J_b, let $K_{d1} = K_{da}$ and $J_1 = J_a$
   (g) If the minimum is J_2, let $K_{d1} = K_{db}$ and $J_1 = J_b$
   (h) Check if: $|K_{d2} - K_{d1}| < \varepsilon$, if not, return to the step of the computation of the criteria J_a and J_b,
6. Let $K_{do} = \dfrac{K_{d1} + K_{d2}}{2}$
7. Stop test: if $|J_m - J_o| < \varepsilon$, otherwise, let $J_o = J_m$, and repeat all the iterative process. ■

It is to be noted that the above iterative procedure reduces the interval of the solution by 1/3 or 2/3. It is also well known that we can use other iterative procedure, particularly, the Fibonacci procedure [7].

In order to obtain aperiodic dynamics, we modify the optimised criterion in the above algorithm, as follows:

$$J = \left| \begin{array}{ll} IAE & \text{if } \max(T) \preceq T_d \\ IAE + 100[\max(T) - T_d] & \text{if } \max(T) > T_d \end{array} \right.$$

The obtained results are presented in figures 1, 2, 3 and 4. Figure 1 represents the response of the system (the temperature in the output of the blower). In this case, the PID regulator parameters are optimised by genetic algorithms. It is obvious that the output temperature presents an overshoot (2.5 %), and the output reach the desired temperature. The value of the criterion is $IAE = 3.82$, and the settling time is equal to 12.3 seconds (the required time for which the absolute value of the error, between the desired and the actual temperatures, becomes less than 5%).

Figure 2 presents the obtained results after an updated optimisation phase of the parameters of the PID regulator. It is clear that the criterion IAE is reduced: $IAE = 2.96$. In this case, the settling time is equal to 7.7 seconds. The overshoot is equal to 4.1 %.

Figure 3 presents the evolution of the output temperature and the input control power for the modified criterion. It is obvious that the response do not present any overshoot. Thus, the response is aperiodic. However, the value of the criterion is then increased: $IAE = 4.13$. The settling time is also increased. It becomes equal to 16.8 seconds. The increases of the settling time results from the fact that the proportional gain of the regulator is decreased in order to eliminate the overshoot.

Figure 4 presents the evolution of the output temperature and the control power of the blower after perturbating the ambient temperature. In fact, we suppose that the blower is placed in a room for which the ambient temperature is regulated by a heating system, giving a constant temperature of the ambient equal to $27°C$. However, the temperature outside of the room is equal to $0°C$. At time $t = 40s$, all doors separating the outside and the inside of the room are opened. Consequently, the ambient temperature decreases suddenly to $0°C$. At time $t = 70s$, these doors are closed, and we suppose that the ambient temperature increases suddenly to $27°C$. Figure 3 illustrates the good perfoprmances obtained by the optimised PID regulator. In these conditions, the variations on the ambient temperature of 27° leads to an increse or a decrease on the power control (about 500 Watt, i.e. 18 Watt/1°), and a perturbation around 60° on the output temperature (about 2° variations on the output for 1° variations on the ambient temperature). The increase or the decrease of the power control is maintained while the perturbation is applied to the system. However, the output variations around the desired temperature are compensated by the control power. The required time, for compensating these perturbations, is less than 10 seconds.

5. Conclusion

This work was aimed at the determination of optimal parameters of a PID regulator of a blower. Mathematical model describing the dynamical behaviour of the system was presented. Being nonlinear and with large scale dimension, the determination of adequate regulator turned to be difficult. Then, a PID regulator was optimised by genetic algorithms, which localised the optimum solution. After that, an updated procedure of optimisation is done by a proposed algorithm based on an unidirectional research of the optimum. Simulation results show the good obtained performances, particularly in the case of variations on the ambient temperature which is considered as a perturbation for the dynamical behaviour of the blower system.

References

[1] Baglia B. R. and Potankar S. V.: *"A new finite element formulation for convection diffusion problems"*. Numerical Heat Transfer, vol. 3, pp. 393-409, 1980.

[2] Darwin C.: *"on the origin of species John Murray"*. London, 1859.

[3] Derbel H.: *"On the Modeling and the Identification of a Blower"*. In French (Sur la modélisation et l'identification paramétrique d'une Soufflerie). Submitted.

[4] Derbel H.: *"PID-Control of a Blower, Optimisation by Genetic Algorithms"*. In French. (Commande d'une Soufflerie par PID Optimisé par Algorithmes Génétiques). Submitted.

[5] Goldberg D.: *"Genetic Algorithms in Search, Optimisation, and Machine Learning"*. Addison-Wesley, Reading, Mass", 1989.

[6] Holland J. H.: *"adaptation in natural and artificial systems"*. University of Michigan Press, Ann Arbor, 1975.

[7] Minoux M.: *"Programmation Mathématique, Théorie et Algorithmes"*. Tome 1, Dunod, 1983.

[8] Sacadura J. F.: *"Initiation aux transferts thermiques"*. Edition Technique et Documentation. Centre d'Actualisation Scientifique et Technique, I.N.S.A., Lyon, 1980.

[9] Sheen H. J., Chen W. J. and Wu J. S.: *"Flow patterns for an annular flow over an axisymmetric sudden expansion"*. Journal Fluids Mechanics, vol. 350, pp. 177-188, 1997.

[10] Taine J. et Petit J. P.: *"Transferts thermiques"*. Dunod, Paris 1995.

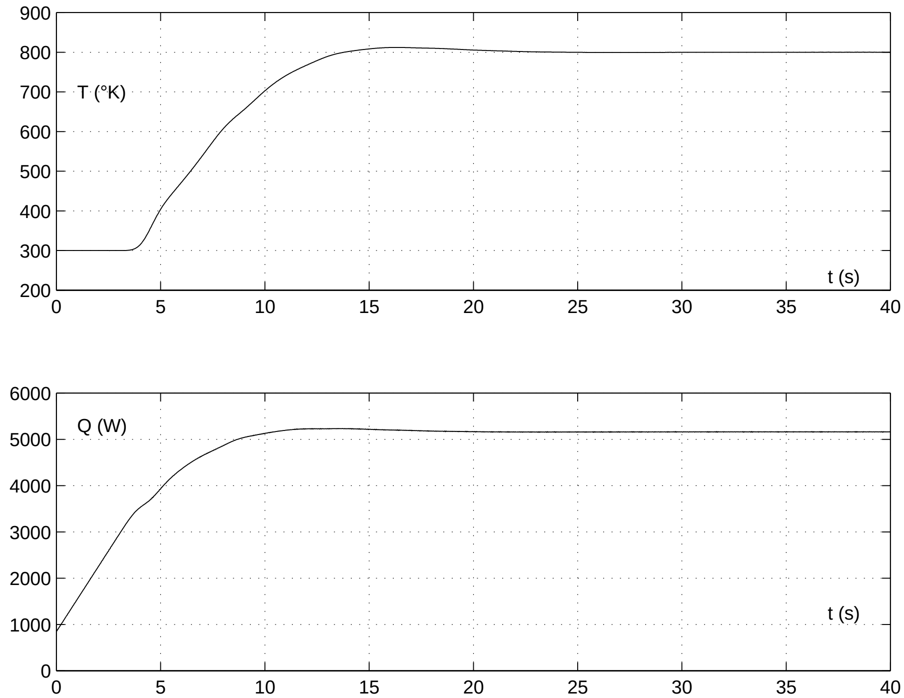

Figure 1: Variations of the output temperature T and of the input control power Q. The parameters of the PID regulator are determined by genetic algorithms.

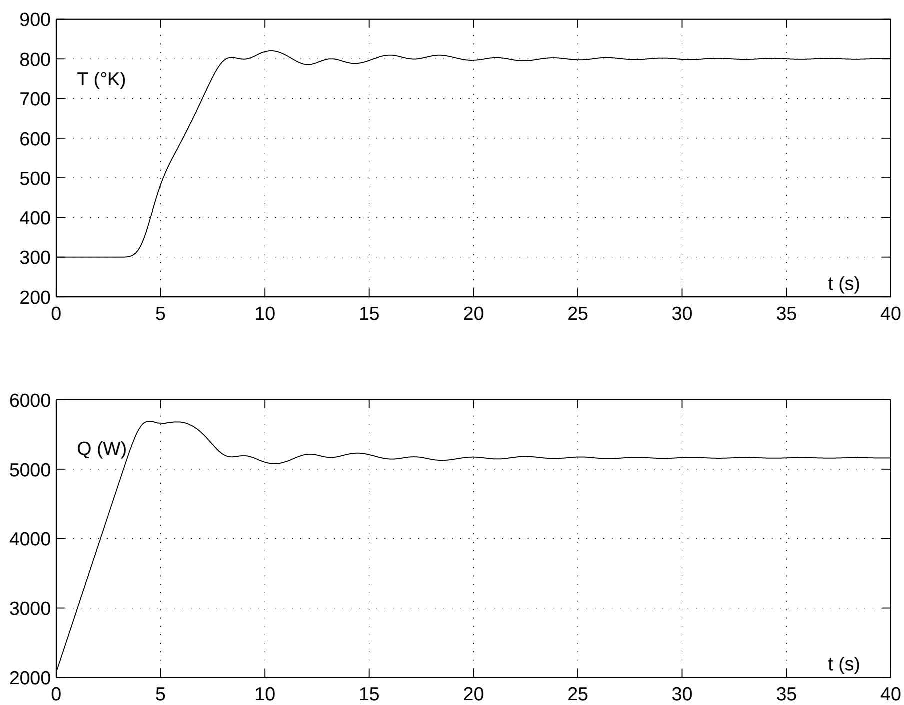

Figure 2: Variations of the output temperature T and of the input control power Q. The parameters of the PID regulator are determined by genetic algorithms, and improved by the iterative optimisation procedure.

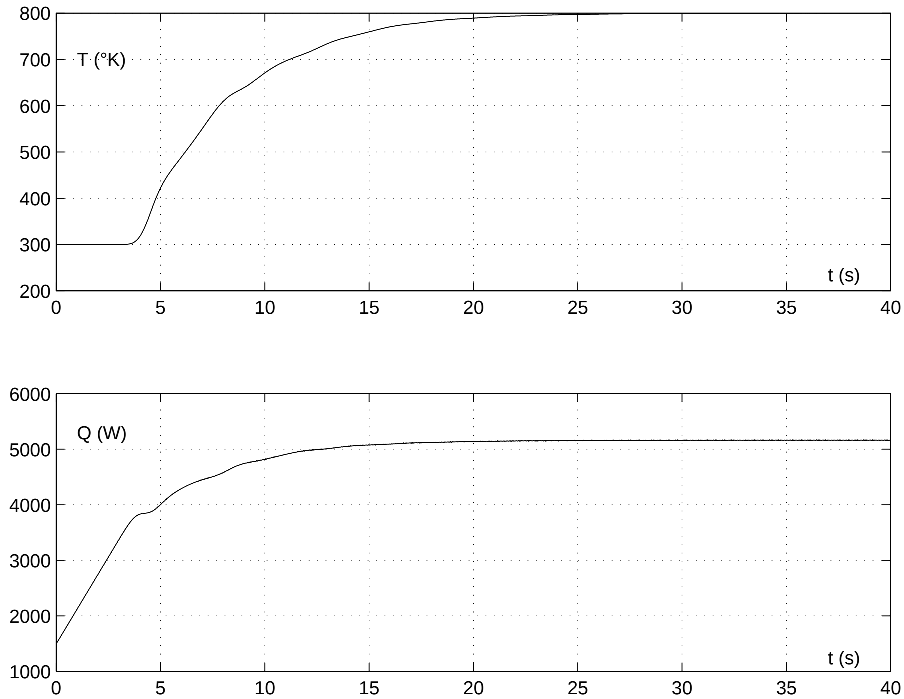

Figure 3: Variations of the output temperature T and of the input control power Q. The parameters of the PID regulator are determined by genetic algorithms, and improved by the iterative optimisation procedure, for the modified criterion (without overshoot).

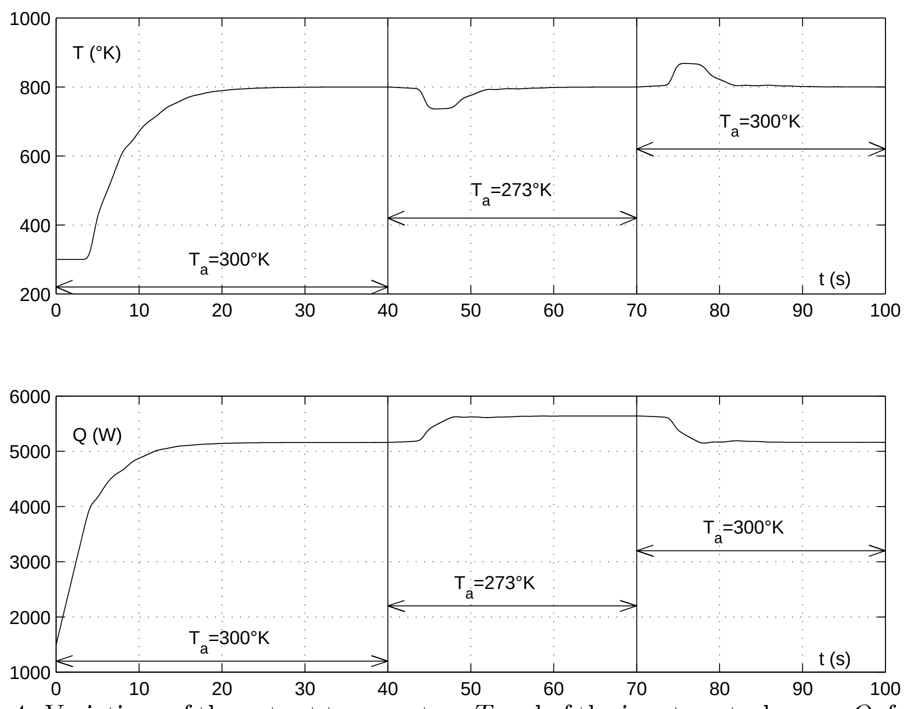

Figure 4: Variations of the output temperature T and of the input control power Q, following perturbations on the ambient temperature T_a. The parameters of the PID regulator are determined by genetic algorithms, and improved by the iterative optimisation procedure, for the modified criterion (without overshoot).

AN ADAPTIVE OUTPUT TRACKING OF LINEARIZABLE NONLINEAR SYSTEMS USING NEURAL NETWORKS

Hassen Mekki
Mohamed Chtourou
Nabil Derbel
Research Unit on Intelligent Control, design and Optimisation of complex System (ICOS)
National School of Engineers of Sfax.:B.P.W 3038, Sfax-Tunisia,
mekkihassen@yahoo.fr ; mohamed.chtourou@enis.rnu.tn ; nabil.derbel@ieee.org

ABSTRACT

This paper proposes an adaptive state feedback controller which achieves asymptotic tracking of a smooth trajectory generated by an auxiliary system for single-input single-output feedback linearizable nonlinear systems. Based on the Lyapunov stability theory, an adaptation law is developed to tune the weights of a radial basis function (RBF) neural network in order to track a predetermined linearizing controller. To show the efficiency of the proposed scheme, numerical simulations are presented.

KEYWORDS: Nonlinear systems, adaptive control, neural network, output tracking, Lyapunov stability.

1. Introduction

Neural network adaptive controllers have been widely used in many practical control problems due to their powerful modelling capability and adaptability. Two types of adaptive control are generally investigated. The first one consists to the indirect adaptive control. The model of the system is first obtained and learned by using the neural network and feedback control law is then designed based on the neural network model (Chen 1990), (Jeon and Lee 1996), Wang and Bao 2000). The second type considers the direct adaptive control. The neural network is directly used as a controller in the feedback control system, i.e., the outputs of the neural network are the control inputs of the system (Chand et al. 2002).
In this paper, we proposed a method which concerns the fully-state linearizable or minimum phase nonlinear systems (Sastry and Isodori 1989). The idea consists in designing a linear feedback controller constructed by a neural network. The weights of the neural network are updated such that the proposed control can track a predetermined input-output linearizing controller. Eventually, using the Lyapunov approach, it can be proved that the desired trajectory is asymptotically tracked by the output signal.
This paper is outlined as follows. In section 2, a brief preliminary on input-output linearizing control for trajectory tracking is given. In section 3, the proposed adaptation law and controller construction is then presented. Finally, in section 4 an illustrative example is considered.

2. Linearizing control

Let's consider a nonlinear continuous-time dynamic system described by:

$$\begin{cases} \dot{x} = f(x) + g(x).u \\ y = h(x) \end{cases} \tag{1}$$

where $x \in \Re^n$: is the state vector, $u \in \Re$ is the control signal and $y \in \Re$ is the output of the system. Moreover let's assume that system (1) has relative degree $\rho \le n$.
Let's define a nonlinear transformation $z = \phi(x)$, where:

$$\phi_1 = h(x),$$
$$\phi_{i+1} = L_f^i h(x),$$

for $i = 1, \dots \rho - 1$, and $\phi_j(x)$, $j = \rho + 1, \dots, n$ are input free functions chosen in such a way that $\phi(x)$ is a diffeomorphism (Isodori 1995). Let's $z = (\xi^T, \eta^T)^T$ with $\xi \in \Re^\rho$. Then using z as the new state variable, system (1) becomes:

$$\begin{aligned} &\dot{\xi}_i = \xi_{i+1}, \quad i = 1, \dots, \rho - 1 \\ &\dot{\xi}_\rho = F(\zeta, \eta) + G(\xi, \eta).u \\ &\dot{\eta} = \psi(\xi, \eta) \\ &y = \xi_1 \end{aligned} \tag{2}$$

where:

$$F(\xi, \eta) = L_f^\rho h(\phi^{-1}(z))$$

$$G(\xi, \eta) = L_g L_f^{\rho-1} h(\phi^{-1}(z)) .$$

We want to design a feedback control that forces the output y to track a smooth (infinitely differentiable) reference trajectory y_r. To accomplish this aim, we define a tracking error $e = Y_r - \xi$ where $Y_r = [y_r, \dot{y}_r, \dots, y_r^{(\rho-1)}]^T$ and we choose an input-output linearizing controller:

$$u = u_0 = \frac{1}{G(\xi,\eta)}(-F(\xi,\eta) + y_r^{(\rho)} + K^T e) \tag{3}$$

where $K = [k_1, \ldots, k_\rho]$ should be a Hurwitz vector, that is all the roots of the polynomial:

$$p(s) = s^\rho + k_\rho s^{\rho-1} + \ldots + k_2 s + k_1 \tag{4}$$

have negative real parts. Then the error is stable at the origin, *i.e.*

$$\lim_{t\to+\infty} e(t) = 0 \Leftrightarrow \lim_{t\to+\infty} \xi(t) = Y_r, \tag{5}$$

and particularly:

$$\lim_{t\to+\infty} y(t) = y_r. \tag{6}$$

Then the closed loop system can be written as

$$\dot{e} = A_c e \tag{7}$$

$$\dot{\eta} = \psi(Y_r - e, \eta) \tag{8}$$

where :

$$A_c = \begin{bmatrix} 0 & 1 & 0 & \ldots & 0 \\ 0 & 0 & 1 & \ldots & 0 \\ \vdots & \vdots & \ddots & \ddots & \vdots \\ \vdots & \vdots & \vdots & \ddots & 1 \\ -k_1 & -k_2 & -k_3 & \cdots & -k_p \end{bmatrix} \tag{9}$$

We notice that if the nonlinear system (1) is full-state linearizable (*i.e.*, $\rho = n$), then it is equivalent to (7) whereas (8) does not exist and thus the output tracking is achieved exponentially. On the other hand, if $\rho < n$, the output tracking is achieved if the system is minimum phase that is $\dot{\eta} = \psi(0,\eta)$ which is asymptotically stable and Y_r is bounded (Sastry and Isodori 1989).

3. The proposed adaptive controller

One of the main drawbacks of the linearizing state feedback law is the difficulty to construct the nonlinear part, in addition to a necessary exact knowledge of the system model (i.e. $F(\xi,\eta)$ and $G(\xi,\eta)$). To solve this problem, we suggest to construct a neural network adaptive controller.
In the RBF neural network model, the output u, is given by the following equation:

$$u(e,W,\phi) = \sum_{i=1}^{N} w_i \phi_i \left[e, c_i, \sigma_i\right] \tag{10}$$

where N is the number of RBFs used, and $\phi_i(e, c_i, \sigma_i)$ are the RBFs expressed as:

$$\phi_i(e, c_i, \sigma_i) = \exp\left(-\frac{\|e - c_i\|^2}{2\sigma_i^2}\right) \tag{11}$$

$c_i \in \Re^\rho, \sigma_i \in \Re^\rho$, are the center value vector and the width value vector of the RBF. These vectors are defined as:

$$c_i = \begin{bmatrix} c_{i1} & c_{i2} & \ldots & c_{i\rho} \end{bmatrix}^T \in \Re^\rho, i = 1, \ldots, N$$

$$\sigma_i = \begin{bmatrix} \sigma_{i1} & \sigma_{i2} & \ldots & \sigma_{i\rho} \end{bmatrix}^T \in \Re^\rho, i = 1, \ldots, N$$

Figure 1 shows the structure of the RBF neural network.

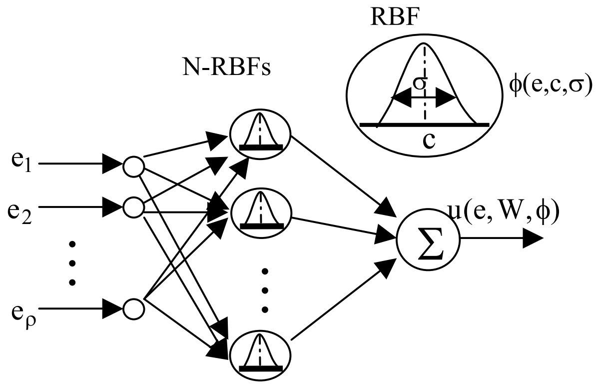

Figure 1 Structure of the RBF Neural Network

Using RBF networks, one typically places the center of the basis functions on regular points of say, a square mesh covering a relevant region of the state space. Denoted by a compact set $\chi_n \subset \Re^n$. This region therefore is the network approximation region, which in general is known for a given system as presented in figure 2.

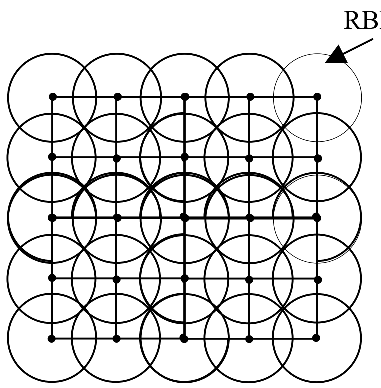

Figure 2: The Network Approximation Region of Two Parameters

Let's the neural network adaptive controller given by :

$$u_1(t) = W^T(t)\phi(e) \tag{12}$$

where $W(t)$ will be adjusted adaptively such that

$$u_1^*(t) = W^{*T}\phi(e) = u_0 \tag{13}$$

W^* denotes the optimal weights.

Substituting u_1, in (2) yields to:

$$\begin{aligned}\dot{\xi}_\rho &= F(\xi,\eta) + G(\xi,\eta)u_1 \\ &= F(\xi,\eta) + G(\xi,\eta)u_0 - G(\xi,\eta)u_0 + G(\xi,\eta)u_1 \\ &= y_r^{(\rho)} + K^T e - G(\xi,\eta)(u_0 - u_1)\end{aligned}$$

$$y_r^{(\rho)} - \dot{\xi}_\rho = -K^T e + G(\xi,\eta)(u_0 - u_1) \tag{14}$$

If we define $B_c = [0,\ldots,0,G(\xi,\eta)]$ then we can write

$$\dot{e} = A_c e + B_c(u_0 - u_1)$$
$$\dot{e} = A_c e + B_c(u_1^* - u_1)$$
$$\dot{e} = A_c e + B_c(W^* - W)^T \phi(e)$$
$$\dot{e} = A_c e + O(W^* - W) \tag{15}$$

Therefore the output tracking problem is reduced to the problem of stabilizing system (13).

Theorem:

Consider the class of nonlinear dynamical systems described by (2). Assume that the state vector z *is measurable and* y_r *is a smooth reference trajectory to be tracked.*

Let $W(t)$ *be the solution of*

$$\dot{W} = -\delta\varphi(e)B_c^T Pe \tag{16}$$

where $\delta > 0$ *is a positive constant. And let P>0 and Q>0 be two positive definite matrices satisfying the following Lyapunov equation*

$$A_c^T P + PA_c = -Q \tag{17}$$

then the controller law defined by (18) leads to asymptotic tracking.

$$u_1 = W^T(t)\phi(e) \tag{18}$$

Proof :

It is shown that the dynamics of the tracking error are described by (4). Let $V(e,W)$ be a Lyapunov function candidate:

$$V(e,W) = e^T Pe + \frac{1}{\delta}(W^* - W)^T(W^* - W) \tag{19}$$

The time derivative of $V(e,W)$ along the trajectories of (7) is given by:

$$\dot{V}(e,W) = e^T(A_c^T P + PA_c)e + 2(W^* - W)\phi B_c^T Pe$$
$$+ (W^* - W)(\phi B_c^T Pe + \frac{1}{\delta}\dot{W})$$

If we choose:

$$\dot{W} = -\delta\phi B_c^T Pe \tag{20}$$

then:

$$\dot{V}(e,W) = -e^T Qe < 0 \tag{21}$$

4. Simulation results

4.1 Example 1

This example illustrates a one-link rigid robotic manipulator. The dynamic equation of the one-link rigid robotic manipulator is given by (Isodori 1995):

$$ml^2\ddot{q} + d\dot{q} + m\lg\cos q = u \tag{22}$$

where the link is of length l and masse m, and q is the angular position with initial value $q(0) = 0.1$ and $\dot{q}(0) = 0$.

The parameters *m, l, d,* and *g* are (in p.u.):

m=1, l=1, d=1, and g=1

The above dynamical equation can be written as the following state equation:

$$\begin{cases}\dot{x}_1 = x_2 \\ \dot{x}_2 = x_2 - \cos(x_1) + u\end{cases} \tag{23}$$

We choose $K = [1 \quad 2]$ so:

$$A_c = \begin{bmatrix} 0 & 1 \\ -1 & -2 \end{bmatrix},\ P = \begin{bmatrix} 4.5 & 1.5 \\ 1.5 & 1.5 \end{bmatrix},\ Q = \begin{bmatrix} 3 & 0 \\ 0 & 3 \end{bmatrix}$$

satisfy the Lyapunov equation of Theorem 1. We have $B_c = [0 \quad 1]$, then the control law expressed by:

$$u(t) = W^T(t)\phi(e), \tag{24}$$

with the following adaptation equation of W:

$$\dot{W} = -\delta(\phi(e)B_c^T Pe) \tag{25}$$

stabilize the nonlinear system (21).

The number of the hidden units is chosen as *N=9* and $\delta = 10$.

To track y_r (a square signal [-0.5; 0.5]), obviously Y_r is bounded and (23) is minimum phase. Figure 3 shows the simulation results of the process using the proposed algorithm. Fig. 3a and fig. 3b show the output response of the system and the corresponding control based on the neural adaptive state feedback controller. It is obvious that satisfactory output tracking performances have been achieved through the proposed control scheme.

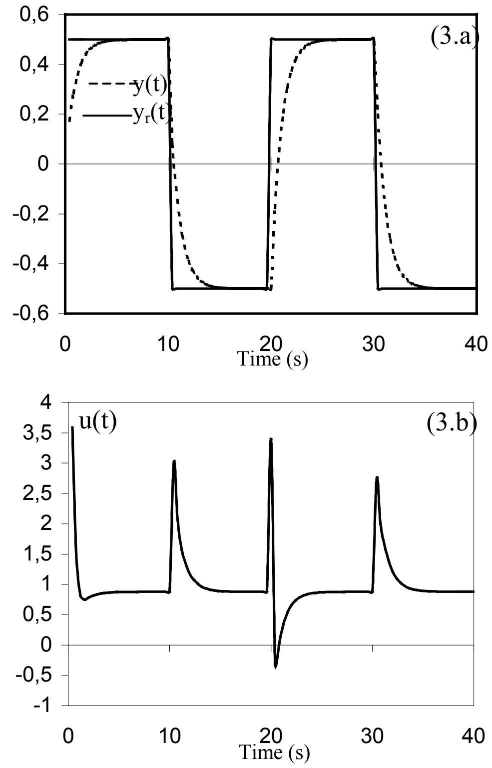

Figure 3: Simulation Results of the Process using the Proposed Algorithm

4.2 Example 2 :

Let's consider the following nonlinear system (Isodori 1995):

$$\begin{cases} \dot{x}_1 = -x_1 + e^{x_2} u \\ \dot{x}_2 = x_1 + x_1 x_2 + u \\ \dot{x}_3 = x_2 \end{cases} \tag{26}$$

and let $y = h(x) = x_3$. It can be easily checked that the system has the relative degree $\rho = 2$ and that the transformation:

$$z_1 = h(x) = x_3$$
$$z_2 = L_f h(x) = x_2$$
$$z_3 = 1 + x_1 - e^{x_2}$$

is a diffeomorphism. The system in the z-space is described as

$$\begin{cases} \dot{z}_1 = z_2 \\ \dot{z}_2 = (-1 + z_3 + e^{z_2})(1 - z_2) + u \\ \dot{z}_3 = (1 - z_3 - e^{z_2})(1 + z_2 e^{z_2}) \end{cases} \tag{27}$$

We choose $K = [1 \quad 2]$, so:

$$A_c = \begin{bmatrix} 0 & 1 \\ -1 & -2 \end{bmatrix}, \; P = \begin{bmatrix} 4.5 & 1.5 \\ 1.5 & 1.5 \end{bmatrix}, \; Q = \begin{bmatrix} 3 & 0 \\ 0 & 3 \end{bmatrix}$$

satisfy the Lyapunov equation of Theorem 1. We have $B_c = [0 \quad 1]$ then the control law expressed by:

$$u(t) = W^T(t)\phi(e),$$

(28)

with the following adaptation equation of W:

$$\dot{W} = -\delta(\phi(e) B_c^T P e)$$

(29)

stabilize the nonlinear system (24). The above system was simulated with the initial conditions

$\delta = 10$; $z_1 = z_2 = z_3 = 0$;

The number of the hidden units is chosen as *N=9*.

To track y_r (a square signal [-0.5; 0.5]), obviously Y_r is bounded and (27) is minimum phase. Figure 4 shows the simulation results of the process using the proposed algorithm. Fig. 4a and fig. 4b show the output response of the system and the corresponding control based on the neural adaptive state feedback controller. It is obvious that satisfactory output tracking performances have been achieved through the proposed control scheme.

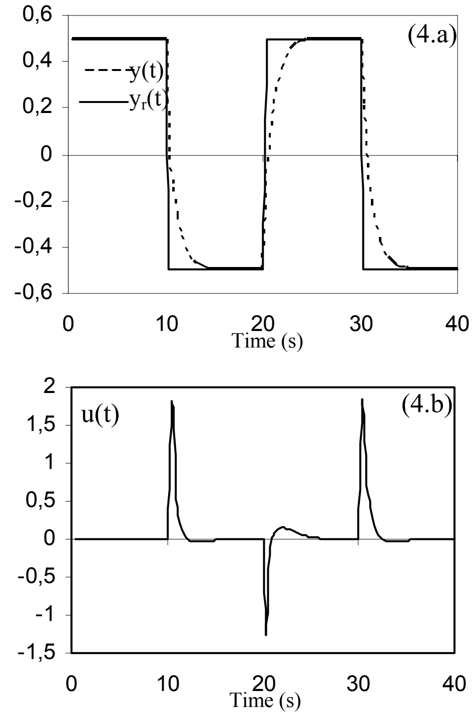

Figure 4 : Simulation Results of the Process using the Proposed Algorithm

5. Conclusion

In this paper, we proposed an adaptive state feedback controller which achieves asymptotic tracking of a smooth trajectory generated by an auxiliary system for single-input single-output feedback linearizable nonlinear systems. Based on the Lyapunov stability theory, an adaptation law is then determined to tune the weights of a radial basis function (RBF) neural network in order to track a predetermined linearizing controller. To demonstrate the efficiency of the proposed scheme, numerical simulation examples are presented.

REFERNCES

Alberto Isodori. 1995. "Nonlinear Control Systems". *Springer Verlag, United Kingdom*, 3rd edition.

D.H. Wang, P. Bao. 2000. "Enhancing the estimation of plant Jacobian for adaptive neural inverse control." *Neurocomputing* 34 , 99-115.

F.C. Chen. 1990."Backpropagation neural networks for nonlinear self-tuning adaptive control.", *IEEE Control System Mag.* 44-48.

G.J. Jeon, I. Lee. 1996. "Neural network indirect adaptive control with fast learning algorithm." *Neurocomputing* 13, 185-199.

S. S. Sastry and A. Isodori. 1989. "Adaptive control of linearizable systems." *IEEE Trans. On Automatic Control*, 34, No.11, 1123-1131.

W. D. Chand et al. 2002, "Stable direct adaptive neural controller of nonlinear systems based on single auto-tuning neuron*."* *Neurocomputing* 48, 541-554.

LATE PAPERS

ADAPTIVE VOLTERRA/HYBRID EQUALIZATION OF NONLINEAR ISI IN A MAGNETO-OPTIC DATA STORAGE CHANNEL

Sunil Gupta
Department of Electrical and Computer Engineering
The University of Texas at Austin
Austin, Texas - 78712
U.S.A.
E-mail: sunil.gupta@mail.utexas.edu or sunil.k.gupta@intel.com

KEYWORDS
ISI (Inter-Symbol Interference), Nonlinear Equalization, Volterra, Optical Data Storage, SNR, eigenvalue, convergence ratio.

ABSTRACT

This paper presents performance analysis of an adaptive Volterra/Hybrid equalizer in a nonlinear magneto-optic data storage channel. In a data storage system, nonlinear intersymbol interference (ISI) is one of the limiting factors for high storage density. Volterra and Hybrid (combination of linear and Volterra) equalizers are proposed and developed for compensation of nonlinear ISI. The use of Volterra/Hybrid equalizers provided an extra 1.3-1.5 dB SNR gain over linear equalizers. Performance and complexity of these equalizers are compared. Convergence issues are also investigated by examining the eigenvalue spread of the covariance matrix. The techniques proposed here can be applied to other communication systems (e.g. wireless, optical) exhibiting nonlinear ISI characteristics.

1. INTRODUCTION

In data storage system the bit sequence is encoded and then marks (symbols) of variable length are generated which are then recorded on the storage medium.

Magneto-Optic data storage is a rewritable storage technology that uses a combination of magnetic and optical methods. Data is written on an M-O disk by both a laser and a magnet. The laser heats the mark to a certain temperature (Curie temperature) at which point the molecules are realigned when subjected to a magnetic field. A magnet then changes the mark's polarity. Reading is accomplished by shining a low power polarized laser beam whose plane of polarization changes depending upon the direction of magnetization.

ISI is defined as the mark (symbol) size deviation between the final readback mark and the original one. This deviation is a function of the mark size itself and its neighboring marks. The readback marks were obtained by recording and reading various data patterns on a magneto-optic drive.

To correct ISI, equalizer is used. Traditionally linear equalizers are used. An adaptive equalizer is used to compensate for channel variations by dynamically adjusting the weights. Linear equalizers were proposed in [6] and RAM (random access memory) based lookup table approach for equalization of nonlinear storage channel was examined in [7]. DFE (decision feedback equalizer) and ADFE (adaptive decision feedback equalizer) are variations of linear equalizer which are implemented using feedforward and feedback linear filters. In the feedback filter decoded symbols are used in the equalization process. In the present work Volterra series which generate nonlinear terms are investigated for compensating the ISI. Modification of Volterra in the form Hybrid equalizer is explored and its performance compared.

The remainder of the paper is organized as follows. Section 2 describes the Volterra equalizer and its mathematical formulations. Section 3 presents the Hybrid equalizer which is a combination of traditional linear and Volterra equalizer. Section 4 covers the convergence analysis of the equalizers. Section 5 develops the SNR expression which is then used as a quantitative figure of merit for performance comparison and finally Section 6 summarizes the main conclusions of this work and its application to other systems.

2. VOLTERRA EQUALIZER

Volterra series has been successfully used in modeling non-linear systems such as Satellite Communication, Machine tools, etc.

Volterra equalizer utilizes an (N-1)-stage tap delay line, just as a linear equalizer. The difference is that Volterra nonlinearly combines received marks which are then used in the equalization process. Volterra series is represented by the following expression.

$$Z_n = \sum_{n1} w_{n1} Y_{n-n1} + \sum_{n1}\sum_{n2}\sum_{n3} w_{n1} w_{n2} w_{n3} Y_{n-n1} Y_{n-n2} Y_{n-n3} \tag{1}$$
$$+ \sum_{n1}\sum_{n2}\sum_{n3}\sum_{n4}\sum_{n5} w_{n1} \cdots Y_{n-n1} Y_{n-n2} \cdots$$

where Z_n = Output symbols, Y_n = Input symbols and w_n = weights of the equalizer.

The number of terms L is related to the order and number of taps N of the filter as –

$$L = \sum_{i=1}^{(order+1)/2} N^{2i-1} \tag{2}$$

The schematic diagram of a 3-tap 3rd order Volterra equalizer is shown in Fig. 1. It is a modification of a 3-tap linear equalizer. There is another intermediate stage where all the nonlinear terms of the Volterra series are terms generated.

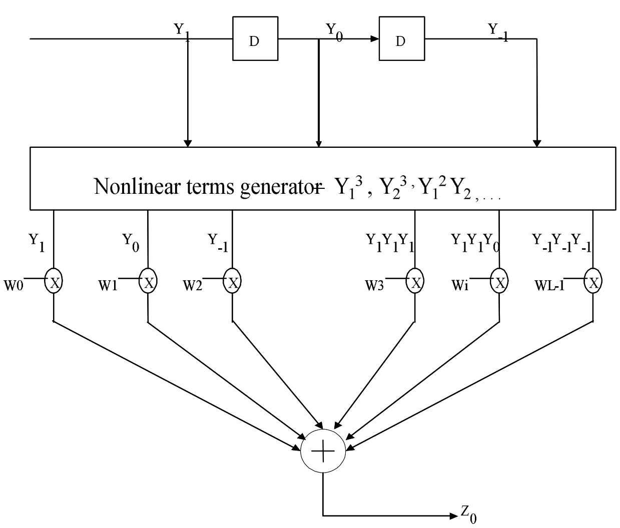

Fig. 1. Schematic diagram of 3-tap 3rd order Volterra Equalizer.

One of the drawbacks of Volterra equalizer is that the number of nonlinear terms generated tends to explode as one goes to higher orders of the series.

Table 1 lists the number of terms generated in the series corresponding to number of taps and the Volterra order used.

Table 1. # of taps, Volterra order and # of terms

# of taps & Volterra order	# of terms
3-tap 3rd order	30
5-tap 3rd order	130
7-tap 3rd order	350
3-tap 5th order	273
3-tap 7th order	2460
5-tap 5th order	3255

3. HYBRID EQUALIZER

To overcome the issue of large number of terms, Hybrid equalizers are proposed which is a combination of linear and short-tap small-order Volterra filter in the middle of the tap delay line. It is based on the assumption that most of the nonlinearity is because of the most adjacent marks to the mark under consideration. Hybrid equalizer considered consisted of a 3-tap 3rd order Volterra filter in the middle and a large N-tap (N=7, 9, 11) linear filter. The short Volterra in the middle compensates for most of the nonlinear ISI. A further reduction in the number of nonlinear terms can be obtained by discarding the terms with very small relative weights.

In the next following sections performance of this hybrid configuration is evaluated and compared with linear and pure Volterra equalizers.

4. CONVERGENCE ANALYSIS

Since the nonlinear combining occurs before the tap weights of the equalizer, the outputs of the nonlinear term generator may be considered as inputs to a linear filter. The weight determination is performed using the traditional LMS (Least Mean Square) algorithm as shown below.

$$W(k+1) = W(k) + \mu e(k) U \tag{3}$$

where W=weight vector, U=output vector of nonlinear terms generator (from Fig. 1), e=error, k=k-th update time and μ =step size.

The output of the equalizer is given by –

$$Z = W^T U \tag{4}$$

where Z=output of the equalizer.

To determine the convergence properties, the eigenvalues of the covariance matrix were examined. The eigenvalue spread is defined as –

$\rho = \frac{\lambda_{max}}{\lambda_{min}}$, where λ_{max} and λ_{min} are the largest and smallest eigenvalues of the covariance matrix ($RW_{opt} = P$ where R=covariance matrix, W_{opt} =optimum weights and P=cross-covariance matrix).

The convergence ration ω is given as -

$$\omega = \frac{(\rho - 1)^2}{(\rho + 1)^2} \quad (5)$$

Intuitively, eigenvalue spread is important as it gives a quantitative measure of degree of correlation of data. Larger the spread, slower the convergence of the algorithm.

Table 2 shows the eigenvalue spread and convergence ratios for various equalizer configurations. From the table one can see that the convergence ratio increases going from linear equalizer to the Volterra equalizer. The convergence ratio of the hybrid equalizer lies in between the linear and pure Volterra equalizer.

Table 2. Equalizer Configuration and Values of Eigenvalue Spread & Convergence Ratio

Equalizer Configuration	Eigenvalue spread	Convergence ratio
5-tap Linear EQ	22.36	0.836
3-tap 3rd order Volterra EQ	29.43	0.873
5-tap 3rd order Volterra EQ	33.45	0.887
7-tap 3rd order Volterra EQ	34.24	0.89
5-tap linear, 3-tap 3rd order Volterra EQ (Hybrid)	31.23	0.879

To improve the convergence one can use multi-step size in the LMS or use Kalman algorithm.

5. SNR COMPUTATION & PERFORMANCE COMPARISON

To quantitatively compare the performance of various configurations of the equalizers, SNR (signal-to-noise) measure was developed. The SNR of the readback marks from the magneto-optic drive is defined as -

$$SNR = 10\log_{10}\left(\frac{W_{unit}^2}{\sigma^2}\right) \quad (6)$$

where W_{unit} is the width of the minimum mark size recorded and

$\sigma^2 = \frac{1}{N}\sum_{i=1}^{N} d_i^2,\ d_i = W_i - \widehat{W_i}$, where W_i & $\widehat{W_i}$ are the original and readback mark sizes.

The above expression shows that for a given spot size (minimum mark size), closer the readback marks are to the original; higher is the SNR since the variance σ^2 decreases. Fig. 2 shows the SNR as a function of the minimum mark width of the raw marks, marks obtained with a linear 3-tap equalizer and marks obtained using a 3-tap 3rd order Volterra equalizer. From the graph it is very clear that the nonlinear equalization using Volterra yields an additional performance gain of about 1.3-1.5 dB over a linear equalizer and about 3 dB gain over un-equalized readback marks.

The SNR increases as the minimum mark width is increased because the relative amount of ISI decreases.

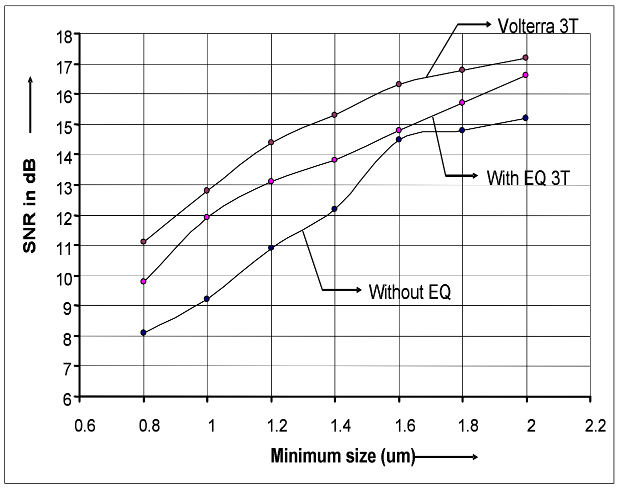

Fig. 2. SNR with and without Volterra Equalization.

Fig. 3 shows the SNR comparison of N-tap linear, N-tap 3rd order Volterra and Hybrid (N-tap linear + 3-tap 3rd order Volterra) equalization versus the # of taps. Using hybrid equalization one can obtain very good performance in signal quality at a modest increase in computational resources. Using pure Volterra does not payoff much as it reaches a point of extreme diminishing return very quickly, in this case after 5 taps. The gain in SNR going from linear to hybrid equalization is about 1.3 dB at 5-taps and beyond.

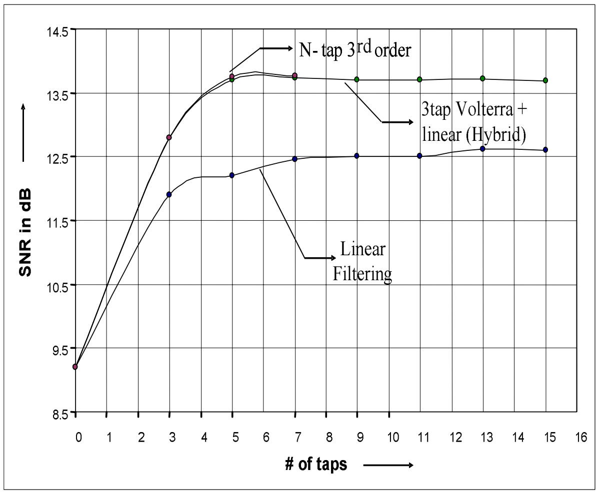

Fig. 3. SNR with Linear, pure Volterra and Hybrid Equalization.

6. CONCLUSION

The Volterra/Hybrid equalizers provided an extra 1.3-1.5 dB SNR gain over linear equalizers. Furthermore, it was observed that going to higher order Volterra equalizers (e.g. 5-tap 5^{th} order or order) does not yield any extra benefit as one reaches a point of diminishing return immediately after 3-tap 3^{rd} order.

Convergence issues related to equalizers were investigated. It was found that the eigenvalue spread of the covariance matrix was large for the Volterra equalizers compared to linear equalizers which resulted in somewhat slower convergence. This can be mitigated by employing a multiple step LMS algorithm.

The Hybrid equalizers provided the best trade-off between computational complexity and performance.

The extra gain in signal quality obtained can be utilized in various ways such as – achieving higher storage density, less expensive read/write optical assembly, lower BER and less stringent FEC (forward error correction) in the overall system design. The Volterra/Hybrid equalizer proposed and developed here can be applied to other communication systems (e.g. wireless, optical) exhibiting nonlinear ISI channel characteristics.

11. REFERENCES

[1] E. D. Daniel and C. D. Mee, *Magnetic Recording Handbook*, McGraw-Hill, 1990.
[2] J. G. Proakis, *Digital Communications*, McGraw-Hill, 1989.
[3] M. Schetzen, *The Volterra and Wiener Theories of Nonlinear Systems*, New York, Wiley, 1980.
[4] Volterra V., *Theory of functions and of integral and integro-differential equations*, Dover Publications, New York, 1959.
[5] Nakamichi U.S.A. Corp., *Optical Memory System*, Nakamichi U.S.A. Corp.
[6] R. W. Lucky, Automatic equalization for digital communications, *BSTJ* 44, April 1965, pp. 547-588.
[7] J. Cioffi, K. Fisher and C. M. Melas, An adaptive dfe for storage channels suffering from nonlinear isi, *IEEE*, 1989.

7. BIOGRAPHY

Sunil Gupta was born in New Delhi, India. He received his B.Tech. (Bachelor of Technology) degree in Electrical Engineering from the Indian Institute of Technology, New Delhi, India in 1989, his M.S. (Master of Science) degree in Electrical and Computer Engineering from The University of Arizona, Tucson, U.S.A. in 1992. He is pursuing his Ph.D. studies in Electrical and Computer Engr. at The University of Texas at Austin, U.S.A. He has worked for the Electrical Engr. Department, I.B.M., Lattice Semiconductor Corp. and Intel Corp.

DIGITAL IMAGE WATERMARKING USING WALSH-CODED HAND-WRIITEN SIGNATURES

Amani Bin Sewaif, Hussain Al-Ahmed and Mohammed Al-Mualla
Multimedia Communication and Signal Processing (MCSP) Research Group,
Etisalat College of Engineering,
P.O.Box: 980, Sharjah, United Arab Emirates
Tel: +971 6 5611333, Fax: +971 6 5611789
e-mail: {alahmad, almualla}@ece.ac.ae

KEYWORDS

Image processing, watermarking, Walsh functions

ABSTRACT

This paper deals with the design and anyalsis of new digital image watermarking techniques using Walsh functions. Different algorithms were implemented in the spatial and frequency domains to Walsh-encode and embed hand-written signatures in digital still images. The effect of watermarking on the quality of the images was studied using single signatures. The effect of changing the length of Walsh functions was also investigated. Test results indicate that the use of Walsh functions results in improved robustness against JPEG attacks. Increasing the length of the Walsh function results in more robustness. This is, however, at the expense of more degradation to the quality of the watermarked image.

INTRODUCTION

In recent years there has been a significant increase in the distribution of images in digital format. The ease in which such images can be copied and modified has created a pressing need for the development of *copyright protection* methods. A promising technique in this direction is *digital image watermarking*.

In digital image watermarking, copyright protection information are embedded in the image in the form of a *watermark*. The image must not be visibly degraded by the presence of this watermark. Another main requirement of watermarking for copyright protection applications is *robustness*. Thus, the watermark must be resistant to unauthorised detection and decoding. In addition, the watermark must be tolerant to normal image processing techniques (e.g. compression), as well as to intentional attacks (attempts to remove the watermark).

There are many digital image watermarking techniques reported in the literature, see (Katzenbeisser and Petitcolas 2000; Cox et al. 2001). They can be classified according to a number of different criteria. One such criterion is the domain in which the watermark is embedded. In this context, there are two main categories: spatial domain techniques, e.g. (Lin 2000; Nikolaidis and Pitas 1998), and frequency-domain techniques, e.g. (Barni et al. 1998; Cheng and Huang 2001).

Another classification of digital image watermarking techniques is based on whether the original image is needed in the watermark extraction process or not. If the original image is *not* needed to recover the watermark from the watermarked image, then the technique is called *complete* (also referred to as *blind* or *oblivious*), otherwise it is called *incomplete* (*non-blind* or *non-oblivious*).

This paper proposes the use of Walsh functions to improve the robustness of digital image watermarking techniques. In the proposed methods, Walsh functions are used to encode the watermark before embedding it in the original image. This approach is tested both in the spatial and in the frequency domains and is compared to the case of no coding. The effect of watermarking on the quality of the image is studied. The effect of changing the length of Walsh functions is also investigated.

It should be mentioned that a unique feature of the proposed techniques in this paper is the use of handwritten signatures as watermarks.

DIGITAL IMAGE WATERMARKING

This paper considers two simple *incomplete* digital image watermarking techniques, one works in the spatial domain and the other works in the frequency domain.

Let **c** be an $X \times Y$ 8-bit grayscale original image and let **s** be an $M \times N$ (where $M \le X$ and $N \le Y$) binary image of a single handwritten signature (watermark). The watermarked image **c'** is an $X \times Y$ 8-bit grayscale image that is produced using the following embedding equation:

$$c'(i,j) = \begin{cases} c(i,j) + s(i,j), & 1 \le i \le M \text{ and } 1 \le j \le N \\ c(i,j), & \text{otherwise} \end{cases} \quad (1)$$

At the decoder an attacked version **c*** of the watermarked image will be received. This can be used with the original image **c** to extract the watermark as follows:

$$s'(i,j) = c^*(i,j) - c(i,j), \quad 1 \le i \le M \text{ and } 1 \le j \le N \quad (2)$$

In the frequency domain technique, the Discrete Cosine Transform (DCT) is first applied to the original image **c** to obtain **C**. The watermark **s** is then embedded directly in the DCT domain as follows:

$$C'(i,j) = \begin{cases} C(i,j) + s(i,j), & 1 \le i \le M \text{ and } 1 \le j \le N \\ C(i,j), & \text{otherwise} \end{cases} \quad (3)$$

The watermarked image **c'** is then obtained by applying the inverse DCT (IDCT) to **C'**.

At the decoder, the DCT is applied to both the received watermarked image **c*** and the original image **c** to obtain **C*** and **C** respectively. The watermark is then extracted using:

$$s'(i,j) = C^*(i,j) - C(i,j), \quad 1 \le i \le M \text{ and } 1 \le j \le N \quad (4)$$

WATERMARKING USING WALSH CODED SIGNATURES

In order to increase the robustness of the above watermarking techniques, it is proposed that the watermark is first encoded using Walsh functions before embedding it into the original image.

Walsh functions consist of square pulses with two states either +1 or –1. Walsh sequences with length k, where $k=2^n$, enable k *orthogonal* codes to be obtained. There are several ways to produce Walsh sequences. The easiest way involves manipulations with Hadamard matrices as detailed in (Beauchamp 1984). As an example, Walsh functions with length k=4 are:

$$\begin{aligned} \mathbf{w}_1 &= [+1 \quad +1 \quad +1 \quad +1] \\ \mathbf{w}_2 &= [+1 \quad +1 \quad -1 \quad -1] \\ \mathbf{w}_3 &= [+1 \quad -1 \quad -1 \quad +1] \\ \mathbf{w}_4 &= [+1 \quad -1 \quad +1 \quad -1] \end{aligned} \quad (5)$$

In the proposed methods, one-dimensional (1-D) coding using Walsh sequences is utilized. Thus, given a vector $\mathbf{v}=[s(i, j), s(i, j+1), \ldots, s(i, j+k)]$ which consists of k horizontally adjacent pixels of the signature image **s**, 1-D Walsh encoding can be applied to this vector as follows:

$$\mathbf{v}' = \sum_{i=1}^{k} v(i) \cdot \mathbf{w}_i \quad (6)$$

Note that this is a form of multiplexing where the data is multiplied by the Walsh sequences and then added together to generate an amplitude modulated signal. Because of orthogonality, the original data can be demultiplexed simply by multiplying again by the same Walsh sequences:

$$\mathbf{v} = \sum_{i=1}^{k} v'(i) \cdot \mathbf{w}_i \quad (7)$$

Figure 1(a) shows the use of 1-D Walsh encoding in the spatial domain, whereas Figure 1(b) shows the frequency domain technique.

RESULTS AND DISCUSSION

A number of 512×512 8-bit grayscale images have been used to test the proposed algorithms. A 128×64 binary handwritten single signature has been used as a watermark. Unless otherwise stated, 1-D Walsh coding was performed using Walsh sequences with length k=8.

Figure 2 shows the signature before and after 1-D Walsh coding.

Figure 3(a) shows the original Lenna image, Figure 3(b) shows the spatial domain watermarked image, whereas Figure 3(c) shows the frequency domain watermarked image. It can be seen that both techniques produce invisible watermarks with imperceptible degradation to the original image.

Figure 4 investigates the performance of watermarking techniques under JPEG compression attacks. In this case, the quality q of JPEG compression was varied between 20 and 90 in steps of 10. The quality of the extracted signature was measured by calculating the Peak Signal to Noise Ratio (PSNR) between the original signature and the extracted signature. Figure 4(a) compares between 'Walsh coding' and 'No Walsh coding' for the spatial domain technique, whereas Figure 4(b) repeats the comparison for the frequency domain technique. It is immediately evident that, regardless of the JPEG compression quality and the embedding domain, the use of Walsh coding results in a significant improvement in robustness against JPEG compression.

Figure 5 illustrates the effect of JPEG compression with a quality factor q=60 on the quality of the extracted signature. Figure 5(a) shows the spatial domain extracted signature, whereas figure 5(b) shows the frequency domain extracted signature. It is immediately evident that frequency domain watermarking is more resistant to JPEG compression attacks.

Figure 6 investigates the effect of changing the length k of Walsh sequences on the quality of the extracted signature with spatial domain watermarking. This effect is investigated for different values of the JPEG compression quality q. Figure 7 repeats the same investigation but for frequency domain watermarking. It is clear from both figures that increasing the length k of Walsh sequences results in an improved robustness against JPEG compression. It must be noted, however, that this improvement in robustness is achieved at the expense of increasing the payload and consequently increasing the degradation to the quality of the watermarked image. Comparing Figures 6 and 7 also confirms the superior performance of frequency domain watermarking.

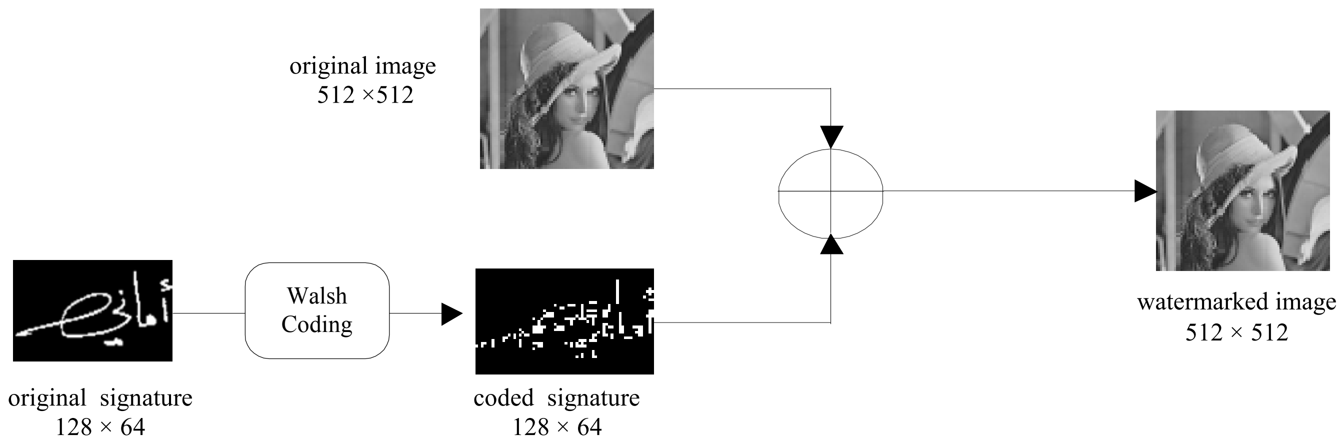

(a) spatial domain embedding

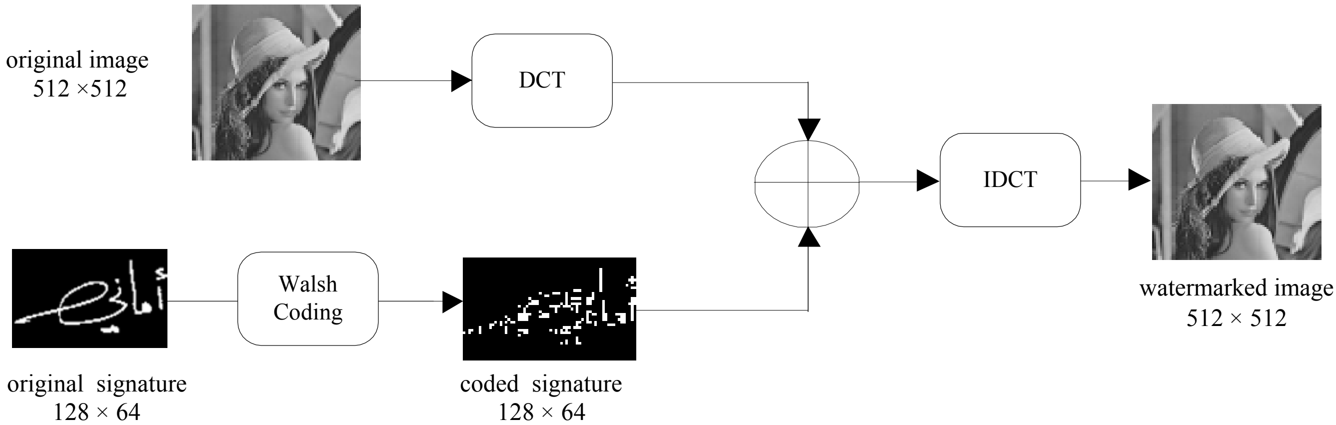

(b) frequency domain embedding

Figure 1: Digital Image Watermarking using 1-D Walsh Coded Signatures

(a) before coding

(b) after coding

Figure 2: 1-D Walsh Coding of 128×64 Handwritten Single Signature

(a) original Lenna

(b) spatial domain watermarked

(c) frequency domain watermarked

Figure 3: Original and Watermarked 512×512 Lenna Images

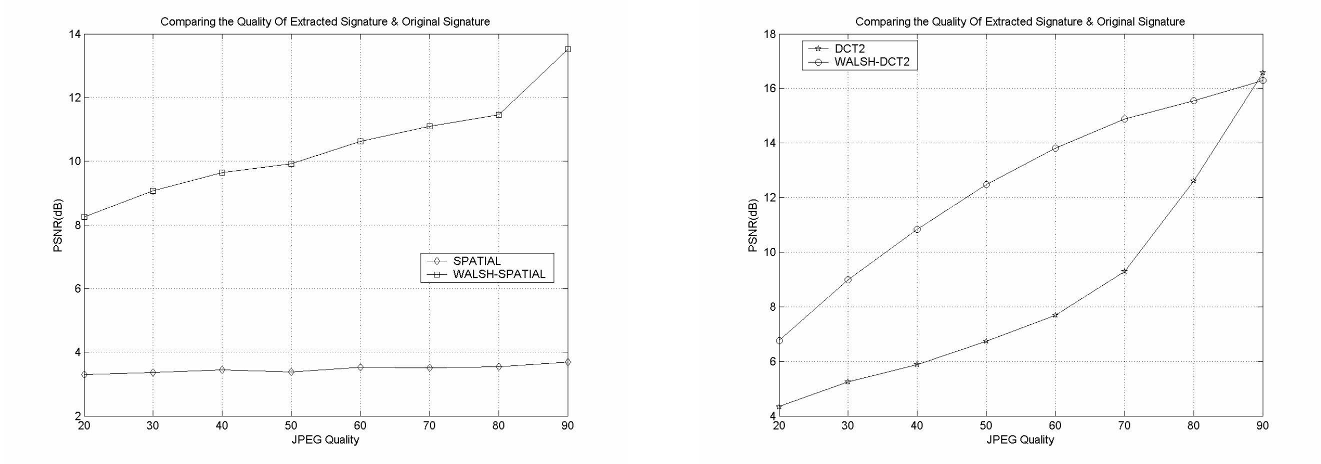

(a) spatial domain (b) frequency domain

Figure 4: Comparison between 'Walsh Coding' and 'No Walsh Coding' under JPEG Compression attacks

(a) spatial domain extracted signature, JPEG quality q=60 (b) frequency domain extracted signature, JPEG quality q=60

Figure 5: Comparison between Spatial and Frequency Domains Extracted Signatures under JPEG Compression

Spatial Domain Without Coding

Spatial Domain With Coding k=2

Spatial Domain With Coding k=4

Spatial Domain With Coding k=8

Spatial Domain With Coding k=16

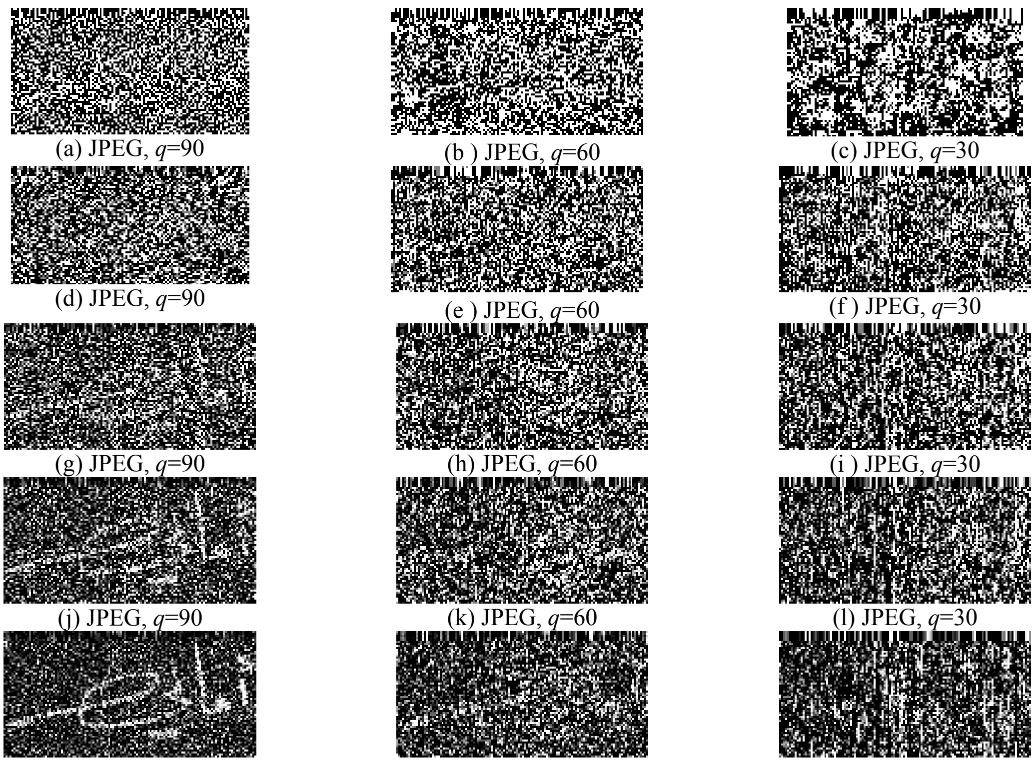

(a) JPEG, q=90 (b) JPEG, q=60 (c) JPEG, q=30

(d) JPEG, q=90 (e) JPEG, q=60 (f) JPEG, q=30

(g) JPEG, q=90 (h) JPEG, q=60 (i) JPEG, q=30

(j) JPEG, q=90 (k) JPEG, q=60 (l) JPEG, q=30

(m) JPEG, q=90 (n) JPEG, q=60 (o) JPEG, q=30

Figure 6 Effect of changing the length k of Walsh sequences on the performance of spatial domain watermarking

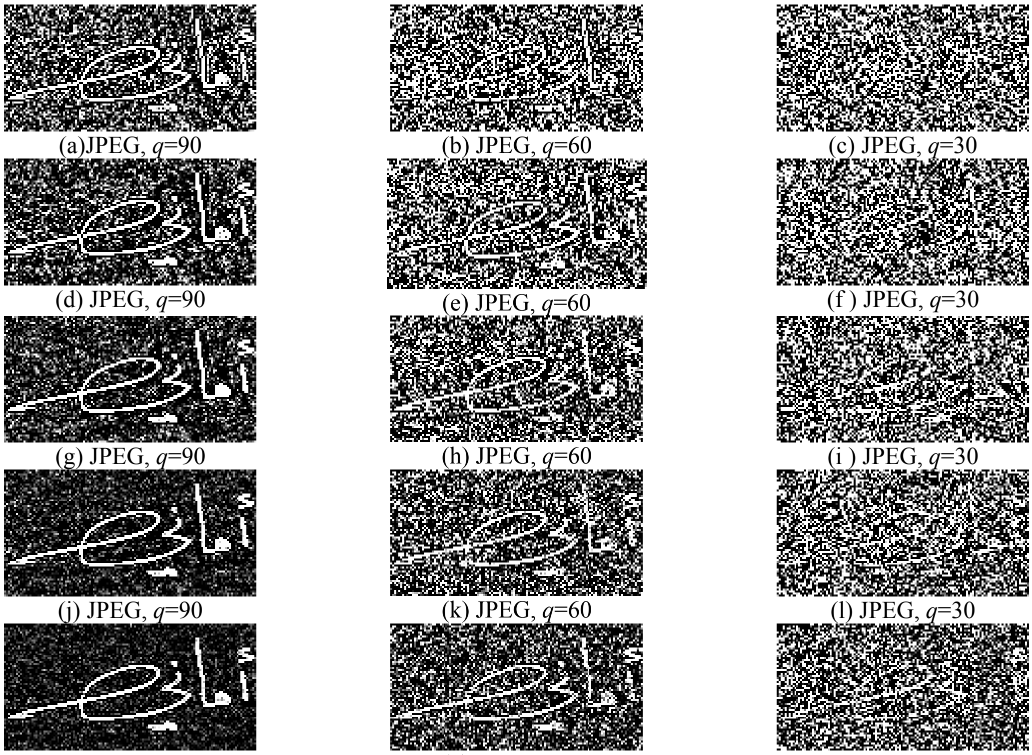

Frequency Domain Without Coding: (a)JPEG, q=90; (b) JPEG, q=60; (c) JPEG, q=30

Frequency Domain With Coding k=2: (d) JPEG, q=90; (e) JPEG, q=60; (f) JPEG, q=30

Frequency Domain With Coding k=4: (g) JPEG, q=90; (h) JPEG, q=60; (i) JPEG, q=30

Frequency Domain With Coding k=8: (j) JPEG, q=90; (k) JPEG, q=60; (l) JPEG, q=30

Frequency Domain With Coding k=16: (m) JPEG, q=90; (n) JPEG, q=60; (o) JPEG, q=30

Figure 7 Effect of changing the length *k* of Walsh sequences on the performance of frequency domain watermarking

CONCLUSIONS

In this paper two new digital image watermarking techniques were proposed, one works in the spatial domain and the other works in the frequency domain. The proposed techniques use Walsh functions to encode a handwritten signature (watermark) before embedding it in the original image. Simulation results showed that, regardless of the JPEG compression quality and the embedding domain, the use of Walsh coding results in a significant improvement in robustness against JPEG compression. It was also observed that frequency domain watermarking is more resistant to JPEG compression attacks than spatial domain watermarking. Simulation results also showed that increasing the length of Walsh sequences results in an improved robustness against JPEG compression. It must be noted, however, that this improvement in robustness is achieved at the expense of increasing the payload and consequently increasing the degradation to the quality of the watermarked image.

ACKNOWLEDGEMENTS

The authors would like to thank Emirates Telecommunication Corporation (ETISALAT) for sponsoring this project.

REFERENCES

Barni, M.; F. Bartolini; V. Cappellini; and A. Piva. 1998. “A DCT-Domain System for Robust Image Watermarking.” *Signal Processing*, vol.66, 357–372.

Beauchamp, K. 1984. *Applications of Walsh and related Functions with an Introduction to sequency Theory*. Academic Press. London.

Cheng, Q and T. Huang. 2001. “An Additive Approach to Transform-Domain Information Hiding and Optimum Detection Structure.” *IEEE Trans. Multimedia*, vol 3, no.3, 273-283.

Cox, I; M. Miller; and J. Bloom. 2001. *Digital Watermarking*. Morgan Kaufmann Publishers, San Francisco.

Katzenbeisser, S and F. Petitcolas. 2000. *Information Hiding techniques for steganography and digital watermarking*. Artech House, London.

Lin, P-L. 2000. “Robust Transparent Image Watermarking System with Spatial mechanisms.” *The Journal of Systems and Software*, vol.50, 107-116.

Nikolaidis, N and I. Pitas. 1998. “Robust Image Watermarking in the Spatial Domain.” *Signal processing*, 66(3), 385-403.

Antenna Sectorisation for Resolving Cell Breathing Problem in CDMA Networks

M. M. Al-Akaidi, H. Ali, O. Alani
School Engineering & Technology
Faculty of Computing Sciences and Engineering
De Montfort University, Leicester, LE1 9BH, UK.
Email: mma@dmu.ac.uk

Keywords:
Antenna, 3G, Mobile, wireless, WCDMA, UMTS.

ABSTRACT

In this paper one of the most interesting and also most confusing items in the 3rd Generation (3G) concept is going to be discussed; Cell breathing in a Universal Mobile Telecommunications System (UMTS) environment. A comparison of the system performance will be made using results obtained from the simulation of a 3 and 6 sectored antenna respectively. In Wideband Code Division Multiple Access (WCDMA) technology, all users share the same common physical resource, frequency band in 5 MHz slices. In Global System for Mobile communications (GSM) the capacity calculation is a relatively straight forward procedure, but in the case of WCDMA the radio interface is handled differently and the system capacity is limited by various factors. In the following report simulations are carried out to investigate the relationship in UMTS capacity and coverage. Since these two elements are inter-dependent and are functions of the radio environment, as the number of users increases, or as the data speed increases, the cell self-interference increases. This lowers the Signal to Noise Ratio (SNR) and thus shrinks the effective coverage of the base station. This may lead to "dead areas", where mobile users cannot access the network as a consequence of the shrinking of the cell. [3] Subscriber traffic is then redirected to a neighbouring cell that is less heavily loaded. This is called "load balancing".

Cells with varying coverage profiles considerably complicate network planning and management. In this paper the simulation results show the reduced impact of cell breathing with the use of micro cells and multi sectored antennas.

1. INTRODUCTION

Compared to GSM, the WCDMA technology for UMTS is considerably more complex. One of the fundamental characteristics of CDMA systems is that the coverage range is intrinsically linked to the capacity of the system. The more traffic being carried by the cell, the smaller the coverage area of the cell becomes. The GSM network capacity is limited by interference, especially from adjacent cells. In UMTS each transmitted signal increases the noise level (N_o) of the overall system. Since capacity is inversely related to the SNR, higher interference leads to higher noise and thus a reduction in the overall capacity.

Since the traffic is constantly changing, depending upon the behaviour of the subscribers and the events of the day (e.g. football match) the coverage range also changes. This phenomenon is known as "Cell Breathing."[7] This dynamic behaviour of the cell makes the cell planning and the network dimensioning a very complex procedure due to the ambiguities of the subscribers. These events can some what be predicted if the nature of the event to attract higher crowds is calendared, again for instance football matches.

Traditional static prediction methods are no longer appropriate so simulation and statistical modelling techniques have to be applied for accurate network calculations. As well as being more accurate the simulation methods have the advantage of being less expensive and effectively more flexible. The simulation tool used in this paper is called the ICS tool and it is developed by ATDI (Advanced Topographical Development & Images Ltd.). It has the capability of simulating both downlink and uplink, voice (8 kbps) and data up to 384 kbps, as well as adjusting user speeds from walking (2 km/h) to using high speed trains of speeds as high as 500 km/h. Finer adjustments can also be made for instance antenna height, sectorisation, electrical and mechanical down tilt, computation of resolution from 1 km to 10 m., the use of the hand sets in various buildings, high rise building offices at different floor heights, open areas, on water expanses, open grass lands, or forested woodland as well as the usual built up area, town/city scenarios, etc.

In this paper average scenarios are used (a maximum of 110 km/h speed) and a part of Paris is take as an example of a typical European city. The simulated scenario is a football match attracting a high number of people for a short while and its effect on the network and how to combat the effect of cell breathing using a combination of macro cells with an array of four micro cells around it, with a combination of either 3 and/or 6 sectored antennas for the cells.

CCI Reduction Techniques

One of the ways in which to reduce Co-Channel Interference (CCI) is through the use of a 12-cell reuse pattern. [1] This may be unacceptable because it reduces the number of users in a specified geographical area covered by a network provider. Thus replacing an omni-directional antenna with a directional antenna reduces the CCI by making sure that some of the interfering signals never reach the primary mobile unit, resulting in an increase of the signal-to-CCI ratio.

This investigation has the aim of simulating the best configuration to enhance reception and reduce CCI. The method adopted will be comparing the number of parented subscribers using a combination of a macro cell with four micro cells in conjunction with either the 3 and/or 6 sectored antennas. (This can be accomplished through use of a 120^o or a 60^o sector antenna respectively.) The term sectorisation refers to the number of sectors belonging to a site. This is primarily used to increase the system capacity as well as increasing service coverage.

Directional Antenna Using Three Sectors

In this scenario the cell is divided in to three equal sectors of 120^o, with each sector having its own set of frequencies. For a seven-cell cluster, the primary mobile unit (MU) will receive interference from only two other cells instead of six, as with an omni-directional antenna. Due to the directional pattern of the antenna seen in Figure 1, the S/I ratio can now be expressed in the worst-case senario, when the MU is at the edge of the its own cell.

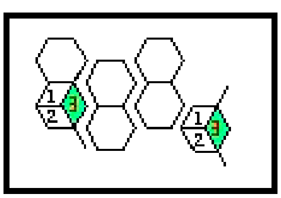

Figure 1. Seven cell reuse pattern with 3 sectored antenna.

Referring to Eqn. 1 we can see the direct relationship between S/I , D and R. [2].

$$S/I = R^{-v} / [D^{-v} + (D+0.7R)^{-v]} \qquad (1)$$

Where v is the loss exponent or loss factor,
D is the distance to the interfering cell
R is the radius of the cell

In the best case scenario, the two interferes will be at distance-D, and the signal-to-CCI ratio for a 120^o sector antenna can now be obtained from the corresponding ratio for the omni-directional antenna by noting that the omni-directional antenna has six interferes:

$$[S/I]_{120o} = [S/I]_{omni} + 10 \log 3 \qquad (2)$$

Comparing the performance of an omni-directional antenna, a 120^o sector antenna provides a signal-to-CCI ratio improvement of 4.77 dB. Using the same ideology with a 6 sectored antenna, the improvement of performance will also be equivalent to 10 log6 plus the $[S/I]_{omni}$ therefore showing an improvement of 7.78 dB with a 60^o sectored antenna.

$$[S/I]_{60o} = [S/I]_{omni} + 10 \log 6 \qquad (3)$$

Using the 6 sectored antennas causes a greater inter-channel interference therefore the theoretical values are much higher than in actual fact. This is clearly seen in the simulations. Also the use of the 6 sectors will require much more careful radio planning in order to minimise the coverage holes between cells, while minimising the overlap of adjacent cells. Upgrading a 3 sectored site to a 6 sectored site simply does not involve installation of three additional aerials, but also requires changing the original three. Thus it is crucial careful planning is carried out before hand in the initial stages of set up. If a site is predicted to have an increase in traffic in the near future it may be advantageous to deploy highly sectorised configurations during initial roll-out to avoid subsequent upgrades. Six sectored antennas are generally used for high capacity macro cell configurations and this is shown later in the results of the simulations.

Multi-tier cellular structures-Macro & Micro cells

As in the scenario set for this particular paper, a sudden increase in traffic, a so called “hot spot”, attracts the deployment of micro cells so as to cope with the sudden increase of the cell load. This is an attractive solution in terms of relative ease of site acquisition, increased air interface capacity and more efficient indoor penetration. This solution can support multiple carriers and multiple cells. Although micro cell sectorisation is significantly more difficult than that for macro cells, it is still able to support dual-branch uplink diversity. Micro cells normally depend on line of sight coverage thus very useful in this football stadium scenario where their multipath coverage is relatively weak. This leads to a high down link orthogonality and correspondingly reduced intra-cell interference.

Referring to table 1 with the capacity related parameters it is noted that the E_b/N_o requirements for the microcell are greater than the macrocell requirements and this is primarily due to the increased fading across the radio channel.

Table 1. A comparison of macrocell and microcell capacity related parameters [2].

Parameter	Macrocell	Microcell
Uplink E_b/N_o (12.2 kbps speech) 4dB	4dB	4.5dB
Increase in inter-cell interference 1dB	1dB	2dB
Downlink E_b/N_o(12.2kbps speech)	6.5dB	9.5dB
Downlink orthogonality	0.5	0.9
Inter-cell interference ratio	0.65	0.25
Soft handover overhead	40%	20%

Cell Breathing

This is a feature of CDMA networks. The effective service area expands and contracts according to the number of users connected. Overlap-regions between cells (which are known as 'handover areas') need careful planning and management. Cell translations and databases must be configured to ensure that handover areas are of optimal size and users furthest from base stations can be successfully 'handed over' to neighbouring cells with lighter traffic loads. If these handover areas are too small, mobiles at the edge of a cell will not receive support from the neighbour cells in time. This will result in too much interference and ultimately a dropped call. If the handover area is set too large then too many mobiles will receive multi-cell support, creating unnecessary links into the network that strain call processing resources and reduce capacity.[6]

In a CDMA network, mobiles operating at the edge of a cell must be simultaneously supported by the surrounding cells. In this way they become a source of signal strength rather than of interference. Such support is known as a 'soft handover', which is not required in GSM, where only one cell at a time is required to support a call. The dynamic behaviour of the cell makes the users at the edge of the cell more vulnerable to dropped or terminated calls. Once a user at the edge of a cell experiences difficulty in maintaining the connection, it tries to increase the transmitting power of the hand set to its maximum value. This in turn increases the overall interference of the cell, making the cell footprint decrease in size, rendering this user at the edge of the cell to become out of range. These areas of no or very limited coverage are called "Dead areas."
As in Eqn. 4 we can see that the power (S) shows a high dependency on the user data rate, R_b, the source activity factor, α and the number of users, N.

$$S = [E_b/I_o . R_b . N_o . W] / [W - {}_{Eb/Io} . R_b\alpha(1+f)(N-1)] \quad (4)$$

Where W is CDMA chip rate = 3.84Mchip/s, E_b/I_o = 7dB, α = 0.5, and the f-factor is the ratio of intercell-to-intracell interference power = 0.55, [6].

2. CASE STUDY

As previously mentioned, the simulations carried out are focused on central Paris with installation of one macro cell and four micro cells surrounding it. The scenario depicted is a sudden increase of the network load at the football stadium. The area includes part of the River Seine in the area of Neuilly Sur Seine. The Grid co-ordinates are, 446485-450625 and 5416090-5413330. The macro-cell parameters used are as follows, base station transmit power: 20 W, antenna gain: 18 dB, transmitter and receiver bandwidth: 5 MHz, receiver sensitivity: -124 dB, base station antenna height :20 m, mobile height: 2m, field strength threshold: 60 dBμv/m, electrical downtilt: 9 degrees, no mechanical downtilt,[4] and frequency used: 1900 MHz, both the 3 and 6 sectored combinations are simulated. The microcell parameters are as follows, transmit power: 5 W, antenna heights: 4 m, Downtilt: 2°.

The simulation aims to find the best configuration to accommodate the maximum amount of subscribers within the given are in times of increased network traffic. The combinations will include four options shown in table 2.

Table 2. Combinations of sectors

Macrocell	3	3	6	6
Microcell	3	6	3	6

The simulations are carried out with randomly generated subscribers and the same numbers of subscribers are used for each scenario. The simulation procedure follows a gradual increase in traffic till kick off time at which the network traffic is at a generally increased level and a maximum sudden increase for instances at times of excitement like a goal, sending off or penalties. The number of parented options will be compared to the total subscribers and an analogy made from the results to the best configuration for such a scenario.

3. RESULTS AND DISCUSSION.

The simulation package has the 3-D option making Base station location much simpler. The Figures 2 and 3 show a 3-D as well as a 2-D representation of the chosen site.

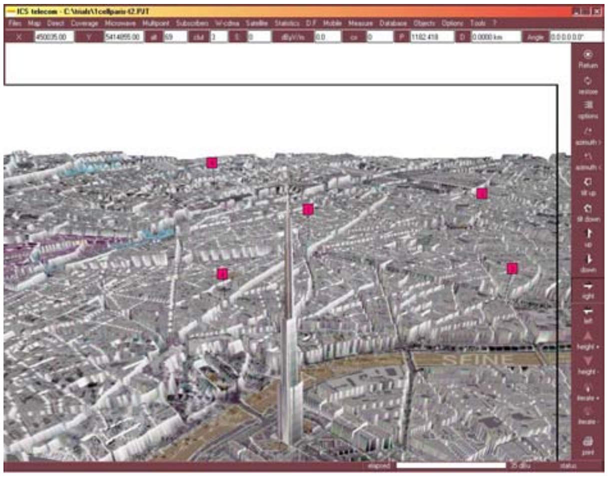

Figure 2. A 3-D view of the area chosen for simulation

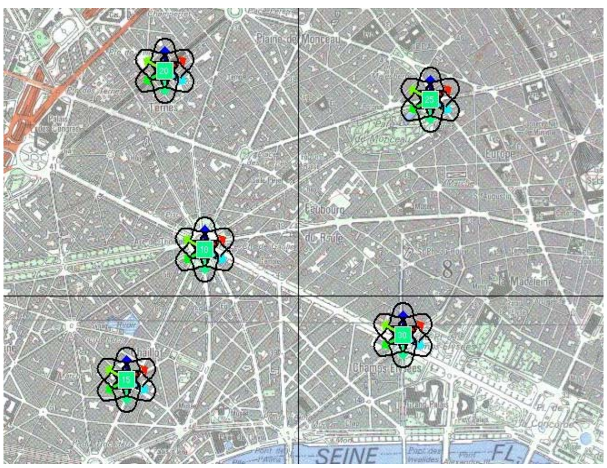

Figure 3. The Planning Site In 2-D, with an example of using all 6 sectored antennas

The results for the simulation are depicted in graphical representation in table 3.The correlation of the results are shown in igure 4.

Table 3. Results of Simulation

Trial type	100sus	500sus	1000sus	2247sus
3M-3m	95	428	921	2003
3M-6m	94	430	932	2016
6M-3m	96	483	961	2105
6M-6m	97	497	990	2196
6M-0	83	387	954	1996
3M-0	73	372	821	1791

Key M=Macro
m=micro

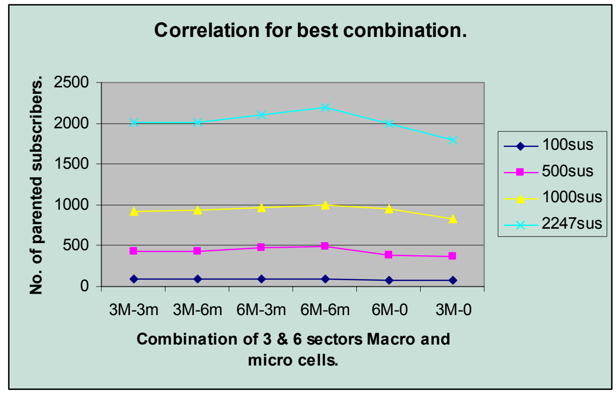

Figure 4. The best combination according to the number of subscribers

We can see in the graph above that there is an increase in the number of parented subscribers coming to a maximum with the 6M&6m combination and this effect is most visible with the maximum number of subscribers (2247). In comparison with the other results the inclusion of the 6 sectored micro cell antennas is not pronounced at all and looking at the table the increase is very minimal with both the 3M and 6M.(a maximum of 30 in 1000 subscribers). This being an improvement of only 3% maximum compared to all the hard ware installation and investment. The 6-sectored Macro cell (with out any micro cell), performs very well against all the 3 sectored antennas and has a higher value of parented subscribers except for the last option -2247, subscribers where the micro cells aid in further cell capacity. As the number of subscribers increase we further recognise the role the micro cells play in increasing the cell coverage. The 6 sectored antennas perform better in all cases but there is not a massive increase in the capacity compared to the three sectored antennas. [7] This might be linked to the intra cell interference caused by the six sectors. Refer to Figure 5. The basic principle is that by using six narrow beam antennas, the coverage area of a cell will be extended due to the increased forward gain, and the capacity will be double that of a three-sectored cell. While it is true that there is an increase in antenna gain, due to the narrow beam width, the gain is typically only two or three dBs, and does not have a significant impact on the coverage.

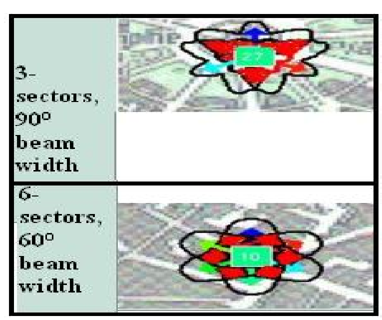

Figure 5. Intra-cell interference

In practical deployment the amount of overlap would be greater due to the effect of the adjacent sites. Also, the use of six sectors will require much more careful radio planning in order to minimise coverage holes between cells, while minimising the overlap of adjacent cells. In the CDMA system, this overlap causes interference, since every cell is on the same carrier, which in turn leads to a reduction in capacity [5]. Despite the soft handover there is still a net reduction in the overall capacity. Thus it is unlikely that there would be a doubling in capacity by moving from three to six sectors, shown in the simulation results.

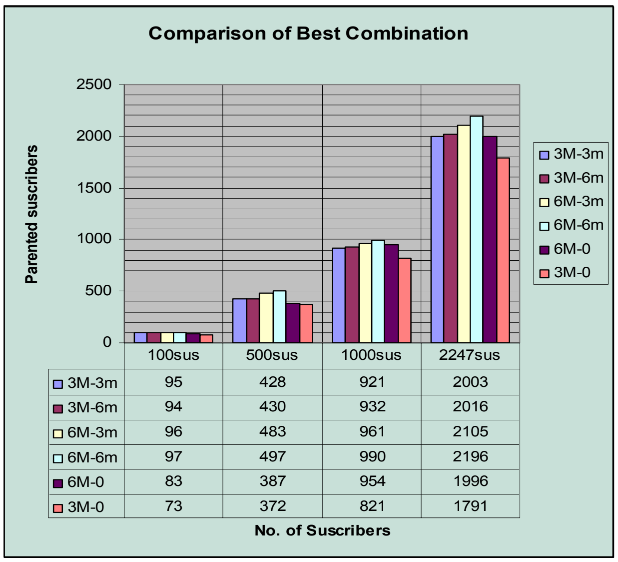

	100sus	500sus	1000sus	2247sus
3M-3m	95	428	921	2003
3M-6m	94	430	932	2016
6M-3m	96	483	961	2105
6M-6m	97	497	990	2196
6M-0	83	387	954	1996
3M-0	73	372	821	1791

Figure 6. Results of best combination

In Figure 6 we can see that there is not a great difference in the use of macro and micro cells when the number of subscribers is low, but as the number increase the micro cell play a vital role in increasing the cell capacity. The added advantage of using the 6 sectored antenna also is more pronounced with greater numbers as we can see with 2247 the 6M*-6m** combination works best covering the maximum amount of subscribers.

Figure 6 shows the individual grouped sections and the performance of the best combination within each section of chosen number of subscribers. Here we can see the differences in comparison to the total parented subscribers the role of the individual Macro and micro cells.

For further in depth comparison the breakdown of the whole configuration is required and specific Macro and micro cell numbers are required this is shown in the Figure 7.

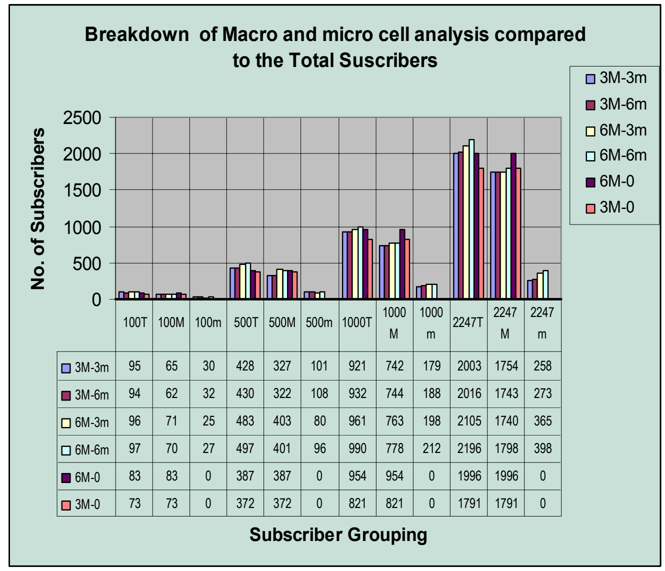

	100T	100M	100m	500T	500M	500m	1000T	1000 M	1000 m	2247T	2247 M	2247 m
3M-3m	95	65	30	428	327	101	921	742	179	2003	1754	258
3M-6m	94	62	32	430	322	108	932	744	188	2016	1743	273
6M-3m	96	71	25	483	403	80	961	763	198	2105	1740	365
6M-6m	97	70	27	497	401	96	990	778	212	2196	1798	398
6M-0	83	83	0	387	387	0	954	954	0	1996	1996	0
3M-0	73	73	0	372	372	0	821	821	0	1791	1791	0

Figure 7. Results of best combination including micro cell performance compared to the macro cell

The use of the micro cells is very limited with the lower end of the subscribers and this performance gradually increases as the cell traffic increases. Example, with 100 subscribers, the use of the micro cell is further reduced in conjunction with the 6 sectored macro cell antenna having an efficiency of just 26% compared to ~ 33% with the 3 sectored Macro-cell. This may be due to the efficiency of the 6 sectored micro cell antenna is greater than the three sectored micro cell antenna.. There is a large variation between just the 3 and 6 sectored antennas and the 6 sectored antenna gives up to a 15% increase in cell capacity compared to just using 3 sectors. As the traffic increases the performance of the micro cell increases and the maximum amount of subscribers are covered by having the 6M-6m combination. Although this is the best combination numbers wise there is only an increase of 4% compared to the 6M-3m combination and ~10% increase to the 3M-3m combination but a massive 20% increase compared to the 3M-0m combination. So compared to the cost of installation of the hard ware there has to be a trade off between performance, cost and efficiency.

In table 4 the raw data is analysed and tabulated to show the percentage increase in capacity of the cell compared to using just a 3 sectored macro cell.

Table 4. Percentage increases compared to 3M-0m/M combination

Trial type	100sus	500sus	1000sus	2247sus	Average In
3M-3m	23	13	11	11	14
3M-6m	22	14	12	11	15
6M-3m	24	23	15	15	19
6M-6m	25	25	17	18	21
6M-0	12	14	14	10	13
3M-0	0	0	0	0	0

There is a definite trend in the table 4 showing a gradual decrease in efficiency the greater the number of subscribers. This is noticed in all the combinations.

4. CONCLUSIONS

Using a Macro cell with a 3 sectored antenna with as the base line comparisons are made as percentage increase from table 4.

There is a general trend as the number subscriber's increase the efficiency of the combined macro-micro cell drops. This trend is continuous with the different sectorisation as well. When comparing the 3M combinations there is no substantial increase in performance when 6 sector-micro cells are used compared to the 3 sectored-micro cell. (Only a difference of 1% increase). With the 6M combinations again the increase is pretty meagre between using 3 or 6 sectors in the micro cells. A difference of 2% increase. In comparison with the 3M and 6M, the increase in performance and coverage is tremendous, between 5-7% increases.
The maximum amount of increase is with the 6M-6m combination at a 21% increase from the 3M-0m combination used as a base line value.

The inclusion of 6 or 3 sectored micro cells does not make a heavy intact on the system. Using 6 sectored Macro cells is shown to be very desirable; the combination either 3 or 6 sectors do not make a massive difference to the system.
Using the 6 sectored micro cells gives an advantage of about 2% over the 3 sectored antennas.

5. REFERENCES

[1] William. C. Y. Lee, 1989 "Mobile cellular telecommunications systems", McGraw Hill Book Company.

[2] J. Laiho, A. Wacker, T. Novosad, 2002 "Radio network planning and optimisation for UMTS", John Wiley & Sons, Ltd.

[3] I. Jami, H. Tao "Micro-cell planning within macro-cells in UMTS" IEE 2002 Vol 489, pg 211-215.

[4] I forkel. A. Kemper, R, Hermans ".Effect of electrical and mechanical antenna down-tilting in UMTS networks." IEE 2002 Vol 489 pg 86-90.

[5] C.Johnson, J.Khalab. "The coexistence of WCDMA macrocell and microcell radio network layers." IEE 2002 Vol 489 pg 81-85.

[6] P.R.Gould "Radio planning of third generation networks in urban areas." IEE 2002 Vol 486 pg 64-68

[7]. Jon Harris, Josef Noll May 2000 "Guidelines For UMTS Radio Access Network Design", EURESCOM.

BIBLIOGRAPHY:

[1] Heikki Kaaranen, Ari Ahtianen, Lauri Laitinen, Saimak Naghian, Valtteri Neimi, 2001. "UMTS Networks, Architecture, Mobility and Services." J.Wiley.

[2]"http://searchnetworking.techtarget.com/sDefinition/0,,sid7_gci820970,00.html"

[3]"http://whatis.techtarget.com/definitionsCategory/0,289915,sid9_tax1686,00.html"

[4] UMTS Quality of Service, UMTS special features, and security issues http://www.computers.toshiba.co.uk/cgi-bin/ToshibaCSG/download_whitepaper.jsp?WHITEPAPER_ID=0000000aa3

[5]. J. D. Parsons, 2001 "The Mobile Radio Propagation Channel", John Wiley & Sons, Ltd.

Robust Field Oriented Control Analysis of an Induction Motor Using an Adaptive Flux Observer Based on Sliding Mode Methodology

Adel Khedher(1,4) , M^{ed} Faouzi Mimouni(2) , Ahmed Masmoudi (3,4) and Nabil Derbel (3,5)

(1)High Institute of Applied Sciences & Technology (ISSAT), City Ibn.Khaldoun 4023 Sousse- TUNISIA.

(2)Monastir Engineering School (ENIM), Road of Kairouan, 5000 Monastir-TUNISIA

(3)Sfax Engineering School (ENIS), BP W, 3038 Sfax-TUNISIA

(4)Research unit on Renewable Energies and Electric Vehicles (RELEV)
(5)Research unit on Intelligent Control, design and Optimisation of Complex Systems (ICOS)

Email: Adel.Khedher@issatso.rnu.tn

Abstract: *This paper deals with the implementation of a field oriented control strategy in an induction motor drive, considering a flux observer based on an approach approximating the rotor resistance. Without flux measurement, the controller has the capability to adapt the estimated rotor resistance. The proposed approach uses a singularly perturbed model to design a sliding mode observer. Then an adaptive sliding mode flux observer is developed. The adaptive technique guarantees that both estimated flux and rotor resistance converge to their values. Simulation results clearly highlight the robustness of the proposed control strategy against parameter variations.*

Key-words: Induction Motor, Sliding mode Observer, adaptive control, Parameter estimation.

LIST OF SYMBOLS

V_{sdq}:	Stator voltages frame dq
$I_{sd}=x_1$, $i_{sq}=x_2$	Stator currents frame dq,
i_{mr}:	magnetizing current,
$\phi_{rd}=x_3$,$\phi_{rq}=x_4$:	Rotor flux frame dq,
Rs, Rr:	Stator and rotor resistances,
Ls, Lr:	Stator and rotor inductances,
M:	Mutual inductance,
σ :	*Blondel* coefficient,
$\omega_r=x_5$	Mechanical speed,
p_L:	*Laplace* operator ,
p:	Numbers of pole pairs,
J:	moment of inertia,
f:	Damping coefficient,
C_{em} :	Electromagnetic torque,
C_r:	Load torque.

I. INTRODUCTION

The induction motor is widely used in the industry because of its popular features such as its simple construction, reliability and low cost [1]-[15]. In most if not all cases, induction motor control strategies are developed with the assumption that either full or partial system state information is available. Examples are partial state feedback for field oriented control (FOC) , full input-output linearisation control (IOLC) and sliding mode control strategy. Practically, the rotor flux is not easily measurable [4],[10]-[15].

Therefore an observer is needed to estimate the unknown states and can also provide, in some circumstances, better estimates of known current states that are contaminated by noise.

In this paper a sliding mode observer is developed. The flux observer model is obtained following the convergence of the d-q stator currents to the sliding mode surface. The gain of the flux observer model is calculated by a further condition obtained by Lyapunov stability theory in order to ensure the convergence of the estimate.

The paper is organized as follows. The mathematical model of the induction motor is reviewed in section II. An adaptive flux observer using sliding mode methodology is proposed in section III. In section IV, simulation results are presented and discussed. Finally, some concluding remarks are distinguished at the end of the paper.

II. MATHEMATICAL MODEL OF THE INDUCTION MOTOR

The electrical differential equations of the machine in the dq-frame can be described by the following [1]-[3] :

$$\begin{cases} V_{sdq}=R_s I_{sdq}+\dfrac{d\Phi_{sdq}}{dt}+\Phi_{sdq}\dfrac{d\Theta_s}{dt} \\ V_{rdq}=R_r I_{rdq}+\dfrac{d\Phi_{rdq}}{dt}+\Phi_{rdq}\dfrac{d\Theta_r}{dt} \end{cases} \quad (1)$$

The expression of the electromagnetic torque is written as follows:

$$C_{em}=\frac{3pM}{2L_r}(\Phi_{rd}I_{sq}-\Phi_{rq}I_{sd}) \quad (2)$$

The mechanical equation is given by:

$$J\frac{d\Omega_m}{dt}+f\Omega_m=C_{em}-C_r \quad (3)$$

The induction motor can be described by five non-linear differential equations with four electrical variables, one mechanical variable and two control variables such as [1]-[8],[10]-[15]:

$$\begin{cases} \dfrac{dx_1}{dt}=-\gamma x_1+\dfrac{k}{Tr}x_3+pkx_4x_5+\dfrac{1}{\sigma Ls}Vsd \\ \dfrac{dx_2}{dt}=-\gamma x_2+\dfrac{k}{Tr}x_4-pkx_3x_5+\dfrac{1}{\sigma Ls}Vsq \\ \dfrac{dx_3}{dt}=\dfrac{M}{Tr}x_1-\dfrac{1}{Tr}x_3-px_4x_5 \\ \dfrac{dx_4}{dt}=\dfrac{M}{Tr}x_2-\dfrac{1}{Tr}x_4+px_4x_5 \\ \dfrac{dx_5}{dt}=\mu(x_2x_3-x_1x_4)-\dfrac{Cl}{J} \end{cases} \quad (4)$$

with

$$\sigma=1-\left(\frac{M^2}{LsLr}\right),\quad \alpha=\frac{1}{\sigma Ls},\quad k=\frac{M}{\sigma LsLr},$$

$$\mu=\frac{pM}{JLr},\quad \gamma=\frac{Rs}{\sigma Ls}+\frac{RrM^2}{\sigma LsLr^2}.$$

III. ADAPTIVE SLIDING MODE OBSERVER

The sliding mode observer design procedure consists of performing the following two steps. First, design the manifold (the intersection of the sliding mode surface SMS) $\boldsymbol{S}$, such that the estimation error trajectories restricted to $\boldsymbol{S}$ have the desired stable dynamics. Second, the observer gain is determined to drive the estimation error trajectories to $\boldsymbol{S}$ and maintain it on the set, once intercepted, for all subsequent time.

Denoting $\mathbf{x_{1e}}$, $\mathbf{x_{2e}}$, $\mathbf{x_{3e}}$, $\mathbf{x_{4e}}$ as estimates of $\mathbf{x_1}$, $\mathbf{x_2}$, $\mathbf{x_3}$, $\mathbf{x_4}$ respectively, the sliding mode observer for this system is designed as [4],[10]-[15]:

$$\begin{cases} \dfrac{dx_{1e}}{dt}=-\gamma x_{1e}+\dfrac{k}{Tr}x_{3e}+pkx_{4e}x_5+\dfrac{1}{\sigma Ls}Vsd+A1Is \\ \dfrac{dx_{2e}}{dt}=-\gamma x_{2e}+\dfrac{k}{Tr}x_{4e}-pkx_{3e}x_5+\dfrac{1}{\sigma Ls}Vsq+A2Is \\ \dfrac{dx_{3e}}{dt}=\dfrac{M}{Tr}x_{1e}-\dfrac{1}{Tr}x_{3e}-px_{4e}x_5+A3Is \\ \dfrac{dx_{4e}}{dt}=\dfrac{M}{Tr}x_{2e}-\dfrac{1}{Tr}x_{4e}+px_{4e}x_5+A4Is \end{cases} \quad (5)$$

The vector sliding surface (S), the vector sign (Is) and the gain matrices for the observer ($A_{1,2}$ and $A_{3,4}$), are given by:

$$s=\begin{pmatrix} S_1 \\ S_2 \end{pmatrix}=D^{-1}*\begin{pmatrix} Isd-Isde \\ Isq-Isqe \end{pmatrix}, \quad (6)$$

$$Is=\begin{pmatrix} sign(S_1) \\ sign(S_2) \end{pmatrix} \quad (7),\qquad D=\begin{pmatrix} \dfrac{k}{Tre} & k*x_5 \\ -k*x_5 & \dfrac{k}{Tre} \end{pmatrix} \quad (8)$$

$$A_{1,2}=\begin{pmatrix} A_{11} & A_{12} \\ A_{21} & A_{22} \end{pmatrix}=D*\begin{pmatrix} \delta_1 & 0 \\ 0 & \delta_2 \end{pmatrix}, \quad (9)$$

$$A_{3,4}=\begin{pmatrix} A_{31} & A_{32} \\ A_{41} & A_{42} \end{pmatrix}=\begin{pmatrix} (q_1-\frac{1}{Tre})*\delta_1 & x_5*\delta_2 \\ x_5*\delta_1 & (q_2-\frac{1}{Tre})*\delta_2 \end{pmatrix} \quad (10)$$

where q_1,q_2, δ_1 and δ_2 are positive constants;

and *Tre*: the estimate of rotor time constant.

The sliding mode observer gains are chosen in such away that Lyapunov stability conditions are satisfied [4],[10]-[15] .Thus:

$$\begin{cases} \delta_1 \geq \left| ((\frac{kM}{Lr}(Rr-Rre)(\frac{x_3}{M}-x_1)+kx_5e_4+\frac{Rre}{Lr}ke_3) \right| \\ \delta_2 \geq \left| ((\frac{kM}{Lr}(Rr-Rre)(\frac{x_4}{M}-x_2)+kx_5e_3+\frac{Rre}{Lr}ke_4) \right| \end{cases} \quad (11)$$

where e_3, e_4 are flux errors in the dq-frame;

It is well Known that sliding mode techniques generate undesirable chattering. This problem can be discarded by replacing the switching function by a smooth continuous function [4],[9],[11],[13].

Then, we propose replace the **Sign** function by the following function:

$$\mathrm{Sat}(S_i)=\begin{cases} 1 & \text{if} \quad S_i > \lambda \\ -1 & \text{if} \quad S_i < -\lambda \\ \frac{S_i}{\lambda} & \text{if} \quad |S_i| < \lambda \end{cases} \quad (12)$$

where λ is a positive small constant, i=1,2.

The estimate of the rotor resistance is based on the Popov criterion [11],[13]. The variation of the rotor estimate is given as follows:

$$\frac{dRre}{dt}=q_3(A_{1,2}I_S)^T C \quad (13)$$

where $q_3 > 0$, and $C=\frac{\Phi_{re}}{Lr}-\frac{M}{Lr}i_s$

V. SIMULATION RESULTS

Following a phase of magnetization of the machine leading to the establishment of the rotor flux, we considered the start-up of the motor according to a ramp of the speed which increases from 0 to 100rad/s started at t=0.05s.

In the simulation works, we considered, in a first step, the case where the machine operates without parameter variations. In a second step and at time t=0.3s, a sudden variation of 20% of the rotor resistance is applied to the machine. In a third step, a second sudden variation of the rotor resistance is applied (the resistance passes to its double values at t=0.6s).

In order to more evaluate the robustness of the proposed approach, we considered the no-loaded operating of the motor. Suddenly, we apply a nominal load to the machine at t=0.3s. A sudden increase of 100% on the rotor resistance is then applied at t=0.6s.

In all simulations, we considered the case where the mutual inductance depends in terms of the magnetizing current such as,[5]:

$$M=0.39+0.4933e^{-3(i_{mr}-0.86)}-0.39e^{-3.65(i_{mr}-0.86)} \quad (14).$$

Simulation results are presented in figures 1 and 2. Figures 1.a and 2.a present the evolution of the machine speed. In figures 1.b and 2.b, the evolution of the actual and estimated fluxes are presented. Actual and estimated stator currents are given in figures 1.c and 2.c. The actual and estimated torques are presented in figures 1.d and 2.d. The parameter variations are presented in figures 1.e, 1.f, 2.e and 2.f. The errors of currents and fluxes are given in figures 1.g, 1.h, 2.g and 2.h.

These figures show that the obtained performances are satisfied.In fact, it is clear that the estimated variables converge to the actual ones with satisfactory dynamics, in both cases of loaded and no-loaded machine.

Consquently, it is obvious that the proposed approach is robust with respect to parameter variations.

VI. CONCLUSION

In this paper, a flux adaptive observer is developed in order to improve the performances of the induction machine under field oriented control. The proposed observer is based on the sliding mode technique.

Simulation results show the robustness of the developed observer which is practically insensitive with respect to parameter variations.

REFERENCES

[1] J. P. Caron et J. P. Hautier, « Modélisation et commande de la machine asynchrone », Editions technip 1995.

[2] B. de Fornel, « Alimentation des machines asynchrones »,Techniques de l'ingénieur D 3620, D3621- Juin 1990.

[3] A. Khedher, M. F. Mimouni, N. Derbel, and A. Masmoudi « Effects of the rotor time constant and the mutual inductance on the behaviour of controlled induction motor », IEEE-SMC'02, October 2002, Hammamet-TUNISIE.

[4] A. Benchaib, A. Rachid, and E. Audrezt « Sliding Mode Input-Output Linearization and Field Orientation For Real-Time Control of Induction Motors » IEEE Trans. Power Electr., vol. 14, no. 1, January 1999.

[5] A. Khedher, M. F. Mimouni, N. Derbel, and A. Masmoudi « Robustness analysis of an induction motor under sliding mode control focused on rotor resistance and mutual inductance variations ». IEEE-SSD'03 , pp.127 (Summary), March 26-28 2003, Sousse-Tunisia.

[6] L. Barazane, Y. Sellami, R. Ouoiguini, and M.S. Boucherit « An approch to field-oriented control of an induction motor using cascade sliding mode controllers», IEEE-JTEA 2002, vol.3, pp 99-106, 21-23 Mars 2002, Sousse Nord, Tunisie.

[7] L.–G. Shiau and J.-L. Lin « Stability of sliding-mode current control for high performance induction motor position drives» , IEE Proc.-Electr. Power Appl. vol. 148 , no. 1, pp. 69-75, January 2001.

[8] R.-J. Wai and F.-J. Lin , « Fuzy neural sliding-mode control for induction servo motor drive» , IEE Proc.-Electr. Power Appl., vol. 146 , no. 3, pp. 297-308, May 1999.

[9] J. Y. Hung, W. Gao and J. C. Hung, « Variable Structure Control: A Survey », IEEE Trans. on Ind. Electronics, vol. 40, no. 1, pp. 2-22, February 1993.

[10] R.-J. Wai, « Adaptive sliding-mode control for induction servomotor drive» , IEE Proc.-Electr. Power Appl., vol. 147 , no. 6, pp. 553-562, November 2000.

[11] G. S. Guillermo « Etude et mise en œuvre d'estimateurs et d'observateurs robustes de flux et de vitesse pour une machine à induction à cage commandée vectoriellement » Thèse, ORSAY, Paris XI – 1998.

[12] H. Rehman , A.Derdiyork , M. K. Guven and L. Xu « A New Current Model Flux Observer for Wide Speed Range Sensorless Control of an Induction Motor », IEEE Trans. Power Electr., vol. 17, no. 6, November 2002.

[13] Y. Zheng, H. A. A. Fattah and K. A. Loparo «Non-linear adaptive sliding mode observer-controller scheme for induction motors », Int. J. Adapt. Control. and Signal .Process., vol. 14, pp.243-273 ; 2000.

[14] M. Djemai, A. Glumineau and R. Boisliveau «Observateur non-linéaire à mode glissant pour machine asynchrone : Etude expérimentale (banc d'essais de l'IRCCyN », CIFA 2000, pp. 489-494 Lille – France.

[15] H. Chen and M.W. Dunnigan «Comparative study of a sliding-mode observer and Kalman flters for full state estimation in an induction machine ». IEE Proc. Electr. Power Appl.., vol. 149, no. 1, January 2002.

APPENDIX : PARAMETERS OF THE MOTOR

Rated power: 1.5 Kw,
Rated stator voltage: 231/400V, 50Hz,
Rated stator current: 3.2/5.5A,
Rr0=4.282Ω, Rs=5.717Ω,
L0=0.0223H,Ls0=Lr0=0.4469H, M0=0.4246H,
σ =0.0973. J=0.0049kgm^2, f=0.029

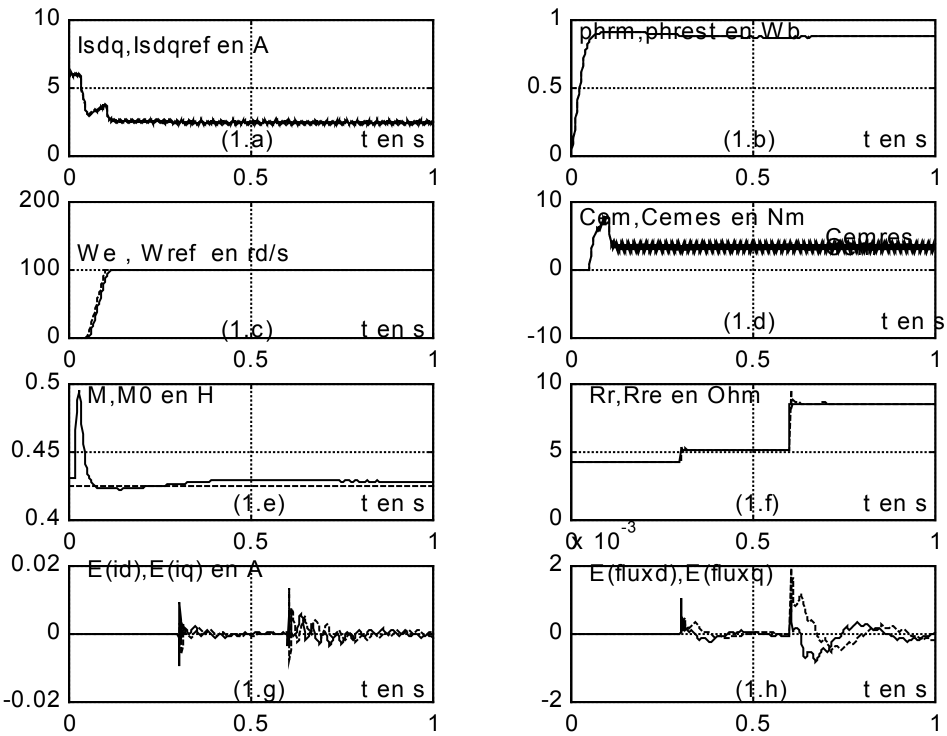

Figure 1: Simulation results for the loaded machine.

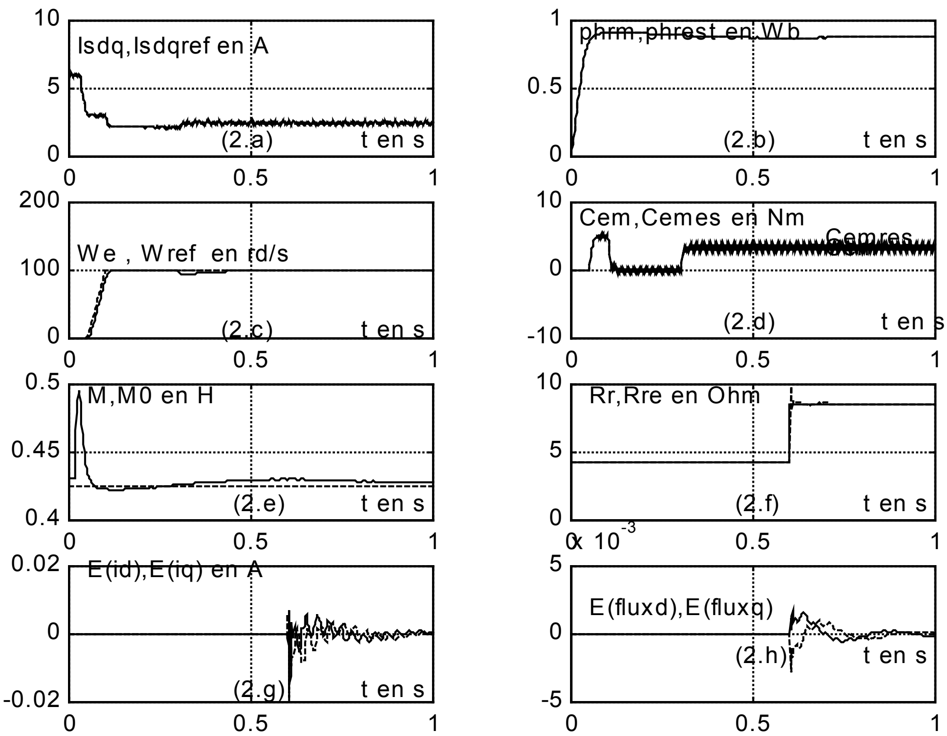

Figure 2: Simulation results for the no-loaded machine.

A REMOTE VIRTUAL ENVIRONMENT FOR MULTILANGUAGE COSIMULATION OF PROGRAMMABLE LOGIC CONTROLLER (PLC) CODE

Mohamed Mhamdi
UR Prince
ISETde Sousse
4023, cité Riadh, Sousse, Tunisia
Mohamed.Mhamdi@isetso.rnu.tn

Rafik Braham
UR Prince
ISITC
H.Sousse, Tunisia
Rafik.Braham@ensi.rnu.tn

Mohamed Moalla
LIP2
Faculty of Sciences of Tunis
ElManar University, Tunis, Tunisia
Mohamed.Moalla@fst.rnu.tn

Hamadou Saliah-Hassane
LICEF
TelUQ
Quebec, Canada
Hamadou_Saliah@teluq.uquebec.ca

KEYWORDS

Learning Object, Virtual Reality, Discrete simulation, Multilanguage simulation, PLC.

ABSTRACT

The use of a PLC (Programmable Logic Controller) within a factory is becoming more and more important. Currently, programmers are often forced to develop and test their PLC code without actual equipment. Most sequence control systems may include software, hardware and mechanical parts. In this case, multilanguage is needed in order to build a significant learning environment enabling learners to achieve real competency gains while simulating the PLC code. The use of a multilanguage simulation requires new validation techniques able to handle a multiparadigm model. Instead of simulation, we will need cosimulation and instead of verification, we will need coverification. Thus the programmer can validate the overall system behavior before the implementation of any of its parts. A visual cosimulation of the behavior of the operative component is possible by using a VRML viewer to validate the conformity of the PLC code with the expected automatism behavior.
The main idea developed in this paper is to be able to achieve a remote virtual environment that allows for the creation and development of a PLC code based on a multilanguage cosimulation where the operative component controlled by the PLC is considered as a learning object that can be used or reused by users connected through a client/server architecture.

INTRODUCTION

A description of the sequence control system design must be structured into an operative part and into a sequence control part. In a teaching context, the operative part is often represented by didactic components. The control part is often represented by a PLC. Building system components into the equipment and programming the control code within a PLC are two major activities in developing the sequence control system[1].
Currently, programmers are often forced to develop and test their PLC code without real equipment, either because the building site is geographically separate from the programming site, or because programming occurs before the building of equipment. Therefore programmers have to assume or predict input and output signals from/to system components in the code programming process.
Moreover they cannot reliably check whether the system functions properly under the control of the developed PLC code before the real system is built. Therefore, the main idea is to be able to achieve an integrated environment, entirely configurable, that allows for the creation and development of programs in a simulation mode[2].
Traditionally, during verification, components are checked in a merely cursory fashion and the integration of the overall system is done only at the final stage. This scheme may induce extra delays and costs because of interface problems. The need for more efficient verification approaches, namely a combined verification of various components, is evident[8].
Experiments with complex system designs prove that there isn't a unique universal language to support the entire cosimulation of components. The simulation may require using different languages. A typical application domain for multilanguage cosimulation is sequence control system simulation. In fact, the combined use of various mechanical parts with the sequence control component, and especially the PLC, requires a multilanguage description and a cosimulation of different components. Multilanguage cosimulation constitutes an important step in this direction. It gives the programmer the ability to validate the whole system's behavior before implementing any of its parts. Multilanguage cosimulation offers many advantages such as efficient verification and less time spent on coming up with solutions. The key idea is to allow for early validation of the overall system through cosimulation[4].
The prime objective of this paper is to research and prototype communication mechanisms that will promote efficient aggregation of disparate components of a cosimulated automatic system into an unified global multilingual network of E-Learning content. Such an integrating platform our system would provide access to a remote PLC to student programming in PLC code. The kernel of the system will provide infrastructure for the student to assemble software components or the learning objects that represent the operative part and PLC to build E-Learning applications.

The next section discusses multilanguage cosimulation concepts and previous work. Section 3 introduces the remote cosimulation architecture system based on the utilization of learning objects. Section 4 shows the feasibility of the multilanguage cosimulation through an example. Finally, Section 5 presents our conclusions.

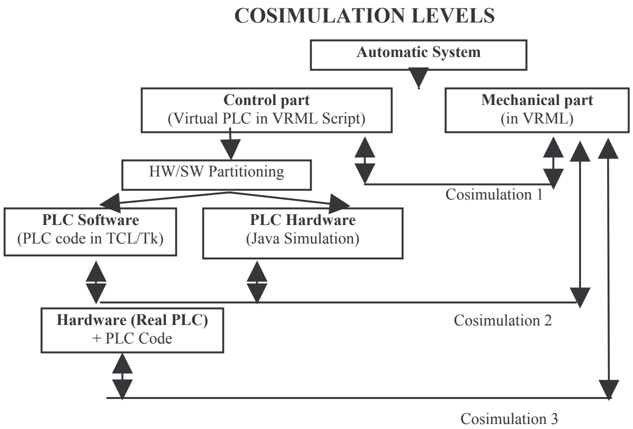

Fig. 1

MULTILANGUAGE COSIMULATION

Most sequence control systems may include both software and hardware. In this case, multilanguage simulation is required. The use of a multilanguage specification requires new validation techniques able to handle a multiparadigm model. Instead of simulation, we will need cosimulation and instead of verification, we will need coverification[9]. Additionally, a multilanguage specification raises the issue of interfacing subsystems that are described in different languages. These interfaces need to be refined when the initial specification is mapped into a prototype[8].

Figure 1 illustrates the flow used for implementing a sequence control system including hardware, software and mechanical parts. Initially, designing such a model involves an analysis of system requirements and a high-level definition of various system functions. The mechanical part is modeled in VRML as modular learning objects wich have nice softaware properties[15], and the control component (PLC) is modeled in JAVA. At this stage, we obtain a multilanguage system-level model given in JAVA-VRML.

The implementation flow handles three cosimulation levels: the local system level, the local optimized system architecture level and the remote accurate level[10-11].

In all cosimulation models, mechanical components are built first into the computer (in VRML), then they [1] are combined with:

- a virtual PLC written in VRML-Script (the first level of cosimulation)
- a virtual remote PLC Engine simulated by a reactive script as is shown in the second level of cosimulation.
- a real remote PLC as is shown in the last level of cosimulation.

SYSTEM ARCHITECTURE

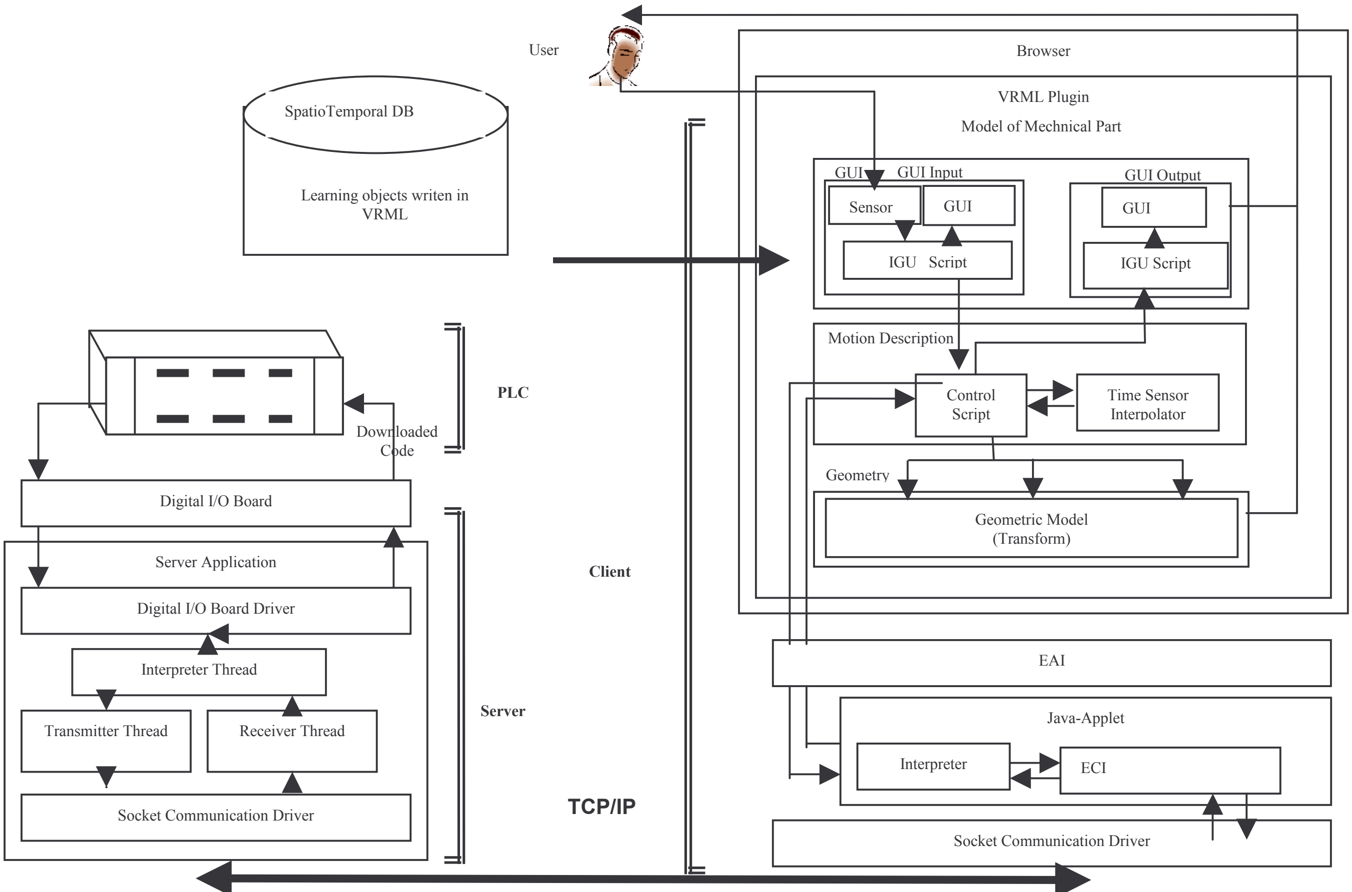

Fig. 2

In our previous work [1], we developed the first two levels of such a model. In this paper, we will give details regarding the third level.
With the third level (cosimulation 3), the behavior of system components controlled by the PLC code can be approximately checked by the programmer. This cosimulation technique can make PLC code testing and debugging processes more reliable.

SYSTEM ARCHITECTURE

This paper deals with designing and implementing a system[flexible operating platform] that allows for an interactive remote cosimulation of the PLC code based on a multilanguage concept. The system works over the WWW, offering Web users a tool for designing and visualizing their sequence control systems. Users may define each mechanical object in the virtual system along with the PLC code that will be executed by a real remote PLC. The system can create a VRML representation of specifications and render it to the client[5].
System architecture follows a three-tier scheme:
- The database, that contains information on the various mechanical components with their virtual representations in VRML[6]. This database is considered as a learning object repositories. The learning objects are not useful only in a single context but they can be used in differents ways, for different purposes, and in different contexts.
- The application server, that is responsible for communicating with the client in order to reply to client requests.
- The application client, that offers a highly interactive interface and communicates with the application server to provide the user with a cosimulation.

In our previous work [1], we presented the spatial characteristics of the didactic component (visual aspect) along with its temporal characteristics (dynamic aspect), items we called spatiotemporal characteristics. We also specified our proposal for storing these characteristics within a format that must meet the following goals:
- Recording the spatiotemporal characteristics of the component within an open format.
- Facilitating the reusability of components and the translation from and to VRML format.
- Allowing a modular description of the component by creating clusters of 3D objects.
- Facilitating the process of verifying and modifying objects encoded in VRML by using a relational language.

The prime objective of our precedent work is to make learning objects throw storing them in a spatio-temporal database, actively able to adapt to the context of their use. More specifically, objects should be adaptative to the pedagogical goals of the learner or learning environment.
As shown in Figure 2, the developed system is based on a client/server (C/S) architecture[3]. The server side consists of a computer connected to a PLC. The application server receives requests for connection to the PLC, programs to be loaded in the PLC memory, commands to be executed by the PLC and input signals in order to modify PLC inputs.
A client is an Internet application that is comprised of the Web browser, a VRML viewer, an EAI and a Java applet that controls communication with the server[15].
Inside a client applet, the VRML sends user/component events into the interpreter. The interpreter translates the incoming events into commands that will be sent to the server. The ECI (external communication interface) receives control frames from the server via the socket communication driver, or delivers outgoing control frames through the socket to the server. The EAI (external authoring interface) enables Java applets to manipulate a VRML world dynamically. The interpreter translates the commands injected into the received control frames into a manipulation of the VRML visualization of the didactic component.
Server and client applications communicate through a TCP/IP connection using the standard socket functions in Visual Basic and Java codes. On the server side, a port is opened to receive possible client requests.
On the client side, once the connection is established, one must specify the address and remote port of the server. The local client port is defined at the compilation stage. The connection is protected, which means that one can be connected through Internet[3].
The communication mechanism is not very fast, but we think that it should be possible to optimize it in order to benefit from the maximal speed of the network connection.
Communication occurs in a synchronous mode. In order to avoid blocking the program during the transfer of information, communication takes place on separate threads. On the server there are two threads that communicate with the PLC, and two other receiver-transmitter threads for controlling communication with the VRML client through a TCP/IP connection.

COMMAND PROTOCOL

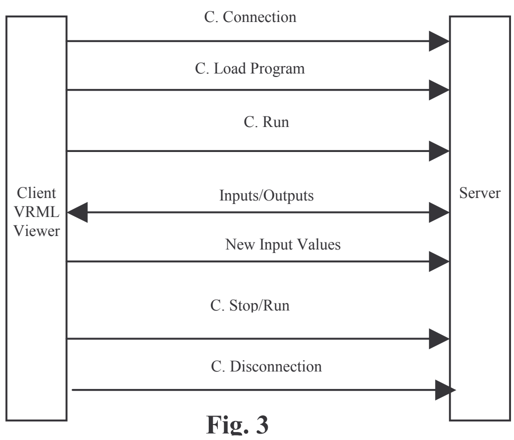

Fig. 3

In the current version, the server accepts one client at a time, but it is possible to modify its behavior in order to serve several clients simultaneously. The server is always ready to receive client commands. Firstly, the client must request a connection to the server. Then the client can request the loading of a code into the PLC memory, the execution or the stopping of this code or the modification of the value of certain PLC inputs. At any time while connected, the client must modify the visualization of the didactic component according to the status of signals sent by the server. Finally the client disconnects to free the server.
The command protocol (Fig. 3) is developed according to the KISS method. The customer sends the server a control frame containing commands; the server answers by one or more information frames. When several successive frames

must be sent in the same direction, the client acknowledges receiving every frame by using a special frame (in order to separate the frames).

A control frame (Fig. 4) consists of:

- 1 control byte (defines the type of command)
- 1 byte of possible parameters
- parameters

COMMAND FRAME

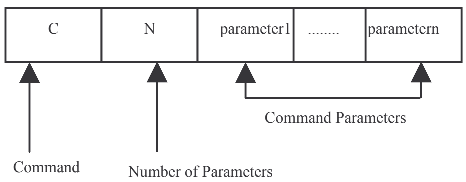

Fig. 4

APPLICATION EXAMPLE

The application is a distribution station controller. The system can be divided into two parts, the festo didactic learning system and a PLC. A real PLC (Siemens S7200 CPU 224) is used to represent the controller and the VRML is used to model component physical behavior.

The simplified distribution station shown in Figure 5 was selected and modeled for an example of equipment controlled by a PLC. This machine currently exists and is used for programmer training purposes.

The station consists of three double-acting cylinders, one pneumatic handling device and eight position sensors. It also has several lamps and switches in the control panel. The station has approximately 6 input signals and approximately 9 output signals.

The purpose of the distribution station is to separate a workpiece from the magazine and to make the workpiece available for a subsequent process. So the station is divided into two subsystems: a feed magazine module and a transfer module.

The feed magazine module separates workpieces from the magazine. A double-acting cylinder pushes out the bottom workpiece from the gravity feed magazine. End position sensing is effected by means of sensors. The filling level of the magazine is monitored. The workpieces supplied may be fed to the magazine in any order. The transfer module is a pneumatic handling device. Workpieces are picked by a vacuum suction cup and can be transferred from between 0° to 180° via a swivel drive. End position sensing is effected by means of sensors.

The PLC code for this control flow specification was programmed and downloaded by using the PLC code programming tool. This distribution station model was developed by directly using the VRML authoring tool and the Java programming environment. The file written by VRML 2.0 for this model becomes 40kbyte size and includes 21 prototype node descriptions that call external the state-transition rules written in 50kbyte JAVA class file[2].

As a result of cosimulation, component models in the VRML viewer can be dynamically moved according to the control code in the PLC. The PLC can adjust the position of the double-acting cylinders as well as the transfer module belonging to the station.

PROTOTYPE EXAMPLE

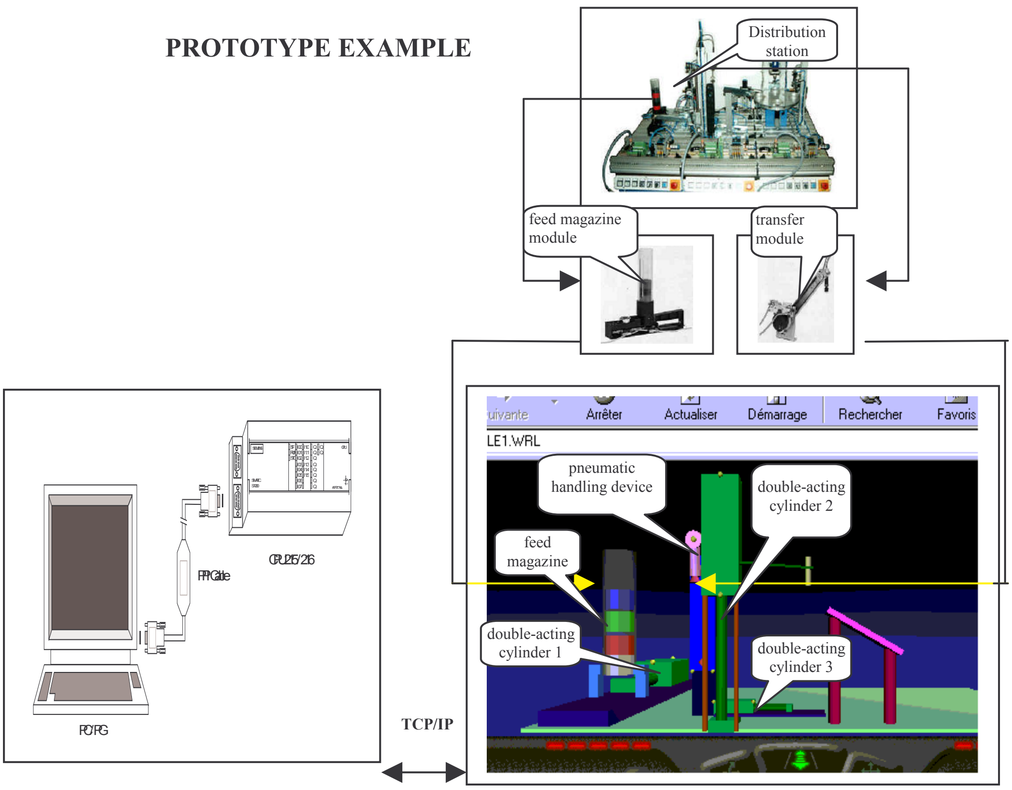

Fig. 5

Twelve signals are exchanged between the VRML Model and the real PLC, two for each component. The interface between the station and the associated controller (PLC board) consists of a standardized I/O interface. This interface allows the connection of 8 sensors, 8 actuators and 24V and 0V to the PLC board. The interface can be plugged to the I/O terminal of the station. The hardware and software environment of this cosimulation is shown in Figure 5. The PLC control code was programmed by using a dedicated programming tool (Step7 S7-200). Due to the difficulties encountered with the JAVA code for direct control of I/O signals[12], the PLC (Simatic S7 200) is connected to another computer controlled by Visual Basic language, and its input and output signals can be transmitted to the computer for cosimulation through TCP/IP socket communication.

The PC Server can be connected to the Siemens Simatic S7-200 family of PLCs. Communication occurs via PLC programming ports using PPI and PPI+ protocols. All available ports on the Simatic S7 200 CPU can be used to connect the PC to the PLC. The cable to be used for point-to-point connection between the panel and a CPU S7-200 is the PC/PPI. The same cable is to be used as a reference to connect the PC to a PPI+ network.

As shown in Figure 5, the RS-232 extremity of the PC/PPI cable is connected to one of the serial connectors of the PC, while the other extremity, RS-485, is connected to the CPU communication interface.

The PLC communication subroutine is a small program transplanted into the PLC memory. It manages the communication with the PC, receives orders (frequency, address and values) and sends the process status. Communication of information is done by means of an interrupt. Every character received through the communication interface is registered by this interrupt in a special memento, then it will be recorded in a special table.

The communication interrupt has an execution time of 5ms to 255ms with an inter-interrupt time equal to 1ms. This interrupt can detect all modifications to PLC I/O signals. Transmission of the PLC I/O to the PC is made by the injection of one or more hexadecimal values in a string made up of four characters, where the first two characters represent the first two input blocks of the PLC and the last two characters represent the two output blocks. Every input block is made up of eight inputs and similarly, every output block is made up of eight outputs.

CONCLUSION

Figure 2 illustrates the prototype we have implemented based on the three main ideas developed in this article: a) multilanguage cosimulation; b) modeling and implementing the virtual didactic component using VRML; c)the use of a TCP/IP connection to execute the cosimulation of the PLC code. Based on the idea of "virtual laboratories"[13-14], which implies an informational rebuilding of the real laboratory and its state through animations and 3D scenes, we attempted, via our system, to allow the teaching of the sequence control system and automatics in a connected mode.

We are currently trying to extend our system to simultaneously support the connection of many clients and to allow for the extraction of a VRML didactic component model from a generic database that resides on the server.

REFERENCES

[1] M. Mhamdi, M. Moalla, "A Virtual Verification and Execution of Grafcet Using VRML", *ICEE 2003*, Valencia, Spain, 2003.

[2] S. Kanai, T. Kishinami, "A Virtual Verification Environment for the Sequence Control System Using Vrml and Java", *Proc. DETC '99/CIE*, 1999.

[3] N. Schoeni, "Librairie de modélisation 3D en VRML pour pocketPC ", *VRAI Group Technical Report*, July 2002.

[4] F. Coste, F. Hessel, P. H. Le Marrek, "Multilanguage Design Of Heterogeneous Systems", *Proc. of the 7th International Workshop on H/S Codesign*, Rome, 1999.

[5] I. Varlamis, M. Vazirgiannis, I. Lazaridis, "Distributed Virtual Authoring Interfaces for the WWW: The VRSHOP Case", *Multimedia Tools and Applications Journal* , 2002.

[6] K. Cibulka, J. Zara, "Using VRML for Creating Interactive Demonstrations of Physical Models", *Proc. of CESCG Conference*, 1998.

[7] G. N. Villec, "Cosimulation of an Automotive Control System using ADAMS and Xmath", *International ADAMS User Conference*, 1998.

[8] I. Bacivarov, S. Yoo, A. A. Jerraya, "Timed HW-SW Cosimulation Using Native Execution of OS and Application SW", *Proc. HLDVT,* October 2002.

[9] G. Pelz, J. Bielefeld, Gunther Hess, "Hardware/Software-Cosimulation for Mechatronic System Design", *Proc. EURO-VHDL '96,* 1996.

[10] C. A. Valderrama, F. Naçabal, P. Paulin, "Automatic Generation of Interfaces for Distributed C-VHDL Cosimulation of Embedded Systems: An Industrial Experience", *7^{th} IEEE Int. Workshop on Rapid System Prototyping (RSP '96)*, 1996.

[11] I. Soetebier, R. Dömer, N. Braun, "A VRML and Java-Based Interface for Retrieving VRML Content in Object-Oriented Databases", *WebNet 1999: 987-992*

[12] J. Douin, "Programmation concurrente et Java", *Cnam,* January 9^{th} 1998.

[13] H. H. Saliah, "Design of a Generic, Interactive, Virtual and Remote Electrical Engineering Laboratory", *20^{th} ASEE/IEEE FEC*, 1999.

[14] H. H. Saliah, L. Villardier, C. Kedowide, "Resource Management Strategies for Remote Virtual Laboratory Experimentation ", *30^{th} ASEE/IEEE,* 2000.

[15] R. S. Pressman, *Software Engineering*, M-Hill, 2000.

BIOGRAPHY

Mohamed Mhamdi received the B.Sc. degree in Computing from the ESPTT, Tunis, 1993. Following a period in industry as a Systems programmer he received the Argegation degree in 1996. In 1997 he received the M.Sc. in Industrial Informatics from the ENSI, Tunis. In the same year he received his Technologue degree after which he moved into the field of Educational Technology in the High Institut of Technology of Sousse where he has remained for the past 6 years. His main areas of interests are in the area of computer science education research, particularly pedagogic and technological innovation.

Enhanced Process Quality and Process Innovation through System Simulation

Paul Stratil[1], Frank Wolf[2]

[1]smart gmbh
71032 Böblingen
Germany

Phone: +49 160 8619828

²Accenture GmbH
61476 Kronberg im Taunus
Germany

Phone: +49 175 5761262

KEYWORDS

CSS (Central Simulation System), Simulation – Minimize evaluation and testing effort – IT Test strategy – Test Management – Process Stability – Process Quality

ABSTRACT

Quality is good, but not quality at any cost. Every day, the business has to make choices about the best use of resources, and it must consider factors other than quality.

With companies merging, growing and becoming more and more international, the complexity and ongoing innovation of the business processes is rising. Processes must be ensured for their quality in order to deliver high class products and services to the customer. The key benefit of this assessment is certainty about the quality of its processes for an organization.

However, this assessment effort is a support function and generally considered overhead because it only supports the core work that generates the product or service the customer is willing to pay for. The challenge is to achieve the aspired level of certainty with a minimum set on resources, thus freeing capacities for the core business.

The objective of this article is to discuss how a business can sensibly manage this challenge and therefore gain a competitive advantage. A practical example from the automotive industry will outline what measurements can be applied by an organization to minimize the assessment effort and how such a new capability can be successfully implemented.

The basic idea is to use a simulation system to simulate the unchanged systems within the overall integration environment instead of testing new or changed processes with an expensive integrated environment. Issues can be identified without involving integrated systems directly, cutting down costs and time of the quality assessment phase.

I. INTORDUCTION "The Cost of Certainty"

On June 4, 1996, the maiden flight of the European Ariane 5 launcher crashed about 40 seconds after takeoff. The amount lost was half a billion dollars - uninsured. The conclusion of the international inquiry board was that the explosion was the result of a software error. It was caused by an internal variable related to the horizontal velocity of the launcher exceeding a limit - the control unit did not catch this exception and became inoperative - possibly the costliest software bug in history (at least in dollar terms, since earlier cases have caused loss of life).

Processes do not always do what they are supposed to do. The more complex it gets, the more options for discrepancies will appear. The possible anomalies during the launch of a rocket are arguably limited only by the imagination of the involved engineers. The consequence is obvious: A process whose malfunction will have a negative impact on people or businesses must be ensured for its faultless function before its first execution under real conditions.

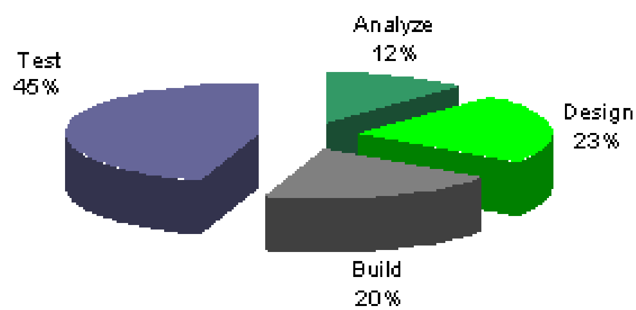

Figure 1: The quota of test effort during a typical software development project [Voas 99].

The common term that expresses to which grade a process has been ensured is "Quality". The goal is therefore to *achieve* quality when a process is designed and set up. Methods, standards or design principles can be used to achieve quality. However, that won't be sufficient in complex cases where the possibility of anomalies rises exponentially with every additional process feature. Quality has therefore to be *assessed* or in another term: to be tested.

As testing results in qualitative and/or quantitative "measures" for processes quality it enables appropriate decision making based on "facts" about the remaining risk for failure of a process. The objective of this article is to provide a better insight about testing as an "unwanted" but necessary (*Figure 1*) support activity to core business and how this support activity can be optimized to achieve the best possible outcome with a minimum effort.

II. A SELECTIVE APPROACH FOR OPTIMIZED PROCESS QUALITY

Structuring the Portfolio of Business Processes

A core process of an organization directly generates value to the customer. Assessing process quality is a support process to it which contributes to product quality indirectly only. Therefore it might be considered overhead if performed too extensively with a tendency to either be neglected or outsourced, if not considered essential to the success of the organization or the required product quality.

Process optimization by focusing of core processes, streamlining support processes and eliminating waste and loss are is one of the key challenges of today's business. The reason is that companies are heavily engaged to improve their efficiency, especially to optimize their operation costs and to free money for investment and innovation. *Figure 2* displays process types according to their benefit for the customer:

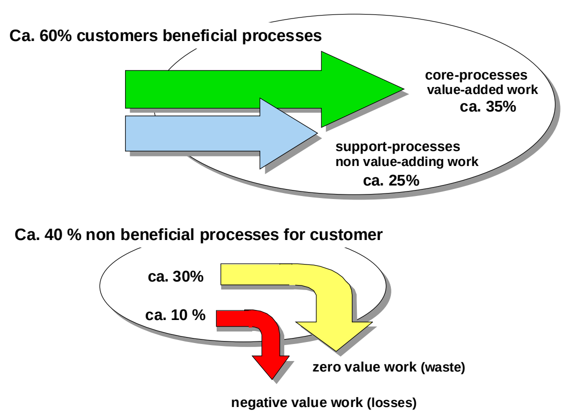

Figure 2: In core processes up to 40% more efficiency can be achieved.

Measuring Support Processes

For some processes – especially if they are mission critical – it has to be proved that they are 100% error free. For complex enterprise-wide business processes such an objective is impossible to achieve due to given time, cost and resource restrictions. A much more reasonable approach is to identify and manage risks according to their anticipated business consequence. This allows reasonable decisions to be made squarely in the context of the business, avoiding both over- or under-spending (McGraw 2003).

Not every system failure will lead to a disaster like a rocket crash. A defective welding robot in a car assembly line can certainly stop the whole production process and cause millions of dollars of loss every unproductive day. A temporary bug in the vehicle ordering functionality of a car manufacturer will cause additional costs and annoy customers but both cases won't spoil the entire mission of the company. The grade of process criticality can vary and an organization must define its required level of certainty about processes and their quality according to the possible business consequences in case of failure.

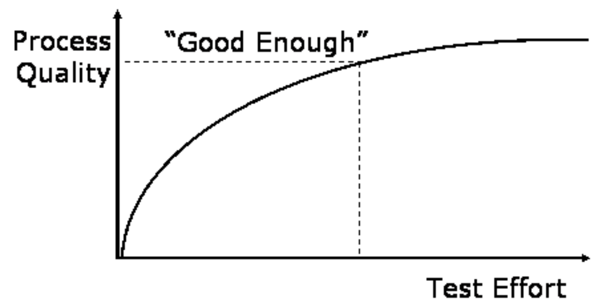

Figure 3: The marginal utility declines with every additional test case

If the desired quality of a process or a product is achieved it is considered sufficient then any further improvements means making an investment that has an inadequate return as depicted in figure 2. The term that is literally used for that approach is "*Good Enough*" [Bac97]. Testing more or less means therefore always moving away from the best possible resource allocation.

Defining Appropriate Selection Criteria for Optimization

The "Good Enough" approach provides a robust set of reminders that can help frame a conversation or make a convincing case about going live of a process, shipping a product, or implementing some better practice. Four factors are used to assess the stage of development:

1. Benefits of the process
2. Problems of the process
3. Process quality
4. Logistics of further improving the process

These factors are compiled under six perspectives (stakeholders, critical purpose, time frame, alternatives, consequence of failure and quality of assessment) to include the interdependences with the business environment [Bac97].

The assessment not only helps to prioritize the process quality towards the business consequences but also generates a better understanding which benefits and problems of a process are critical to the desired result. The strategic choice (which part of the overall budget do we spend on assessing process quality) produces therefore also input for the operative question which parts of the process need the most thorough review.

No Time to Rest – Innovation and Process Quality Optimization

The economy is led by those who innovate - create, find and/or combine knowledge into new products, services, and distribution methods - faster than their competitors. Innovation is the ability of an organization to deal with the dynamics of the environment, to differentiate or implement a plan whereby success is more probable [ZvA02].

Innovations may change products, processes, organizations, technology and even business models. But what's the consequence for a business that constantly renews its processes compared to one that is just operated?

Innovation is a learning process, the product of new applied knowledge. Operations is an established process driven by existing knowledge. The primary difference between operations and innovation is *uncertainty*. Innovation complicates planning, prediction and issue containment.

It is obvious that the assessment of process quality becomes even more important and costly for businesses in today's environment of permanent change. The good news is that the recurring verification effort offers also new opportunities for organizations to manage process quality.

The most apparent option is the automation of appropriate quality assessment steps. The repeated use of test support tools such as test automation systems or test management systems will make the initial required investment pay off. Automation in the context of innovation might seem a contradiction; it is therefore important to stress that these automated processes must be flexible enough to cope with the changing process and system landscape.

Another option for innovative businesses is to extend its view of desirable process attributes. Quality as the grade to which a process has been ensured is important but does not describe how predictable a process acts when it is changed. The term that shall be used for this attribute is "Stability".

A process is then stable if it behaves predictably under changed conditions. Stable processes would therefore ease the major drawback of innovations: uncertainty about the quality of changed processes. In stable processes, quality can be achieved in the design phase through analysis of the impact of a change. A quality assessment is in the most cases still required for stable processes but to a much lesser degree. As displayed in Figure 4: Stable processes allow a stronger emphasis on quality achievement.

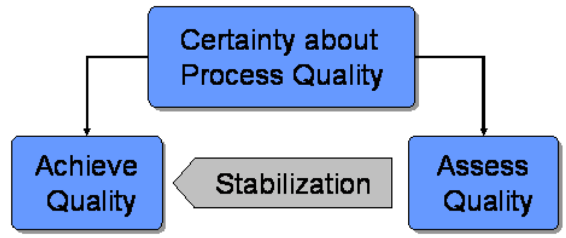

Figure 4: Stable processes allow a stronger emphasis on quality achievement.

Practical measures to stabilize processes are system and process documentation, training of those executing the process, fixing of bugs in the involved systems or system and process modeling. Stabilization is about learning to better understand the existing processes, their interconnection, and their behavior under impacting factors. Innovative businesses must establish a learning process that systematically confronts the unknown with hypotheses, tests them, and eventually creates new knowledge.

III. OPTIMIZING THE ASSESSMENT

The different ways a program can behave are almost unquantifiable, and the number of potential tests for that program is, therefore, limited only by the imagination of the tester. Moving further to a highly integrated system landscape with different master data sets for each system will ultimately result in an unmanageable amount of possible test cases. That complex combination of systems, software and data makes "complete" testing an impossible goal in all but the most trivial systems.

One approach to reduce the required test effort is to limit the testing to that which is required to make the process performance "Good Enough". The effort is further reduced by obtaining certainty at an early stage in the development process ("Achieve Quality" through stabilization). However, there will remain a significant amount of test cases that need to be assessed for their quality. The optimization of this process leads to a quantitative and a qualitative aspect:

The quantitative optimization defines how many test cases can be selected for the test. The task is about the composition of test infrastructure (available test systems, available timeframe), test resources (number, available timeframe and skill level of testers) and other support functions (test automation, issue management, release management) within the given budget and time constrains. This also includes the option to automate parts of the test process in continuously changing systems of innovative businesses. The better an organization is able to manage these functions, the more extensive the final test scope will be in relation to the size of the "bin" in which all selected test cases have to finally fit.

The qualitative optimization determines which test cases will be selected for the test. The task covers the selection of test cases that are relevant towards the test's quality goal from the total number of possible test cases. An important input to this selection comes from the assessment that prioritizes the process quality towards the business consequences ("Good Enough"). That process generates valuable input for the operative question which parts of the process need the most thorough review.

The amount of selectable cases has been set by the quantitative optimization and will be in the most cases considerably lower that the total number of imaginable test cases. The selection will be dependent on the scope of the new functionality (in the context of existing functions), the occurrence of interdependencies (between systems, software functions, data, the operating system) and other models for test case prioritization (statistical models, standard test procedures for regression tests). The better an organization is able to manage these functions, the more objective the final assessment will be, as these tasks define the best possible content of the "bin". *Figure 5* summarizes the discussed selective approaches towards process quality.

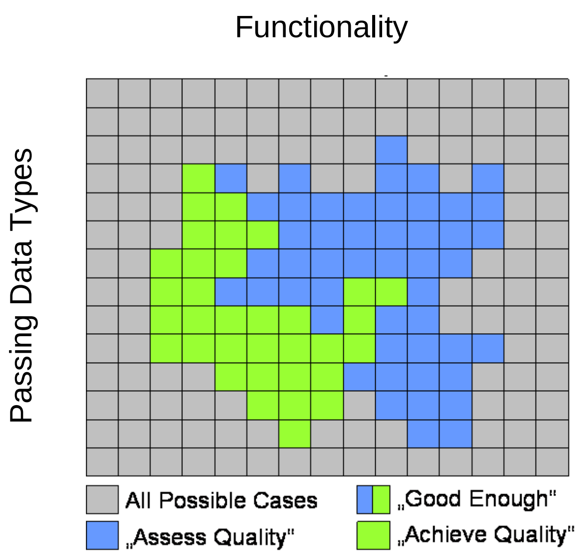

Figure 5: Joint approaches to reduce the overall quality assessment effort.

IV. CASE STUDY: Innovation as a Matter of Economic Survival

This chapter provides an example of how the described approaches to certainty about processes can be brought to life within the organization of an automotive manufacturer.

Increasing competitive pressure, individual customer requirements and growing customer demands have deeply changed the market environment. Process integration and innovative and integrated IT solutions are decisive in many cases for the international competitiveness of products and companies. That is especially true for the automotive industry.

A German carmaker provides a case study example. This carmaker established a virtual enterprise accompanied by the development of a new type of car. A network of business partners, located on the plant site preassembles car modules and delivers them just-in-time and in-sequence. The final assembly process is very lean and operates completely stockless, without material receipts for the car components and modules. Financial transactions for the payment of modules and components are triggered after consumption when each car passes the final assembly check point.

The decentral systems for sales and service in the network of more than 300 dealers operate fully integrated with the central systems of marketing, finance, assembly and spare parts logistics. A very short car order-to-cash processing time allows the company to react flexibly to dynamic market situations and customer requirements.

The automotive industry currently faces major challenges as cost and price pressure are hitting as the industry struggles through the current global economic downturn. Developing innovative products at the right time, the right place, and for the right customers has become a matter of economic survival. The carmaker realized that necessity and pushed towards cost reduction and expansion through new products and new markets to achieve further growth. The three major measures taken heavily impacted the existing process and system landscape:

Measure 1: Process and System Integration as Result of a Merger

This long-term project includes virtually all core and supporting processes of the company. A major part is the integration of the Ordering Systems with the processes Planning, Ordering, Distribution and Invoicing. This extremely complex system integration will enable the dealers of both companies to use one database for the online order processing of vehicles.

A key requirement during each phase of the project is to retain the full operability of all value creating processes thus minimizing the noticeable impact on customers and the affected departments.

Measure 2: New Products

The automotive market environment requires new product innovation in faster cycles, requiring shortened product time-to-market. It is planned to establish two new models in the next two years. These new products implicate new factories, new processes, new human resources, an extenstion to the available functionality of the IT systems and a considerable amount of new product master data, that has to be set up, tested and maintained, as well.

Regarding the historical development, only one car model was planned and the IT systems were, therefore, established for only that configuration. New product models require a reengineering of existing systems to integrate the new requirements. New products obviously require new data to be handled by the processes and systems. It must be ensured that the processes function correctly with this new master and transactional data.

Measure 3: New Markets

The carmaker has discovered potential growth in new markets in Europe, Asia and the USA for the current and planned products. To take advantage of this, the new business models and distribution channels for vehicles and parts have to be developed and implemented. This also impacts the IT and process landscape and adds new complexity to the overall solution.

Due to the highly integrated nature of the present vehicle sales solution it must be assured that changes to specific processes and applications do not have an unexpected impact on other existing processes and systems. This is especially true given the scope of the described three major requirements.

A further ongoing task is the continuous optimization of processes and systems in order to generate stable processes with a high quality.

Certainty as Competitive Advantage

Considering the innovative and dynamic business environment and the complex system and process landscape the **competence of generating certainty about process quality** is regarded as a major support process in the organization and as a success factor to effectively deal with the dynamics of the environment. This competence ensures the delivery of processes and systems that meet the requirements and the needed quality standards with a minimum set on resources, thus freeing capacities for the core business.

The main goal of the companies' quality insurance process is to bring together experts, thus knowledge to generate the best possible decision on how to receive the required level of certainty for its processes and systems that have been changed. *Figure 6* displays the central planning instance ("round table") that optimizes the balance between the validation requirements and the available validation resources.

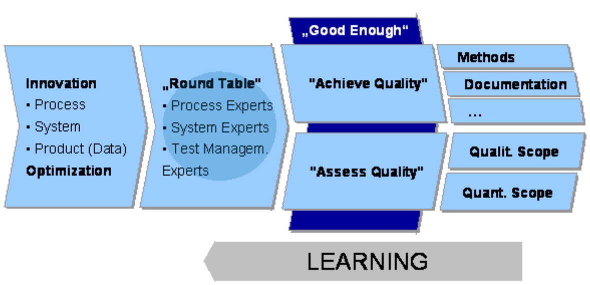

Figure 6: Knowledge concentration to define the best possible validation procedure.

V. SYSTEM SIMULATION TO OPTIMIZE THE ASSESSMENT PROCESS

The IT department that is responsible for all sales systems has alone more than 60 systems to maintain. Considering the highly dynamic environment (e.g. several releases per year in the main order processing system (one of 60)) one may imagine the required test effort. Though not every system is as dynamic as the order system and not every release requires passing the full stage test models (some systems and functionalities have well defined interfaces to the other systems thus limiting the integration and regression test effort); testing accounts for the major part of the carmakers IT budget.

As more and more tests focus on testing new data (new models, new markets), the automation of tests has become a major topic on the agenda. That includes tools for automated testing but also a new approach to test environment management. Maintaining a copy of the production system for testing purposes requires significant effort to:

- configure hardware and network
- maintain the most actual release level on each of the connected systems and
- validate master and working data to ensure the tests correctness.

These conditions made test environment management one of the major cost drivers in the IT budget and led to repeated time delays and quality issues during various software development projects because of their complexity.

To improve this situation, it was decided to simulate parts of the test environment instead of using an exact copy of the production system. This allows the testing process to be sped up, reducing costs for the test environment setup and guaranteeing a consistent high quality of the delivered software. The detailed development and setup of the simulation system will be further detailed below.

Though the simulation system is mainly driven as a "technology" initiative, its implementation is inseparably connected to the successful implementation of the associated organizational and process changes.

VI. THE CENTRAL SIMULATION SYSTEM (CSS)

A simulation is the execution of a model, represented by a computer program that gives information about the system being investigated. The purpose of the simulation is to make better decisions and avoid wrong decisions that could have bad consequences to affected people or companies [SEGR98]

In which cases do "simulation systems" have to be set up? Sometimes, it is not possible to examine processes under real conditions due to time and / or budget restrictions and / or incalculable dangers. In such cases, an artificial environment can be created that allows hypotheses to be examined under the influence of several parameters [Dia02].

Test Rationalization via a Simulation

The idea was to create a simulation system that could reduce the ever growing time for validation and test execution. This tool would rationalize dramatically the whole test process with a positive impact on time and resources. It would not be used as a “classical simulation” to actually gain further insights, to learn, about the real system. This learning aspect is a possible goal for further releases but was not the focus of the initial system setup.

The Definition of the Model and its Properties as Crucial Step to a Successful Simulation

The first step in the model definition process was the selection of the systems in scope of the model (Johansson 1996). It was obvious that not all present systems in the existing landscape could be simulated. The selection of the systems in scope was made in consideration of:

- the number of test relevant business processes supported by the system,
- the required effort to setup a production copy of the system in the test environment and
- the strategic relevance of the system within the changing IT and process world.

Systems were selected for simulation if all criteria were in the upper level compared to all other systems. The final selection and system model was thoroughly discussed with the most experienced testers and system experts to receive valuable feedback and validate the result. This selection ensures that the simulation system delivers a maximum of business value in comparison with the implementation costs to the test processes and will be a long-term investment.

The next step in the model definition process was the determination what the important properties of the system really are. A property sheet for each system was created to capture the systems master data, transaction data, business logic and the interfaces. The respective system experts were responsible for this task.

The last step in the model creation was then to make the choices of simplification that means to determine what properties to include or ignore. This selection cannot only be done by looking at each system itself; the system may interact within the simulation system with other systems and require therefore functionalities for a proper interaction in the whole simulation model. This very complex and challenging task was performed by the respective systems experts together with the system simulation team in a two-day workshop.

The result of the modeling phase was the decision to simulate the order to delivery process as this core process is part of most of the regression test models. It includes the central ordering system and the production system as these require the biggest effort to set up a production copy in the test environment and will remain a valid test case for the next years. The model will simulate the following business process flow:

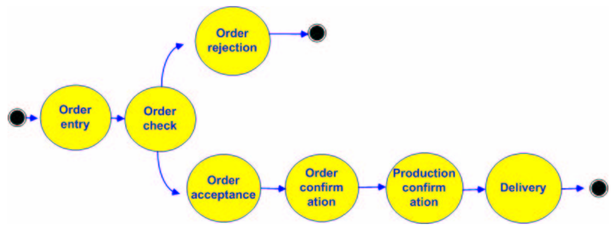

Figure 7: The Business Process Model

During the model creation phase a lot of system and process related expert knowledge was captured and documented in the simulation system and its documentation. This puts the organization in the position to perform tests with the involvement of very complex systems without the persistent support of a system expert thus saving the time of its most valuable human resources.

The System Architecture Decision and the Implementation Strategy

Technology principles were derived from the business requirements to provide a guideline for the architecture selection process:

- *Availability* – The system has to be available to various users at different locations. No specific client software has to be installed. 7X24 availability is not required as the system is not part of the core production environment
- *Hardware/ Software Selection* - Simplify hardware/software implementation by leveraging a few key vendor relationships. Focus on balancing technology principles, rather than the cost of software.
- *IT Development* - Utilize strategic partnerships to bring in leading-edge technology skills to accelerate implementation.
- *Maintainability* - The architecture can be modified easily and should be flexible enough to cope with the rapid pace of change in the IT landscape.
- *Buy vs. Build* - Purchasing packaged-based solutions minimizes the total cost of ownership of the applications and technology architecture.

The CSS application architecture is implemented in Java, especially using the standard J2EE. The business logic and data access have been coded in Enterprise Java Beans (EJB). The graphical user interface has been realized using servlet. The business logic for the data transformation of read files is processed in Session Beans. For storage or retrieving data from the underlying database, Entity Beans are in use. For accessing the application a standard browser was used.

The implemented components are using the frameworks GRNDS (General and Reusable Net centric Delivery Solution) and JUNA. GRNDS provides reusability and a wide range of technical architecture components. The JUNA Java based framework provides the protocol mechanism for the CSS.

The application runs under the IBM Websphere application server – one of the market leaders in J2EE application server technology and one of the preferred application servers in the company, where there is a lot of know how within the organization. The server provides embedded security, robustness, performance, extensibility, scalability and network enabled to access heterogeneous and worldwide placed IT systems and consequently provides an option for further integration. The application itself is user-friendly, multi-user-enabled, high reliable and module based and consequently extensible as well. The application is intuitively usable and accessible from everywhere using a standard web browser.

The main focus of the implementation strategy was to gather quick acceptance within the sponsoring departments to ensure the ongoing support of the project and the associated goals of various stakeholders. A release plan was defined with the most important and business-critical functionality in Release 1. The chosen architecture supported this goal by allowing a very fast implementation (4 weeks) that nevertheless had high maintainability. Release 2 covered the remaining parts of the selected order-to-delivery process.

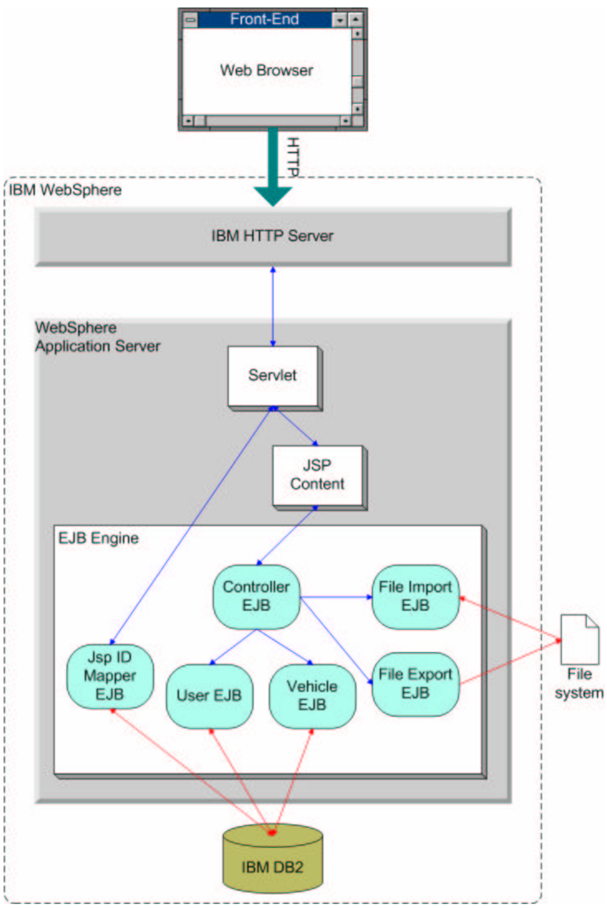

Figure 8: The CSS Application Architecture

The step-by-step implementation turned out to be very positive for the overall acceptance of the project within the company. This is especially true as some concerns about the necessity of the simulation system came up asking if another system to develop and maintain will be the right way to reduce complexity. The involved departments started to use the CSS for their tests right away and directly requested the functionalities of Release 2.

The CSS Validation and Process Setup Phase

The validation phase focused on ensuring that each part of the model functions as the corresponding part in the real system and getting control over the model and its use, so that it is possible to tell the difference between phenomena observed due to the shortcomings of the model and phenomena that are related to the real system.

Being itself a validation tool makes the CSS a very critical application as far as the quality and validity of the implemented logic is concerned. The system experts of the simulated systems were intensively involved in this verification to achieve the best possible quality and correctness.

A process had to be established to update the CSS with all changes to the respective production environment. It became, therefore, an essential part of the change approval process for systems to check if the change is relevant for the CSS. If that is the case, the CSS has to be updated with the new configuration. The implemented architecture ensures that this procedure is easy to execute. That is especially true for interface definition changes.

The CSS features also a test management support functionality that allows the user to open, maintain and save multiple projects and simulation scenarios. This enables the parallel access of different projects to the simulation environment and marks the first step from just being a test simulation to a test management platform.

Getting Started – The CSS in Use

The elapsed time between the first discussions about the simulation model and the live start of Release 1 in a production test environment was two months. The completion of Release 2 took then another month. This very tight timeframe could only be met by involving all relevant departments from the beginning and by dedicating highly skilled technical resources from third party suppliers to accelerate the implementation.

A mixed team completed the project to ensure the knowledge transfer from the beginning of the project on and increase the acceptance of the tool by its future users.

The conclusion one year after the CSS implementation is that the tool fully confirmed its business case, reducing significantly the runtime costs of the test environment, saving valuable time of system experts, enabling system knowledge transfer and setting the basis for a fully integrated test management system.

According to a rough estimation after the projects completion a return on investment will be achieved within one year. This short amortization time is especially caused by the extensive use of the CSS to deliver the large number of software changes in time and high quality.

VII. SUMMARY AND OUTLOOK

Improving and accelerating the test phase leads to considerable savings of time and resources. The proposed simulation architecture model is able to cope with flexible requirements in a changing environment and makes the assessment process significantly more efficient. The company gains a competitive advantage as innovations (even in its core processes and applications) can be realized more quickly and cheaply.

The simulation system is one part of the company's effort to retain certainty about its highly complex and constantly changing system and process landscape. Only all measurements taken together, along with continuous verification and learning will lead to a successful fulfillment of this task. It is about learning on the job, learning from failure and coping with complexity. It encourages the idea that benefits always come with problems. The task is not to blindly eliminate all problems, but to understand the problems and benefits of a situation well enough to eliminate the right problems and also deliver the right benefits.

REFERENCES

[Bac97] Bach, James, "Good Enough Quality: Beyond the Buzzword.", *IEEE Computer*, 30 (8), August 1997, pp. 96-98.

[Dia02] Diamond, Bob, "Concepts of Modeling and Simulation,"; 2002; *www.imaginethatinc.com*

[ZvA02] Zyl, Jay vanAlec, "Process Innovation Imperative" 2002, *www.tsa.ac.za/itweb/research/process. pdf*

[SEGR98] Stickel, Eberhart, Hans-Dieter Groffmann, Karl Heinz Rau, Gabler Wirtschaftsinformatik Lexikon, 1998, Wiesbaden

[SHB99] P. Stratil, A. Homolla, U. Baake, *"Introduction of Best Practice Processes for Product Innovation and Engineering"*, ECEC99

[JS96] Johansson, Sverker, "Computer Modeling and Simulation"; 1996; *http://www.ida.liu.se/labs/aslab/groups/ct/resources/mod_sim.html*

[MGG03] McGraw, Gary, "Making Essential Software Work", 2003, *www.cigital.com*

[MC99] Mindrum, Craig, et al. "Systems Thinking and Computer Simulation as an Aid to Project and Risk Management"; 1999; *www.accenture.com*

[Voas 99] Voas, Jeffrey M., Reducing Uncertainty about Software Safety, 1999, *http://www.rstcorp.com*

AUTHOR BIOGRAPHY

The author **PAUL STRATIL**, age 42, is Senior Manager for Information Management of DCAG. In his current assignment he works for smart gmbh, a member of the MercecesBenz Car Group.

As head of the *IT department Marketing, Sales and Aftersales* his responsibility is to ensure and support all *order fulfillment processes*, being *traditional sales channels* via dealer network or *digital sales channels* via eBusiness platforms and CRM. This responsibility includes a support function to central systems which undergoes both a *continuous evaluation* process validating its business contribution and a *continuous improvement* process boosting its performance by using efficient simulation concepts and tools, such as described in this paper.

In more than 16 years including 7 years in overseas assignments, the author has gained conceptual knowledge and practical experience in the optimization of business processes in various business areas of DaimlerChrysler´s Passenger Car Divisions, Commercial Vehicle Divisions and as member of the ITM board of this company.

Over the last nine years, the author has published several articles and papers for international conferences to contribute to the discussion on process, IT and organizational challenges in multinational companies.

FRANK WOLF, age 28, is a Senior Consultant at Accenture GmbH in Germany. He supported smart over the last years in various projects within the ITM Organization. His main focus was smarts process and system integration into the DaimlerChrysler system landscape, where he was a member of the system architecture design team and later responsible for the design of the core integration application the "smart Mercedes connector". He is a specialist for automotive sales processes, system modeling and integration, test strategies and Knowledge Management.

AUTHOR LISTING

AUTHOR LISTING

AUTHOR LISTING